# Stony Brook University

# Trace Element (Ni, Zn, Cr) and Halogen (Br, Cl) Geochemistry

# During Surficial Processes on Mars

A Dissertation Presented

by

**Yuyan Zhao**

to

The Graduate School

in Partial Fulfillment of the

Requirements

for the Degree of

**Doctor of Philosophy**

in

**Geosciences**

Stony Brook University

**August 2014**

**Stony Brook University**

The Graduate School

**Yuyan Zhao**


We, the dissertation committee for the above candidate for the

Doctor of Philosophy degree, hereby recommend

acceptance of this dissertation.


**Scott M. McLennan – Dissertation Advisor**
**Professor, Department of Geosciences**


**A. Deanne Rogers – Chairperson of Defense**
**Assistant Professor, Department of Geosciences**


**Martin A. A. Schoonen**
**Professor, Department of Geosciences**


**Joel A. Hurowitz**
**Research Associate Professor, Department of Geosciences**


**Suniti Karunatillake**
**Assistant Professor, Department of Geology & Geophysics**
**Louisiana State University**


This dissertation is accepted by the Graduate School


Charles Taber
Dean of the Graduate School

Abstract of the Dissertation

# Trace Element (Ni, Zn, Cr) and Halogen (Br, Cl) Geochemistry

# During Surficial Processes on Mars

by

**Yuyan Zhao**

**Doctor of Philosophy**

in

**Geosciences**

Stony Brook University

**2014**

Trace elements (Ni, Zn, and Cr) and halogens (Br and Cl) can be used as powerful tracers for evaluating Martian surficial processes, and are broadly relevant to intriguing questions such as aqueous chemistry and history, brine and mineral stability, and potential habitability of the Red Planet. Large volumes of geochemical data recently have become available for Ni, Zn, Cr, Br and Cl from Mars in the form of SNC meteorite analyses and in situ measurements by rovers, and, in the case of Cl, from orbital gamma-ray spectroscopy. In order to best interpret these geochemical data or utilize them to test models relevant to understanding the surface of Mars, a variety of simulation experiments are important to gain better understanding of the fundamental geochemistry of these elements. In this study, a series of laboratory simulation experiments were conducted to investigate the behavior of trace elements (Ni, Zn, and Cr) and halogens (Br and Cl) during (1) post-depositional diagenetic oxidation processes of ferrous sulfate to ferric oxide and (2) photochemical related processes during evaporation of halide saline systems.

A model of post-depositional oxidation of ferrous sulfate (melanterite; $FeSO_4 \cdot 7H_2O$) to ferric oxide (hematite; $\alpha\text{-}Fe_2O_3$) via two major pathways is well-established as a possible diagenetic process affecting certain Martian sedimentary systems: (1) via schwertmannite ($Fe_8O_8(OH)_6(SO_4)$) and/or goethite ($\alpha\text{-}FeOOH$) intermediaries; (2) via a jarosite (($H_3O,K$)$Fe_3(OH)_6(SO_4)_2$) intermediary. For initial solutions with equal concentrations of $Cr^{3+}$, $Ni^{2+}$ and $Zn^{2+}$, uptake of $Cr^{3+}$ by the precipitates was orders of magnitude greater than $Ni^{2+}$ and $Zn^{2+}$ for both pathways, due to probable substitution of $Cr^{3+}$ for $Fe^{3+}$ in mineral structures, in contrast to $Ni^{2+}$ and $Zn^{2+}$, which were mainly adsorbed onto mineral surfaces. Preferred uptake of $Ni^{2+}$ and $Zn^{2+}$ by schwertmannite and goethite was in the order $Ni^{2+} > Zn^{2+}$, but was reversed in the case of jarosite ($Zn^{2+} > Ni^{2+}$). By comparing these experimental results to in-situ rover measurements at Meridiani Planum, important constraints on the diagenetic pathways that produced the hematitic spherules (interpreted as sedimentary concretions) are obtained. The observed high Ni ($\geq$ 2,000 ppm) content and high Ni/Zn mass ratios (2~4) in the hematitic spherule-bearing samples of the Burns formation, relative to Martian crust (Ni = 337 ppm and mass Ni/Zn = 1.05), can be readily explained by the evolution pathway involving goethite. Other diagenetic pathways, such as via jarosite, could be valid only with an additional source of Ni (e.g., meteoritic or especially high-Ni basalt provenance).

The anions $Br^-$ and $Cl^-$, present in such diagenetic solutions, also demonstrate different partitioning behavior via different mineralogical evolution pathways. For solutions with initial molar $Cl^-/Br^- > 1$, jarosite incorporated at least an order of magnitude more Br than Cl and greatly enriched Br over Cl in its structure. Such preferential Br-enrichment was not found in goethite. Incorporation of large amounts of $Br^-$ would greatly decrease jarosite stability during aqueous alteration. Accordingly, it is concluded that jarosite could be a plausible candidate

holding elevated Br and fractionated Br/Cl ratios at the Martian surface. The changes in decomposition rates of jarosite, observed when incorporating halide anions, should be considered when attempting to interpret the aqueous history of Meridiani Planum by using jarosite as a "stopwatch".

Based on detailed statistical examination of Cl, Br, and S distributions of Martian soil profiles at Gusev Crater and Meridiani Planum, it is suggested that photochemical processes could play an important role in controlling halogen behavior at the Martian surface. Laboratory experiments demonstrate that photo-oxidation (ultraviolet $\lambda$ = 254 nm) of evaporative saline systems containing Br$^-$ and Cl$^-$ are able of producing perchlorate and chlorate at up to ~2% levels of total chlorine under conditions relevant to Mars. In addition, significant Br/Cl fractionation was present in the resulting evaporites due to preferential volatilization of Br over Cl into the atmosphere. Experimental evaluation of variables such as brine compositions, pH, sediment grain size, atmospheric conditions, and length of UV irradiation indicate an efficient heterogeneous reaction pathway, rather than commonly proposed atmospheric gas-gas reactions, for perchlorate and chlorate to form. Bromine is strongly influenced by photochemical processes and at high abundance is capable of competing with Cl for available oxidants, reacting with Cl radicals, forming oxy-bromine species, and cycling at the Martian surface. Consequently, such processes could cause substantial local variations in Br concentrations, which is consistent with the highly variable Br abundances that have been detected on the Martian surface.

**Dedication**

*To Huarong and Vincent Wenhao, for love and courage*

*To Mom and Dad, with love*

**Table of Contents**

# List of Figures

Chapter 4

Appendix 1

Appendix 2

# List of Tables

# Acknowledgments

My most sincere thanks go to my advisor and mentor, Scott McLennan. He showed me the standard of a good work, patiently shaped my way of thinking and expression to be like a scientist, and is always happy to share his experiences and thoughtful advice about working in the academia. Scott is the role model for me in many ways -- a great scientist with unwavering enthusiasm, a great mentor truly caring about his students, and a wise man living a well-balanced life. I feel so fortunate to be able to work with him in the last several years, and his encouragement and understanding have helped me through some of the most difficult time. I wish I could carry on his enthusiasm, devotion and wisdom in my own work and life, and could someday become a good scientist and mentor myself, in appreciation to his selfless help to my career.

I would like to thank my committee members: Deanne Rogers (Chair), Suniti Karunatillake (Louisiana State University), Joel Hurowitz, and Martin Schoonen. They have provided, with kindness, their insights and suggestions, which are precious to me.

An old Chinese proverb says, "When we see men of worth, we should think of equaling them". I have been very fortunate to work with some of the smartest people that have made up our research group, and I've learned much from each of them: Brian Hahn, Lauren Beavon, Suniti Karunatillake and Erwin Dehouck, and also two former members, Nick Tosca and Joel Hurowitz.

I greatly appreciate my collaborators for their contributions to the work presented here. I thank Martin Schoonen for helping me develop the XRF method to analyze halogens in my samples, which was a crucial part of that work (in Chapter 3). My many thanks to Andrew Jackson from Texas Tech Univ. for helping me analyze the oxy-chlorine species in highly concentrated matrices, which was a big challenge (in Chapter 4). My appreciations go to Suniti Karunatillake for inspiring discussion of my experimental UV-halogens project (in Chapter 4), and the invitation to contribute in his *Icarus* paper (Appendix 3), which was a great working experience. I would also like to take this opportunity to thank all the people who have helped me with my projects: Nick Tosca, Jim Quinn, Wenqian Xu, Lisa Hlinka, Alex Smirnov, Wei Li, and Congcong Che.

I must extend thanks to the entire faculty, staff, and fellow students of the Geosciences Department who make this department a big family. Thanks for giving me the fondest memories that I will always enjoy. The warmness and support you give me make the stressful journey of graduate school a much more of fun. Special thanks to: Owen Evans, for always keeping the building and labs well-organized; Lorreta Budd, for helping me arrange a smooth transition of my maternity leave in 2009-2010; and Diane Isgro, Yvonne Barbour, and Laura Colucci, for much appreciated help.

I'm so grateful to be a part of a wonderful family. My deepest love goes to my dear Mom and Dad, thanks for encouraging me to experience the diverse world, and always be there for me. My appreciations to Uncle Juming and Aunt Su, for many encouragements and helps along this journey to my PhD. Special thanks to my in-law parents and family, who have been extremely understanding. My appreciation also goes to Che Xiao, thank you for always being positive and optimistic. Your laughter has a curing power.

Last and most important, this thesis is dedicated to my love, Huarong, who has sacrificed so much for so long to make this happen. Thank you so much for your respect, patience, support and encouragement, which granted me a precious opportunity to pursue my dream. Even though we are apart by thousands of miles, I'm always inspired by your insights and confidence, and gain the strength from you to face my deepest fear. I'm so grateful to have you to face the world with. This thesis is also dedicated to my little Vincent, without whom, this work should have been finished at least two years ago. Thank you for openning my mind to a whole new world, and teaching me the most precious lesson of life: responsibility and unconditional love. Exploring the world with you is another journey that I'm looking forward to.

**Chapter 1: Introduction**

Over the past 15 years, large volumes of high quality chemical and mineralogical data obtained from nine successful surface and orbital missions to Mars, have greatly improved our knowledge of the Red Planet. One highlight of Martian data return, relevant to this dissertation, is the large number of measurements for the trace elements (Ni, Zn, and Cr) and halogen elements (Br and Cl) on the Martian surface, as observed by the 1975 Viking 1 and 2 landers (Cl abundances; Clark et al., 1976, 1982; Clark and van Hart, 1981), 1996 Pathfinder rover *Sojourner* (Cl abundances; Wänke et al., 2001; Brückner et al., 2003; Foley et al., 2003), 2001 Mars Odyssey orbital gamma-ray spectrometer (global Cl near-surface distribution; Boynton et al., 2007), 2003 Mars Exploration Rovers (MER), *Spirit* and *Opportunity* (Cl, Br, Cr, Ni, Zn abundances; Brückner et al., 2008), 2007 *Phoenix* Mars Lander (soluble Cl abundances and speciation; Hecht et al., 2009; Kounaves et al., 2010) and the 2011 Mars Science Laboratory (MSL) rover *Curiosity* (Cl, Br, Cr, Ni, Zn abundances and Cl speciation; Blake et al., 2013; Leshin et al., 2013; McLennan et al., 2014; Ming et al., 2014).

These measurements along with SNC meteorite analyses (e.g., Dreibus and Wänke, 1987; Wänke and Dreibus, 1994; Rao et al., 2005, 2009; Kounaves et al., 2014) provide us valuable tools to evaluate the surficial processes on Mars, broadly relevant to the aqueous chemistry and history, brine and mineral stability, detection of organics, and potential habitability. In order to better understand some of the possible controls on the distributions and speciation of these elements on the Martian surface, and utilize these geochemical data to test models relevant to

understanding the surface of Mars, a variety of theoretical modeling and laboratory simulation experiments are indeed important.

Two surficial processes of great interest that can be evaluated using trace elements (Ni, Zn and Cr) and halogen elements (Br and Cl) are the focus of this study: (1) post-depositional diagenetic Fe-oxidation processes that are especially relevant at Meridiani Planum; (2) photochemical related evaporation of saline systems at the Martian surface. Specifically, I experimentally investigated the behavior of trace elements and halogen elements in these two scenarios in order to provide constraints on the following questions:

(1) The origin of hematitic spherules present in the sedimentary rocks of the Burn formation at Meridiani Planum.

(2) The reasons accounting for Br enrichment and variation, and highly variable Br/Cl ratios, detected in Martian surface samples.

(3) Any photochemical influences on halogen distributions at Martian surface, and the possible formation mechanism of oxy-chlorine species and volatilization of Br and Cl into the Martian atmosphere.

## 1.1 Trace element constraints on hematitic spherules formation

Of all settings examined by the Mars Exploration Rovers *Spirit* and *Opportunity*, Meridiani Planum is distinct in its well-established sedimentological and stratigraphic context and so far is the only site where hematitic spherules have been directly observed on Mars (Grotzinger et al., 2005; McLennan et al., 2005; Squyres et al., 2009). One question has been the object of great interest is the origin of these hematitic spherules present in the sedimentary rocks of Burns formation. Although several models have been proposed (e.g., Barrón et al., 2006; Golden et al.,

2008; Knauth et al., 2005; Sefton-Nash and Catling, 2008; Tosca et al., 2008; Zolotov and Shock, 2005), most agree that these spherules are sedimentary concretions, but there is no consensus about the mechanisms or aqueous conditions of their formation.

A model of diagenetic oxidation of ferrous sulfate (melanterite; $FeSO_4 \cdot 7H_2O$) to ferric oxide (hematite; $\alpha\text{-}Fe_2O_3$) via two major pathways (1) goethite ($\alpha\text{-FeOOH}$) intermediary and (2) jarosite ($KFe_3(OH)_6(SO_4)_2$) intermediary have been relatively well-established, accounting for some of the jarosite and crystalline hematite (and/or hematitic spherules) detected at the outcrops of Meridiani Planum (McLennan et al., 2005; Tosca et al., 2008; Sefton-Nash and Catling, 2008). This model might have a broader implication for some other locations across the Martian surface, including regions of Valles Marineris and Magaritifer Terra, where closely associated Fe oxides (e.g., hematite) and sulfates (e.g., polyhydrated sulfates) have been detected remotely (Bibring et al., 2007).

Mass balances suggest hematitic spherules have approximately Ni $\geq 2000$ ppm; Zn ~500-600 ppm; Cr $\leq 1000$ ppm (Taylor and McLennan, 2009) and compared to Martian crustal abundances (Ni = 337 ppm; Zn = 320 ppm; Cr = 2600 ppm), these trace elements are enriched by factors of >6 (Ni), ~1.5-2 (Zn), and <0.4 (Cr). Accordingly, the trace element features of high Ni content, high Ni/Zn ratios and low Cr/Ni ratios of the hematitic spherules, need to be explained.

Yen et al. (2006) evaluated the high Ni content of the hematite-rich soils at Meridiani, and concluded that the enrichment could not be reproduced by physically mixing of any known materials from Mars. Therefore, whether the high Ni features originated from a previously unrecognized high-Ni magma, thus representing a provenance signature, or is enriched by surficial processes such as evaporation and/or diagenesis, or both are still unclear. Direct detection of Fe-Ni meteorites, such as "Meridiani Planum" (also informally named

"Heatshield"), on the surface of Meridiani Planum (Schröder et al., 2008) suggests a possibility of exogenic meteoritic components contributing to elevated Ni in this area. Contributions of Ni from meteoritic sources have been discussed by McLennan et al. (2005) for Meridiani sediments and Yen et al. (2006) for Gusev/Meridiani soils, and each constrained the contribution to be less than 6% and 1-3% respectively. Nevertheless, as shown in Figure 1.1, the trend of increasing Ni correlating to increasing Fe and hematite-rich samples indicates the possibility that Ni may be mobile and thus could be enriched through groundwater-related processes.

The basalt alteration and evaporation concentration processes from which the diagenetic fluids were derived were also evaluated experimentally in the laboratory, to provide further constraints on the trace element features of the diagenetic fluids. Acidic alteration of crystalline basalt, likely a dominant process on Mars (Tosca and McLennan, 2009), can produce a relative order of release: Ni > Cr > Zn, providing for aqueous fluids with a lower Cr/Ni and higher Ni/Zn than average crustal abundances (Beavon et al., 2009). Preliminary mineral-solution free-drift experiments further suggest significant substitution of $Ni^{2+}$, $Zn^{2+}$, and $Cr^{3+}$ into sulfates could occur from concentrated brines during Martian evaporite formation. $Ni^{2+}$ and $Zn^{2+}$ would preferentially replace $Fe^{2+}$ in ferrous sulfates (e.g., melanterite) and $Cr^{3+}$ preferentially replace $Fe^{3+}$ in ferric sulfates (e.g., jarosite) in more oxidized evaporating fluids (Hahn et al., 2009). Accordingly, the initial trace element concentrations in the diagenetic solutions were set at a similar level (300-500 µg/g), to see if any fractionation of Ni/Zn and Cr/Ni could occur during the final stage of the diagenetic processes, with an understanding that initial brines may in fact have borne lower Cr/Ni and higher Ni/Zn signatures.
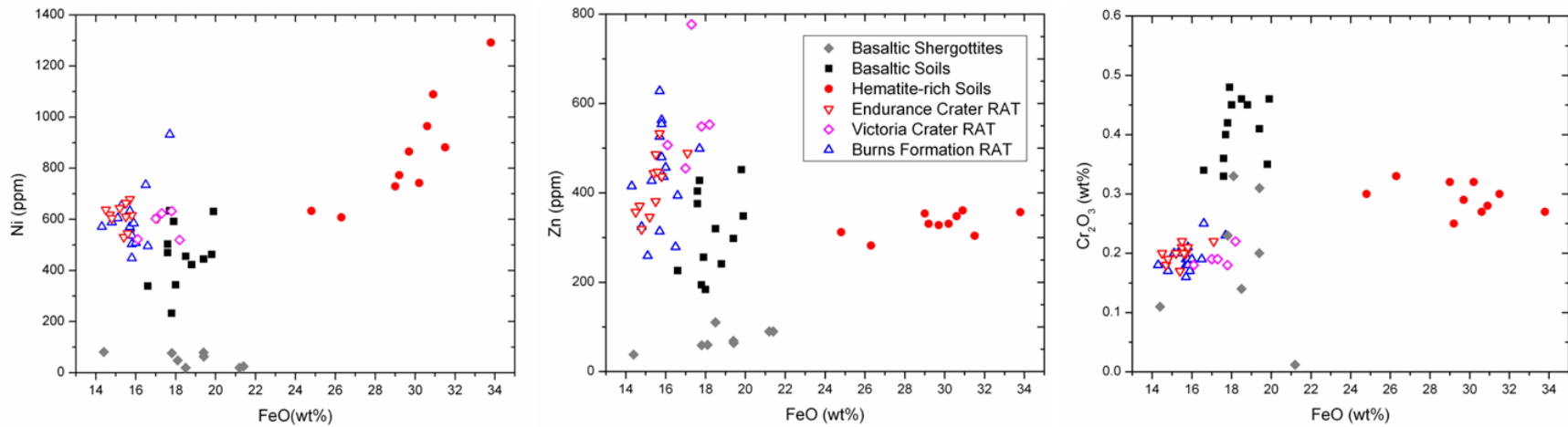
**Figure 1.1.** Plots of Ni, Zn and $Cr_2O_3$ versus FeO (as total Fe) for Meridiani undisturbed (commonly spherule-rich) soils, RAT-abraded outcrop rocks, and basaltic shergottites. Meridiani outcrop material is enriched in Ni and Zn but less so in Cr compared to basaltic shergottites and basaltic soil samples examined in situ by the Spirit rover. Ni concentrations in hematitic spherules are high and its enrichment is strongly associated with Fe in hematite-rich soil samples, but less so for Zn; (3) Cr concentrations, though elevated in soils compared to outcrop rocks with similar FeO concentration, are lower in the hematite-rich soils than basaltic soils. Data source: Brückner et al. (2008).

## 1.2 Possible Br enrichment and Br/Cl fractionation during diagenetic Fe-oxidation processes

Average SNC meteorites (shergottites, nakhlites, and chassignites) have a Cl/Br ratio of ~180 (Dreibus and Wänke, 1987; Banin et al., 1992; Brückner et al., 2008), which is close to the CI chondrite ratio of 199 (Cl 698 ppm and Br 3.5 ppm; Palme and Jones, 2003). Consistent with these findings in meteorites, APXS measurements on rocks found at the Martian surface show that Br concentrations are low or undetectable in basalt samples, but enriched in the samples that have undergone a variety of sedimentary processes, such as weathering, evaporation, and diagenesis (Rieder et al., 2004; Clark et al., 2005). As shown in Figure 1.2, the highly variable Cl/Br mass ratios are primarily controlled by variable Br abundances, which in turn vary by more than three orders of magnitude.

Due to the 8% difference in ionic radius ($Br^-$ 1.96 Å vs. $Cl^-$ 1.81 Å), $Br^-$ can substitute for $Cl^-$ in most mineral lattices but preferentially remains in the brine as $Cl^-$ forms halide minerals (Edmunds, 1996; Worden, 1996; Seimann and Schramm, 2002). During evaporation of terrestrial waters, both $Br^-$ and $Cl^-$ act conservatively through to the point of $Cl^-$ precipitation, beyond which Cl/Br ratios decrease in evaporating brines with Cl/Br ratios of precipitates being higher than the complementary ambient brines. However, the possible behavior of $Br^-$ and $Cl^-$ present in the diagenetic solutions during Fe-sulfates to Fe-oxides transformation (as described in Section 1.1), is largely unknown. In addition, $Cl^-$ ion has been suggested to be able to substitute for the hydroxyl ion in the jarosite (and related) structures (Morris et al., 2006), and the tunnel structure of schwertmannite (a likely precursor of both jarosite and goethite during the proposed diagenetic processes; Tosca et al., 2008) is able to accommodate $F^-$ and $Cl^-$, but not $Br^-$ due to its

larger ionic radius (Eskandarpour et al., 2008). Consequently, diagenetic Fe-oxidation processes may have the potential for incorporating and fractionating halide anions near the Martian surface.
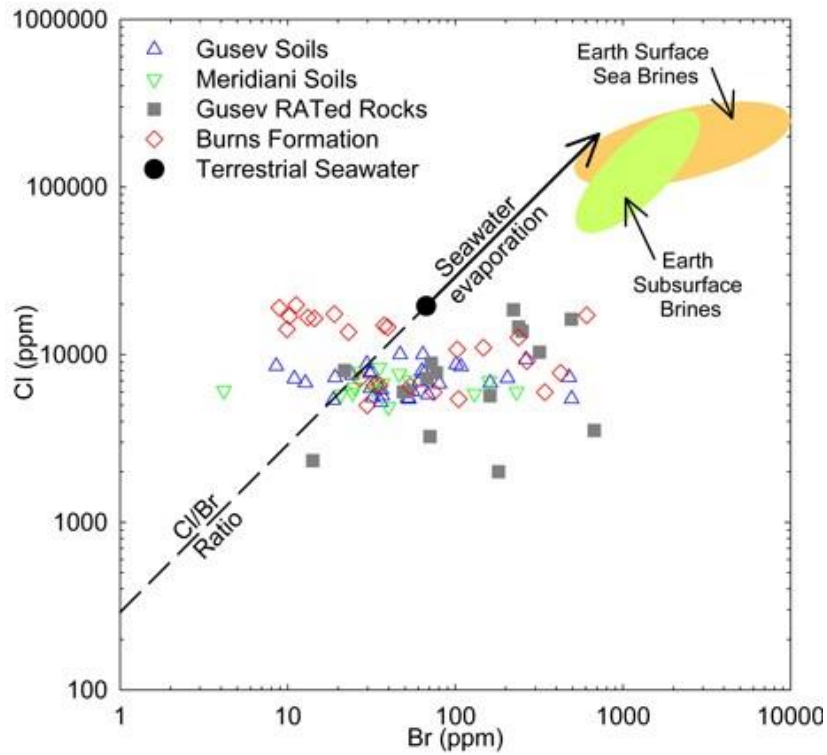
**Figure 1.2.** Cl (ppm) vs. Br (ppm) for selected APXS analyses. Also shown are the Cl/Br path of evaporating terrestrial seawater and fields for terrestrial brines (low Cl/Br) from which halite (high Cl/Br) has precipitated. The Cl/Br ratio in Martian samples is highly variable and the variation of Cl/Br ratios is mainly controlled by Br abundances. Data source: Brückner et al. (2008).

### 1.3 Photochemical influences on halogens at the Martian surface

Besides highly variable Br abundances in Martian surface samples, direct measurements of Cl on Mars reveal that: (1) Cl is widely distributed (Boynton et al., 2007; Clark et al., 1982; Gellert et al., 2004; Keller et al., 2006; Rieder et al., 2004). (2) Perchlorate ($ClO_4^-$) is present at two widely separated locations (Phoenix and Curiosity landing sites) and in three different lithologies (surface soils, aeolian fines, ancient sedimentary rock) (Hecht et al., 2009; Leshin et al., 2013; Ming et al., 2014), suggesting that oxy-chlorine species may be important components of Cl, ubiquitous on the Martian surface, and persistent through its history. These observations suggest that photochemical oxidation processes, which appear to have been underappreciated, may play an important role influencing Cl distributions. Such processes could also affect Br (Sander et al., 2003), and may be one of the explanations for considerable Br variability observed on the Martian surface (Karunatillake et al., 2013; see Appendix 3 for details).

Due in part to limited understanding of how natural perchlorate forms on Earth, some key questions remain unclear including formation pathways, types of effective reactions (i.e., atmospheric gas-gas, heterogeneous solid-gas or liquid-gas), roles of intermediate oxidation species between $Cl^-$ and $ClO_4^-$ (i.e., $ClO_3^-$, $ClO^-$, and $ClO_2^-$), type of oxidants, and other variables such as pH and temperature. Thus, for Mars, questions of great interest remain unanswered, such as (1) whether $ClO_3^-$, $ClO_2^-$ and $ClO^-$ are also present on the Martian surface; (2) what likely are the most efficient formation pathways; (3) which natural oxidants account for perchlorate formation, and so forth. In addition, due to the more attenuated atmosphere of Mars compared to Earth, relatively well-established atmospheric origins of perchlorate on Earth (Bao and Gu, 2004; Catling et al., 2010; Jackson et al., 2010) may not be quantitatively sufficient to explain the

apparently abundant perchlorate detected on Mars, thus demanding alternative pathways yet to be identified, such as heterogeneous reactions (Smith et al., 2014).

Studies of terrestrial tropospheric Br suggest that Br preferentially volatilizes over Cl in brines having Br/Cl ratios greater than seawater (e.g., Enami et al., 2007; Finlayson-Pitts, 2010; Lary, 2005) and such surface-atmosphere transfer is sufficient to influence Br mass balance and fractionate Br/Cl ratios in local regions (Risacher et al., 2006; Wood and Sanford, 2007). Some tropospheric Br sources identified on Earth may be relevant to Mars, including evaporative brine and saltpan environments (Hönninger et al., 2004; Risacher et al., 2006; Wood and Sanford, 2007), brine films on suspended dust (Sander et al., 2003), and aerosol release from newly-formed ice on seawater (Kaleschke et al., 2004; Yang et al., 2008). At present, it is unknown if Br species other than Br$^-$ (e.g., Br, BrO, and BrO$_3$) are present on Mars, and how any Br would influence Cl during any photochemical processes.

Accordingly, this thesis is organized into five chapters, with Chapters 2-4 each focusing on one main question stated above. Chapter 2 "Behavior of Ni, Zn and Cr during low temperature aqueous Fe(II) oxidation processes on Mars" is a journal paper that was published in *Geochimica et Cosmochimica Acta*. Chapter 3 "Behavior of bromide, chloride and phosphate during low temperature aqueous Fe(II) oxidation processes on Mars" is a journal paper that was published in *Journal of Geophysical Research-Planets*. Chapter 4 "Photochemical controls on oxychlorine production and Br/Cl fractionation on the Martian surface" is currently in preparation for submission and is formatted accordingly. Chapter 5 summarizes the conclusions of the dissertation and provides recommendations for future work. Three appendices follow the main chapters. Appendix 1 is the supplementary materials for Chapter 3 that was published with the paper. Appendix 2 is the supplementary materials for Chapter 4 that will be submitted with the

manuscript. Appendix 3 "Does Martian soil release reactive halogens to the atmosphere" is a journal paper that was published in *Icarus* on which I am a co-author.  It is based on Martian data analyses, and is greatly relevant to the experimental work described in Chapter 4.

A brief overview of the major findings of each of the chapters is provided below.

**Overview of Chapter 2:**

The results of experimental investigations of trace element Ni, Zn and Cr behaviors and controlling factors during Fe(II)-oxidation processes are presented in Chapter 2. The experimental approaches were designed to simulate groundwater recharge diagenesis events after evaporite deposition and infiltration of water into sediments under conditions of high ionic strength. Depending on the pH of the system, the transformation from melanterite ($FeSO_4 \cdot 7H_2O$) to hematite ($\alpha$-$Fe_2O_3$) could occur by way of three major pathways, involving intermediate species schwertmannite ($Fe_8O_8(OH)_6(SO_4)$), goethite ($\alpha$-FeOOH), and jarosite ($(H_3O,K)Fe_3(OH)_6(SO_4)_2$).

Path 1: Melanterite → Jarosite → Hematite

Path 2: Melanterite → Schwertmannite → Goethite → Hematite

Path 3: Melanterite → Schwertmannite → Goethite plus Jarosite → Hematite

For initial solutions with equal concentrations of $Cr^{3+}$, $Ni^{2+}$ and $Zn^{2+}$, uptake of $Cr^{3+}$ by the precipitates was orders of magnitude greater than $Ni^{2+}$ and $Zn^{2+}$ for both goethite and jarosite pathways, due to structural incorporation and probable substitution of $Cr^{3+}$ for $Fe^{3+}$, in contrast to $Ni^{2+}$ and $Zn^{2+}$ which were mainly adsorbed onto mineral surfaces. Preferred uptake of $Ni^{2+}$ and $Zn^{2+}$ by schwertmannite and/or goethite was in the order $Ni^{2+} > Zn^{2+}$, but was reversed in the case of jarosite ($Zn^{2+} > Ni^{2+}$). Path 3 (melanterite → schwertmannite → goethite plus jarosite → hematite), which effectively represents a combination of Path 1 and 2, could exhibit intermediate

trace element behavior depending on the proportion of goethite and jarosite in the mixtures (Figure 1.3).

Given that the Martian crust has similar levels of Ni and Zn (337 ppm and 320 ppm; (Taylor and McLennan, 2009), the elevated Ni ($\geq$ 2000 ppm) and high Ni/Zn mass ratios (2~4) observed in Meridiani hematitic spherule-bearing samples can be explained best by Path 2 via goethite, without need for additional high Ni sources in this region. Although the lack of goethite at Meridiani renders it uncertain if goethite ever served as a precursor to facilitate hematite formation, dehydration of nano-crystalline goethite is thermodynamically favored and thus cannot be ruled out. However, if hematitic concretions were formed by dissolution of jarosite (Path 1), then Ni concentrations in the spherules could not readily be accounted for by this process alone and a higher initial Ni/Zn ratio than adopted in our initial fluids would be needed, possibly contributed by high Ni magmas or Fe-Ni meteoritic components.

The Cr(III), when assumed to be in equal amounts as Ni and Zn in the initial solution, accumulated in all Fe(III)-phases by at least two orders of magnitude greater than Ni and Zn. Given that Cr concentrations are within about an order of magnitude of Ni and Zn in samples measured by the Opportunity rover, Cr concentrations may have been much lower than Ni and Zn in the initial diagenetic fluids. Significantly lower ratios of Cr/Ni and Cr/Zn in the diagenetic fluids, than the Martian crustal abundances, suggests that mobility of Cr was greatly limited during basalt weathering or evaporation processes prior to diagenesis compared to Ni and Zn. These findings are generally in agreement of the experimental results of trace element behavior during Martian basalt alteration (Beavon et al., 2009) and subsequent evaporation concentration (Hahn et al., 2009), the processes which may constrain the initial characteristics of the diagenetic fluids.
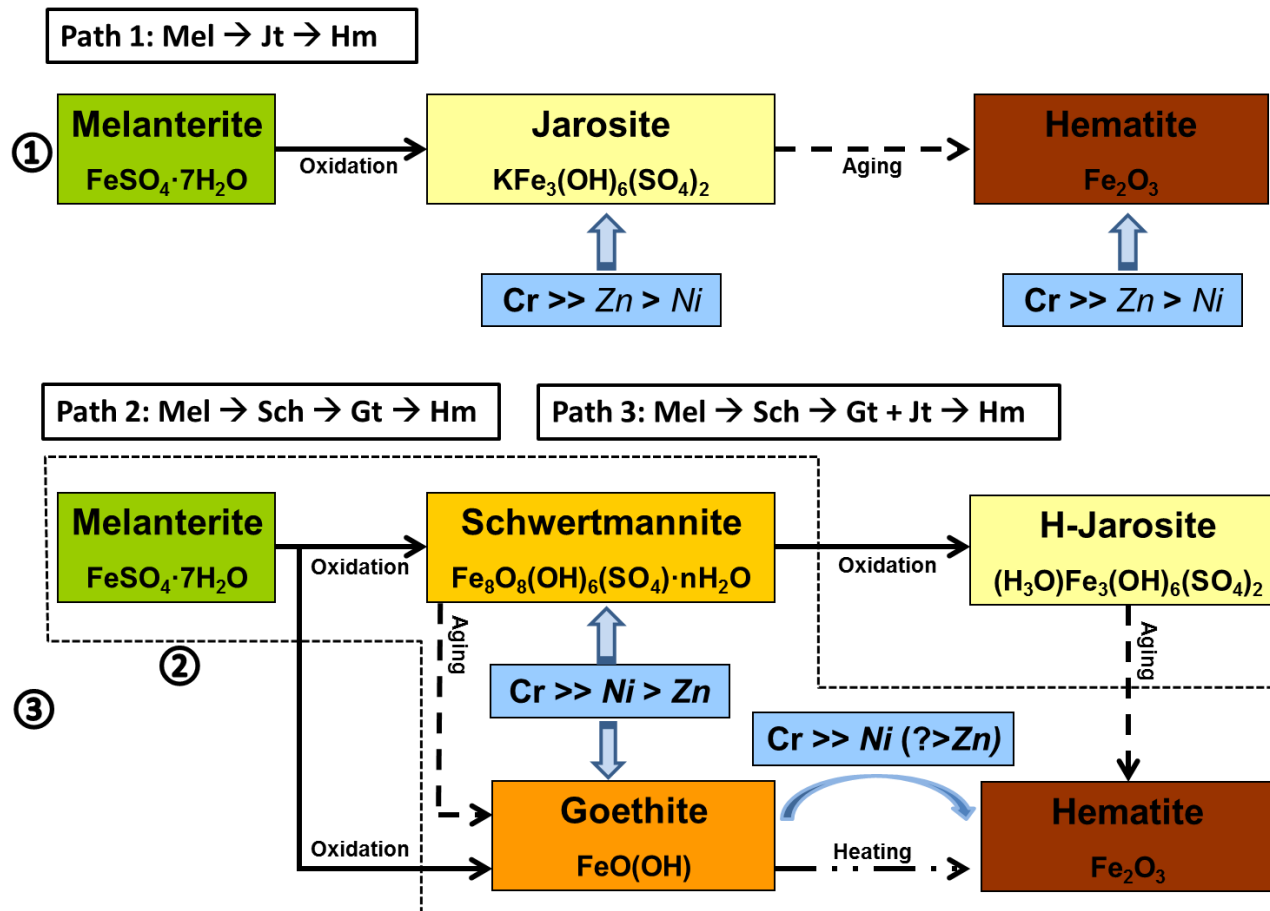
**Figure 1.3.** Schematic outline of mineralogical evolution pathways established, and the relative order of trace element partitioning into each mineral phase suggested by the experimental results described in Chapter 2. Different arrows indicate oxidation experiments (solid arrow), aging experiments (simple dashed arrow) and heating experiments (dash-dot arrow). Circled numbers represent pathways described in the text. Path 2 is effectively a part of Path 3, and is outlined by the dashed polygon. The main mechanisms accounting for trace element partitioning behavior are labeled by the font of each element name, where **bold** represents incorporation, *italic* represents adsorption/desorption, and ***bold italic*** represents uncertain or both mechanisms.

**Overview of Chapter 3:**

The results of experimental investigations of bromide, chloride and phosphate behavior during diagenetic oxidation from melanterite ($FeSO_4 \cdot 7H_2O$) to hematite ($\alpha$-$Fe_2O_3$) via jarosite ($KFe_3(OH)_6(SO_4)_2$) and goethite ($\alpha$-$FeOOH$) pathways are presented in Chapter 3. In this scenario of post-depositional diagenetic processes, hematite-rich concretions within the Burns formation sandstones grew within the phreatic zone during slow recharge of a high ionic strength groundwater system, which was likely dominated by the sulfate anion, but also likely contained chloride and bromide. Phosphate anion could also have been present in such a fluid, but likely at limited concentrations due to the relatively low solubility of Ca-, Mg- and Fe-phosphates compared to sulfates and halides.

Our results demonstrate that for solutions with initial molar $Cl^-/Br^- > 1$, jarosite incorporated at least an order of magnitude more Br than Cl and greatly enriched Br over Cl in its structure (Table 1.1). Such preferential Br-enrichment was not found in goethite. This observation indicates that jarosite could be a plausible candidate holding elevated Br and fractionated Br/Cl ratios at the Martian surface. The fluids from which jarosite formed could be originally depleted in $Br^-$ with respect to $Cl^-$, but still yield high Br precipitates. In the case of Meridiani Planum, it is thus possible that some high Br abundances detected by Opportunity rover are associated with jarosite, and such jarosite precipitates might originate from brines that were depleted in $Br^-$ concentration initially.

Incorporation of large amounts of $Br^-$ would greatly decrease jarosite stability during aqueous alteration. As shown in Figure 1.4, the dissolution rates of four types of jarosite, at both 25 ºC and 70 ºC, were in the same order: Br,Cl-bearing > Br-only > halogen-free > Cl-only. It is suggested that weight percent levels of $Br^-$ incorporated into jarosite may distort its structure and

make the bonds more susceptible to being attacked during aqueous alteration and thus reduce the stability relative to halogen-free jarosite. The changes in decomposition rates of jarosite, by incorporating halide anions, should be considered when attempting to interpret the aqueous history of Meridiani Planum using the kinetics of jarosite dissolution as a "stopwatch". In addition, the initial $Cl^-/Br^-$ ratio from which the jarosite formed may be an important factor influencing jarosite stability.

Preliminary competitive adsorption experiments for $Cl^-$, $Br^-$, $SO_4^{2-}$ and $H_2PO_4^-$ on halogen-free -hematite, -goethite and -jarosite show that, in a sulfate-dominant solution system where $SO_4^{2-}$ is much higher in abundance than any other anions (as is likely the case at Meridiani), $Cl^-$, $Br^-$ and $H_2PO_4^-$ could not compete with $SO_4^{2-}$ on these Fe-mineral surfaces. Therefore, in the diagenetic fluid system where sulfate is most likely the highest abundance component, adsorption may not result in an enrichment of $Cl^-$, $Br^-$ or phosphate onto hematite, goethite, or jarosite. This observation is consistent with the findings from APXS soil data that there are no significant correlations between Cl or P and nanoparticle Fe oxides in soils at both MER landing sites (Greenwood and Blake, 2006).

**Table 1.1.** Concentrations of Cl$^-$ and Br$^-$ in precipitated jarosite solids and the molar ratios of Cl$^-$ and Br$^-$ concentrations between precipitates and initial solutions.

| Type of jarosite | $C_{aq}$ (mmol/L) | | $C_s$ (mmol/kg) | | $C_s/C_{aq}$ | |
|---|---|---|---|---|---|---|
| | Cl$^-$ | Br$^-$ | Cl$^-$ | Br$^-$ | Cl$^-$ | Br$^-$ |
| Cl-jarosite | 374 | - | 39.4 | - | 0.105 | - |
| Br-jarosite | - | 367 | - | 642 | - | 1.75 |
| Br,Cl-jarosite | 370 | 186 | 22.5 | 493 | 0.061 | 2.65 |

*$C_s$ denotes the concentration of final jarosite solid. $C_{aq}$ denotes the concentration of initial parent solution.

16
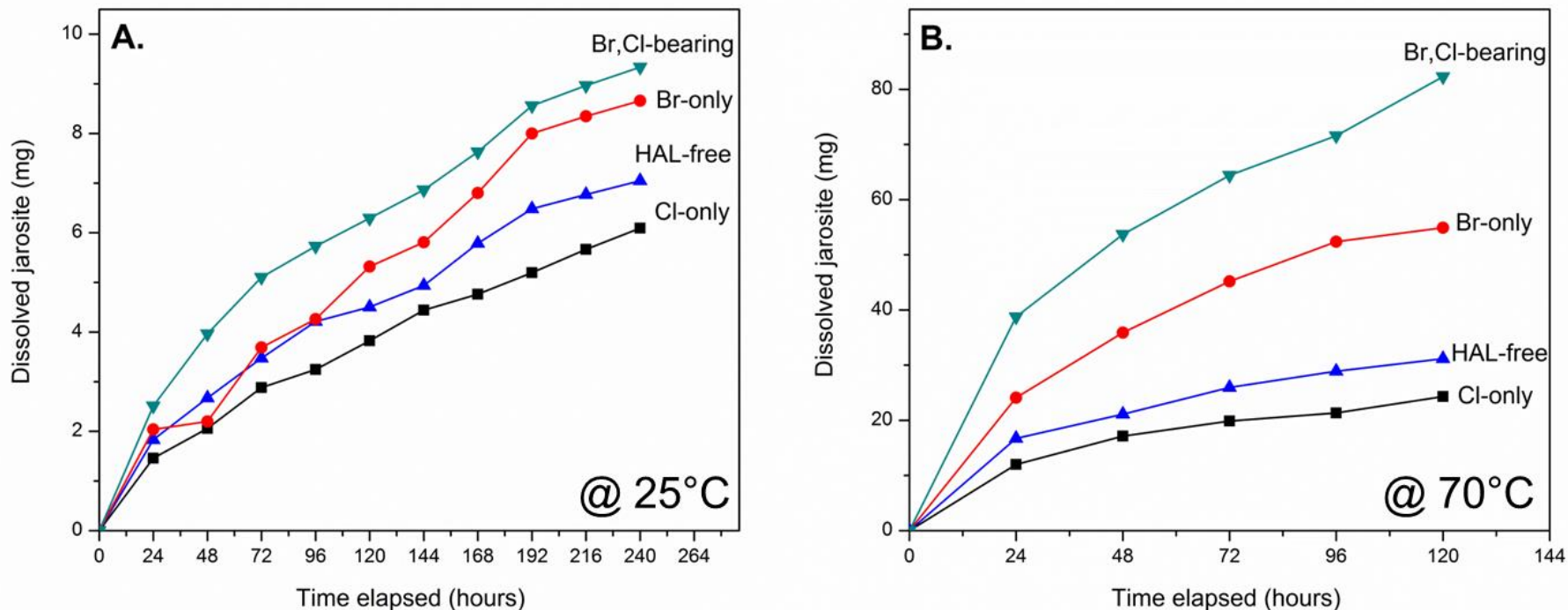
**Figure 1.4.** Aqueous alteration of halogen-bearing jarosite in ultrapure water at 25 °C and 70 °C. Regardless of temperature, the amount of jarosite dissolved increased according to the following sequence: Br,Cl-jarosite > Br-jarosite > HAL-free jarosite > Cl-jarosite. The difference was (A) at 25 ℃, the amount of dissolved jarosite was low and no obvious phase change was observed; (B) at 70 °C, the amount of dissolved jarosite was much higher than at 25 °C, and significant amounts of hematite were detected in the final mixture.

**Overview of Chapter 4:**

Based on detailed statistical examination of Cl, Br, and S distributions of Martian soil profiles at Gusev Crater and Meridiani Planum, it is suggested that photochemical processes could play an important role in controlling halogen behavior at the Martian surface (Karunatillake et al., 2013; see Appendix 3 for details). Accordingly, a series of photochemical related evaporation experiments of saline systems were conducted to investigate the influences on halogen geochemistry by UV radiation. Variables including brine compositions, pH, sediment grain size, atmospheric conditions, and length of UV irradiation were evaluated. Major results are summarized as follows:

1. Photo-oxidation (ultraviolet $\lambda = 254$ nm) of evaporative saline systems containing $Br^-$ and $Cl^-$ produced substantial amounts of oxy-chlorine species ($ClO_4^-$ and $ClO_3^-$), and in some cases, bromate ($BrO_3^-$), under current Earth or Mars atmospheric conditions. Production of $ClO_4^-$ and $ClO_3^-$ increased with prolonged UV irradiation (Figure 1.5).

2. Solid-gas heterogeneous reactions are likely more efficient at forming oxy-chlorine compared to solution-gas and gas-gas reactions. Inert sediment particles (e.g., quartz) facilitated the reactions, likely by providing effective interfaces, i.e., higher oxy-chlorine yields were observed on finer grain sediment particles.

3. Neutral to alkaline pHs facilitated preservation of $ClO_3^-$, and lower pH preferentially led to decomposition of $ClO_3^-$ and additional formation of $ClO_4^-$. This suggests that the nearly neutral environments at Gale Crater and the Phoenix landing site likely preserve $ClO_3^-$ along with $ClO_4^-$ in the analyzed samples.

4. Br was strongly influenced by photochemical processes. At high abundance, it appeared to compete with Cl for available oxidants, react with Cl radicals, form oxy-bromine

species, and thus could be cycled at the Martian surface (Figure 1.6). Sulfate behaved conservatively during photo-oxidation, that is, the sulfate variations were primarily controlled by precipitation of sulfate-containing minerals. Accordingly, the variation of Br/S and Cl/S ratios of these evaporating systems were mainly controlled by the variation of Br and Cl. These observations from the experiments are consistent with the statistical analyses of Cl and Br in Martian soil profiles (Karunatillake et al., 2013).

5. Supplementary experiments confirmed that without UV radiation, interaction of hydrogen peroxide ($H_2O_2$) with $Br^-$ and $Cl^-$ containing brines could not produce detectable oxy-chlorine species or fractionate $Br^-/Cl^-$ in the solution.
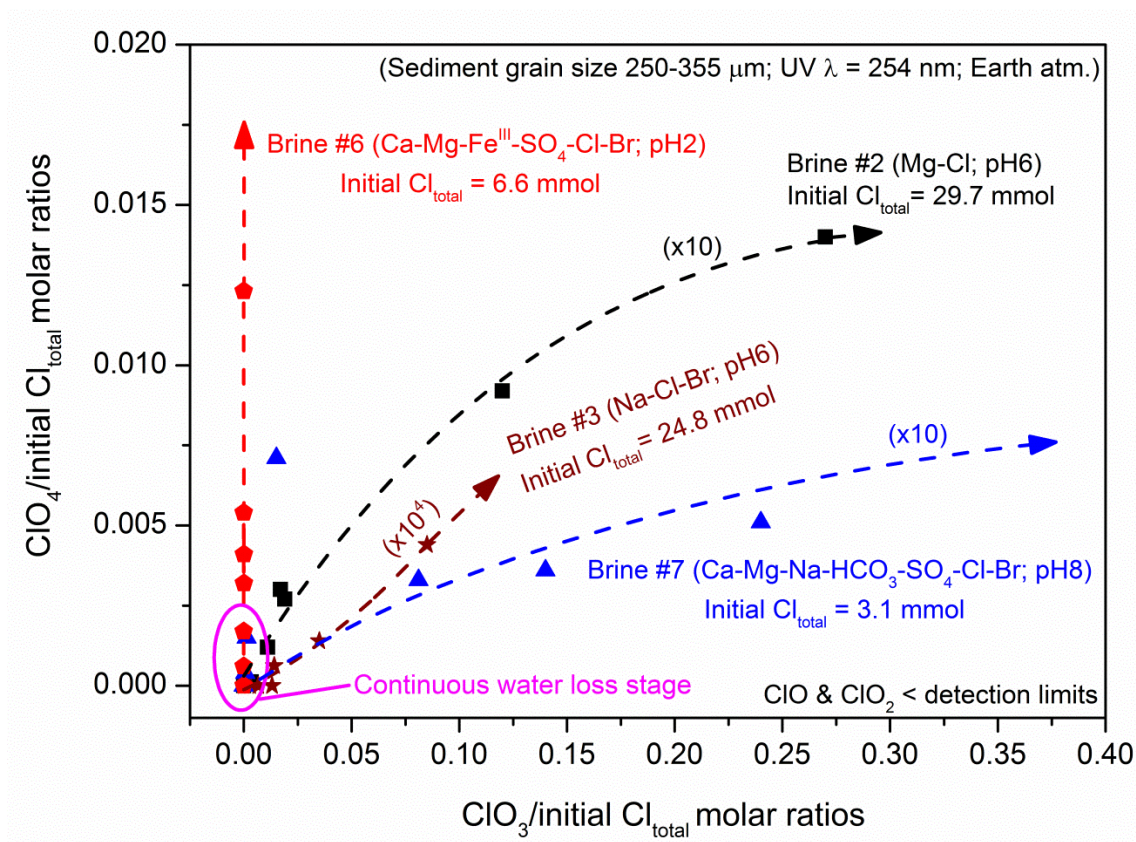
**Figure 1.5.** Molar ratios of $ClO_4^-/Cl_{total}$ versus $ClO_3^-/Cl_{total}$ in evaporating materials during extended time UV exposure experiments (UV time = 384 h) with Brines #2, #3, #6 and #7. Solid symbols represent samples collected every 48-72 h, and arrows show direction of increasing UV exposure time. In order to plot results on the same scale, perchlorate and chlorate concentrations were multiplied 10 times in Brines #2 (black) and #7 (blue), and $10^4$ times in Brine #3 (brown). Orders of magnitude lower yields of oxy-chlorine in Brine #3 was likely due to bromate production, which was $10^4$ times greater than levels of oxy-chlorine species. Samples within the pink oval formed under "wet" conditions (i.e., excess water lost via evaporation > 0.2 g). Orders of magnitude differences in oxy-chlorine yields between "wet" and "dry" conditions indicate that heterogeneous solid-gas reactions better facilitate oxy-chlorine production.
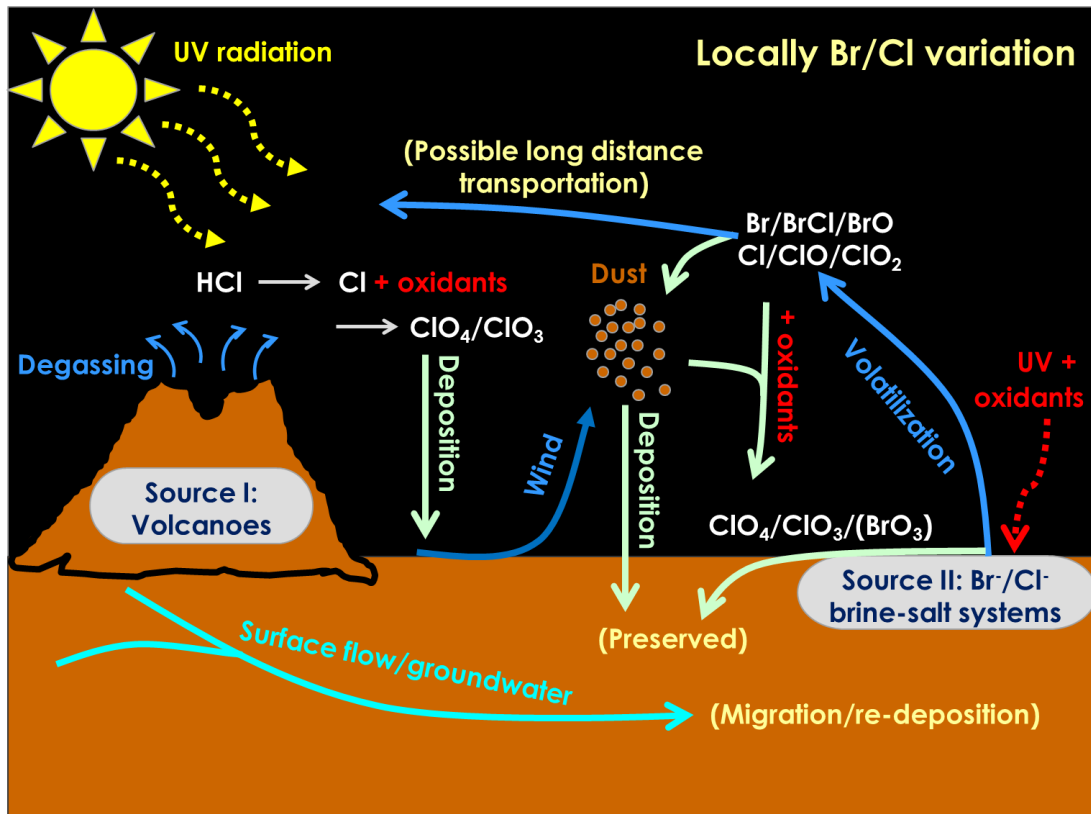
**Figure 1.6.** Model of photochemical controls on Br and Cl at the Martian surface. The two main sources of halogens on the Martian surface are: (1) volcanic degassing and (2) Br$^-$- and Cl$^-$-containing brine-salt systems. With UV radiation, Br$^-$ and Cl$^-$ can be photo-oxidized and mobilized, and follow three major transfer pathways: (1) direct transfer into the atmosphere (blue); (2) direct deposition from the atmosphere (light yellow), and (3) migration via aqueous activity (light green). Mobility of Br compared to Cl is greater than previously thought due to preferential volatilization into the atmosphere, and may result in local variations of Br/Cl ratios. Br variation and Br/Cl fractionation observed in this model are consistent with Br and Cl measurements in in-situ samples on the Martian surface.

# References

Banin, A, Clark, B.C., Wänke, H. (1992) Surface chemistry and mineralogy. *In: Mars* (eds by Kieffer, H. H. et al.). Univ. Arizona Press, Tucson, AZ, pp 594-625.

Bao, H. M. and Gu, B.H. (2004) Natural perchlorate has a unique oxygen isotope signature. *Environ. Sci. Technol.,* **38**, 5073-5077.

Barrón, V., Torrent, J., Greenwood, J. P. (2006) Transformation of jarosite to hematite in simulated Martian brines. *Earth Planet. Sci. Lett.,* **251**, 380-385.

Beavon, L. J., Lindsley, D. H., McLennan, S. M., Tosca, N. J. (2009) Experimental constraints on trace element mobility in Martian basalt: progress report. 40th Lunar Planet Sci. Conf., Abst. #1879, Lunar Planetary Institute, Houston, TX.

Bibring, J. P., Arvidson, R. E., Gendrin, A., Gondet, B., Langevin, Y., Le Mouelic, S., Mangold, N., Morris, R. V., Mustard, J. F., Poulet, F., Quantin, C., Sotin, C. (2007) Coupled ferric oxides and sulfates on the Martian surface. *Science,* **317**, 1206-1210.

Blake, D. F., Morris, R. V., Kocurek, G., Morrison, S. M., Downs, R. T., Bish, D., Ming, D. W., Edgett, K. S., Rubin, D., Goetz, W., Madsen, M. B., Sullivan, R., Gellert, R., Campbell, I., Treiman, A. H., McLennan, S. M., Yen, A. S., Grotzinger, J., Vaniman, D. T., Chipera, S. J., Achilles, C. N., Rampe, E. B., Sumner, D., Meslin, P. Y., Maurice, S., Forni, O., Gasnault, O., Fisk, M., Schmidt, M., Mahaffy, P., Leshin, L. A., Glavin, D., Steele, A., Freissinet, C., Navarro-Gonzalez, R., Yingst, R. A., Kah, L. C., Bridges, N., Lewis, K. W., Bristow, T. F., Farmer, J. D., Crisp, J. A., Stolper, E. M., Marais, D. J. D., Sarrazin, P. and Team, M. S. (2013) Curiosity at Gale Crater, Mars: Characterization and analysis of the Rocknest sand shadow. *Science*, **341 (6153)**, doi: 10.1126/science.1239505.

Boynton, W. V., Taylor, G. J., Evans, L. G., Reedy, R. C., Starr, R., Janes, D. M., Kerry, K. E., Drake, D. M., Kim, K. J., Williams, R. M. S., Crombie, M.K., Dohm, J. M., Baker, V., Metzger, A. E., Karunatillake, S., Keller, J. M., Newsom, H. E., Arnold, J. R., Bruckner, J., Englert, P. A. J., Gasnault, O., Sprague, A. L., Mitrofanov, I., Squyres, S. W., Trombka, J. I., d'Uston, L., Wanke, H., Hamara, D. K. (2007) Concentration of H, Si, Cl, K, Fe, and Th in the low- and mid-latitude regions of Mars. *J. Geophys. Res.***112**, E12S99, doi: 10.1029/2007JE002887.

Brückner, J., Dreibus, G., Gellert, R., Squyres, S., Wänke, H., Yen, A., Zipfel, J. (2008) Mars Exploration Rovers: chemical composition by the APXS. In *The Martian Surface: composition, mineralogy, and physical properties* (ed. J. F. Bell). Cambridge Univ. Press, Cambridge. pp. 58-101.

Brückner, J., G. Dreibus, R. Rieder, Wänke, H. (2003) Refined data of Alpha Proton X-ray Spectrometer analyses of soils and rocks at the Mars Pathfinder site: Implications for surface chemistry, *J. Geophys. Res.,* **108**, 8094, doi:10.1029/2003JE002060, E12.

Catling, D. C., Claire, M. W., Zahnle, K. J., Quinn, R. C., Clark, B. C., Hecht, M. H., Kounaves, S. (2010) Atmospheric origins of perchlorate on Mars and in the Atacama. *J. Geophys. Res.,* **115**, E00E11.

Clark, B. C., Baird, A. K., Weldon, R. J., Tsusaki, D. M., Schnabel, L., Candelaria, M. P. (1982) Chemical composition of Martian fines, *J. Geophys. Res.,* **87(B12)**, 10059-10067, doi:10.1029/JB087iB12p10059.

Clark, B. C. and van Hart, D. C. (1981) The salts of Mars, *Icarus*, **45(2)**, 370-378, doi:10.1016/0019-1035(81)90041-5.

Clark, B. C., Morris, R. V., McLennan, S. M., Gellert, R., Jolliff, B., Knoll, A. H., Squyres, S. W., Lowenstein, T. K., Ming, D. W., Tosca, N. J., Yen, A., Christensen, P. R., Gorevan, S., Bruckner, J., Calvin, W., Dreibus, G., Farrand, W., Klingelhoefer, G., Waenke, H., Zipfel, J., Bell, J. F., Grotzinger, J., McSween, H. Y., Rieder, R. (2005) Chemistry and mineralogy of outcrops at Meridiani Planum. *Earth Planet. Sci. Lett.,* **240**, 73-94.

Clark, B. E., Baird, A. K., Rose Jr., H. J., Toulmin III, P., Keil, K., Castro, A. J., Kelliher, W. C., Rowe, C. D., Evans, P. H. (1976) Inorganic analyses of Martian surface samples at the Viking landing sites, *Science*, **194**, 1283-1288, doi:10.1126/science.194.4271.1283.

Dreibus, G. and Wänke, H. (1987) Volatiles on Earth and Mars - a comparison. *Icarus,* **71**, 225-240.

Edmunds, W. M. (1996) Bromine geochemistry of British groundwaters. *Mineral. Mag.,* **60**, 275-284.

Enami, S., Vecitis, C. D., Cheng, J., Hoffmann, M. R., Colussi, A. J. (2007) Global inorganic source of atmospheric bromine, *J. Phys. Chem. (A),* **111 (36)**, 8749-8752.

Eskandarpour, A., Onyango, M. S., Ochieng, A., Asai, S. (2008) Removal of fluoride ions from aqueous solution at low pH using schwertmannite, *J. Hazard. Mater.,* **152(2)**, 571-579, doi: 10.1016/j.jhazmat.2007.07.020.

Finlayson-Pitts, B. J. (2010) Halogens in the Troposphere. *Anal. Chem.,* **82 (3)**, 770-776, doi: 10.1021/ac901478p.

Foley, C. N., T. Economou, and Clayton, R. N. (2003) Final chemical results from the Mars Pathfinder alpha proton X-ray spectrometer, *J. Geophys. Res.,* **108(E12)**, 8096, doi:10.1029/2002JE002019.

Gellert, R., Rieder, R., Anderson, R. C., Brückner, J., Clark, B. C., Dreibus, G., Economou, T., Klingelhöfer, G., Lugmair, G. W., Ming, D. W., Squyres, S. W., d'Uston, C., Wänke, H., Yen, A., Zipfel, J. (2004) Chemistry of rocks and soils in Gusev crater from the alpha particle x-ray spectrometer. *Science,* **305**, 829-832.

Golden, D. C., Ming, D. W., Morris, R. V., Graff, T. G. (2008) Hydrothermal synthesis of hematite spherules and jarosite: Implications for diagenesis and hematite spherule formation in sulfate outcrops at Meridiani Planum, Mars. *Am. Mineral.,* **93**, 1201-1214.

Greenwood, J. P. and Blake, R. E. (2006) Evidence for an acidic ocean on Mars from phosphorus geochemistry of Martian soils and rocks, *Geology,* **34(11)**, 953-956, doi: 10.1130/G22415a.1.

Grotzinger, J. P., Arvidson, R. E., Bell, J. F., Calvin, W., Clark, B. C., Fike, D. A., Golombek, M., Greeley, R., Haldemann, A., Herkenhoff, K. E., Jolliff, B. L., Knoll, A. H., Malin, M., McLennan, S. M., Parker, T., Soderblom, L., Sohl-Dickstein, J. N., Squyres, S. W., Tosca, N. J., Watters, W. A. (2005) Stratigraphy and sedimentology of a dry to wet eolian depositional system, Burns formation, Meridiani Planum, Mars. *Earth Planet. Sci. Lett.,* **240**, 11-72.

Hahn, B. C., McLennan, S. M., Tosca, N. J., Reeder, R. J. (2009) Trace element behavior in Martian evaporite minerals: experimental constraints. *40th Lunar Planet Sci. Conf.,* Abst. #1194, Lunar Planetary Institute, Houston, TX.

Hecht, M. H., Kounaves, S. P., Quinn, R. C., West, S. J., Young, S. M. M., Ming, D. W., Catling, D. C., Clark, B. C., Boynton, W. V., Hoffman, J., DeFlores, L. P., Gospodinova, K., Kapit, J., Smith, P. H. (2009) Detection of perchlorate and the soluble chemistry of Martian soil at the Phoenix lander site. *Science,* **325 (5936)**, 64-67, doi: 10.1126/science.1172466.

Hönninger, G., Bobrowski, N., Palenque, E.R., Torrez, R. and Platt, U. (2004) Reactive bromine and sulfur emissions at Salar de Uyuni, Bolivia. *Geophys. Res. Lett.,* 31, L04101, doi: 10.1029/2003GL018818.

Jackson, W. A., Böhlke, J. K., Gu, B. H., Hatzinger, P. B. and Sturchio, N. C. (2010) Isotopic composition and origin of indigenous natural perchlorate and co-occurring nitrate in the southwestern United States. *Environ. Sci. Technol.,* **44**, 4869-4876.

Kaleschke, L., Richter, A., Burrows, J., Afe, O., Heygster, G., Notholt, J., Rankin, A. M., Roscoe, H. K., Hollwedel, J., Wagner, T. and Jacobi, H. W. (2004) Frost flowers on sea ice as a

source of sea salt and their influence on tropospheric halogen chemistry. *Geophys. Res. Lett.,* **31**, L16114, doi: 10.1029/2004GL020655.

Karunatillake, S., Zhao, Y. Y. S., McLennan, S. M., Skok, J. R. and Button, N. E. (2013) Does Martian soil release reactive halogens to the atmosphere? *Icarus,* **226 (2)**, 1438-1446, http://dx.doi.org/10.1016/j.icarus.2013.07.018.

Keller, J. M., Boynton, W. V., Karunatillake, S., Baker, V. R., Dohm, J. M., Evans, L. G., Finch, M. J., Hahn, B. C., Hamara, D. K., Janes, D. M., Kerry, K. E., Newsom, H. E., Reedy, R. C., Sprague, A. L., Squyres, S. W., Starr, R. D., Taylor, G. J., Williams, R. M. S. (2006) Equatorial and midlatitude distribution of chlorine measured by Mars Odyssey GRS. *J. Geophys. Res.,* **111,** E03S08, doi: 10.1029/2006JE002679.

Knauth, L. P., Burt, D. M. and Wohletz, K. H. (2005) Impact origin of sediments at the Opportunity landing site on Mars. *Nature,* **438**, 1123-1128.

Kounaves, S. P., Carrier, B. L., O'Neil, G. D., Stroble, S. T. and Claire, M. W. (2014) Evidence of martian perchlorate, chlorate, and nitrate in Mars meteorite EETA79001: Implications for oxidants and organics. *Icarus*, **229**, 206-213.

Kounaves, S. P., Hecht, M. H., Kapit, J., Gospodinova, K., DeFlores, L., Quinn, R. C., Boynton, W. V., Clark, B. C., Catling, D. C., Hredzak, P., Ming, D. W., Moore, Q., Shusterman, J., Stroble, S., West, S.J. and Young, S. M. M. (2010) Wet Chemistry experiments on the 2007 Phoenix Mars Scout Lander mission: Data analysis and results. *J. Geophys. Res.,* **115**, E00E10, doi: 10.1029/2009JE003424.

Lary D. J. (2005) Halogens and the chemistry of the free troposphere. *Atmos. Chem. Phys.,* **5**, 227-237, doi: 10.5194/acp-5-227-2005.

Leshin, L. A., Mahaffy, P. R., Webster, C. R., Cabane, M., Coll, P., Conrad, P. G., Archer, P. D., Atreya, S. K., Brunner, A. E., Buch, A., Eigenbrode, J. L., Flesch, G. J., Franz, H. B., Freissinet, C., Glavin, D. P., McAdam, A. C., Miller, K. E., Ming, D. W., Morris, R. V., Navarro-Gonzalez, R., Niles, P. B., Owen, T., Pepin, R. O., Squyres, S., Steele, A., Stern, J. C., Summons, R. E., Sumner, D. Y., Sutter, B., Szopa, C., Teinturier, S., Trainer, M. G., Wray, J. J., Grotzinger, J. P., Team, M. S. (2013) Volatile, isotope, and organic analysis of Martian fines with the Mars Curiosity rover. *Science,* **341 (6153)**, doi: 10.1126/science.1238937.

McLennan, S. M., Bell, J. F., Calvin, W. M., Christensen, P. R., Clark, B. C., de Souza, P. A., Farmer, J., Farrand, W. H., Fike, D. A., Gellert, R., Ghosh, A., Glotch, T. D., Grotzinger, J. P., Hahn, B., Herkenhoff, K. E., Hurowitz, J. A., Johnson, J. R., Johnson, S. S., Jolliff, B., Klingelhofer, G., Knoll, A. H., Learner, Z., Malin, M. C., McSween, H. Y., Pocock, J., Ruff, S. W., Soderblom, L. A., Squyres, S. W., Tosca, N. J., Watters, W. A., Wyatt, M. B., Yen, A. (2005) Provenance and diagenesis of the evaporite-

bearing Burns formation, Meridiani Planum, Mars. *Earth Planet. Sci. Lett.,* **240(1)**, 95-121.

McLennan, S.M., Anderson, R.B., Bell, J.F., Bridges, J.C., Calef, F., Campbell, J.L., Clark, B.C., Clegg, S., Conrad, P., Cousin, A., Des Marais, D.J., Dromart, G., Dyar, M.D., Edgar, L.A., Ehlmann, B.L., Fabre, C., Forni, O., Gasnault, O., Gellert, R., Gordon, S., Grant, J.A., Grotzinger, J.P., Gupta, S., Herkenhoff, K.E., Hurowitz, J.A., King, P.L., Le Mouelic, S., Leshin, L.A., Leveille, R., Lewis, K.W., Mangold, N., Maurice, S., Ming, D.W., Morris, R.V., Nachon, M., Newsom, H.E., Ollila, A.M., Perrett, G.M., Rice, M.S., Schmidt, M.E., Schwenzer, S.P., Stack, K., Stolper, E.M., Sumner, D.Y., Treiman, A.H., VanBommel, S., Vaniman, D.T., Vasavada, A., Wiens, R.C., Yingst, R.A. and Team, M.S. (2014) Elemental Geochemistry of Sedimentary Rocks at Yellowknife Bay, Gale Crater, Mars. *Science*, 343(6169), doi: 10.1126/science.1244734.

Ming, D. W., Archer, P. D., Glavin, D. P., Eigenbrode, J. L., Franz, H. B., Sutter, B., Brunner, A. E., Stern, J. C., Freissinet, C., McAdam, A. C., Mahaffy, P. R., Cabane, M., Coll, P., Campbell, J. L., Atreya, S. K., Niles, P. B., Bell, J. F., Bish, D. L., Brinckerhoff, W. B., Buch, A., Conrad, P. G., Des Marais, D. J., Ehlmann, B. L., Fairen, A. G., Farley, K., Flesch, G. J., Francois, P., Gellert, R., Grant, J. A., Grotzinger, J. P., Gupta, S., Herkenhoff, K. E., Hurowitz, J. A., Leshin, L. A., Lewis, K. W., McLennan, S. M., Miller, K. E., Moersch, J., Morris, R. V., Navarro-Gonzalez, R., Pavlov, A. A., Perrett, G. M., Pradler, I., Squyres, S. W., Summons, R. E., Steele, A., Stolper, E. M., Sumner, D. Y., Szopa, C., Teinturier, S., Trainer, M. G., Treiman, A. H., Vaniman, D. T., Vasavada, A. R., Webster, C. R., Wray, J. J., Yingst, R. A., Team, M. S. (2014) Volatile and organic compositions of sedimentary rocks in Yellowknife Bay, Gale Crater, Mars. *Science,* **343(6169)**, doi: 10.1126/science.1245267.

Morris, R. V., Klingelhöfer, G., Schröder, C., Rodionov, D. S., Yen, A., Ming, D. W., de Souza, P. A., Wdowiak, T., Fleischer, I., Gellert, R., Bernhardt, B., Bonnes, U., Cohen, B. A., Evlanov, E. N., Foh, J., Gütlich, P., Kankeleit, E., McCoy, T., Mittlefehldt, D. W., Renz, F., Schmidt, M. E., Zubkov, B., Squyres, S. W., Arvidson, R. E. (2006) Mössbauer mineralogy of rock, soil, and dust at Meridiani Planum, Mars: Opportunity's journey across sulfate-rich outcrop, basaltic sand and dust, and hematite lag deposits, *J. Geophys. Res.,* **111, E12S15**, doi: 10.1029/2006je002791.

Palme, H. and Jones, A. (2003) Solar system abundances of the elements. In *Treatise on Geochemistry* (eds. H. D. Holland and K. K. Turekian), Elsevier, vol. **1**, Section 1.03, Table 3, pp. 49.

Rao, M. N., Nyquist, L. E., Sutton, S. R., Dreibus, G., Garrison, D. H., Herrin, J. (2009) Fluid-evaporation records preserved in salt assemblages in Meridiani rocks. *Earth Planet. Sci. Lett.,* **286 (3-4)**, 396-403.

Rao, M. N., Sutton, S. R., McKay, D. S., Dreibus, G. (2005) Clues to Martian brines based on halogens in salts from nakhlites and MER samples. *J Geophys. Res.,* **110**, E12S06, doi: 10.1029/2005JE002470.

Rieder, R., Gellert, R., Anderson, R. C., Bruckner, J., Clark, B. C., Dreibus, G., Economou, T., Klingelhoffer, G., Lugmair, G. W., Ming, D. W., Squyres, S. W., d'Uston, C., Wanke, H., Yen, A., Zipfel, J. (2004) Chemistry of rocks and soils at Meridiani Planum from the alpha particle X-ray spectrometer. *Science*, **306**, 1746-1749.

Risacher, F., Fritz, B. and Alonso, H. (2006) Non-conservative behavior of bromide in surface waters and brines of Central Andes: A release into the atmosphere? *Geochim. Cosmochim. Acta,* **70**, 2143-2152.

Sander, R., Keene, W.C., Pszenny, A.A.P., Arimoto, R., Ayers, G.P., Baboukas, E., Cainey, J.M., Crutzen, P.J., Duce, R.A., Hönninger, G., Huebert, B.J., Maenhaut, W., Mihalopoulos, N., Turekian, V.C. and Van Dingenen, R. (2003) Inorganic bromine in the marine boundary layer: a critical review. *Atmos. Chem. Phys.,* **3**, 1301-1336.

Schröder, C., Rodionov, D. S., McCoy, T. J., Jolliff, B. L., Gellert, R., Nittler, L. R., Farrand, W. H., Johnson, J. R., Ruff, S. W., Ashley, J. W., Mittlefehldt, D. W., Herkenhoff, K. E., Fleisher, I., Haldemann, A. F., Klingelhöfer, G., Ming, D. W., Morris, R. V., de Souza, P.A., Squyres, S. W., Weitz, C., Yen, A., Zipfel, J., Economou, T. (2008) Meteorites on Mars observed with the Mars Exploration rovers. *J. Geophys. Res.,* **113**, E06S22, doi: 10.1029/2007JE002990.

Sefton-Nash, E. and Catling, D. C. (2008) Hematitic concretions at Meridiani Planum, Mars: Their growth timescale and possible relationship with iron sulfates, *Earth Planet. Sci. Lett.,* **269**, 365-375.

Seimann, M. G. and Schramm, M. (2002) Henry's and non-Henry's law behavior of Br in simple marine systems. *Geochim. Cosmochim. Acta,* **66**, 1387-1399.

Smith, M. L., Claire, M. W., Catling, D. C., Zahnle, K. J. (2014) The formation of sulfate, nitrate and perchlorate salts in the martian atmosphere. *Icarus,* **231**, 51-64.

Squyres, S. W., Knoll, A. H., Arvidson, R. E., Ashley, J. W., Bell, J. F., Calvin, W. M., Christensen, P. R., Clark, B. C., Cohen, B. A., de Souza, P. A., Edgar, L., Farrand, W. H., Fleischer, I., Gellert, R., Golombek, M. P., Grant, J., Grotzinger, J., Hayes, A., Herkenhoff, K. E., Johnson, J. R., Jolliff, B., Klingelhöfer, G., Knudson, A., Li, R., Mccoy, T. J., McLennan, S. M., Ming, D. W., Mittlefehldt, D. W., Morris, R. V., Rice, J. W., Schroder, C., Sullivan, R. J., Yen, A., Yingst, R. A. (2009) Exploration of Victoria Crater by the Mars Rover Opportunity. *Science,* **324**, 1058-1061.

Taylor S. R. and McLennan S. M. (2009) *Planetary Crusts: Their Composition, Origin, and Evolution*. Cambridge Uni. Press, Cambridge. pp. 404.

Tosca, N. J. and McLennan, S. M. (2009) Experimental constraints on the evaporation of partially oxidized acid-sulfate waters at the martian surface. *Geochim. Cosmochim. Acta*, **73**, 1205-1222.

Tosca, N. J., McLennan, S. M., Dyar, M. D., Sklute, E. C., Michel, F. M. (2008) Fe oxidation processes at Meridiani Planum and implications for secondary Fe mineralogy on Mars. *J. Geophys. Res.,* **113**, E05005.

Wänke, H. and Dreibus, G. (1994) Chemistry and accretion history of Mars. *Philos. T. Roy. Soc. (A),* **349**, 285-293.

Wänke, H., J. Brückner, G. Dreibus, R. Rieder, Ryabchikov, I. (2001) Chemical composition of rocks and soils at the Pathfinder site, *Space Sci. Rev.,* **96**, 317-330, doi: 10.1023/A:1011961725645.

Wood, W. W. and Sanford, W. E. (2007) Atmospheric bromine flux from the coastal Abu Dhabi sabkhat: A ground-water mass-balance investigation. *Geophys. Res. Lett.,* **34**, L14405, doi: 10.1029/2007GL029922.

Worden, R. H. (1996) Controls on halogen concentrations in sedimentary formation waters. *Mineral. Mag.,* **60**, 259-274.

Yang, X., Pyle, J. A. and Cox, R. A. (2008) Sea salt aerosol production and bromine release: Role of snow on sea ice. *Geophys. Res. Lett.,* **35**, L16815, doi: 10.1029/2008GL034536.

Yen, A. S., Mittlefehldt, D. W., McLennan, S. M., Gellert, R., Bell, J. F., McSween, H. Y., Ming, D. W., McCoy, T. J., Morris, R. V., Golombek, M., Economou, T., Madsen, M. B., Wdowiak, T., Clark, B. C., Jolliff, B. L., Schroder, C., Brückner, J., Zipfel, J., Squyres, S. W. (2006) Nickel on Mars: Constraints on meteoritic material at the surface. *J. Geophys. Res.,* **111**, E12S11, doi: 10.1029/2006JE002797.

Zhao, Y. -Y. S. and McLennan, S. M. (2013) Behavior of Ni, Zn and Cr during low temperature aqueous Fe oxidation processes on Mars. *Geochim. Cosmochim. Acta,* **109**, 365-383.

Zhao, Y. -Y. S., McLennan, S. M., Schoonen, M. A. A. (2014) Behavior of bromide, chloride, and phosphate during low-temperature aqueous Fe(II) oxidation processes on Mars, *J. Geophys. Res.,* **119**, doi: 10.1002/2013JE004417.

Zolotov, M. Y. and Shock, E. L. (2005) Formation of jarosite-bearing deposits through aqueous oxidation of pyrite at Meridiani Planum, Mars. *Geophys. Res. Lett.,* **32**, L21203, doi: 10.1029/2005GL024253.

# Chapter 2: Behavior of Ni, Zn and Cr during Low Temperature Aqueous Fe(II) Oxidation Processes on Mars

**Abstract**

The behavior of Ni(II), Zn(II) and Cr(III) during the melanterite ($FeSO_4 \cdot 7H_2O$) to hematite ($\alpha\text{-}Fe_2O_3$) oxidative transformations involving evolution pathways via jarosite (($H_3O,K$)$Fe_3(OH)_6(SO_4)_2$), schwertmannite ($Fe_8O_8(OH)_6(SO_4)$) and goethite ($\alpha\text{-}FeOOH$) were investigated in an acidic saturated $MgSO_4$ matrix. Results provide important clues about how elevated levels of trace elements are incorporated into the secondary Fe mineralogy assemblages found on Mars and the mechanism for formation of hematitic concretions at Meridiani Planum on Mars. Our results demonstrate that starting at the same concentrations in the initial solution, final amounts of Ni, Zn and Cr in hematite via different pathways are very different. In Path 1 (melanterite → jarosite → hematite), partitioning of Ni, Zn and Cr into jarosite and hematite (formed through dissolution of jarosite) is most likely in the order: Cr > Zn > Ni. In Path 2 (melanterite → schwertmannite → goethite → hematite), schwertmannite and goethite exhibited strong affinities for divalent Ni and Zn. During such a pathway, Ni should accumulate more than

Zn by at least a factor of two, and partitioning of Ni, Zn and Cr to the hematite is most likely in the order: Cr > Ni > Zn. Therefore, our results suggest that the high Ni and moderate Zn distribution pattern observed in Meridiani hematitic spherule-bearing samples can be explained best by the schwertmannite-goethite to hematite pathway (Path 2), without need for an additional high Ni source in this region. Although the lack of goethite at Meridiani renders it uncertain if goethite ever served as a precursor to facilitate hematite formation, dehydration of nano-crystalline goethite is thermodynamically favored and cannot be ruled out. On the other hand, if hematitic concretions were formed by dissolution of jarosite (Path 1), then much higher initial Ni/Zn ratios than 1 in initial diagenetic fluids may be necessary to explain the elevated levels of Ni in the spherules. The Cr(III), when starting in equal amounts as Ni and Zn in the solution, accumulated at least two orders of magnitude more than Ni and Zn in all Fe(III)-phases. Given that Cr concentrations are of the same order of magnitude as Ni and Zn in most rocks and soils measured by the rover Opportunity, Cr concentrations should be much lower than Ni and Zn in the initial diagenetic fluids. Mobility of Cr was greatly limited by precipitation of Fe(III)-phases, due to substitution for Fe(III) and sequestration in the solids.

## 2.1 Introduction

The Alpha-Particle X-ray Spectrometers (APXS) onboard the Mars Exploration Rovers (MER) Spirit and Opportunity have obtained elemental abundances of more than 350 in situ soil and rock samples in at least five distinct geological settings (Meridiani Planum, Endeavour Crater, Gusev Plains, Columbia Hills and Inner Basin) (e.g., Gellert et al., 2004; Rieder et al., 2004; Clark et al., 2005). Besides major elements, a selection of trace element (TE) concentrations, including those for Ni, Zn and Cr, are also available (as well as Br and in a few

cases, Ge), which can be used as powerful tracers in understanding Martian sedimentary processes. However, our understanding of the behavior of these trace elements in fluids derived from the aqueous alteration of basalt and during other aqueous processes is very poor which unavoidably hinders our interpretation of these data to better constrain the surficial processes on Mars.

Of all settings examined by the MER rovers, Meridiani Planum is distinct in its well-established sedimentological and stratigraphic context and so far is the only site where hematitic spherules have been directly observed on Mars (Grotzinger et al., 2005; McLennan et al., 2005; Squyres et al., 2009). The presence of jarosite and hematite in the outcrop (Klingelhöfer et al., 2004), mm-scale diagenetic secondary porosity in the form of elongated vugs and crystal molds presumably of a highly soluble mineral (McLennan et al., 2005), as well as widespread hematitic concretions all suggest that these Late Noachian to Early Hesperian layered outcrops experienced multiple stages of diagenesis resulting from episodes of groundwater interaction (Grotzinger et al., 2005; McLennan et al., 2005; Sefton-Nash and Catling, 2008). Perhaps similar to Meridiani Planum, closely associated Fe oxides (e.g., hematite) and sulfates (e.g., polyhydrates sulfates) have also been detected remotely at several locations across the Martian surface, including regions of Valles Marineris and Magaritifer Terra (Bibring et al., 2007). This suggests a possible broader genetic relationship between these two associated mineral occurrences, and perhaps that acidic sulfate aqueous conditions found at Meridiani were indeed widespread for at least certain times during Mars geological history. In addition, since approximately 90% of the total Fe resides as Fe(III) in the outcrop of Meridiani (Klingelhöfer et al., 2004), the conditions of evaporation and/or diagenesis were oxidizing, although the nature of the oxidant is as yet

unclear. Therefore, Fe oxidation processes are likely to be very important in the development of ferric sulfates (i.e., jarosite) and oxides (i.e., hematite).

To date, several models have been proposed to explain the mineral assemblages in the Meridiani outcrops, particularly for crystalline hematite and hematitic spherules (e.g., Barrón et al., 2006; Golden et al., 2008; Tosca et al., 2008). Morris et al. (2005) and Golden et al. (2008) proposed a formation mechanism for jarosite and hematite spherules by gradual hydrolysis of Fe(III) under hydrothermal condition (e.g., 150 °C), based on field observations from the Mauna Kea in Hawaii and laboratory simulations. However, unlike Gusev Crater, the lack of diverse alteration minerals at Meridiani does not support the hypothesis of widespread hydrothermal fluid activity in this area. Alternatively, Barrón et al. (2006) proposed that hematite can be formed by dissolution of jarosite in Martian brines under acidic conditions at low temperature. In a second model, Tosca et al. (2008) suggested that dissolution of highly soluble Fe(II) sulfate minerals (e.g., melanterite ($FeSO_4 \cdot 7H_2O$)) followed by sequential oxidation to ferric oxides, which in turn may be responsible for the secondary porosity present in the outcrops. Calculations for an Fe(III) source of the hematite concretions based on diffusion models (Sefton-Nash and Catling, 2008) suggested that acid dissolution of jarosite was plausibly the dominant contributor to Fe(III) in the hematitic concretions, and melanterite oxidation could also have been an important iron source. Speciation calculations for formation of a jarosite-goethite-gypsum assemblage at Meridiani (Zolotov and Shock, 2005) argued that such an assemblage can be obtained through aqueous oxidation of pyrite, which was originally deposited by sulfide-rich hydrothermal waters in this region. Transformation of goethite to hematite can be facilitated by regional heating, although there is no known evidence for such an event. Hurowitz et al. (2010) demonstrated that reduced subsurface waters of near-neutral pH and rich in Fe(II) can be rapidly

acidified once exposed to oxidants at the Martian surface. Oxidation of Fe(II) and the precipitation of oxidized Fe(III) minerals were the critical driver of acidification at Meridiani Planum surface water and potentially elsewhere on the late Noachian surface of Mars.

Since Fe is one of the most important components at Meridiani, plots of Ni, Zn and Cr against FeO (as total Fe) of undisturbed soil and RAT-abraded outcrop samples reveal a number of interesting features (Figure 2.1): (1) Meridiani outcrop material is enriched in Ni and Zn but less so in Cr compared to basaltic shergottites and basaltic soil samples examined in situ by the Spirit rover; (2) Ni concentrations in hematitic spherules are high and its enrichment is strongly correlated to Fe in hematite-rich soil samples, but less so for Zn; (3) Cr concentrations, though elevated in soils compared to outcrop rocks with similar FeO concentration, are lower in hematitic-rich soils than basaltic soils.

Of these three elements, Ni is the most intriguing at Meridiani. Due to its high concentration (average ~650 ppm) in outcrops and spherule-rich soils, it is significantly higher than can be reproduced by physically mixing any known materials from Mars (Yen et al., 2006). The origin of elevated Ni remains an open question. Whether it originated from a high-Ni magma thus representing a provenance signature, or is enriched by surficial processes such as evaporation and/or diagenesis, or both are still unclear. In addition, direct detection of Fe-Ni meteorites, such as "Meridiani Planum" (also informally named "Heatshield"), on the surface of Meridiani Planum (Schröder et al., 2008) suggests a possibility of exogenic meteoritic components contributing to elevated Ni in this area. Contribution of Ni from meteoritic sources has been discussed by McLennan et al. (2005) for Meridiani sediments and Yen et al. (2006) for Gusev/Meridiani soils, and each constrained the contribution to be less than 6% and 1-3% respectively. Nevertheless, the trend of increasing Ni correlating to increasing Fe and hematite

34

establishes the possibility that Ni may be mobile and be enriched through groundwater-related mechanisms that do not necessarily involve the simple addition of meteoritic material.

In this study, we report on a series of experiments to investigate trace element behaviors and controlling factors during Fe-oxidation processes, which in turn may directly account for some of the jarosite and hematite formation on Mars (Tosca et al., 2008). We investigated three pathways of precipitate evolution by oxidation of ferrous sulfate (melanterite) to Fe-oxide (hematite), with Ni(II), Zn(II) and Cr(III) added:

Path 1 – Melanterite → Jarosite → Hematite;

Path 2 – Melanterite → Schwertmannite → Goethite → Hematite;

Path 3 – Melanterite → Schwertmannite → Goethite plus Jarosite → Hematite.

The experimental approaches were designed to simulate groundwater recharge diagenesis events after evaporite deposition or infiltration of water into sediments under conditions of high ionic strength. Trace element distribution patterns during different pathways were evaluated, which provide important clues about the mechanism for hematite concretion formation and how elevated levels of trace elements are incorporated into secondary Fe mineralogy assemblages.

Since characteristics of such concretion forming diagenetic solutions are largely unconstrained, in designing our experiments we chose to study each element individually to avoid various complications such as mixing ratios and competing TE controls on precipitated mineral morphologies, with an understanding that this approach may be less representative of the natural conditions. Future studies of more complex systems are certainly warranted. For initial trace element concentrations in our aqueous solutions, we used a range of 300-500 µg/g. Several factors were taken into account in selecting these initial trace element concentrations. Hematite-rich soils analyzed by Opportunity's APXS showed that Ni, Zn and Cr range from 600-1300
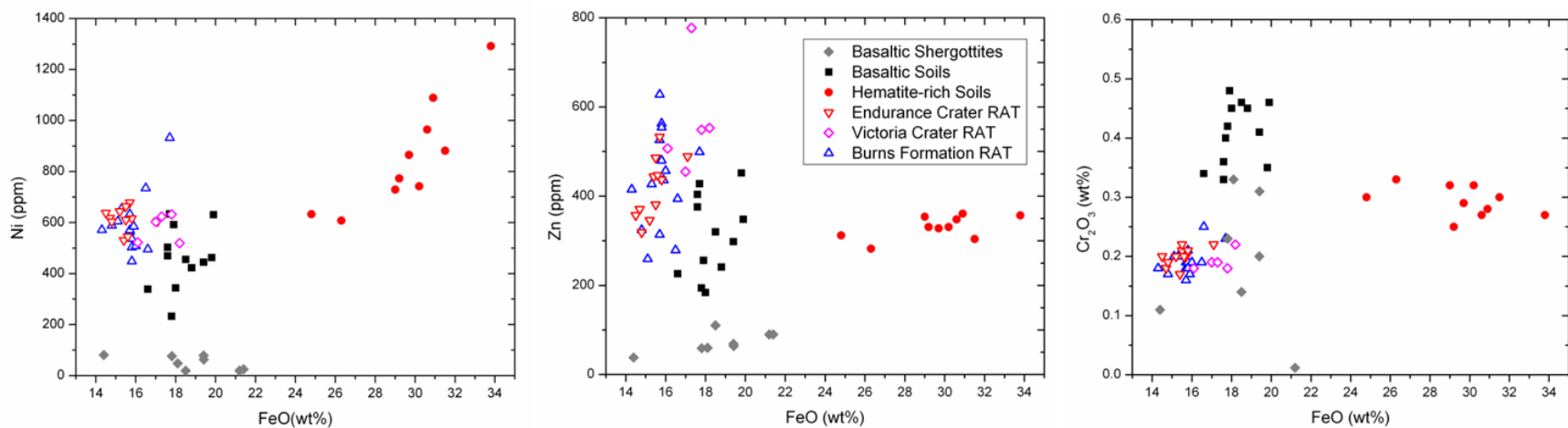
35

**Figure 2.1.** Plots of Ni, Zn and $Cr_2O_3$ versus FeO (as total Fe) for Meridiani undisturbed soils, RAT-abraded outcrop rocks, and basaltic shergottites. Data groups are the same as Table 2.1. Note that Ni and Zn are very high in soils and outcrop compared to basaltic rocks but that Cr has broadly overlapping abundances. Ni correlates with Fe in hematite rich soils.

μg/g, 300-360 μg/g and 840-1150 μg/g, respectively (Table 2.1), and the Martian crust has similar levels of Ni and Zn (337 μg/g and 320 μg/g) although much higher levels of Cr at 2600 μg/g (Taylor and McLennan, 2009).

Although there is no reason that aqueous solutions would have the same concentrations as solids, such levels are commonly found in many terrestrial acidic mine drainage systems (e.g., Acero et al., 2006), which are acidic, sulfate rich and low temperature environments similar to our target systems. Finally, we selected concentrations that were sufficient to be analytically detected in all of our experimental procedures.

## 2.2 Experimental Methods

### 2.2.1 Precipitation of schwertmannite, goethite and jarosite via Fe(II)-oxidation experiments

Detailed experimental and analytical methods were similar to those described by Tosca et al. (2008), but with $Ni^{2+}$, $Zn^{2+}$ and $Cr^{3+}$ added respectively as $NiSO_4 \cdot 6H_2O$, $ZnSO_4 \cdot 7H_2O$ and $Cr(NO_3)_3 \cdot 7H_2O$. A.C.S. reagents were used in this study. In each experiment, 500 mL of 1.6 M $MgSO_4$ solution (made with $MgSO_4 \cdot 7H_2O$) was placed in Pyrex beakers as a high ionic strength matrix. Two sets of melanterite loadings (added as $FeSO_4 \cdot 7H_2O$) were then added to the beakers at 10 and 200 g/L (equivalent to adding 5 g and 100 g of melanterite to the 500 mL of matrix solution respectively), termed low Fe and high Fe oxidation experiments, respectively. In the low Fe oxidation experiments, Ni and Zn were at initial levels of 500 μg/g and Cr at initial levels of 300 μg/g in the solution. In the high Fe loading experiments, all three elements were set at same initial levels of 400 μg/g in the solution. To facilitate precipitation of pure jarosite rather than goethite/jarosite mixtures in the high Fe oxidation experiment, 1-2 g of KCl solid was also added into the starting solution.

**Table 2.1.** Averages, standard deviations, and approximate ranges of Ni, Zn and Cr abundances from undisturbed soil and RATed rock targets detected by APXS onboard on Opportunity rover at Meridiani Planum (Brückner et al., 2008). For comparison, the compositions of basaltic shergottites are also listed.

| Group/Samples | Ni (µg/g) | Zn (µg/g) | Cr (µg/g) | Notes |
|---|---|---|---|---|
| | Avg. ± Std. Dev (Approx. range) | Avg. ± Std. Dev (Approx. range) | Avg. Std. Dev (Approx. range) | |
| Basaltic Shergottites (n=8) (including "BounceRock") | 52 ± 27 (40-80) | 72 ± 23 (40-110) | 577 ± 415 (40-1230) | Indigenous to Mars; unlikely to contain additional meteoritic material |
| Basaltic Soils[a] (n=12) | 461± 66 (230-630) | 310 ± 26 (180- 450) | 1400 ± 149 (1100-1600) | Soil samples are divided into "basaltic soils" and "hematite-rich soils", depending on the presence of hematitic spherules. |
| Hematite-rich Soils[a] (n=10) | 858 ± 68 (600-1300) | 331 ± 23 (300-360) | 998 ± 124 (840-1150) | |
| Burns Formation RAT[b,c] (n=26) | 604 ± 54 (450-1000) | 429 ± 20 (250-630) | 673 ± 113 (550-860) | Outcrop samples. Not including Endurance Crater and Victoria Crater samples |
| Endurance Crater RAT[b,c] (n=11) | 614 ± 57 (530-700) | 419 ± 22 (320-530) | 684 ± 117 (600-750) | Samples of Karatepe section and Burns Cliff. Endurance Crater is approximately 700 m away from original rover landing site. |
| Victoria Crater RAT[b,c] (n=5) | 581 ± 46 (500-630) | 568 ± 18 (450-800) | 658 ± 103 (600-750) | Samples of the crater wall. Victoria Crater is approximately 7 km away from original rover landing site. |
| Meteorite "Meridiani Planum" | 70000 | 125 ± 12 | 0 | High Ni-Fe meteoritic sample found on Martian surface |
| Mean CI chondrite [d] | 10770 | 323 | 2646 | Volatiles included |

a. APXS measurements for these samples were of the undisturbed soil surface.
b. The "RATed rock" samples are the rock surface ground by Rock Abrasion Tool (RAT) before the APXS measurement, thus exposed lesser weathered or unweathered interior which represented the original composition of the rocks. RATed samples are grouped by locations.
c. "Burns Formation RAT", "Endurance Crater RAT" and "Victoria Crater RAT" all belong to the Burns Formation; a geological formation named after "Burns Cliff" and composed of sulfate rich sandstones.
d. Data source: Palme and Jones (2003)

All beakers were covered by paraffin film with a 2 cm hole to accommodate sampling and a pH electrode monitor port. In this design, the beakers maintained contact with ambient atmosphere ($pO_2 = 0.21$ atm), which acted as the oxidant, and solutions were continuously stirred at 25 ºC. Solutions were also corrected for evaporation through daily weighing and the addition of small amounts of de-ionized water (DI water).

The low Fe (10 g/L) oxidation experiments were allowed to run approximately 52 days for the Ni and Zn experiments, and 42 days for the Cr experiment until the pH of the solution was stable and the anticipated phases had precipitated. Suspension samples were collected every 12 h in the first day and then daily afterwards until jarosite precipitated. After jarosite appeared, the sampling frequency adjusted to once every 2-3 days.

The high Fe (200 g/L) oxidation experiments were run for approximately 40 days to attain a steady-state condition in the solution, such that amounts of solids and solution were largely invariant. The suspension samples were collected every 2-3 days.

The suspensions were then centrifuged at 5000 rpm at 25 ºC for 40 min. The supernatant solutions were collected and diluted immediately to prevent any further precipitation. The extracted solid samples were then washed with DI water and air dried at room temperature. Detailed analysis methods of solution and solid samples are described in Section 2.2.6.

## 2.2.2 Transformation of jarosite to hematite and schwertmannite to goethite via aging experiments

To further evaluate the processes controlling TE behavior during the transformation of jarosite to hematite and schwertmannite to goethite, TE-bearing jarosite and TE-bearing schwertmannite were aged in either DI water or 400 µg/g solution of individual TE for 21 days, during which the phase transformation of these mineral phases occurred.

In the jarosite aging experiment, about 0.2 g of synthetic TE-bearing jarosite was dispersed into ~60 g aging solution (i.e., solution to solid weight ratio range of 300-350). The suspensions were ultrasonicated for 10 min in LDPE bottles and then placed in a water bath at 70 ℃. The system was then agitated on a regular basis, and small amounts of suspension were collected every 7-8 days. The pH and temperature were measured at the time of sampling. The solution and suspension processing methods are described in Section 2.2.6.

The schwertmannite aging experiment was similar to jarosite aging, starting with 0.2 g synthetic TE-bearing schwertmannite dispersed into DI water and individual TE solution respectively, with an initial solution to solid weight ratio around 200-300.

### 2.2.3 Transformation of goethite to hematite

In the work of Tosca et al. (2008), an attempt was made to realize the goethite to hematite transition at low temperature, in a high ionic strength solution, over a period of 4 months. However, even this timescale was apparently too short and the transition was not observed. The dehydroxylation process, which has a potential influence on TE behavior due to mineral structural alteration, however, may be broadly similar regardless of the alteration temperature. Therefore, in an attempt to observe the transition in our short-term experiments, a high transition temperature was adopted with an understanding that such conditions impose significant caveats.

Approximately 3 g each of synthetic Ni- and Cr-goethite were heated in air in a furnace at 300 ℃ for 48 h and then cooled slowly to room temperature. To make it comparable to the initial goethite, which was thoroughly washed after synthesis, the final product of hematite was also thoroughly washed with DI water, and air dried and digested for bulk composition.

**2.2.4 TE adsorption on jarosite and goethite**

In order to estimate the retention of TE by surface adsorption of jarosite and goethite, TE-free jarosite and TE-free goethite (so called "control group") were used for adsorption comparisons.

In the jarosite adsorption experiment, 400 µg/g $Ni^{2+}$, $Zn^{2+}$ and $Cr^{3+}$ solutions were prepared respectively by dissolving $NiSO_4 \cdot 6H_2O$, $ZnSO_4 \cdot 7H_2O$ and $Cr(NO_3)_3 \cdot 7H_2O$ solids in DI water. Aliquots of synthetic TE-free jarosite were placed into the Ni, Zn and Cr solutions, with a solution to solid weight ratio around 100, for 24 h. The initial TE concentration and solid to solution ratio of these experiments were similar to the conditions of the high Fe oxidation experiments. The suspensions were then collected and centrifuged to separate supernatants from solids. To make the bulk composition of these solids comparable to those yielded from high Fe oxidation experiments which were washed by DI water after sampling, the solids here were also washed with DI water and air dried, and then digested for bulk composition.

The goethite adsorption experiments were similar to the jarosite adsorption experiments. 0.06 g of synthesized TE-free goethite was put into 30 g of a 500 µg/g TE solution (i.e., solution to solid weight ratio equal to 500) for 36 h, after which both solid and solution samples were collected and processed the same way as described above in the jarosite adsorption experiments.

**2.2.5 Synthesis of TE-bearing and TE-free Fe-phases**

Ni-, Zn-, and Cr-substituted schwertmannite were prepared using a method adapted from Schwertmann and Cornell (2000). Two liters of 0.01 M Ni-, Zn-, and Cr-solutions were prepared respectively and preheated in an oven at 60 ℃. To these solutions 10.8 g of $FeCl_3 \cdot 6H_2O$ and 3 g of $Na_2SO_4$ were quickly added and heated for a further 12 min at 60 ℃. After cooling at room temperature, the suspensions were aged for a period of 30 days. After that, supernatants were

discarded and the solid products were repeatedly washed with DI water and air dried at room temperature.

Cr-substituted goethite ($Fe_{1-x}Cr_xOOH$) was prepared using a recipe adapted from Schwertmann and Cornell (2000). Alkaline Cr solution were prepared by mixing 600 mL of 0.5 M $Cr(NO_3)_3$ solution with 360 mL of 5 M KOH in a 2 L Erlenmeyer flask. 90 mL of 1 M $Fe(NO_3)_3$ solution was added to 270 mL of the alkaline Cr solution. The mixing suspension was brought to 0.3 M KOH with addition of 128 mL of 5 M KOH and diluted by DI water resulting in a final volume of 1.8 L. The suspension was stored in a water bath at 70 ºC for 30 days and agitated occasionally. The final product was washed twice with 0.1 M KOH and then with DI water to remove the electrolytes and dried. Amorphous Cr-hydroxides and adsorbed Cr were removed by a 12 h treatment with 2 M $H_2SO_4$ at 80 ºC.

The Ni-substituted goethite was synthesized by aging Ni-containing ferric hydroxides for 60 h at 70 ºC (Carvalho-E-Silva et al., 2003). The hydroxides were obtained by precipitation from 100 mL 1 M $Fe(NO_3)_3$ and 600 mL 0.5 M $Ni(NO_3)_2$ with 500 mL 5 M KOH solutions in a final volume of 1.2 L. The supernatant was discarded and the products were repeatedly washed with DI water and dried at 50 ºC for 12 h. Amorphous material was removed by leaching the products with a solution of 3 M $H_2SO_4$ at 50 ºC for 12 h. The final products were again repeatedly washed with DI water.

TE-free goethite was prepared from an alkaline Fe(III) system described in Schwertmann and Cornell (2000). 100 mL of 1 M $Fe(NO_3)_3$ solution was placed into a 2 L polyethylene flask, followed by rapid addition and stirring of 180 mL of 5 M KOH. Red-brown 2-line ferrihydrite precipitated at once. The suspension was immediately diluted to 2 L with DI water and held in a

closed polyethylene flask at 70 ℃ for 60 h. The suspension was then removed from the oven, centrifuged, washed and the precipitate dried in air at room temperature.

Ni-, Zn- and Cr-bearing jarosite and TE-free jarosite were synthesized by the same procedures as the high Fe oxidation experiments.

### 2.2.6 Analytical methods

A gel-filled paper pulp pH electrode with temperature compensation was used to measure pH and was calibrated regularly with standard buffer solutions of pH 1.6, 4 and 7. Eh was measured with a platinum combination oxidation-reduction potential (ORP) electrode (Orion model 9678).

During the experiments, suspension samples were periodically collected and centrifuged at 5000 rpm at 25 ℃ for 40 min. The extracted solid samples were then washed with DI water and air dried at room temperature. Solids were identified with Powder X-ray Diffraction (XRD), Fourier Transform Infrared Spectroscopy (FTIR), and Scanning Electron Microscopy (SEM) with Energy Dispersive X-ray Spectrometer (EDS). Powder XRD data were collected using a Scintag PAD-V Bragg-Brentano diffractometer at 45 kV and 25 mA with Cu-Kα radiation (λ = 1.5418 Å). Data were collected between 10 and 60 degrees $2\theta$, with a scan step of 0.02 degrees and between 2 and 6 s of counting time per step. SEM measurements were taken using a LEO 1550 SFEG SEM at 15 kV and using a 30 mm aperture. Sizes of nano-scale particles were estimated by XRD data using the Scherrer formula (Patterson, 1939), in which the goethite characteristic peak (1 0 1) and schwertmannite characteristic peak (2 1 2) were used. The surface area of solid samples were determined by B.E.T. surface analysis (BET), using a NOVA 2200e surface area & pore size analyzer. Proportions of each mineral in the final products of the aging experiments were also estimated from XRD data by comparing them with XRD patterns of

standards with known proportions of schwertmannite-goethite mixtures, and jarosite-hematite mixtures.

At the end of each experiment, a small fraction of all solid samples were digested with concentrated HCl at an elevated temperature to determine the TE concentrations. All supernatant samples collected during the experiments, as well as digested products, were filtered with a 0.2 μm membrane and analyzed for Mg, $Fe_{total}$, K, Ni, Zn and Cr with a direct current argon plasma emission spectrophotometer (DCP-AES). Solutions were diluted with 4% $HNO_3$ and external solution standards were prepared in a 4% $HNO_3$ matrix with concentrations bracketing the unknown sample range as closely as possible. A HACH DR 4000 UV/Vis spectrophotometer was used for determining ferrous iron and $SO_4$ concentration in solution, with standard methods suggested by instrumental procedures manual: 1,10-phenanthroline method and SulfaVer4 method, respectively.

The quality of analytical data was monitored by parallel samples and duplicated analyses. Low Fe and high Fe oxidation experiments of each element were performed in duplicate, to ensure the behavior of trace elements observed in the solution was the true trend instead of random error occurring in one analysis. Average analytical precision for trace elements determined by DCP is estimated to be about ±5%.

All the major experiments conducted in this study are summarized in Table 2.2, except for the synthesis of mineral phases described in Section 2.2.5.

## 2.3 Results and Discussion

### 2.3.1 TE evolution during jarosite precipitation via high Fe(II)-oxidation experiments

Due to hydrolysis of $Fe^{2+}$ and $Fe^{3+}$, and possible occurrence of low levels of $Fe^{3+}$ in the initial $FeSO_4 \cdot 7H_2O$ phase, dissolution of melanterite is a fast acid generating process (Hurowitz

et al., 2009). During high Fe oxidation experiments precipitating jarosite, the pH decreased from 3.0 to 1.6 in all three trace element experiments.

In the solutions, acidic conditions (initial pH < 3) and the presence of $K^+$ led to direct precipitation of jarosite from the first day and the jarosite persisted until the end of the experiment (Figure 2.2 (E)). Small amounts of metastable hexahydrite ($MgSO_4 \cdot 6H_2O$) also precipitated at the beginning of the experiment, mixed with jarosite and re-dissolved back into the solution after the first two days. The jarosite yielded in all high Fe oxidation experiments had similar grain sizes, about 1 micron in diameter, and the surface area was about 3 $m^2/g$.

Ni, Zn and Cr concentrations of the solutions during the course of the oxidation experiments are shown in Figure 2.3. All three elements witnessed a sharp decrease in concentration at the beginning. Ni concentration dropped to the range of 300-350 µg/g, while Zn varied within the range of 350-400 µg/g. Trivalent Cr, on the other hand, demonstrated a more systematic trend of decrease from 400 µg/g to 325 µg/g. Similar trends in trace element behavior were observed in duplicated experiments. Ni varied twice as much as Zn in the solution.

**Table 2.2.** Summary of major experiments conducted in this study, except for synthesis of mineral phases described in Section 2.2.5.

| Experiments | Initial Settings | Objectives |
|---|---|---|
| 1A: High Fe oxidation | Either Ni(II), Zn(II) or Cr(III) was 400 μg/g in 500 ml 1.6 M MgSO$_4$ matrix solution; 200 g/L FeSO$_4$·7H$_2$O solid; 1-2 g KCl solid. 25°C; 40 days. | Precipitation of pure Jt |
| 1B: Low Fe oxidation | Either Ni(II) or Zn(II) was 500 μg/g and Cr(III) was 300 μg/g in 500 ml 1.6 M MgSO$_4$ matrix solution; 10 g/L FeSO$_4$·7H$_2$O solid; 25°C; 42~55 days. | Precipitation of mixture of Sch, Gt and Jt. |
| 2A: Jt aging in DI water | Synthetic Ni-Jt/Zn-Jt/Cr-Jt were put into DI water, respectively; solution (wt)/ solid (wt) = 300; 70°C; 21 days. | TE releases during TE-Jt to Hm transition without additional TE in ambient solution |
| 2B: Jt aging in TE solution | Synthetic Ni-Jt was put into 400 μg/g Ni-SO$_4$ solution; Zn-Jt was put into 400 μg/g Zn-SO$_4$ solution, Cr-Jt was put into 400 μg/g Cr-NO$_3$ solution; solution (wt)/ solid (wt) = 350; 70°C; 21 days. | Interaction of TE with Jt-Hm mixture during TE-Jt to Hm transition with additional TE in ambient solution |
| 2C: Sch aging in DI water | Synthetic Ni-Sch/Zn-Sch/Cr-Sch were put into DI water, respectively; solution (wt)/ solid (wt) = 200; 70°C; 21 days. | TE behavior during TE-Sch to Gt transition without additional TE in ambient solution |
| 2D: Sch aging in TE solution | Synthetic Ni-Sch was put into 400 μg/g Ni-SO4 solution; Zn-Sch was put into 400 μg/g Zn-SO4 solution, Cr-Sch was put into 400 μg/g Cr-NO3 solution, respectively; solution (wt)/ solid (wt) = 300; 70°C; 21 days. | Interaction of TE with Sch-Gt mixture during TE-Sch to Gt transition with additional TE in ambient solution |
| 3A: Gt to Hm transformation | Synthetic Ni- and Cr- Gt were heated in air in a furnace at 300°C; 48 h. | To compare the Ni and Cr amounts in Hm after transition from Gt |
| 4A: Jt adsorption | Synthetic TE-free Jt was put into 400 μg/g either Ni(II), Zn(II) or Cr(III) solution; solution (wt)/ solid (wt) = 100; 25°C; 24 h. | To estimate the amount of TE adsorbed on Jt surface |
| 4B: Gt adsorption | Synthetic TE-free Gt was put into 500 μg/g either Ni(II), Zn(II) or Cr(III) solution; solution (wt)/ solid (wt) = 500; 25°C; 36 h. | To estimate the amount of TE adsorbed on Gt surface |

*Sch = schwertmannite; Gt = goethite; Jt = jarosite; Hm = hematite.
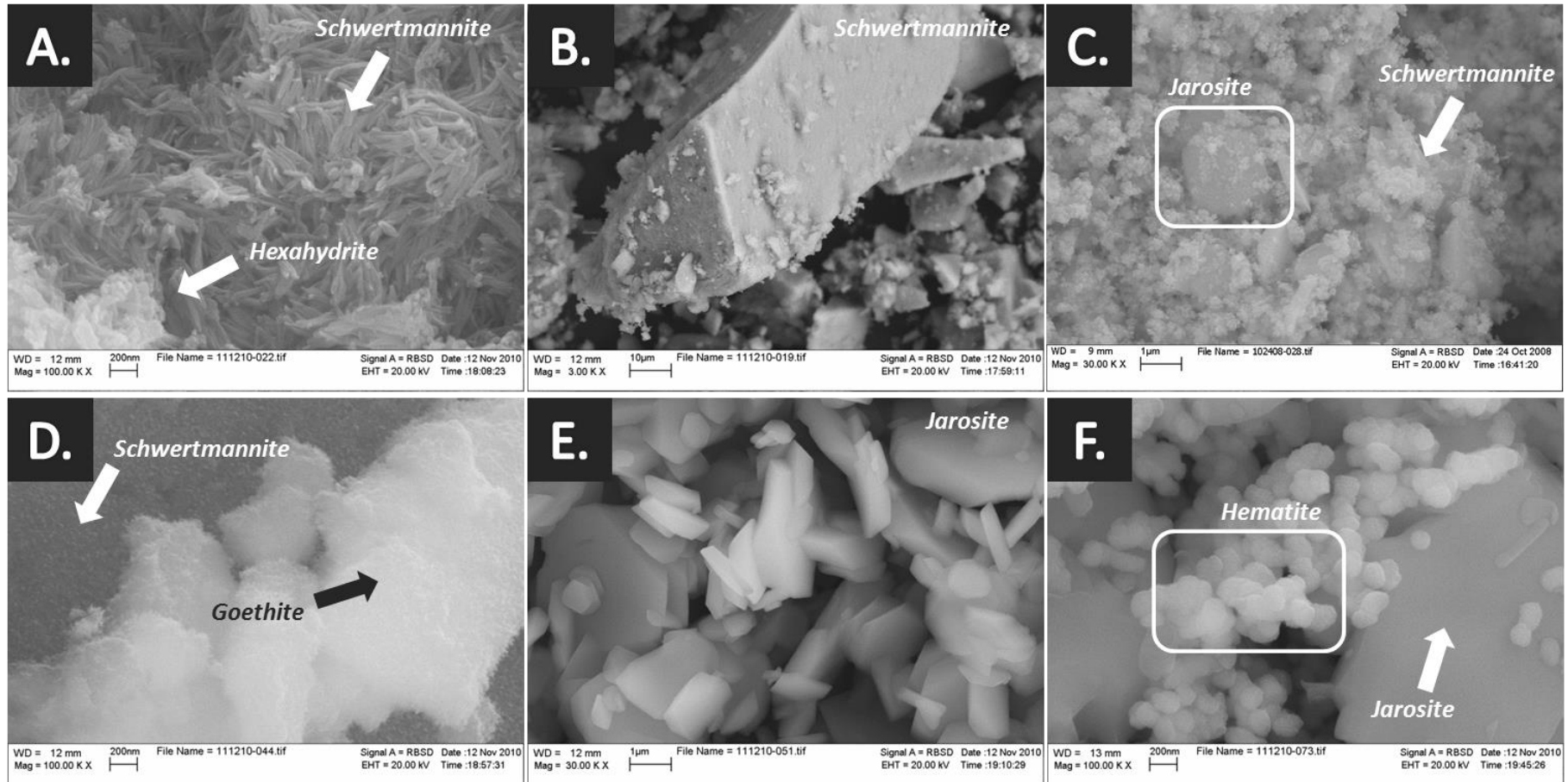
**Figure 2.2.** Scanning electron micrographs of Fe-oxidation products from experiments described in this study. (A) Schwertmannite and metastable hexahydrite ($MgSO_4 \cdot 6H_2O$) precipitated on the 17th day (the first day schwertmannite precipitated) of Cr experiment in the low Fe oxidation. Hexahydrite re-dissolved back into the solution on the following day. (B) Schwertmannite precipitated in the Ni experiment of low Fe oxidation. (C) Breakdown of precursor schwertmannite and growth of H-jarosite observed in the Zn experiment of low Fe oxidation. Goethite was also present in this sample but was too small to be resolved under SEM. (D) Schwertmannite and goethite in the schwertmannite aging experiment. (E) Jarosite precipitated in the TE-free high Fe oxidation experiment. (F) Dissolution of jarosite and neo-formed hematite in Zn-jarosite aging experiment in DI water.

47
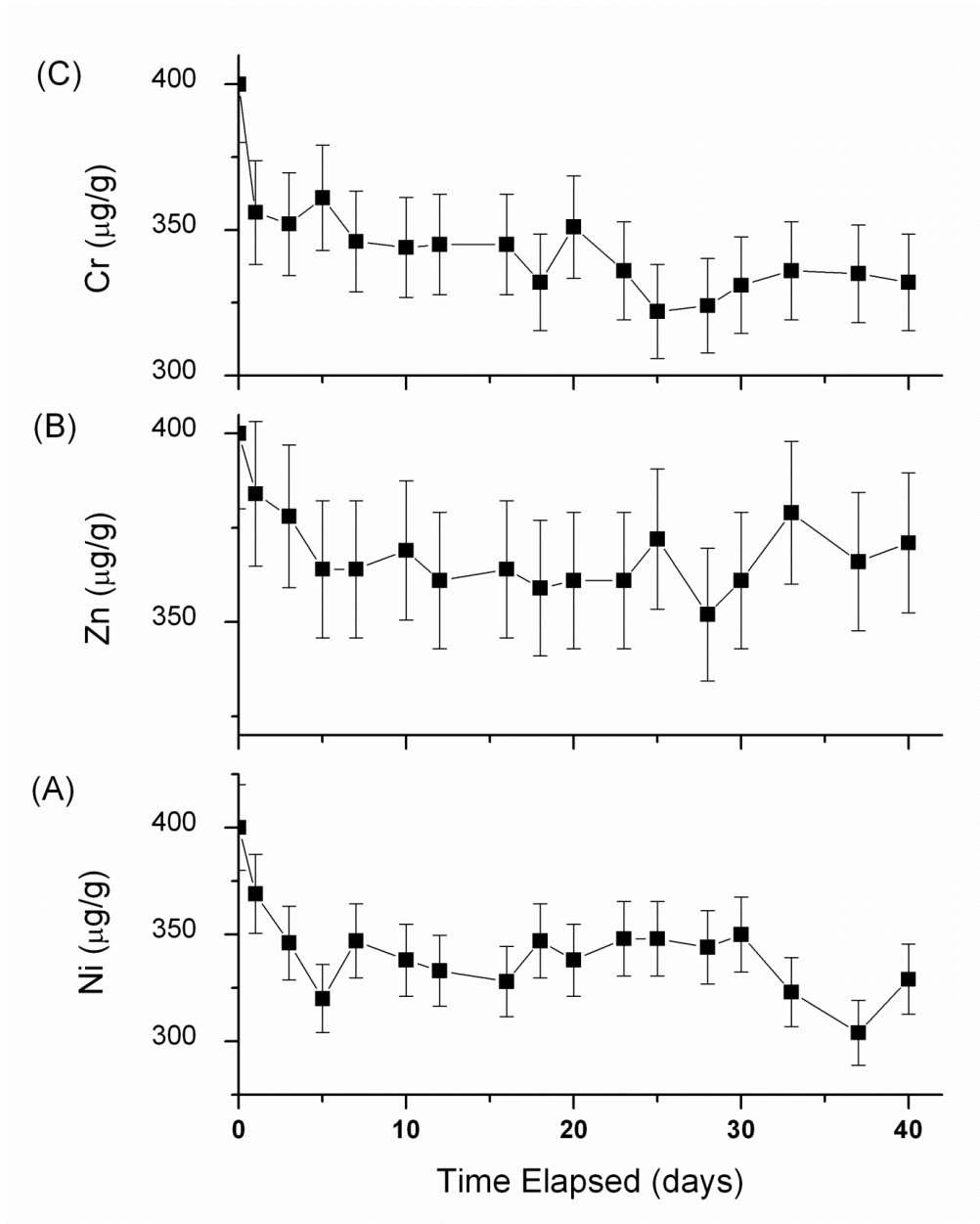
**Figure 2.3.** TE concentrations of solution during precipitation of pure jarosite in the high Fe oxidation experiments. Initial Ni, Zn and Cr concentrations in the solution were each 400 µg/g. All three elements witnessed a sharp decrease at the beginning. Ni concentration dropped to the range of 300 - 350 µg/g, while Zn varied within the range of 350 - 400 µg/g. Cr demonstrated a more systematic trend of decrease from 400 µg/g to 325 µg/g. Ni and Zn behavior was more likely controlled by adsorption-desorption on the jarosite surface, which was unstable. Thus their concentrations varied from day to day in the solution.

At the end of the experiments, Ni was 71 µg/g and Zn was 29 µg/g less than their respective initial concentrations. Because Ni decreased more than Zn in the solutions, it was expected that in the corresponding jarosite samples, Ni concentrations would be higher than Zn. However, in contrast to expectation, Ni (18 µg/g) was much less than Zn (157 µg/g) (Table 2.3). One explanation for this apparent discrepancy is that all the solids were washed by DI water after sampling; thus it is very possible some adsorbed TE were removed from the solids during this treatment. Compared to the control group TE-free jarosite adsorption data (Table 2.3), Ni concentration in precipitated jarosite was lower than its adsorption-only counterpart (71 µg/g), whereas Zn concentration was slightly higher than surface adsorption amounts (131 µg/g).

The removal of Ni and Zn from the solution did not result from substantial partitioning into precipitated jarosite. Therefore, Ni and Zn behavior was more likely controlled by adsorption-desorption processes on the jarosite surface rather than incorporation into its structure. Ni adsorbed onto jarosite was very unstable and readily re-released. This resulted in a greater amount of Zn remaining adsorbed onto the jarosite surface than Ni.

Although no compelling evidence of Ni and Zn incorporation into jarosite was observed in our experiment, Papike et al. (2006) suggested that divalent cations such as Zn can substitute for Fe(III) in the jarosite structure, and the expected trends both for incorporation and for adsorption of Ni and Zn are similar. The order of incorporation of divalent metals by jarosite has been determined to be: Cu > Zn > Co ~ Ni ~ Mn > Cd, where Zn concentrations may be about two times the levels of Ni in jarosite (Dutrizac and Jambor, 2000). In this study, increases of the pH of the parent solution increased the extent of hydrolysis and promoted the structural incorporation of the divalent metals. On the other hand, elevated concentrations of ferric sulfate

**Table 2.3.** Comparison of TE concentrations in solids by precipitation and surface adsorption. Adsorption experiments were conducted with similar initial TE concentration and solid/solution ratios to the oxidation experiments.

| TE conc. in solid (μg/g) | Precipitates of high Fe oxidation | TE-free Jt adsorption | TE conc. in solid (μg/g) | Precipitates of low Fe oxidation[1] | TE-free Gt adsorption[2] |
|---|---|---|---|---|---|
| Ni | 18 (Jt) | 71 | Ni | 8355 (Sch+Gt) | 4841 |
| Zn | 157 (Jt) | 131 | Zn | 1255 (Sch+Gt) | 4955 |
| Cr | 889 (Jt) | 250 | Cr | 39507 (Sch only) | 860 |

*Sch = schwertmannite; Gt = goethite; Jt = jarosite.
1. Solids were sampled the day before jarosite precipitated in the low Fe oxidation experiments.
2. The TE sorbate solution had different anions. In the Ni and Zn experiment, the anion was sulfate; in the Cr experiment, the anion was nitrate. The anion difference may play an important role in TE adsorption to Gt.

reduced the extent of incorporation (Dutrizac and Chen, 2004). In jarosite, the maximum reported Zn content was 2.1 wt% and Ni was less than 1.35 wt%. Similarly, in Na-jarosite, the maximum reported Zn content was about 1 wt%, whereas the Ni was less than 0.5 wt% (Dutrizac and Chen, 1984; Dutrizac and Oreilly, 1984). The key factor controlling the incorporation of divalent cations into jarosite group compounds is the extent of hydrolysis. Accordingly, the high temperature and high pH would encourage structural incorporation. In our experiments, the low temperature and highly acidic conditions may account for the inhibition of Ni and Zn incorporated into jarosite.

Trivalent Cr, in contrast to divalent Ni and Zn, demonstrated a clearer trend of decrease from the solution during jarosite precipitation. At the end of the experiment, the Cr concentration of precipitated jarosite was 889 µg/g (Table 2.3), much higher than in the surface adsorption only sample (250 µg/g). The decrease of Cr in the solution was likely due to a combination of incorporation and adsorption. Since Cr can readily be incorporated into the jarosite structure by substituting for Fe(III), incorporation might be the dominant factor.

To summarize, partitioning of Ni, Zn and Cr to precipitated jarosite (regardless of whether by adsorption and/or incorporation) was most likely in the order: Cr > Zn > Ni.

**2.3.2 TE evolution during jarosite to hematite transformation**

The jarosite used in the aging experiment was the final products obtained from the high Fe oxidation experiment (discussed in detail in Section 2.3.1), where Ni and Zn were mainly adsorbed onto the jarosite surface and Cr was mainly incorporated into the structure. The initial concentrations of Ni, Zn and Cr in the jarosite were 18 µg/g, 157 µg/g and 889 µg/g, respectively.

At the end of the aging experiments, the color of solids changed from yellow to red and XRD patterns of the new phase best matched hematite (Figure 2.4). SEM confirmed the dissolution of jarosite crystals and precipitation of hematite spherules clustered in bundles near dissolved jarosite crystal edges (Figure 2.2 (F)). The neo-formed hematite has a diameter around 100-200 nm. The phase change was via reaction (1) shown below. Detailed concentration of solution and solid during the aging process are listed in Table 2.4.

$$2\ KFe_3(SO_4)_2(OH)_6\ (Jt) \rightarrow 3\ Fe_2O_3\ (Hm) + 4\ SO_4^{2-} + 2\ K^+ + 6\ H^+ + 3\ H_2O \tag{1}$$
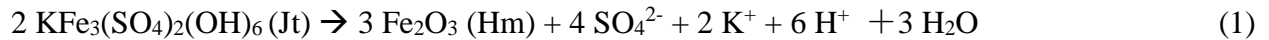
During aging in DI water, Ni, Zn and Cr were not detected in the ambient solutions. However, in the final solids, Ni and Zn were below detection limit, whereas Cr concentrations remained almost unchanged (844 µg/g). Therefore, the Ni and Zn were indeed released into the solution during this phase conversion, but were greatly diluted due to the initial solution to solid mass ratio. Cr, on the other hand, was not released much during the jarosite to hematite transformation.

During aging in 400 µg/g TE solutions, pH, K and $SO_4$ in the solution demonstrated identical trends of evolution during the jarosite to hematite transformation (shown in Figure 2.5 (A-C)). All three trace elements in the initial solutions showed affinity for the solids (Figure 2.5 (D)). Ni and Zn in the solution behaved similarly as they both continuously decreased from the solution at the beginning but then remained constant until the end. The final concentrations of Ni and Zn in the solutions were similar, at 306 µg/g and 307 µg/g respectively. Cr in the solution decreased much more than Ni and Zn. It continuously dropped about 300 µg/g in the first 2 weeks, and recovered slightly from about 50 µg/g to about 125 µg/g at the end. Ni, Zn and Cr concentrations in the final solid mixtures were 442 µg/g, 1055 µg/g and 3017 µg/g, respectively (Table 2.4).
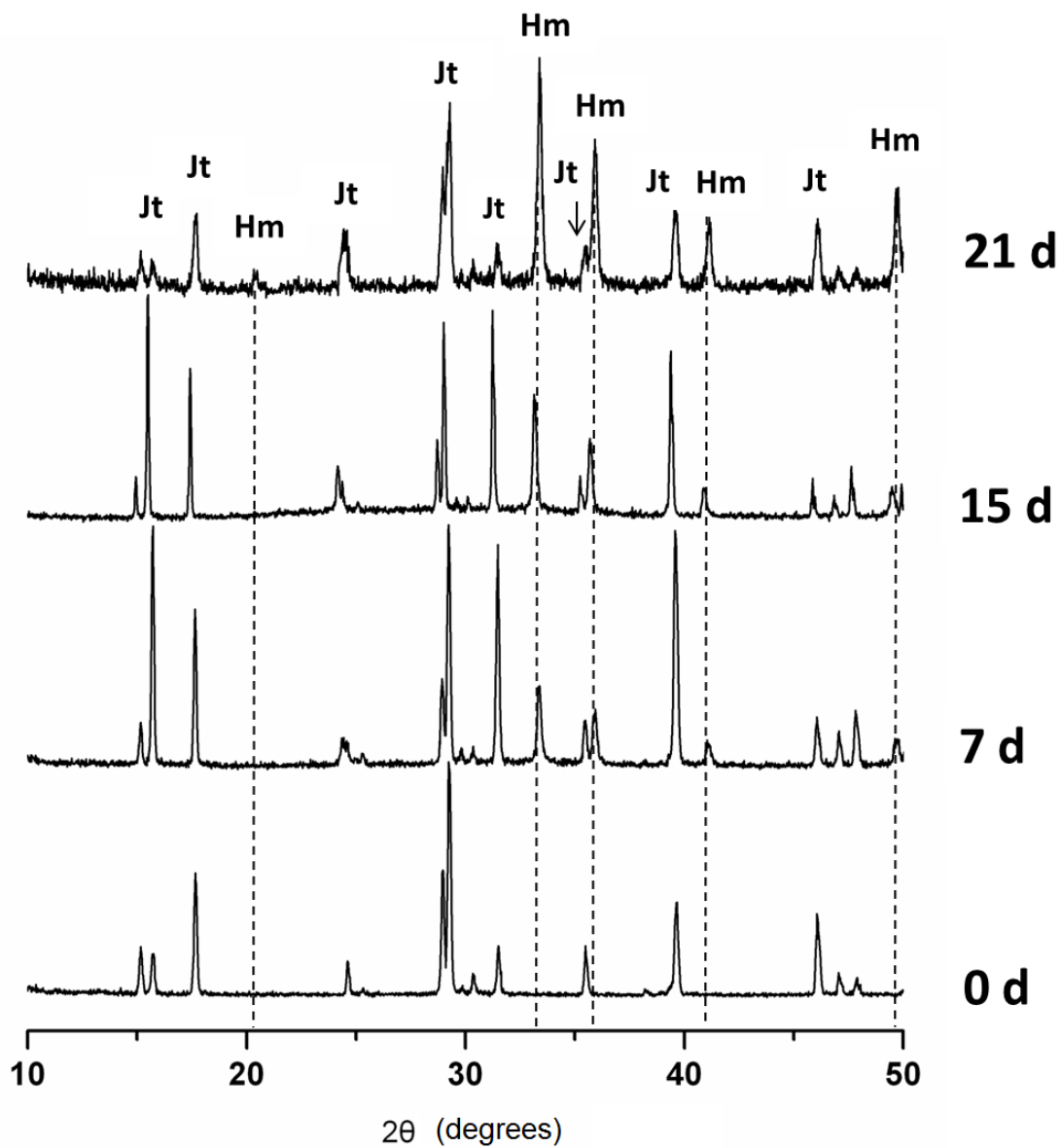
**Figure 2.4.** Powder X-ray diffractograms of the aging experiment of the synthetic Ni-bearing jarosite (and hematite) aging in Ni solution. A mixture of jarosite and hematite was observed at the end of the experiment.

**Table 2.4.** TE concentrations of solutions and solids during transformation of jarosite to hematite in DI water and TE solutions. In TE-solution aging experiments, TE concentrations in neo-formed Hm was calculated based on the final TE concentrations in Jt-Hm mixture and their proportions. This estimate did not consider the TE interaction with jarosite during the aging process.

| Initial TE-Jt solid (µg/g) | | Final product composition (wt%) | TE in final mixture (µg/g) | Final TE conc. in DI water (initially 0) |
|---|---|---|---|---|
| *Aging jarosite in DI water* | | | | |
| Ni | 18 | 55% Hm; 45%Jt | <DL | <DL |
| Zn | 157 | 40% Hm; 60%Jt | <DL | <DL |
| Cr | 889 | 15% Hm; 85% Jt | 844 | <DL |

| Initial TE-Jt solid (µg/g) | | Final product composition (wt%) | TE in final Jt-Hm mixture (µg/g) | Final TE conc. in TE solution (initially 400 µg/g) | Calculated TE conc. of neo-formed Hm (µg/g) |
|---|---|---|---|---|---|
| *Aging jarosite in TE-solution* | | | | | |
| Ni | 18 | 55% Hm; 45%Jt | 442 | 306 | 788 |
| Zn | 157 | 40% Hm; 60%Jt | 1055 | 307 | 2402 |
| Cr | 889 | 15% Hm; 85% Jt | 3017 | 130 | 15000 |

*Jt = jarosite; Hm = hematite. Solution detection limit (DL) for Ni = 0.05 µg/g; Zn = 0.01 µg/g; Cr = 0.01 µg/g. Solid detection limit (DL) for Ni = 6.5 µg/g; Zn = 3 µg/g.
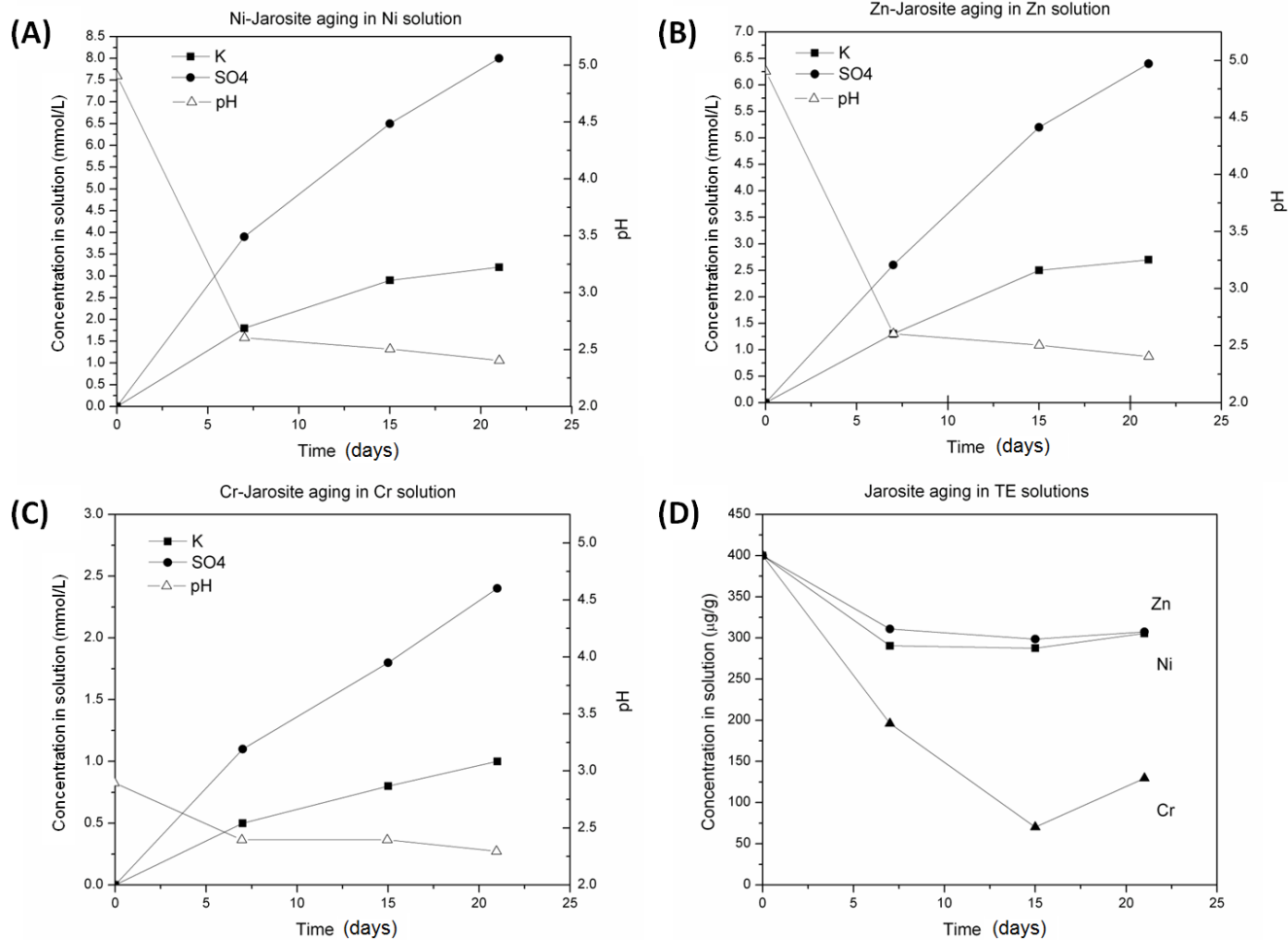
**Figure 2.5.** Cation and anion concentrations in solution during the TE-bearing jarosite to hematite transformation in TE solutions. The evolution of K, $SO_4$ and pH in these aging experiments was nearly identical, although absolute concentrations were different.

Using the jarosite and hematite proportions of the solid mixtures and initial TE concentrations in the jarosite, the concentrations of Ni, Zn and Cr in the neo-formed hematite were estimated to be 788 µg/g, 2402 µg/g, and 1.5 wt% (Table 2.4). This calculation assumed that no TE partitioned to jarosite during such a process, and thus provides an upper limit of TE concentrations in the neo-formed hematite. Based on these results, during the phase change from jarosite to hematite, trivalent Cr had higher affinity for hematite than divalent Ni and Zn. Zn concentration was higher than Ni in hematite derived from jarosite when additional TE were available in the ambient solution. The amount of Ni, Zn and Cr partitioning into the hematite via dissolution of jarosite was likely in the order of Cr > Zn > Ni.

Therefore, if hematite formed via the dissolution of jarosite within a TE solution where three trace elements were initially equal, the TE partitioning into hematite would be higher than for jarosite but would inherit the same general TE pattern. That is, Ni should be lower than Zn in the hematite if it formed via the dissolution of jarosite.

## 2.3.3 Precipitation of mixtures of schwertmannite, goethite and jarosite via low Fe(II)-oxidation experiments

The evolution of precipitates in low Fe oxidation experiments can be divided into two stages. The first stage was mixtures of schwertmannite and goethite, and the second was mixtures of schwertmannite, goethite and hydronium-jarosite (H-jarosite).

In the first stage, before the precipitation of jarosite, the pH started at 4.4 and continuously decreased to 3.3 in the Ni and Zn experiments, and decreased from 3.8 to 3.0 in the Cr experiment. The slightly lower initial pH for the Cr experiment is due to the soluble salt used as the source of Cr (III), $Cr(NO_3)_3 \cdot 6H_2O$, which itself is acidic in solution.

In the Ni and Zn experiments, the precipitation started with schwertmannite (Figure 2.2 (B)), thus acting as a precursor for the following precipitates, goethite and H-jarosite, where goethite appeared earlier than H-jarosite. The stage during which schwertmannite existed alone was just a few hours long at the beginning of the experiments. After 24 h, the precipitates were mixtures of schwertmannite and goethite, and after 15 days, the H-jarosite appeared. The breakdown of schwertmannite and growth of H-jarosite was observed (Figure 2.2 (C)). The Cr experiment was slightly different. Colloids formed and persisted in the solution without any precipitates during the first 16 days. On the 17th day, schwertmannite started to precipitate. Beginning on the 30th day, H-jarosite started to appear and then a mixture of schwertmannite and H-jarosite coexisted until the end of the experiment (i.e., total of 42 days). The colloid particles were thus an intermediate in the precipitate formation process. Although the exact phase/mineralogy of those colloids was not identified, based on others studies of chromium speciation in an acid aqueous system (e.g., Palmer and Wittbrodt, 1991) at pH conditions 3.0-3.7, similar to our experiment, hydrolysis of Cr(III) likely yields trivalent chromium hydroxyl species such as $CrOH^{2+}$ and $Cr(OH)_2^+$. With the presence of Fe(III), chromium hydroxide is likely to generate an amorphous hydroxide co-precipitate in the form of $Cr_xFe_{1-x}(OH)_3$ (Palmer and Wittbrodt, 1991).

Similar to the observation in the high Fe oxidation experiment, schwertmannite precipitated at the beginning and was mixed with metastable hexahydrite ($MgSO_4 \cdot 6H_2O$), which re-dissolved back into the solution after about 1 or 2 days (e.g., Figure 2.2 (A)). It is worth noting that schwertmannite displayed fibrous morphology in the Cr experiment (Figure 2.2 (A)) but formed nano-scale crystallites that accumulated into small chunks in the Ni and Zn experiments (Figure 2.2 (B)). In addition, similar to the findings of Tosca et al. (2008), goethite appeared as nano-

crystalline particles, and although confirmed by XRD and FTIR, it was not possible to resolve individual crystallites by SEM in any of the low Fe oxidation experiment samples.

The grain size of schwertmannite precipitated in the Zn experiment was ~4 nm and precipitated goethite was around 10 nm. The sample from the 15th day (the last day before H-jarosite appeared) was a mixture of schwertmannite and goethite and had a specific surface area ~70 m$^2$/g. The mineral phase yielded from the Ni experiment had similar grain size and surface area to that of the Zn experiment. The schwertmannite precipitated in the Cr experiment had a larger size, ~200-400 nm in length. Proportions of components in the final products of the low Fe oxidation experiment could not be estimated, because well-crystallized H-jarosite overwhelmed the schwertmannite signal and resulted in the absence of a schwertmannite peak in the XRD pattern.

The breakdown of schwertmannite, presence of goethite and growth of H-jarosite particles are consistent with precursor schwertmannite transformation to goethite and H-jarosite, a process that has been observed in other studies (Acero et al., 2006; Tosca et al., 2008). However, the conversion of schwertmannite to goethite has been found to be greatly inhibited by increasing sulfate concentration and decreasing pH (Jönsson et al., 2005). Given the short time frame, decreasing pH and high ionic strength sulfate matrix conditions in our low Fe oxidation experiments, it is very likely that the goethite was formed by direct precipitation due to Fe$^{3+}$ hydrolysis rather than by transformation from schwertmannite (Bigham et al., 1996). This could also be the explanation for the lack of goethite in the Cr experiment, in which only jarosite was found to have precipitated after schwertmannite. The lower pH condition in the Cr experiment may have inhibited either the conversion of schwertmannite to goethite, or the direct precipitation of goethite. Therefore, in general, the most likely mineralogical evolution in the low

Fe oxidation experiment was that schwertmannite precipitated first, followed by direct precipitation of goethite, after which the jarosite was formed by the breakdown of precursor schwertmannite.

**2.3.4 TE evolution during precipitation of mixtures of schwertmannite, goethite, (and jarosite)**

Ni, Zn and Cr behaved differently during schwertmannite and goethite precipitation (Figure 2.6). Ni demonstrated higher affinity for the mixture of schwertmannite and goethite than did Zn. Ni concentrations in solution decreased continuously by about 80 µg/g correlating to schwertmannite precipitation, whereas Zn remained almost unchanged. As the proportion of goethite increased, the overall trend of Ni concentration in the solution was to decrease, by another 100 µg/g, though the concentrations jumped up at certain points and dropped again afterward. On the other hand, Zn concentrations in solution dropped by about 70 µg/g upon goethite appearance, and remained relatively constant afterwards. Ni and Zn concentrations in mixture of schwertmannite and goethite collected on the last day before appearance of jarosite were 8355 µg/g and 1255 µg/g respectively (Table 2.3).

In the Cr experiment, the Cr concentration in solution rapidly dropped by about 70 µg/g and remained fairly constant from the state in which colloids dominated through to the state in which schwertmannite dominated. The final schwertmannite contained 3.95 wt% of Cr (Table 2.3).

Furthermore, the second stage of mineral phase evolution during which schwertmannite broke down and H-jarosite precipitated in the Fe-oxidation experiments did not cause significant change of the trace elements in the solution. Concentrations of Ni and Zn in the solution

remained almost constant, whereas Cr, on the other hand, rose by about 20 µg/g in the solution and then decreased back as H-jarosite increased in amount and dominated the solid phases.

For comparison, the results of the TE-free goethite adsorption experiment are also listed in Table 2.3. The surface area of synthetic TE-free goethite was 20 $m^2$/g, which was less than the precipitates yielded from the oxidation experiment. However, it can still provide some clues about the capability for retention of TE by the goethite surface. The amount of Ni and Zn adsorbed onto the goethite surface were similar (Table 2.3), therefore, the large difference in Ni and Zn observed in the precipitates might be due to a certain level of incorporation, especially in the case of Ni. The amount of Ni and Zn adsorbed on goethite surface were much greater than Cr. However, we cannot conclude that the adsorption of Cr was less than Ni and Zn by the goethite surface. The sulfate anion in the Ni and Zn sorbate solution could play a role in increasing the adsorption, compared to the Cr sorbate solution, which was nitrate. The anion difference in influencing the adsorption capacity of goethite to the trace elements will be discussed in greater detail in Section 2.3.6.


**2.3.5 TE evolution during schwertmannite to goethite transformation**

Synthetic schwertmannite was light ochreous in color, with a particle size of ~4 nm. Ni, Zn and Cr concentrations measured in the synthetic schwertmannite were 959 µg/g, 1000 µg/g and 1.69 wt%, respectively (Table 2.5).

In principle, schwertmannite is metastable with respect to goethite and H-jarosite (Tosca et al., 2008), and thus can transform to either or both phases via reactions shown below:

$$Fe_8O_8(OH)_6(SO_4) \ (Sch) + 2 \ H_2O \rightarrow 8 \ FeO(OH) \ (Gt) + 2 \ H^+ + SO_4^{2-} \tag{2}$$

$$0.5 \ Fe_8O_8(OH)_6(SO_4) \ (Sch) + 1.5 \ SO_4^{2-} + 6 \ H^+ \rightarrow (H_3O)Fe_3(OH)_6(SO_4)_2 \ (H\text{-}Jt) + Fe^{3+} \tag{3}$$
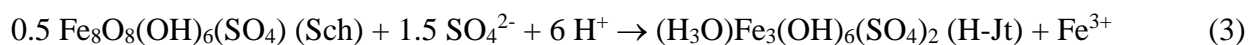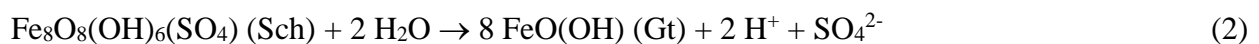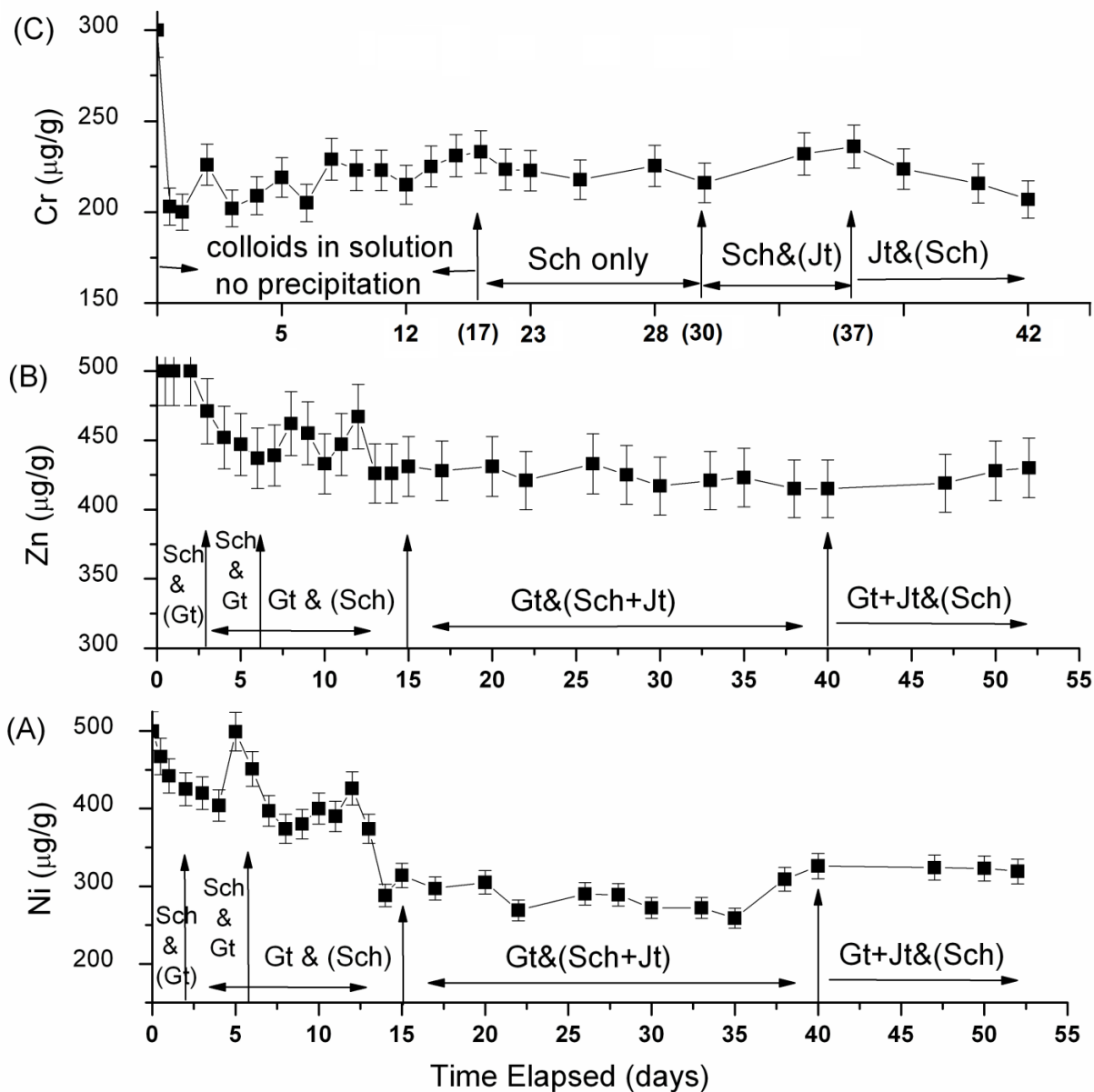
**Figure 2.6.** TE concentrations of solution during low Fe oxidation experiments in which schwertmannite, jarosite and/or goethite precipitated. Also shown are the observed mineral assemblages. Sch = schwertmannite; Gt = goethite; Jt = jarosite. Ni demonstrated higher affinity for mixture of schwertmannite and goethite than Zn. Cr concentration rapidly dropped by about 70 µg/g and remained fairly constant from the state in which colloids dominated through to the state in which schwertmannite dominated. Additional breakdown of schwertmannite and precipitation of H-jarosite did not cause significant change of these trace elements in the solution.

**Table 2.5.** TE concentrations of solutions and solids during transformation of schwertmannite to goethite in DI water and TE solutions. For comparison, in DI water aging experiment, expected maximum TE in DI water were calculated by assuming altered schwertmannite released all the TE without retention. In TE-solution aging experiment, TE concentrations in neo-formed Gt were calculated based on the final TE concentration in Sch-Gt mixture and their proportions. This estimate was based on the assumption of no TE interaction with Sch during the aging process.

| Initial TE-Sch solid (µg/g) | | Final product composition (wt%) | TE in final Sch-Gt mixture (µg/g) | Final TE conc. in DI water (initially 0) | Calculated maximum TE in DI water (µg/g) |
|---|---|---|---|---|---|
| *Aging schwertmannite in DI water* | | | | | |
| Ni | 959 | 60% Sch; 40% Gt | 698 | 0.92 | 1.9 |
| Zn | 1000 | 30% Sch; 70% Gt | 324 | 2.96 | 3.4 |
| Cr | 16900 | 90% Sch; 10% Gt | 17400 | <DL | 8.2 |

| Initial TE-Sch solid (µg/g) | | Final product composition (wt%) | TE in final Sch-Gt mixture (µg/g) | Final TE conc. in TE solution (initially 400 µg/g) | Calculated TE conc. of neo-formed Gt (µg/g) |
|---|---|---|---|---|---|
| *Aging schwertmannite in TE-solution* | | | | | |
| Ni | 959 | 60% Sch; 40% Gt | 1702 | 355 | 2817 |
| Zn | 1000 | 40% Sch; 60% Gt | 1875 | 347 | 2458 |
| Cr | 16900 | 90% Sch; 10% Gt | 29400 | 311 | 141900 |

*Sch = schwertmannite; Gt = goethite; DL= detection limit. Solution detection limit (DL) for Ni = 0.05 µg/g; Zn = 0.01 µg/g; Cr = 0.01 µg/g.

If schwertmannite transforms to goethite, decreasing pH and increasing $SO_4$ should be observed in the solution. In contrast, if schwertmannite transforms to H-jarosite, increasing pH and decreasing $SO_4$, and release of Fe (III) into the solution is expected.

At the end of the aging experiments, no jarosite group compounds were detected by XRD, FTIR or SEM-EDS. Consistent with mineral phase identifications, chemical analyses of all aging solutions demonstrated significant pH decrease and $SO_4$ release. During aging experiments in DI water, the pH of the Zn and Cr experiments dropped from 3.6 to 2.6, and the pH of the Ni experiment dropped from 3.1 to 2.3. When schwertmannite was aged in the 400 µg/g TE solution, pH decreases in the Ni, Zn and Cr experiments were 3.3 to 2.5, 3.5 to 2.4, and 2.9 to 2.2, respectively.

These results indicate that during the short-term aging process, schwertmannite was transformed exclusively to goethite without forming significant amounts of H-jarosite. Neo-formed goethite was also nano-crystalline, with particle sizes around 10 nm (Figure 2.2 (D)). Figure 2.7 shows the changing XRD patterns during the aging process of Zn-schwertmannite in DI water. The alteration rates of TE bearing schwertmannite in each aging experiment were different. The proportions of final solid products in each experiment are listed in Table 2.5.

During aging in DI water, both Ni and Zn were released during dissolution of schwertmannite, but no release of Cr was detected in the solution. Zn concentration in the solution kept increasing while Ni initially increased but then began to decrease starting at about 15 days, possibly due to re-trapping by neo-formed goethite. Calculation of the final conditions suggested that if the portion of altered schwertmannite released all of the TE it initially contained, then concentrations of Ni, Zn and Cr in the final solution are expected to be 1.9 µg/g, 3.4 µg/g and 8.2 µg/g, respectively. However, the actual concentrations measured in the
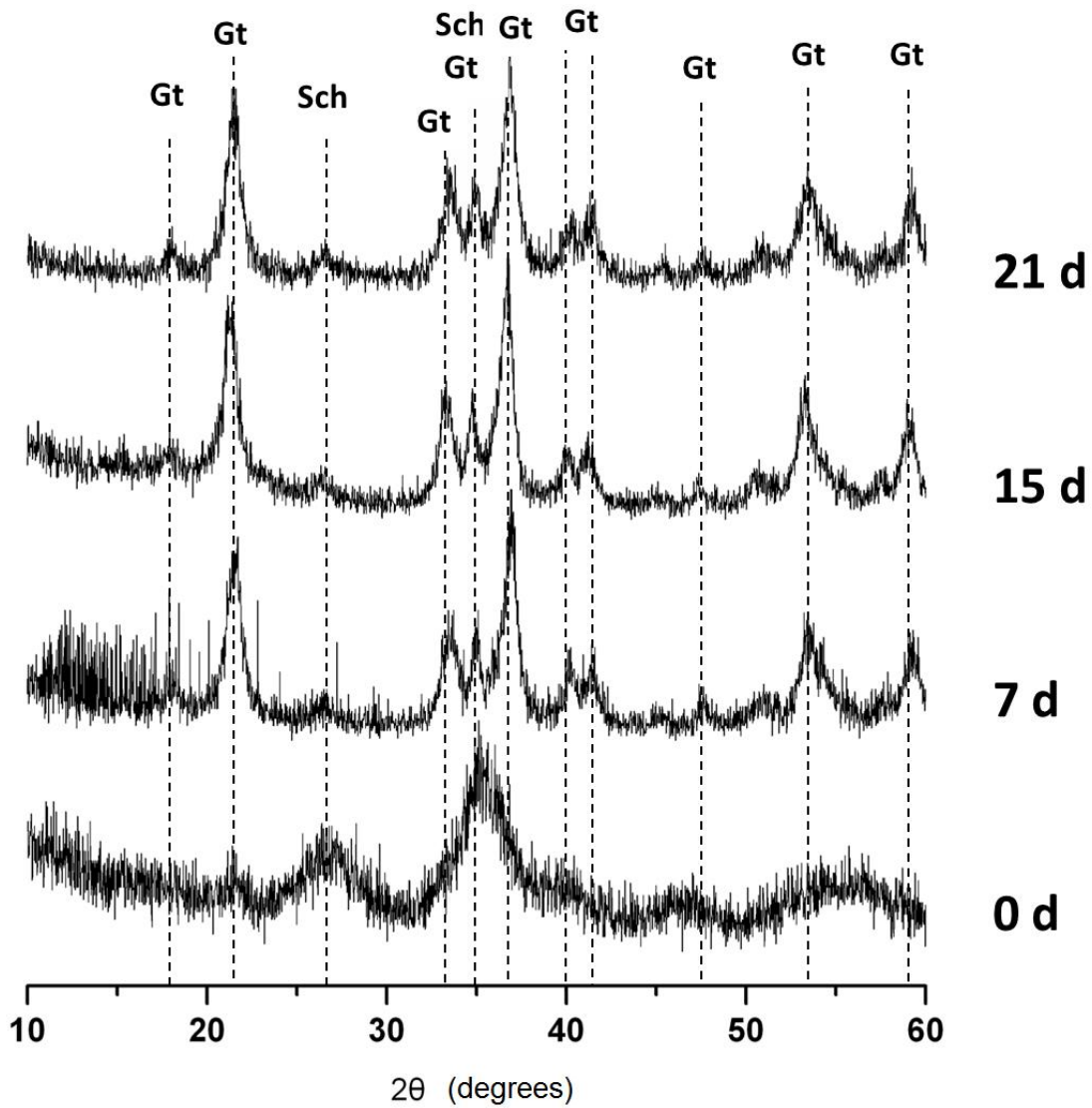
**Figure 2.7.** Powder X-ray diffractograms of the aging experiment of synthetic Zn-bearing schwertmannite aging in DI water. Schwertmannite transformed exclusively to goethite, and H-jarosite was not detected in any of the samples.

solutions were lower than these calculated amounts. In the final solutions, Ni was 0.92 µg/g and Zn was 2.96 µg/g, and Cr was lower than detection limit (DL for Cr = 0.01 µg/g). Therefore, the release of Zn was more complete than Ni (Figure 2.8 (A)). The final solid products had a Ni concentration of 698 µg/g and a Zn concentration of 324 µg/g. On the other hand, the rate of alteration of Cr-schwertmannite was much lower than for Ni- and Zn- schwertmannite, and no obvious release of Cr into the solution was observed.  Accordingly, the concentration of Cr in the solids remained almost unchanged (1.74 wt%).

During aging in the 400 µg/g TE solutions (Figure 2.8 (B); Table 2.5), Ni concentrations varied greatly, over a range of about 200 µg/g in the solution, suggesting that significant amounts of release and re-trapping of Ni may have taken place during the aging process. Over the course of the experiment, Zn in solution behaved similar to Ni but with much less variability. At the end of the experiment, the final concentrations of Ni and Zn were similar in the solution, at 355 µg/g and 347 µg/g respectively. Accordingly, concentration of Ni in the final solids increased from 959 µg/g to 1702 µg/g, and concentration of Zn increased from 1000 µg/g to 1875 µg/g. When calculated based on the proportion of schwertmannite and goethite and initial TE concentration in schwertmannite solids (same calculation discussed above in Section 2.2 for the jarosite to hematite aging experiment), the Ni concentration (2817 µg/g) in goethite is higher than Zn (2458 µg/g). In addition, the solid continually incorporated more trivalent Cr during the course of the aging process resulting in a significant decrease in Cr in the solution (Figure 2.8 (B)). At the end, Cr concentration of the solid increased from initial 1.69 wt% to 2.94 wt%.
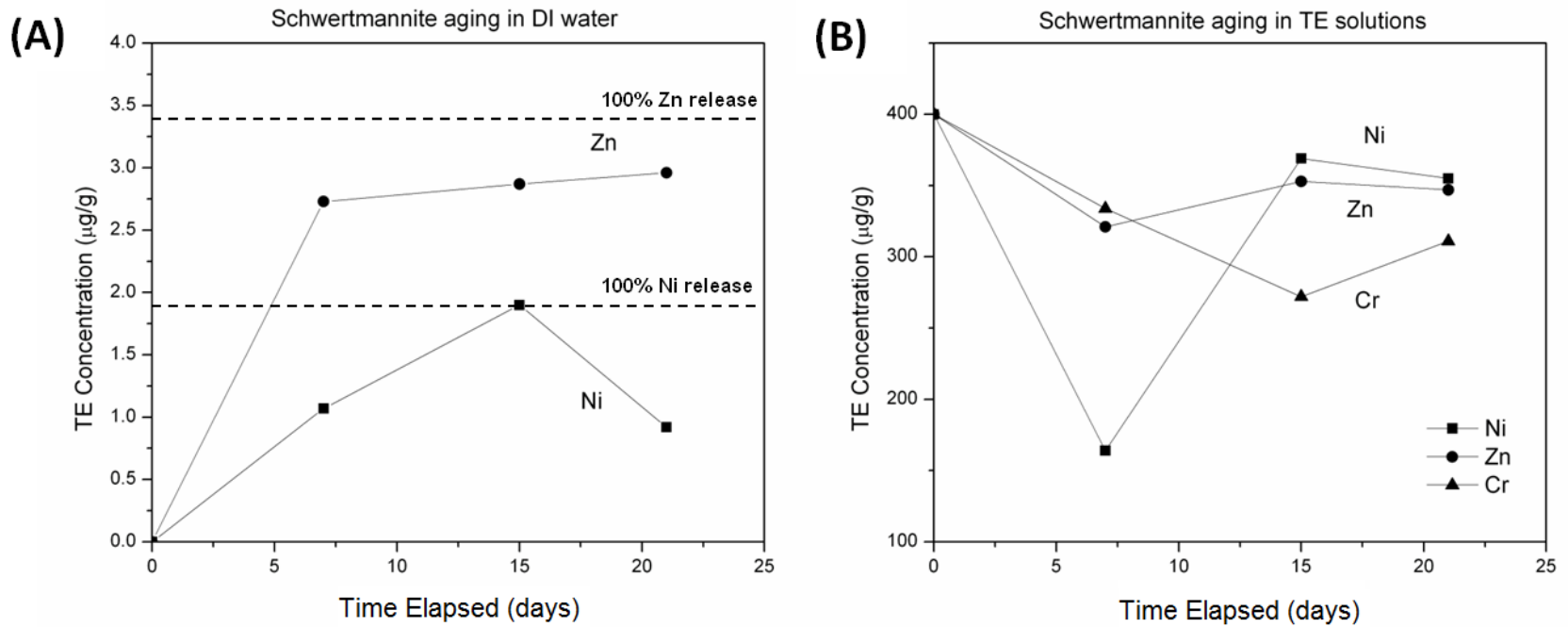
**Figure 2.8.** TE behavior in solution during synthetic TE-bearing schwertmannite to goethite transformation in DI water and TE-bearing solutions. Note that for the DI water aging experiment, Cr in solution was below detection limits throughout. Detection limit for Cr is 0.01 µg/g.

### 2.3.6 TE interaction with schwertmannite and goethite

Generally, TE interactions with schwertmannite and goethite are controlled by both incorporation and surface adsorption. In the case of incorporation, substitutions of Ni, Zn and Cr for Fe (III) in goethite result in stable removal of TE from the solution and constant retention by the solids. Trivalent Cr can substitute for Fe(III) by isomorphous substitution without significantly distorting the mineral structure and form a solid solution $Fe_{1-x}Cr_xOOH$. The upper limit of such Cr-for-Fe substitution is about 12 mol% (Schwertmann and Cornell, 2000). Divalent cations such as Ni can also be incorporated into goethite by substituting for Fe(III) in the octahedral position with a proton capture, forming $NiO_2(OH)_4$ octahedra which locally distorts and opens the mineral structure (Carvalho-E-Silva et al., 2003). Therefore, the upper limit of Ni-for-Fe substitution in goethite is 5 mol% (Singh et al., 2002). At present no data for the upper limit on Zn-for-Fe substitution in goethite has been reported. In addition, no substantial data relevant to TE incorporation into schwertmannite has been reported, and these matters clearly require further work.

Surface adsorption is also a very important mechanism for immobilizing TE from the solution. Ni and Zn sorption may occur in the form of a combination of ion exchange and surface complexation. Generally, low pH results in low TE sorption on geological materials, such as goethite (Ticknor, 1994). However, when combined with excessive $SO_4^{2-}$ anions in the solution, adsorption of TE onto the Fe-oxide surfaces in turn will be significantly enhanced. Although we did not attempt to collect any data confirming sulfate adsorption from our experiment, similar acidic sulfate rich solutions investigated by other researchers provide good analogues to our fluid systems. Fe-oxide surfaces are positively charged under very acidic conditions, and capable of adsorbing large amounts of $SO_4^{2-}$ anion. The adsorbed $SO_4^{2-}$ can then interact with Zn to form ternary surface complexes (Swedlund and Webster, 2001), thus removing it from the solution.

The adsorbed $SO_4^{2-}$ anions can form a continuum of outer- and inner-sphere surface complexes on goethite, which is similar to the structure of schwertmannite (Peak et al., 1999). And the $SO_4$-adsorbed goethite exhibits a greater affinity for Zn, compared to schwertmannite, ferrihydrite or pure goethite (Webster et al., 1998). This trend could also be the case for Ni, based on extrapolation of our experimental results, in which Ni and Zn are both divalent cations. No adsorption data of Cr(III) onto schwertmannite or goethite surfaces have been reported, although Fe-oxides are found to be good sorbents of chromate oxyanion when Cr is in its highest oxidation state of (VI) (e.g., Palmer and Wittbrodt, 1991; Regenspurg and Peiffer, 2005).

In summary, it is clear that Ni, Zn and Cr behave differently during the precipitation of schwertmannite and its subsequent transformation into goethite (Section 2.3.4 and 2.3.5). $SO_4$-adsorbed goethite was the most important sink for Ni and Zn by both enhanced surface adsorption and structural incorporation, especially in the case of Ni. The absolute amount of Ni in mixtures of schwertmannite and goethite is significantly higher than that of Zn. Cr was immobilized by both incorporation and absorption, although the proportion of incorporation is at least an order of magnitude higher than that of adsorption. The amounts of these elements partitioning into the precipitating schwertmannite and goethite were likely in the order: Cr > Ni > Zn.

**2.3.7 TE behavior during goethite to hematite transformation**

We focused only on Ni- and Cr-goethite. Synthetic Ni- and Cr-goethite were both dark brown powders with the color of Cr-goethite being darker. Both samples were crystalline at a size of about 10 nm. After 48 h of heating at 300 ºC, goethite completely altered to crystalline hematite and remained nano-scaled. No residual goethite was detected by XRD (Figure 2.9).

Chemical compositions of synthetic TE bearing goethite and final altered phase hematite are listed in Table 2.6. The synthetic Ni-goethite had 1.94 wt% Ni. After alteration, Ni in the neo-formed hematite was 1.88 wt%. Synthesized Cr-goethite had about 3.89 wt% of Cr. After alteration, the amount of Cr was 5.04 wt% in the resulting hematite. Note that all the altered hematite samples were washed before digestion; therefore, some elements might be leached out during washing. Based on the digestion results, Ni and Fe concentrations of goethite and hematite are within 5% analysis error range, therefore, Ni was not significantly mobilized during the dehydroxylation of goethite. The proportion of Cr in hematite was increased; however, the amount was higher than can be accounted for by loss of water and hydroxyl compound during heating. The apparent discrepancy might be due to greater uncertainty in the treatments of Cr-goethite and Cr-hematite, or some unrecognized analytical issue, although duplicate samples were examined and yielded similar results. In any case, we conclude here that Cr was not significantly mobilized during thermal-transformation from goethite to hematite.

Similar to goethite, which has an upper limit of structural incorporation of Ni at 5.5 mol%, hematite has an upper limit of 5.3 mol% obtained by combustion of metal oxinates (Saragovi et al., 2004). After the transformation to hematite by heating at 230-250 ºC, leaching experiments showed that Ni dissolved congruently with Fe (i.e., constant Fe/Ni ratios), which suggested that surface absorbed Ni might move toward the center of hematite crystals and become more concentrated (Landers and Gilkes, 2007). On the other hand, Cr(III) can substitute for Fe in the goethite structure without the need for charge imbalance compensation; Cr substitution for Fe thus can reach up to 12 mol% in goethite (Schwertmann and Cornell, 2000).
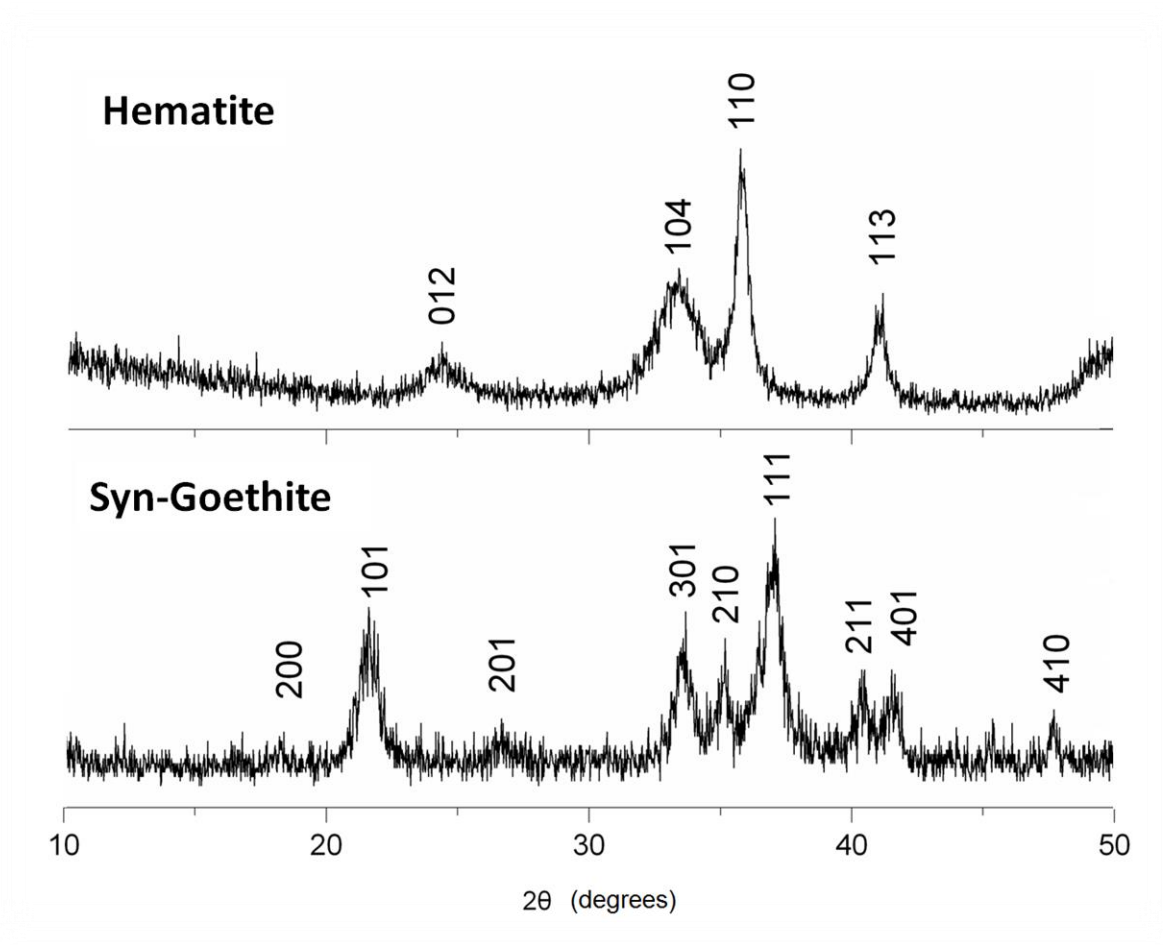
**Figure 2.9.** Powder X-ray diffractograms of synthetic goethite and the hematite yielded after heating at 300 °C for 48 h.

**Table 2.6.** Chemical analysis of synthetic Ni- and Cr-goethite and their hematite products after heat treatment at 300 °C for 48 h.

|  | Ni-Gt | Ni-Hm | Cr-Gt | Cr-Hm |
|---|---|---|---|---|
| M (Wt%) | 1.94 | 1.88 | 3.89 | 5.04 |
| Fe (Wt%) | 52.7 | 55.3 | 51.9 | 54.4 |
| *M/(M+Fe) mol% | 3.4 | 3.1 | 7.5 | 9.2 |

*M represents Ni or Cr in corresponding Gt and Hm samples. Gt = goethite; Hm = hematite.

Comparatively few studies have been reported on the incorporation of Ni and Zn into hematite, partly because the usual wet chemical synthesis methods produce hematite with little or no trace element content (Barrero et al., 2004). Ayub et al. (2001) synthesized Zn-bearing hematite from mixtures of Fe(III) chloride hexahydrate and Zn(II) chloride with aqueous ammonia by hydrothermally processing the suspension in a Teflon-lined autoclave at 200 ℃ and 15 atm. However, the Zn-for-Fe substitution was still very low and attempts to increase the Zn content were unsuccessful. Barrero et al. (2004) applied a method based on the combustion of mixed $Fe(III)_{0.95}$ and $Zn(II)_{0.05}$-oxinates, however, it was still difficult to determine if Zn-for-Fe substitution in hematite had taken place. Sidhu et al. (1980; 1981) suggested that during the thermal transformation of Ni- and Zn-doped magnetites to hematite, Ni and Zn were excluded and formed a surface layer rich in these elements. The exclusion was more pronounced for Zn than Ni, mainly due to the fact that the normally occupied trivalent iron sites in hematite were octahedral, and $Zn^{2+}$ does not have any octahedral crystal-field stabilization energy and may not be incorporated into the hematite lattice because of its large size (0.74Å) and low valency. Indeed, it is possible that all of the Zn migrated to the surface of the particles.

As discussed above, it is obvious that the incorporation of Ni and Zn into hematite was difficult, especially under the aqueous conditions examined. Compared to Ni, Zn is preferentially excluded from the hematite lattice, so that hematite likely contains less Zn than Ni in its structure assuming aqueous conditions where Ni and Zn were initially at the same concentration.

In the case of surface adsorption, some studies have demonstrated that surface adsorptive capacity of Ni and Zn by goethite is significantly higher than for hematite (Novikov et al., 2006). Accordingly, surface adsorbed Ni and Zn may be released during the transformation from goethite to hematite in aqueous conditions. However, there is no substantial data to support this

possibility since it is very difficult to study this alteration under laboratory timescales at low temperature.

When considering TE behavior during the Path 2, discussed in the next section, we assume that goethite is the dominant sink controlling TE behavior and that hematite will inherit the same levels of TE after alteration.  In reality however, it is more likely to be that while the Ni and Zn partitioning patterns may be the same during the goethite to hematite transformation, the absolute TE amounts in hematite are less than in goethite.

**2.3.8 TE behavior during pathways of mineralogical evolution**

In this work, we established three pathways for the transformation from melanterite to hematite in a high ionic strength $MgSO_4$ matrix by oxidation processes.

Path 1:  Melanterite→ Jarosite→ Hematite;

Path 2:  Melanterite → Schwertmannite → Goethite → Hematite;

Path 3:  Melanterite → Schwertmannite → Goethite plus Jarosite→ Hematite.

For Ni, Zn and Cr concentrations of 400 µg/g in the starting solutions, the subsequent removal of the trace elements and approximate partitioning into each mineral component can be calculated based on the experimental results discussed in this study.

In Path 1, jarosite is precipitated directly from the solution, and then transforms to hematite. During this process, Ni concentrations are very low in the jarosite, at about 18 µg/g (Table 2.3). When the jarosite continued to dissolve in a solution with additional Ni, the Ni concentrations in the neo-formed hematite can reach up to 788 µg/g (Table 2.4).  Zn concentration is higher in jarosite than Ni, at about 157 µg/g (Table 2.3), and increases to 2402 µg/g in hematite via dissolution of jarosite (Table 2.4). During the precipitation of jarosite, the Ni and Zn decreased in the solution, by about 100 µg/g and 50 µg/g respectively. During

subsequent transformation, Ni and Zn decreases in the solution were about 100 µg/g (Figure 2.5 (D); Table 2.4). Therefore, for 400 µg/g of initial TE in solutions, Path 1 resulted in relatively minor depletion of Ni and Zn in the solution. Cr(III) can be incorporated at higher levels in jarosite than either Ni or Zn, reaching around 889 µg/g (Table 2.3). During the transformation, Cr is incorporated into neo-formed hematite, and thus hematite has a Cr concentration of about 1.5 wt% (Table 2.4). Cr removal from the solution is very substantial. Cr in the solution decreased about 75 µg/g during jarosite precipitation (Figure 2.3 (C)) and dropped about 270 µg/g during jarosite dissolution (Figure 2.5 (D)), indicating that Cr mobility is much lower than Ni and Zn during such process. The amounts of TE partitioning to jarosite and hematite during this pathway is in the order: Cr > Zn > Ni. Zn is likely at least a factor of two higher than Ni.

In Path 2, schwertmannite and goethite are formed as precursors before transformation to the final stable hematite. During this pathway, Ni is strongly associated with schwertmannite and goethite by both surface adsorption and structural incorporation. In goethite, Ni can reach 8355 µg/g in the solid mixture (Table 2.3; based on 500 µg/g initial Ni of solution). Zn also accumulates in the solids during Fe(II)-oxidation, however, not to the same extent as Ni. Zn in the schwertmannite and goethite mixture is around 1255 µg/g (Table 2.3; based on 500 µg/g initial Zn of solution). For transformation starting with similar Ni and Zn in the original schwertmannite (959 µg/g and 1000 µg/g respectively, Table 2.5), the Ni and Zn in neo-formed goethite was 2817 µg/g and 2458 µg/g respectively, which was more than 2 times higher than in the original schwertmannite. Assuming hematite retains all TE after transformation from goethite, the final hematite would then have a higher concentration of Ni than Zn. Note that Ni exhibited a higher affinity for schwertmannite than did Zn during the precipitation of schwertmannite (discussed in Section 2.3.4; Figure 2.6 (A) and (B)), and so the initially different

concentrations of Ni and Zn in the starting schwertmannite would further enhance the difference. Therefore, during Path 2, the resulting hematite would have much higher Ni than Zn.

On the other hand, Cr partitions into schwertmannite and goethite to a greater degree than into jarosite. Cr in the precipitated schwertmannite is about 3.95 wt%. After transformation to goethite with additional Cr in the ambient solution, the Cr concentration of neo-formed goethite reaches up to 14.19 wt% (Table 2.5), much higher than the original 1.69 wt% in the schwertmannite. Hematite would very likely inherit the Cr from its precursor goethite since Cr(III) can readily substitute for Fe(III) and remain relatively stable during such phase transformation.

Based on the combination of data shown in Figs. 5D and 6, Cr removal from solution is very substantial, about 200 µg/g from its initial 300 µg/g. Ni and Zn varied in the solution in the range of 300 µg/g and 200 µg/g respectively comparing to their initial 500 µg/g. The relatively rapid removal of Cr is similar in both Path 1 and Path 2.

Path 3, which effectively represents a combination of Paths 1 and 2, exhibits intermediate trace element behavior.

Each of the mineralogical pathways, along with the experimental approaches used to establish it (i.e. oxidation, aging, heating), and the relative order of trace element partitioning into each newly formed mineral phase are summarized schematically in Figure 2.10.

## 2.4 Implications for Mars

One of the major results from the rover Opportunity is that groundwater-mediated diagenesis may have occurred within the evaporite-bearing sedimentary rocks at Meridiani
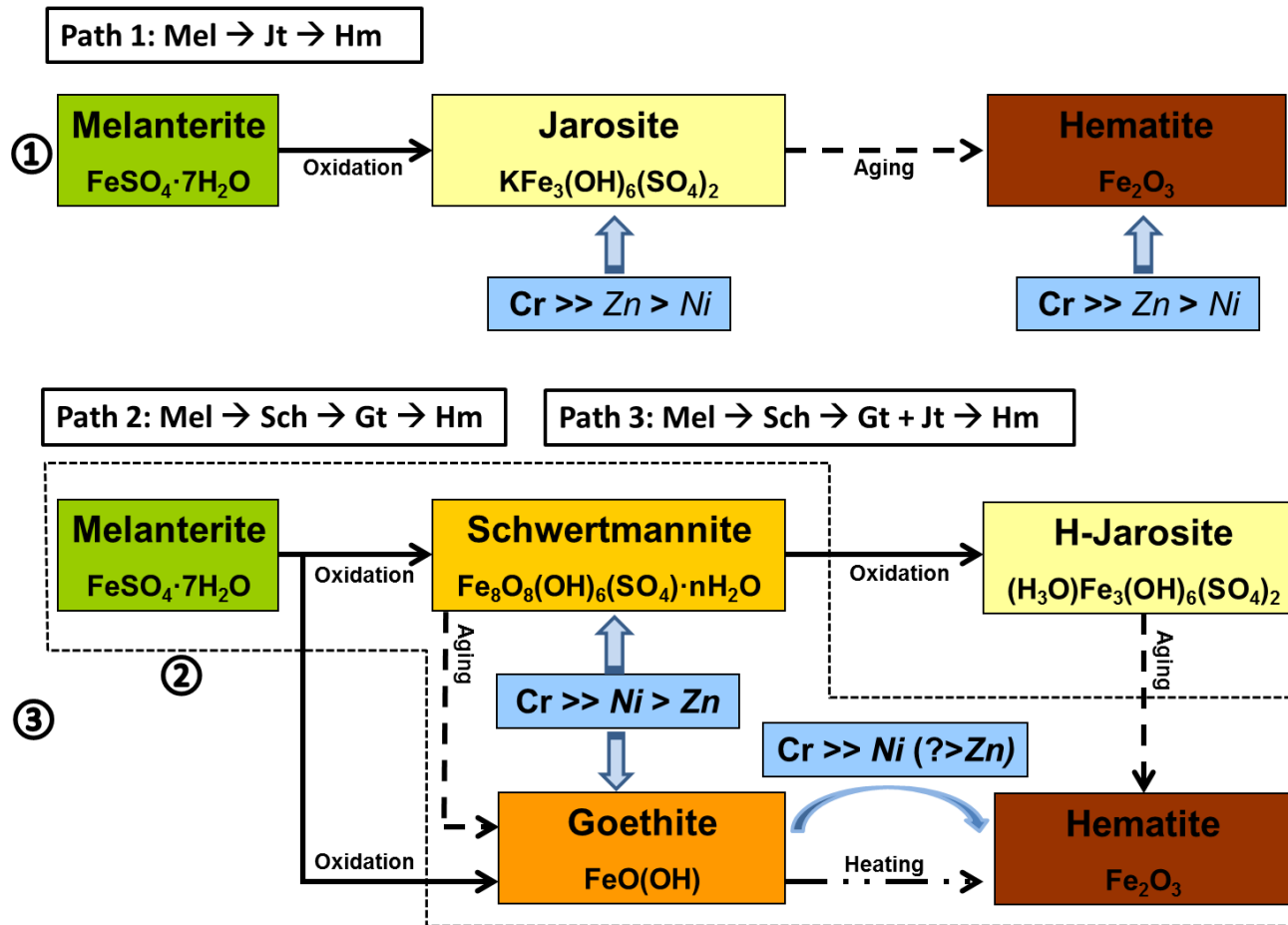
**Figure 2.10.** Schematic outline of mineralogical evolution pathways established in this study, and the relative order of trace element partitioning into each mineral phase suggested by the experimental results described in this study. Different arrows indicate oxidation experiments (solid arrow), aging experiments (simple dashed arrow) and heating experiments (dash-dot arrow). Circled numbers represent pathways described in the text. Path 2 is a part of Path 3, and is outlined by the dashed polygon in the Path 3 area. The main mechanisms accounting for trace element partitioning behavior are labeled by the font of each element name, where **bold** represents incorporation, *italic* represents adsorption/desorption, and ***bold italic*** represents uncertain or both mechanisms.

Planum. However, it is still unclear when the oxidation of Fe(II) occurred during Martian history and whether jarosite or goethite already existed prior to the diagenetic events. Nevertheless, oxidation of Fe(II) can occur as part of the diagenesis process by leaching soluble Fe-bearing sulfate components (e.g., melanterite) and account for the majority of Fe-bearing secondary phases detected at Meridiani Planum (i.e. hematite and jarosite) (e.g., McLennan et al., 2005; Tosca et al., 2005, 2008; Sefton-Nash and Catling, 2008). Goethite, a missing piece from Meridiani, could also be included in such a model, acting as a precursor of hematite.

An important concern about the partitioning behavior of these trace elements is whether they are incorporated into or just adsorbed onto the precipitates, since adsorbed cations are potentially much more mobile in terrestrial sedimentary systems and not likely to be retained during aqueous diagenesis. However, this concern might not matter as much on Mars. The occurrence of opaline silica (McLennan et al., 2005) and Fe-Mg-smectites (McLennan et al., 2005; Mustard et al., 2008) in ancient sedimentary deposits suggest that Martian sedimentary rocks are diagenetically under-developed, such that relatively little liquid water interaction has taken place since the time of their formation (Tosca and Knoll, 2009). Therefore, in a case of such limited liquid water interaction after formation of the current mineral assemblages, trace elements, regardless of whether initially being held by either incorporation or adsorption would be more likely to remain in place associated with the precipitates and thus contribute to the bulk concentration measured by the MER Opportunity's APXS.

The pathways of iron sulfate oxidation are mainly controlled by initial pH, which effectively translates to the initial ratio of water to Fe-sulfates, a value that would have been controlled by porosity, permeability and the mass fraction of melanterite (or other Fe-sulfates) that was present in the initial evaporite assemblages (Tosca et al., 2008). When the initial ratio of

water to melanterite is relatively high (~120 in our experiments), the resulting conditions are characterized by pH >3, and schwertmannite, goethite and/or jarosite should precipitate and subsequently convert to hematite. Accumulations of Ni, Zn and Cr into goethite are substantial and such partitioning patterns may in turn be inherited by hematite after transformation. Therefore, if Ni, Zn and Cr are sufficiently high in the starting solution (a reasonable likelihood if the evaporating solution was derived from acidic alteration of Martian basalt; Tosca et al., 2004), high concentrations of these elements could be expected in hematite. Ni would accumulate more than Zn during such processes when they start at the same concentration in the initial solution.

If the initial ratio of water to melanterite is relatively low (~6 in our experiments), the resulting solution will begin with pH < 3 and jarosite would precipitate directly and in due course could subsequently transform to hematite. Jarosite is not a good sink for divalent Ni and Zn, and even trivalent Cr concentrations are lower in jarosite than in schwertmannite and goethite. Hematite formation via dissolution of jarosite in TE-bearing brines would accumulate more TE in hematite than in jarosite. However, if this is the case, the resulting Zn concentration in hematite should be equal or higher than Ni, for a system with an initial Ni/Zn ratio of 1, a value similar to the average Martian crust (see below).

At Meridiani Planum, Ni and Zn behavior in fluids derived from acid alteration of basaltic rocks and subsequent evaporation processes is not well constrained. For the discussion below, it is assumed that these two divalent elements behaved similarly prior to Fe-oxidation processes, and that they started at the same concentrations in the initial fluid. Note that the Martian crust is estimated to have similar levels of Ni and Zn, at 337 ppm and 320 ppm, respectively (Taylor and McLennan, 2009). Under this scenario, the much higher Ni compared to Zn in the Meridiani

hematite concretions (Figure 2.1) can be explained by the evolution Path 2, involving goethite. If this is the case, then any additional high Ni sources would not be necessary since Fe-oxidation processes alone could account for the high Ni and moderate Zn distribution patterns in hematite spherules. Nevertheless, given the occurrence of Fe-Ni meteorites on the Meridiani surface (Schröder et al., 2008), addition of any extra meteoritic components would further elevate Ni over Zn.

Because of the lack of goethite in the Meridiani outcrop (Klingelhöfer et al., 2004; Clark et al., 2005), it is still debatable if goethite ever formed from the Martian brines, or whether the goethite-to-hematite conversion took place. However, we cannot rule out this possibility. In the acidic and sulfate rich brine at Meridiani, the nature of goethite is expected to be nanocrystalline since this is the most common occurrence of goethite on Earth under such conditions (Cornell and Schwertmann, 2003; Waychunas et al., 2005). Langmuir (1971) demonstrated that nano-particle goethite is thermodynamically unstable relative to coarse-grained hematite at all relative humidities and temperatures from 0 to 100 °C. Therefore, nano-particle goethite is indeed unlikely to have survived under likely prevailing Martian conditions. The rates of the goethite-hematite conversion are typically too slow to study experimentally over laboratory timescales at low temperatures and pressures. On the other hand, on Earth, goethite dehydration may occur fairly rapidly at the surface of dry, sun baked soils at temperatures lower than 100 °C (Langmuir, 1971), which is a possible environment of the Martian surface. Kinetically, dehydration of goethite may not compete with dissolution of jarosite or re-crystallization of amorphous oxyhydroxides. Nevertheless, it is still possible that the nano-crystalline goethite serves as precursor to facilitate hematite formation under low-temperature high ionic strength acid sulfate conditions (Tosca et al., 2008).

On the other hand, if the hematite concretions were formed by dissolution of jarosite as shown in Path 1, Ni concentrations in the spherules could not readily be accounted for by this process alone, and Zn would be expected to be equal to or higher in concentration than Ni in the spherules. Therefore, to explain the higher level of Ni than Zn observed in hematite-rich soils, a higher initial Ni/Zn ratio than adopted in our fluids would be needed, perhaps by originally high Ni magma in this region, or through addition of meteoritic components.

Mobility of these trace elements is greatly enhanced by decreasing pH, and this is particularly true for divalent Ni and Zn. However, precipitation of all of the Fe-oxide phases, including jarosite, results in efficient removal of Cr(III) from solution due to substitution for Fe(III) and thus greatly constrains the mobility of Cr. Assuming equal amounts of Cr as for Ni and Zn in the starting solutions, Cr was at least two orders of magnitude higher in all of Fe-oxides and jarosite than Ni and Zn from our experiments. Given that Cr concentrations are within an order of magnitude of Ni and Zn in rocks and soils measured by Opportunity (Table 2.1), Cr concentration would need to be much lower than Ni and Zn in the initial diagenetic fluids. Note that Cr abundance in the Martian crust is estimated to be 2600 ppm (Taylor and McLennan, 2009), significantly higher than Ni and Zn, therefore such lower ratios of Cr/Ni and Cr/Zn in the diagenetic fluids might suggest that mobility of Cr was greatly limited during basalt weathering and evaporation processes prior to diagenesis compared to Ni and Zn.

## 2.5 Conclusions

In this study, the behavior of Ni(II), Zn(II) and Cr(III) during the melanterite to hematite oxidative transformation via three pathways involving jarosite, schwertmannite and goethite were evaluated in an acidic $MgSO_4$ saturated matrix. The experimental approaches were

designed to simulate groundwater recharge diagenesis events after evaporite deposition and infiltration of water into sediments under conditions of high ionic strength.

Assuming a system that started with the same concentrations in the initial solution, our results demonstrate that final amounts of Ni, Zn and Cr in hematite via different pathways are very different (Figure 2.10). In Path 1 (melanterite → jarosite → hematite), partitioning of Ni, Zn and Cr into jarosite and hematite (formed by dissolution of jarosite) is most likely in the order: Cr > Zn > Ni. In Path 2 (melanterite → schwertmannite → goethite → hematite), schwertmannite and goethite exhibited strong affinities for Ni and Zn. During such a pathway, Ni should accumulate more than Zn by at least a factor of two, and partitioning of Ni, Zn and Cr into the hematite is most likely in the order: Cr > Ni > Zn. Path 3 (melanterite → schwertmannite → goethite plus jarosite → hematite), which effectively represents a combination of Path 1 and 2, could exhibit intermediate trace element behavior depending on the proportion of goethite and jarosite in the mixtures.

Given that the Martian crust has similar levels of Ni and Zn (337 ppm and 320 ppm; (Taylor and McLennan, 2009), the elevated Ni over Zn observed in Meridiani hematitic spherule-bearing samples can be explained best by Path 2 via goethite, without need for additional high Ni sources in this region. Although the lack of goethite at Meridiani renders it uncertain if goethite ever served as a precursor to facilitate hematite formation, dehydration of nano-crystalline goethite is thermodynamically favored and thus cannot be ruled out. However, if hematitic concretions were formed by dissolution of jarosite (Path 1), then Ni concentrations in the spherules could not readily be accounted for by this process alone and a higher initial Ni/Zn ratio than adopted in our initial fluids would be needed, contributed by high Ni magmas or Fe-Ni meteoritic components. The Cr(III), when assumed to be in equal amounts as Ni and Zn in the

initial solution, accumulated at least two orders of magnitude higher than Ni and Zn in all Fe(III)-phases. Given that Cr concentrations are within about an order of magnitude of Ni and Zn in samples measured by the Opportunity rover (Table 2.1), Cr concentrations may have been much lower than Ni and Zn in the initial diagenetic fluids. Significant lower ratios of Cr/Ni and Cr/Zn in the diagenetic fluids than the Martian crustal abundances suggests that mobility of Cr was greatly limited during basalt weathering or evaporation processes prior to diagenesis compared to Ni and Zn.

# References

Acero, P., Ayora, C., Torrento, C., Nieto, J. M. (2006) The behavior of trace elements during schwertmannite precipitation and subsequent transformation into goethite and jarosite. *Geochim. Cosmochim. Acta*, **70**, 4130-4139.

Ayub, I., Berry, F. J., Bilsborrow, R. L., Helgason, O., Mercader, R. C., Moore, E. A., Stewart, S. J., Wynn, P. G. (2001) Influence of zinc doping on the structural and magnetic properties of alpha-$Fe_2O_3$. *J. Solid State Chem.,* **156**, 408-414.

Barrero, C. A., Arpe, J., Sileo, E., Sanchez, L. C., Zysler, R., Saragovi, C. (2004) Ni- and Zn-doped hematite obtained by combustion of mixed metal oxinates. *Physica. B.,* **354**, 27-34.

Barrón, V., Torrent, J., Greenwood, J. P. (2006) Transformation of jarosite to hematite in simulated Martian brines. *Earth Planet. Sci. Lett.,* **251**, 380-385.

Bibring, J. P., Arvidson, R. E., Gendrin, A., Gondet, B., Langevin, Y., Le Mouelic, S., Mangold, N., Morris, R. V., Mustard, J. F., Poulet, F., Quantin, C., Sotin, C. (2007) Coupled ferric oxides and sulfates on the Martian surface. *Science,* **317**, 1206-1210.

Bigham, J. M., Schwertmann, U., Pfab, G. (1996) Influence of pH on mineral speciation in a bioreactor simulating acid mine drainage. *Appl. Geochem.,* **11**, 845-849.

Brückner, J., Dreibus, G., Gellert, R., Squyres, S., Wänke, H., Yen, A., Zipfel, J. (2008) Mars Exploration Rovers: Chemical composition by the APXS. In *The Martian Surface: Composition, mineralogy, and physical properties* (ed. J. Bell). Cambridge Univ. Press, Cambridge, pp. 58-101.

Carvalho-E-Silva, M. L., Ramos, A. Y., Tolentino, H. C. N., Enzweiler, J., Netto, S. M., Alves, M. D. C. M. (2003) Incorporation of Ni into natural goethite: An investigation by X-ray absorption spectroscopy. *Am. Mineral.,* **88**, 876-882.

Clark, B. C., Morris, R. V., McLennan, S. M., Gellert, R., Jolliff, B., Knoll, A. H., Squyres, S. W., Lowenstein, T. K., Ming, D. W., Tosca, N. J., Yen, A., Christensen, P. R., Gorevan, S., Brückner, J., Calvin, W., Dreibus, G., Farrand, W., Klingelhöefer, G., Waenke, H., Zipfel, J., Bell, J. F., Grotzinger, J., McSween, H. Y., Rieder, R. (2005) Chemistry and mineralogy of outcrops at Meridiani Planum. *Earth Planet. Sci. Lett.,* **240**, 73-94.

Cornell, R. M. and Schwertmann, U. (2003) *The Iron Oxides: Structure, Properties, Reactions, Occurrences and Uses.* John Wiley, Weinheim, Germany. pp. 607.

Dutrizac, J. E. and Chen, T. T. (1984) A mineralogical study of the jarosite phase formed during the autoclave leaching of zinc concentrate. *Can. Metall. Quart.,* **23**, 147-157.

Dutrizac, J. E. and Chen, T. T. (2004) Factors affecting the incorporation of cobalt and nickel in jarosite-type compounds. *Can. Metall. Quart.,* **43**, 305-319.

Dutrizac, J. E. and Jambor, J. L. (2000) Jarosites and their application in hydrometallurgy. In *Reviews in Mineralogy and Geochemistry,* vol. **40** (eds. C. N. Alpers, J. L. Jambor, D. K. Nordstrom). Mineralogical Society of America. pp. 405-452.

Dutrizac, J. E. and Oreilly, J. B. (1984) The origins of zinc and brass. *Cim. Bull.,* **77**, 69-73.

Gellert, R., Rieder, R., Anderson, R. C., Brückner, J., Clark, B. C., Dreibus, G., Economou, T., Klingelhöfer, G., Lugmair, G. W., Ming, D. W., Squyres, S. W., d'Uston, C., Wänke, H., Yen, A., Zipfel, J. (2004) Chemistry of rocks and soils in Gusev crater from the alpha particle x-ray spectrometer. *Science,* **305**, 829-832.

Golden, D. C., Ming, D. W., Morris, R. V., Graff, T. G. (2008) Hydrothermal synthesis of hematite spherules and jarosite: Implications for diagenesis and hematite spherule formation in sulfate outcrops at Meridiani Planum, Mars. *Am. Mineral.,* **93**, 1201-1214.

Grotzinger, J. P., Arvidson, R. E., Bell, J. F., Calvin, W., Clark, B. C., Fike, D. A., Golombek, M., Greeley, R., Haldemann, A., Herkenhoff, K. E., Jolliff, B. L., Knoll, A. H., Malin, M., McLennan, S. M., Parker, T., Soderblom, L., Sohl-Dickstein, J. N., Squyres, S. W., Tosca, N. J., Watters, W. A. (2005) Stratigraphy and sedimentology of a dry to wet eolian depositional system, Burns formation, Meridiani Planum, Mars. *Earth Planet. Sci. Lett.,* **240**, 11-72.

Hurowitz, J. A., Fischer, W. W., Tosca, N. J., Milliken, R. E. (2010) Origin of acidic surface waters and the evolution of atmospheric chemistry on early Mars. *Nature Geosci.,* **3**, doi:10.1038/NGEO831.

Hurowitz, J. A., Tosca, N. J., Dyar, M. D. (2009) Acid production by $FeSO_4$ center dot $nH(2)O$ dissolution and implications for terrestrial and martian aquatic systems. *Am. Mineral.,* **94**, 409-414.

Jönsson, J., Persson, P., Sjoberg, S., Lovgren, L. (2005) Schwertmannite precipitated from acid mine drainage: Phase transformation, sulphate release and surface properties. *Appl. Geochem.,* **20**, 179-191.

Klingelhöfer, G., Morris, R. V., Bernhardt, B., Schroder, C., Rodionov, D. S., de Souza, P. A., Yen, A., Gellert, R., Evlanov, E. N., Zubkov, B., Foh, J., Bonnes, U., Kankeleit, E., Gutlich, P., Ming, D. W., Renz, F., Wdowiak, T., Squyres, S. W., Arvidson, R. E.

(2004) Jarosite and hematite at Meridiani Planum from Opportunity's Mössbauer spectrometer. *Science,* **306**, 1740-1745.

Landers, M. and Gilkes, R. J. (2007) Dehydroxylation and dissolution of nickeliferous goethite in New Caledonian lateritic Ni ore. *Appl. Clay Sci.,* **35**, 162-172.

Langmuir, D. (1971) Particle size effect on reaction goethite = hematite + water. *Am. J. Sci.,* **271**, 147-156.

McLennan, S. M., Bell, J. F., Calvin, W. M., Christensen, P. R., Clark, B. C., de Souza, P. A., Farmer, J., Farrand, W. H., Fike, D. A., Gellert, R., Ghosh, A., Glotch, T. D., Grotzinger, J. P., Hahn, B., Herkenhoff, K. E., Hurowitz, J. A., Johnson, J. R., Johnson, S. S., Jolliff, B., Klingelhöfer, G., Knoll, A. H., Learner, Z., Malin, M. C., McSween, H. Y., Pocock, J., Ruff, S. W., Soderblom, L. A., Squyres, S. W., Tosca, N. J., Watters, W. A., Wyatt, M. B., Yen, A. (2005) Provenance and diagenesis of the evaporite-bearing Burns formation, Meridiani Planum, Mars. *Earth Planet. Sci. Lett.,* **240**, 95-121.

Morris, R. V., Ming, D. W., Graff, T. G., Arvidson, R. E., Bell, J. F., Squyres, S. W., Mertzman, S. A., Gruener, J. E., Golden, D. C., Le, L., Robinson, G. A. (2005) Hematite spherules in basaltic tephra altered under aqueous, acid-sulfate conditions on Mauna Kea volcano, Hawaii: Possible clues for the occurrence of hematite-rich spherules in the Burns formation at Meridiani Planum, Mars. *Earth Planet Sci. Lett.,* **240**, 168-178.

Mustard, J. F., Murchie, S. L., Pelkey, S. M., Ehlmann, B. L., Milliken, R. E., Grant, J. A., Bibring, J. P., Poulet, F., Bishop, J., Dobrea, E. N., Roach, L., Seelos, F., Arvidson, R. E., Wiseman, S., Green, R., Hash, C., Humm, D., Malaret, E., McGovern, J. A., Seelos, K., Clancy, T., Clark, R., Des Marais, D., Izenberg, N., Knudson, A., Langevin, Y., Martin, T., McGuire, P., Morris, R., Robinson, M., Roush, T., Smith, M., Swayze, G., Taylor, H., Titus, T., Wolff, M. (2008) Hydrated silicate minerals on mars observed by the Mars reconnaissance orbiter CRISM instrument. *Nature,* **454**, 305-309.

Novikov, G. V., Vikent'ev, I. V., Bogdanova, O. Y. (2006) Sorption of heavy metal cations by low-temperature deposits of Pacific hydrothermal fields. *Geol. Ore Deposit,* **48**, 304-325.

Palme, H. and Jones, A. (2003) Solar system abundances of the elements. In *Treatise on Geochemistry* (eds. H. D. Holland and K. K. Turekian), Elsevier, vol. **1**, Section 1.03, Table 3, pp. 49.

Palmer, C. D. and Wittbrodt, P. R. (1991) Processes affecting the remediation of chromium-contaminated sites. *Environ. Health Persp.,* **92**, 25-40.

Papike, J. J., Karner, J. M., Shearer, C. K. (2006) Comparative planetary mineralogy: Implications of martian and terrestrial jarosite. A crystal chemical perspective. *Geochim. Cosmochim. Acta,* **70**, 1309-1321.

Patterson, A. L. (1939) The Scherrer Formula for X-ray particle size determination. *Phys. Rev.,* **56**, 978-982.

Peak, D., Ford, R. G., Sparks, D. L. (1999) An in situ ATR-FTIR investigation of sulfate bonding mechanisms on goethite. *J. Colloid. Interf. Sci.,* **218**, 289-299.

Regenspurg, S. and Peiffer, S. (2005) Arsenate and chromate incorporation in schwertmannite. *Appl. Geochem.,* **20**, 1226-1239.

Rieder, R., Gellert, R., Anderson, R. C., Brückner, J., Clark, B. C., Dreibus, G., Economou, T., Klingelhöffer, G., Lugmair, G. W., Ming, D. W., Squyres, S. W., d'Uston, C., Wänke, H., Yen, A., Zipfel, J. (2004) Chemistry of rocks and soils at Meridiani Planum from the alpha particle X-ray spectrometer. *Science,* **306**, 1746-1749.

Saragovi, C., Arpe, J., Sileo, E., Zysler, R., Sanchez, L. C., Barrero, C. A. (2004) Changes in the structural and magnetic properties of Ni-substituted hematite prepared from metal oxinates. *Phys. Chem. Miner.,* **31**, 625-632.

Schröder, C., Rodionov, D. S., McCoy, T. J., Jolliff, B. L., Gellert, R., Nittler, L. R., Farrand, W. H., Johnson, J. R., Ruff, S. W., Ashley, J. W., Mittlefehldt, D. W., Herkenhoff, K. E., Fleisher, I., Haldemann, A. F., Klingelhöfer, G., Ming, D. W., Morris, R. V., de Souza, P.A., Squyres, S. W., Weitz, C., Yen, A., Zipfel, J., Economou, T. (2008) Meteorites on Mars observed with the Mars Exploration rovers. *J. Geophys. Res.,* **113**, E06S22, doi: 10.1029/2007JE002990.

Schwertmann, U. and Cornell, R. M. (2000) *Iron Oxides in the Laboratory: Preparation and Characterization,* second, completely revised and extended edition. Wiley-Vch, Weinheim.

Sefton-Nash, E. and Catling, D. C. (2008) Hematitic concretions at Meridiani Planum, Mars: Their growth timescale and possible relationship with iron sulfates. *Earth Planet. Sci. Lett.,* **269**, 365-375.

Sidhu, P. S., Gilkes, R. J., Posner, A. M. (1980) Behavior of Co, Ni, Zn, Cu, Mn, and Cr in Magnetite during Alteration to Maghemite and Hematite. *Soil Sci. Soc. Am. J.*, **44**, 135-138.

Sidhu, P. S., Gilkes, R. J., Posner, A. M. (1981) Oxidation and Ejection of Nickel and Zinc from Natural and Synthetic Magnetites. *Soil Sci. Soc. Am. J.,* **45**, 641-644.

Singh, B., Sherman, D. M., Gilkes, R. J., Wells, M. A., Mosselmans, J. F. W. (2002) Incorporation of Cr, Mn and Ni into goethite (alpha-FeOOH): Mechanism from extended X-ray absorption fine structure spectroscopy. *Clay Miner.,* **37**, 639-649.

Squyres, S. W., Knoll, A. H., Arvidson, R. E., Ashley, J. W., Bell, J. F., Calvin, W. M., Christensen, P. R., Clark, B. C., Cohen, B. A., de Souza, P. A., Edgar, L., Farrand, W. H., Fleischer, I., Gellert, R., Golombek, M. P., Grant, J., Grotzinger, J., Hayes, A., Herkenhoff, K. E., Johnson, J. R., Jolliff, B., Klingelhöfer, G., Knudson, A., Li, R., Mccoy, T. J., McLennan, S. M., Ming, D. W., Mittlefehldt, D. W., Morris, R. V., Rice, J. W., Schroder, C., Sullivan, R. J., Yen, A., Yingst, R. A. (2009) Exploration of Victoria Crater by the Mars Rover Opportunity. *Science,* **324**, 1058-1061.

Swedlund, P. J. and Webster, J. G. (2001) Cu and Zn ternary surface complex formation with $SO_4$ on ferrihydrite and schwertmannite. *Appl. Geochem.,* **16**, 503-511.

Taylor S. R. and McLennan S. M. (2009) *Planetary Crusts: Their Composition, Origin, and Evolution.* Cambridge Uni. Press, Cambridge. pp. 404.

Ticknor, K. V. (1994) Sorption of nickel on geological-materials. *Radiochim. Acta,* **66-7**, 34-348.

Tosca, N. J., McLennan, S. M., Clark, B. C., Grotzinger, J. P., Hurowitz, J. A., Knoll, A. H., Schröder, C. and Squyres, S. W. (2005) Geochemical modeling of evaporation processes on Mars: Insight from the sedimentary record at Meridiani Planum. *Earth Planet. Sci. Lett.,* **240**, 122-148.

Tosca, N. J., McLennan, S. M., Lindsley, D. H. and Schoonen, M. A. A. (2004) Acid-sulfate weathering of synthetic Martian basalt: The acid fog model revisited. *J. Geophys. Res.,* **109**, E05003, doi:10.1029/2003JE002218.

Tosca, N. J. and Knoll, A. H. (2009) Juvenile chemical sediments and the long term persistence of water at the surface of Mars. *Earth Planet. Sci. Lett.,* **286**, 379-386.

Tosca, N. J., McLennan, S. M., Dyar, M. D., Sklute, E. C., Michel, F. M. (2008) Fe oxidation processes at Meridiani Planum and implications for secondary Fe mineralogy on Mars. *J. Geophys. Res.,* **113**, E05005, doi:10.1029/2007JE003019.

Waychunas, G. A., Kim, C. S., Banfield, J. F. (2005) Nanoparticulate iron oxide minerals in soils and sediments: unique properties and contaminant scavenging mechanisms. *J. Nanopart. Res.,* **7**, 409-433.

Webster, J. G., Swedlund, P. J., Webster, K. S. (1998) Trace metal adsorption onto an acid mine drainage iron(III) oxy hydroxy sulfate. *Environ. Sci. Technol.,* **32**, 1361-1368.

Yen, A. S., Mittlefehldt, D. W., McLennan, S. M., Gellert, R., Bell, J. F., McSween, H. Y., Ming, D. W., McCoy, T. J., Morris, R. V., Golombek, M., Economou, T., Madsen, M. B., Wdowiak, T., Clark, B. C., Jolliff, B. L., Schroder, C., Brückner, J., Zipfel, J., Squyres, S. W. (2006) Nickel on Mars: Constraints on meteoritic material at the surface. *J. Geophys. Res.,* **111**, E12S11, doi: 10.1029/2006JE002797.

Zolotov, M. Y. and Shock, E. L. (2005) Formation of jarosite-bearing deposits through aqueous oxidation of pyrite at Meridiani Planum, Mars. *Geophys. Res. Lett.,* **32**, L21203, doi: 10.1029/2005GL024253.

# Chapter 3: Behavior of Bromide, Chloride and Phosphate during Low Temperature Aqueous Fe(II) Oxidation Processes on Mars

**Abstract**

The behaviors of bromide, chloride and phosphate were studied experimentally under previously proposed Martian diagenetic conditions, involving jarosite ($KFe_3(OH)_6(SO_4)_2$), goethite ($\alpha$-FeOOH) and hematite ($\alpha$-$Fe_2O_3$). Experiments evaluated (1) the behavior of $Cl^-$/$Br^-$ with and without aqueous phosphate during oxidation of $Fe^{2+}$ to $Fe^{3+}$, (2) the stability of halogen-bearing jarosite, and (3) the uptake of $Cl^-$, $Br^-$, $H_2PO_4^-$ and $SO_4^{2-}$ by halogen-free -hematite, -goethite, and -jarosite through adsorption. Our results demonstrate that when precipitated from a solution in which $Cl^-$ is higher than $Br^-$, jarosite preferentially incorporated at least an order of magnitude more $Br^-$ than $Cl^-$. Such enrichment of $Br^-$ over $Cl^-$ in the solids compared to initial solutions suggests that jarosite could be a host for elevated Br on the Martian surface, and the fluids from which jarosite forms could be depleted in $Br^-$ with respect to $Cl^-$. Moreover, the incorporation of halogens in jarosite would affect its stability during aqueous alteration, and the dissolution rates of four types of jarosite at both 25 ℃ and 70 ℃ were in the same order: Br,Cl-bearing > Br-only > halogen-free > Cl-only. In addition, competitive adsorption of $Cl^-$, $Br^-$, $SO_4^{2-}$

and $H_2PO_4^-$ on halogen-free -hematite, -goethite and -jarosite demonstrates that in a sulfate-dominant aqueous system, $Cl^-$, $Br^-$ and $H_2PO_4^-$ could not compete with $SO_4^{2-}$. This observation suggests that the adsorption may not result in an enrichment of phosphate or halogens in Fe oxides in a sulfate-dominant aqueous system like Meridiani Planum, consistent with the absence of significant correlations of Cl and P with nanoparticle Fe oxides found in Martian soils.


## 3.1 Introduction

Characterizing the geochemistry of chlorine, bromine, and phosphorus during a variety of sedimentary alteration processes is essential for understanding their distributions on the Martian surface and provides constraints on brine evolution and aqueous history of the red planet. In sedimentary systems, anions $Cl^-$ and $Br^-$ are especially important, due to their large-scale transfer capability into aqueous environments (Shilling et al., 1978). The aqueous geochemistry of phosphorus on Mars is also intriguing due to its potential for supporting prebiotic synthesis, early microbial nutrition and space-based agriculture (Mautner and Sinaj, 2002).

The Br concentrations of the abraded (or Rock Abrasion Tool (RAT)ed) rock samples at Meridiani Planum range from 35 to 471 ppm (Sols 11-1481), and Cl/Br molar ratios range from 40 to 1094 (e.g., Brückner et al., 2008). Such data were obtained by the Opportunity rover using its Rock Abrasion Tool (RAT) to grind rock surfaces to expose lesser weathered or unweathered interiors before Alpha Particle X-ray Spectrometer (APXS) analyses and thus represent the best measure of the original chemical compositions of the rocks. For comparison, in CI-type carbonaceous chondrites Cl and Br concentrations average 698 ppm and 3.5 ppm, respectively, with a Cl/Br molar ratio of about 449 (Palme and Jones, 2003). In addition, SNC meteorites (shergottites, nakhlites, and chassignites), of Martian origin, have an average Cl/Br molar ratio of

about 405 (Dreibus and Wänke, 1987). Consistent with these findings in meteorite studies, APXS measurements on rocks found at the Martian surface show that Br concentrations are low or undetectable in basalt samples, but enriched in the samples that have undergone a variety of sedimentary processes, such as weathering, evaporation, and diagenesis (Rieder et al., 2004; Clark et al., 2005). As shown in Figure 3.1, the highly variable Cl/Br mass ratios are primarily controlled by variable Br abundances, which in turn vary by more than three orders of magnitude.

On the other hand, neither Cl nor Br is significantly correlated with P or S in the Meridiani soil samples (Greenwood and Blake, 2006; Karunatillake et al., 2013). In addition, nanoparticle Fe oxides (Np-Ox) in soils at both Martian Exploration Rover (MER) landing sites (Klingelhöfer et al., 2004; Morris et al., 2004) show no significant correlation with Cl and P, which may suggest that phosphate has not been concentrated in Martian soils due to adsorption onto Fe oxides (Greenwood and Blake, 2006). At this point, however, the geochemical behavior of chloride, bromide, sulfate, and phosphate on the Martian surface, appears to be largely unconstrained.

At Meridiani Planum, the presence of jarosite and hematite in the outcrop (Klingelhöfer et al., 2004), millimeter-scale diagenetic secondary porosity (McLennan et al., 2005), and widespread hematitic concretions all suggest that these Late Noachian to Early Hesperian outcrops experienced multiple stages of diagenesis resulting from episodes of groundwater interaction (Grotzinger et al., 2005; McLennan et al., 2005; Sefton-Nash and Catling, 2008). Not limited to Meridiani Planum, a correlation between Fe oxides and sulfate minerals has been observed remotely by orbital spectroscopy at several locations across the Martian surface (e.g., Bibring et al., 2007; Murchie et al., 2009; Roach et al., 2010), and suggests a fairly common diagenetic transformation of ferrous sulfate to iron oxides under Martian surface conditions
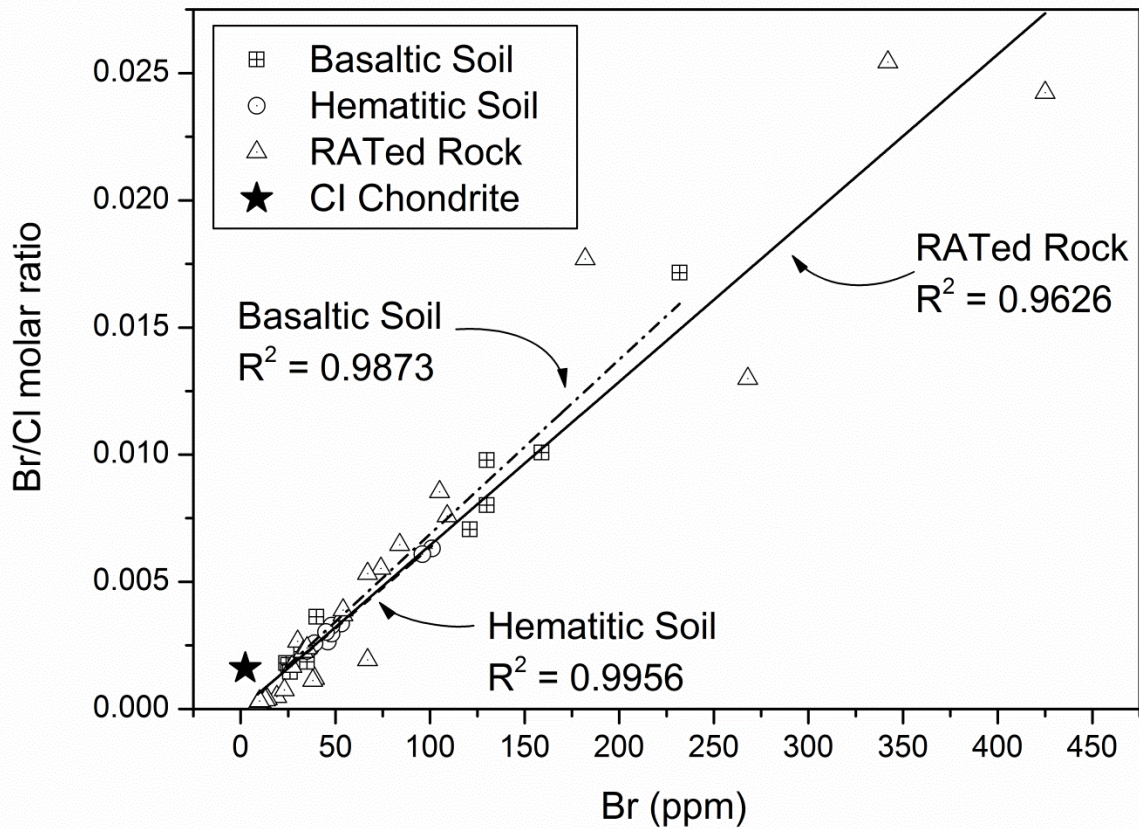
**Figure 3.1.** Variations of Br/Cl molar ratios versus Br concentration at Meridiani Planum (by the Mars Exploration Rover Opportunity, Sols 11-1481). In all the three categories of basaltic soil, hematitic soil, and RATed rocks, Br/Cl mass ratios are highly correlated to Br concentration. CI chondrite has a much lower Br concentration and Br/Cl ratio than the APXS data from the Martian surface. Data source: Brückner et al. (2008).

(McLennan et al., 2005; Navrotsky et al., 2005; Tosca et al., 2005; Golden et al., 2008; Sefton-Nash and Catling, 2008; Tosca et al., 2008).

One likely mineralogical pathway for such Fe(II) to Fe(III) transformation is the oxidation of ferrous sulfates, involving ferric sulfates and oxides, including schwertmannite $(Fe_8O_8(OH)_6(SO_4) \cdot nH_2O)$, jarosite $(K,Na,H_3O)Fe_3(OH)_6(SO_4)_2)$, goethite $(\alpha\text{-FeOOH})$, and hematite $(\alpha\text{-Fe}_2O_3)$ (Tosca et al., 2008). During such processes, $Cl^-$ can substitute for the hydroxyl ion in the jarosite (and related) structures (Morris et al., 2006), and the tunnel structure of schwertmannite is able to accommodate $F^-$ and $Cl^-$, but likely not $Br^-$ due to its larger ionic radius (Eskandarpour et al., 2008). Consequently, diagenetic Fe-oxidation processes have the potential for incorporating and fractionating halogen elements near the Martian surface.

As for phosphorus, the interactions of phosphates with Fe oxides in Martian brines potentially control the distributions of halide species on the Martian surface. The uptake of phosphate by Fe-oxides (e.g., goethite, hematite, and schwertmannite) and by terrestrial basalt and granite powders have been studied extensively (Torrent et al., 1992; 1994; Dreibus and Haubold, 2004; Eskandarpour et al., 2006). The presence of phosphate in brines may prevent certain Fe oxides forming from $Fe^{3+}$ hydrolysis, which could in turn control secondary assemblages observed on Mars (e.g., Barrón et al., 2006). Alternatively, the presence of phosphate may affect the morphology of precipitating Fe oxides (e.g., Galvez et al., 1999; Cumplido et al., 2000). In addition, competitive sorption among phosphate, sulfate, chloride, and bromide on Fe-oxide surfaces is likely to exert an important role on the fate of these species on Mars (Greenwood and Blake, 2006), much the same way as it controls their partitioning and distribution in terrestrial soil and aquatic systems (e.g., Parfitt, 1982).

In this work, we focused on the behavior of $Br^-$, $Cl^-$ and $H_2PO_4^-$ during three parts of the well-established reaction pathway from ferrous sulfate to ferric oxides (Tosca et al., 2008; Zhao and McLennan, 2013). As shown in Figure 3.2, we experimentally investigated (1) how $Cl^-$, $Br^-$ and/or $H_2PO_4^-$ behave during the precipitation of goethite and jarosite via Fe(II) oxidation; (2) how the incorporation of $Cl^-$ and $Br^-$ into the jarosite structure would affect its stability during aqueous alteration; and (3) how $Cl^-$, $Br^-$, $SO_4^{2-}$ and $H_2PO_4^-$ would interact with the surfaces of halogen-free (HAL-free) -hematite, -goethite and -jarosite by adsorption.

## 3.2 Experimental Methods

### 3.2.1 Fe(II) oxidation experiments

Four initial conditions for Fe(II) oxidation experiments were employed. In each, 0.9 or 1.8 L of 0.45 M $MgSO_4$ solution (made with $MgSO_4 \cdot 7H_2O$) was placed in Pyrex beakers as a matrix (A.C.S reagents and 18.2 m$\Omega$ EasyPure ultrapure water were used in all experiments). Two loadings of melanterite (added as $FeSO_4 \cdot 7H_2O$) were then added. According to the amount of melanterite added, the experiments were named low-Fe oxidation experiments (melanterite at 31 g/L) and high-Fe oxidation experiments (melanterite at 268 g/L). To examine the possible influence of phosphate on halogen distributions during oxidation, a small amount of $KH_2PO_4$ was added to one of the low-Fe and one of the high-Fe oxidation experiments, at the initial concentration of 4.4 mM and 4.7 mM, respectively. Hence, the four settings can be characterized as: (1) low-Fe without $PO_4$ (low-Fe-Pht-free); (2) low-Fe with $PO_4$ (low-Fe-Pht); (3) high-Fe without $PO_4$ (high-Fe-Pht-free); (4) high-Fe with $PO_4$ (high-Fe-Pht). To each experiment, $Cl^-$ and $Br^-$ were added according to the total amount of $SO_4^{2-}$ in the solution, in order to make the initial $SO_4^{2-} : Cl^- : Br^-$ molar ratio 8 : 2 : 1. In the low-Fe oxidation experiments designed to form
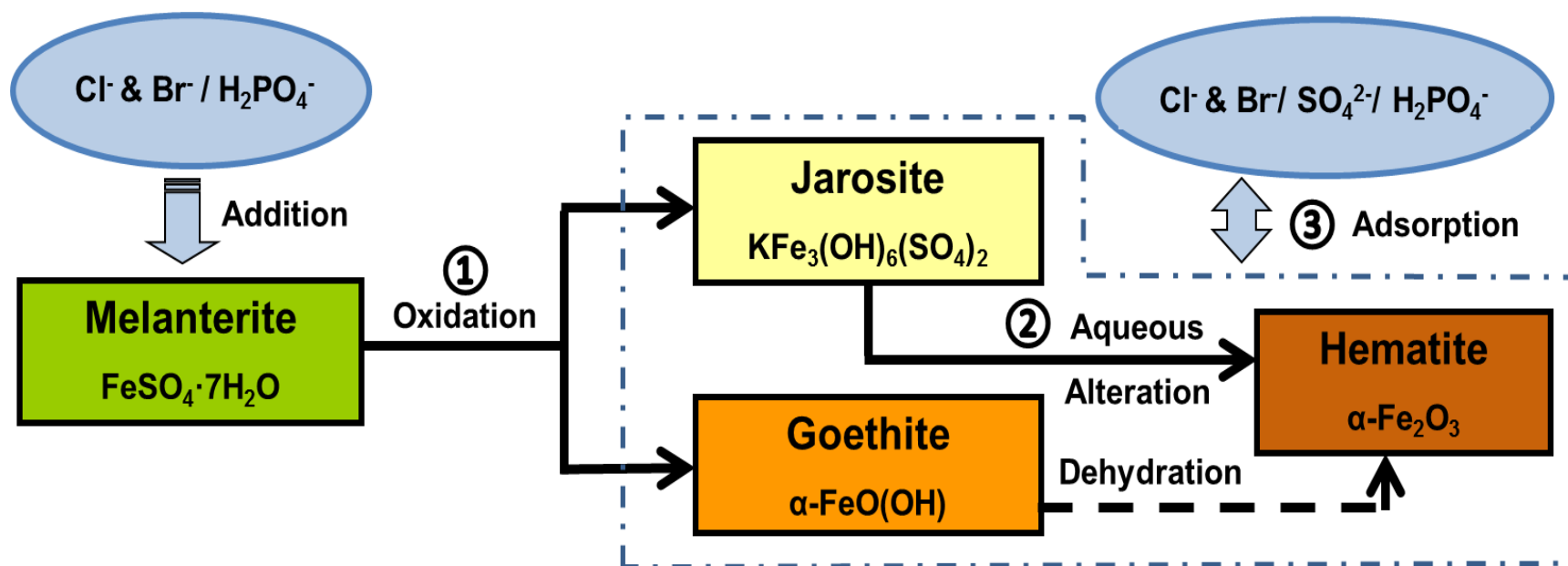
**Figure 3.2.** Schematic outline of mineralogical evolution pathways studied in this work. The oxidation of melanterite ($FeSO_4 \cdot 7H_2O$) formed jarosite ($KFe_3(OH)_6(SO_4)_2$) and goethite ($FeO(OH)$)) which in turn, by aqueous alteration and dehydration, can transform to hematite. Solid arrows indicate steps that were experimentally examined, whereas the dashed arrow indicates an additional pathway (Tosca et al., 2008; Zhao and McLennan, 2013) that was not experimentally examined in this study. Circled numbers identify the major experiments in the same order as they described in Sections 3.2.1-3.2.3. Dash-dotted polygon outlines the key minerals jarosite, goethite, and hematite. Halogen-free samples of these three minerals were synthesized and used for $Cl^-/Br^-/SO_4^{2-}/H_2PO_4^-$ adsorption experiments.

goethite, $Cl^-$ and $Br^-$ were added as $MgCl_2 \cdot 6H_2O$ and $MgBr_2 \cdot 6H_2O$. In the high-Fe oxidation experiments designed to form jarosite, $Cl^-$ and $Br^-$ were added as $KCl$ and $KBr$, in order to also supply $K^+$ to facilitate jarosite precipitation.

All beakers were covered by paraffin film with a 2 cm hole to accommodate sampling and pH monitoring. In this design, the beakers maintained contact with ambient atmosphere ($pO_2 = 0.21$ atm), which acted as the oxidant, and the solutions were continuously stirred at 25 ℃. The solutions were also corrected for evaporation through daily weighing and the addition of small amounts of ultrapure water.

All oxidation experiments were run for 15 days until the pH of solutions was largely invariant and the anticipated minerals had precipitated. Suspension samples were collected every day, and centrifuged at 5000 rpm at 25 ℃ for 40 min. The supernatant solutions were collected and diluted immediately to prevent further precipitation. The extracted solid samples were then thoroughly washed by ultrapure water until the leachate was halogen free (determined using a 0.65 M $AgNO_3$ solution) and air dried at room temperature.

The $SO_4^{2-} : Cl^- : Br^-$ molar ratio 8 : 2 : 1 in our initial solutions was chosen due to the analytical limitation of the ion chromatography (IC) used in our analyses. In a solution composed of $SO_4^{2-}$, $Cl^-$ and $Br^-$, this ratio was the upper limit for the IC to clearly discriminate the conductivity peak of $Br^-$ from $SO_4^{2-}$. Any higher concentration of $SO_4^{2-}$ would overwhelm the $Br^-$ signal, resulting in a poor analysis. Therefore, in design of our experiments, we chose not to use solutions with the exact S/Cl, S/Br, and Cl/Br molar ratios found in Martian *in situ* analysis. Instead, like the Mars case, we used a solution dominated by sulfate, with molar concentration of $Cl^-$, $Br^-$ and $H_2PO_4^-$ in the sequence $Cl^- > Br^- > H_2PO_4^-$. Table 3.1 provides initial solution compositions of each setting.

**Table 3.1.** Initial and final compositions of four Fe(II)-oxidation experiment conditions (unit of concentration: mM).

| Components of solution | Added as | Low-Fe oxidation experiments | | | | Added as | High-Fe oxidation experiments | | | |
| | | Soln [1] Pht-free | | Soln [2] Pht | | | Soln [3] Pht-free | | Soln [4] Pht | |
| | | Initial conc. (meas.) | Final conc. (meas.) | Initial conc. (meas.) | Final conc. (meas.) | | Initial conc. (meas.) | Final conc. (meas.) | Initial conc. (meas.) | Final conc. (meas.) |
|---|---|---|---|---|---|---|---|---|---|---|
| $Fe_{total}$ | $FeSO_4 \cdot 7H_2O$ | 109 | 104 | 108 | 107 | $FeSO_4 \cdot 7H_2O$ | 736 | 634 | 770 | 590 |
| $Mg^{2+}$ | $MgSO_4 \cdot 7H_2O$ | 868 | 862 | 570 | 565 | $MgSO_4 \cdot 7H_2O$ | 398 | 384 | 395 | 315 |
| $K^+$ | | - | - | 4.40 | 4.10 | | 555 | 539 | 552 | 494 |
| $Cl^-$ | $MgCl_2 \cdot 6H_2O$ | 190 | 192 | 188 | 187 | KCl | 369 | 358 | 365 | 370 |
| $Br^-$ | $MgBr_2 \cdot 6H_2O$ | 84.3 | 84.0 | 83.4 | 86.4 | KBr | 186 | 177 | 182 | 184 |
| $SO_4^{2-}$ | | 840 | 835 | 541 | 532 | | 1135 | 1082 | 1165 | 942 |
| $H_2PO_4^-$ | $KH_2PO_4$ | - | - | 4.4[a] | <DL | $KH_2PO_4$ | -- | -- | 4.7* | <DL |
| pH | | 3.4 | 2.1 | 3.6 | 2.5 | | 3.2 | 1.8 | 2.9 | 1.8 |
| Precipitates | | | Gt | | Jt and Phts (Phts dominant)[b] | | | Jt [b] | | Jt and Phts (Jt dominant) [b] |

[a]Initial phosphate concentration was by calculation due to immediate precipitation of amorphous phases after adding $KH_2PO_4$.
[b]Pht-free = phosphate free; Pht = phosphate; Jt = jarosite; Gt = goethite; Conc. Meas. = measured; DL = detection limit. DL for phosphate = 0.0001mM.

**3.2.2 Aqueous alteration of jarosite by batch experiments**

Four synthetic jarosite samples (HAL-free-, Cl-, Br-, and Br,Cl-bearing) were used for aqueous alteration batch experiments in ultrapure water at two temperatures: 25 ℃ and 70 ℃. Methods of synthesizing jarosite are described in Section 3.2.4. Details of each synthetic jarosite sample are listed in Table 3.2.
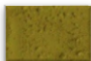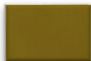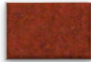
In the 25 ℃ batch experiments, 0.2 g of each jarosite was dispersed into 200 g ultrapure water in 600 mL Pyrex beakers, with magnetic Teflon stir bars stirring throughout the experiment. The beakers were covered by paraffin film. Stirring speed for each beaker was calibrated to the same rate to eliminate any influence on dissolution rate by discrepant stirring speeds. Ten milliliters of suspension samples were collected every 24 h for 10 days.

In the 70 ℃ batch experiments, 0.1 g of each jarosite was dispersed into 100 g ultrapure water in 125 mL wide mouth high-density polyethylene (HDPE) bottles with a magnetic Teflon stir bar. The bottles were placed in a water bath at constant 70 ℃. The system was then magnetically agitated daily and a 15 mL of suspension was collected daily for 5 days. The pH was measured at room temperature after the collected samples had cooled down. The suspension was centrifuged and processed for further analyses of K and $Fe_{total}$ concentrations. Section 3.2.5 provides methods for the solution and suspension processing.

**3.2.3 Adsorption batch experiments**

Preliminary adsorption experiments were conducted to investigate the adsorption behavior of $Cl^-$, $Br^-$, $SO_4^{2-}$ and $H_2PO_4^-$ on synthetic HAL-free -hematite, -goethite and -jarosite. See Section 3.2.4 for synthesis methods and Table 3.2 for details of the three HAL-free phases.

**Table 3.2.** Bulk chemical composition (wt %), formula and physical properties of synthetic Fe minerals.

| Index | Phase[a] | K | Fe | S | Cl | Br | Chemical formula[b] | Surface area $(m^2/g)$ | Munsell color[C] | Color | |
|-------|----------|------|-------|-------|------|------|---------------------|------------------------|------------------|-------|---|
| [1] | HAL-free Jt | 7.77 | 33.55 | 12.74 | - | - | $KFe_{3.0}(SO_4)_{2.0}(OH)_{6.0}$ | 3.1 | 5Y 8/6 | Pale yellow |  |
| [2] | Cl-Jt | 8.32 | 33.33 | 12.52 | 0.14 | - | $KFe_{2.81}(SO_4)_{1.84}(OH)_{5.73}Cl_{0.02}$ | 3.3 | 2.5Y 6/6 | Dark yellow |  |
| [3] | Br-Jt | 7.90 | 32.01 | 12.08 | - | 5.13 | $KFe_{2.84}(SO_4)_{1.86}(OH)_{5.46}Br_{0.32}$ | 2.7 | 5Y 5/6 | Dark greenish yellow |  |
| [4] | Br,Cl-Jt | 8.47 | 32.11 | 12.02 | 0.08 | 3.94 | $KFe_{2.66}(SO_4)_{1.73}(OH)_{5.26}Br_{0.23}Cl_{0.01}$ | 2.9 | 5Y 4/4 | Dark greenish yellow |  |
| [5] | HAL-free Gt[d] | 0.88 | 62.1 | - | - | - | $(K)_{0.02}(Fe)_{0.993}O(OH)$ | 19.9 | 10Y 8/8 | Light brown |  |
| [6] | HAL-free Hm[d] | 1.02 | 69.18 | - | - | - | $K_{0.04}Fe_{1.99}O_3$ | 24.3 | 10R 4/8 | Dark red |  |

[a] Jt = jarosite; Gt = goethite; Hm = hematite. HAL-free = halogen-free.
[b] Formula of jarosite based on K = 1. OH values were calculated, based on charge balance.
[c] The Munsell color of minerals was determined by visually comparing the powder samples prepared for XRD measurement with Munsell color charts [Munsell color, 1994].
[d] The K detected in the HAL-free Gt and HAL-free Hm samples are due to the impurity introduced by KOH from the goethite synthetic solution.

Before making multi-adsorbate solutions of Cl-, Br-, $SO_4^{2-}$ and $H_2PO^{4-}$, the adsorption isotherms of single adsorbate $Cl^-$ and $Br^-$ of the three HAL-free minerals were determined and are summarized in the Appendix 1 (part B).

After determining the adsorption isotherms in single-adsorbate solutions, three types of multi-adsorbate systems were synthesized as $Cl^-$-$Br^-$, $Cl^-$-$Br^-$-$SO_4^{2-}$, and $Cl^-$-$Br^-$-$SO_4^{2-}$-$H_2PO_4^-$. In the $Cl^-$-$Br^-$ system, to investigate the influence of initial concentrations of $Cl^-$and $Br^-$, three $Cl^-$-$Br^-$ adsorbate solutions were made at 10-10 mM, 20-20 mM, and 20-10 mM, respectively. In the $Cl^-$-$Br^-$-$SO_4^{2-}$ system, $Cl^-$ to $Br^-$ ratio was set at 10-10 mM and 20-10 mM initially, with $SO_4^{2-}$ varied from 10 to 40 mM with 10 mM intervals. In the $Cl^-$-$Br^-$-$SO_4^{2-}$-$H_2PO_4^-$ system, initial adsorbate concentration was set at 20-10-40-10 mM.

In each experiment, 25 mL of adsorbate solution (unbuffered) were transferred to a 50 mL centrifuge tube and then a 1 mL of mineral slurry (0.1 g/mL) was added to the tube. These tubes were then capped and put in a water bath maintained at 25 ºC for 3 days for the reactions to reach equilibrium. The time required for reaching the equilibrium was chosen based on previous kinetic studies dealing with similar systems (e.g., Gao, 2001; Chitrakar et al., 2006). During the reaction period, the tubes were agitated by hand every 24 h. In the end, all the tubes were centrifuged and the supernatant solutions were collected and passed through 0.2 μm filters. The pH of each solution was measured immediately after sampling.

### 3.2.4 Synthesis of Fe-bearing phases

All final synthetic phases described in this section were confirmed by Powder X-ray Diffraction (XRD), Fourier Transform Infrared (FTIR) spectroscopy and Scanning Electron Microscopy (SEM) with Energy Dispersive X-ray Spectrometer (EDS). Details of characterization methods are described in Section 3.2.5 and Table 3.2 lists the chemical

composition and physical properties of each synthetic sample. See the Appendix 1 (Part A) for SEM images.

3.2.4.1 Four types of jarosite

All four types of jarosite were prepared in a similar manner as for the high-Fe oxidation experiment. For HAL-free jarosite, 100 g $FeSO_4 \cdot 7H_2O$ was added to 454 mL of a 0.45 M $MgSO_4$ solution, along with 3 g of $K_2SO_4$ solid to facilitate jarosite precipitation.  For Cl-jarosite and Br-jarosite, 80 g of $FeSO_4 \cdot 7H_2O$ was added to 454 mL of 0.32 M $MgSO_4$ solutions, and then 12.8 g of KCl was added to the Cl-jarosite solution, whereas 20.2 g of KBr was added to the Br-jarosite solution. The Br,Cl-bearing jarosite (Br,Cl-jarosite) was the final product obtained from the high-Fe-Pht-free experiment (initial conditions listed in Table 3.1). After 15-20 days, the suspensions were removed from the beaker and centrifuged. The precipitate was thoroughly washed by ultrapure water until the leachate was halogen-free (determined using a 0.65 M $AgNO_3$ solution) and dried in air at room temperature.

3.2.4.2 Halogen-free goethite

The halogen-free goethite (HAL-free goethite) was prepared from an alkaline Fe(III) system as described in Schwertmann and Cornell (2000). One hundred milliliters of a 1 M $Fe(NO_3)_3$ solution was placed into a 2 L polyethylene flask, followed by rapid addition and stirring of 180 mL of 5 M KOH. Red-brown poorly crystalline ferrihydrite precipitated at once. The suspension was immediately diluted to 2 L with ultrapure water and held in the closed flask at 70 ºC for 60 h. The suspension was then removed from the oven and centrifuged. The precipitate was repeatedly washed and dried in air at room temperature.

3.2.4.3 Halogen-free hematite

The halogen-free hematite (HAL-free hematite) was prepared by heating of HAL-free goethite at 300 ºC for 48 h.


**3.2.5 Analytical methods**

A gel-filled paper pulp pH electrode with temperature compensation was used to measure pH and was calibrated regularly against standard buffer solutions of pH 1.6, 4 and 7.

During the experiments, the suspension samples were collected and centrifuged at 5000 rpm at 25 ºC for 40 min, and the supernatants were then filtered by 0.2 µm syringe filter units. The extracted solid samples were washed with ultrapure water and air dried at room temperature. Solids were identified with XRD. The prepared powder XRD samples formed a 2.5 cm by 2.5 cm square and 0.05 mm in thickness sitting on a flat glass plate. Powder XRD data were collected using a Scintag PAD-V Bragg-Brentano diffractometer at 45 kV and 25 mA with Cu-Kα radiation ($\lambda = 1.5418$ Å). Data were collected between 10 and 60 degrees $2\theta$, with a scan step of 0.02 degree and 6 s of counting time per step. Infrared spectra were acquired using a Nicolet 6700 FTIR spectrometer. The specific surface area of solid samples was determined by a five-point $N_2$ Brunauer-Emmett-Teller (BET) gas adsorption isotherm method, using a NOVA 2200e surface area and pore size analyzer.

The concentrations of Br, Cl and other major elements in synthetic samples were determined by X-ray fluorescence spectrometry (Bruker AXS S4 Pioneer), with calibration standard sets bracketing the sample concentrations and conditions as closely as possible. One analytical issue we had to overcome stemmed from the difference in analyzed layer depth for Br and Cl in the calibration standards. The analyzed layer of Cl (3-4 µm) was much shallower than that of Br (50 µm), and accordingly, sample heterogeneity exerts a far more pronounced effect

on the quantification of Cl than it does for Br. For instance, in the standards prepared in the same manner by mixing HAL-free goethite with KBr (varying Br from 0 to 5 wt %) or KCl (varying Cl from 0 to 3 wt %), Br was detected easily, but Cl was not detectable in any standard. To overcome this problem, we used crystal violet ($C_{25}N_3H_{30}Cl$), an organic compound with a much lower Cl content (8.7 wt % of Cl) than KCl (47.55 wt % of Cl). Using crystal violet rather than KCl greatly reduced sample heterogeneity and improved the detection limit for Cl. In our standard sets, a four-point calibration curve of Cl using crystal violet has an $R = 0.9984$ and of Br using KBr has an $R = 0.9997$, which represents a consistent and reliable analysis. The detection limits for Br and Cl are 0.219 and 0.046 wt % respectively, and analyzed layer depths are very similar to the unknown samples, which make XRF a suitable method to determine Br and Cl concentrations in our samples.

All filtered solution samples were analyzed for Mg, $Fe_{total}$, K, and P with a direct current argon plasma emission spectrophotometer (DCP-AES). The solutions were diluted with 0.96 M $HNO_3$ and external solution standards were prepared in a 0.96 M $HNO_3$ matrix. The concentrations of $Cl^-$, $Br^-$ and $SO_4^{2-}$ in solution were determined by Dionex DX-500 ion chromatography, using an AS4A-SC column and $Na_2CO_3/NaHCO_3$ eluent. Each sample was analyzed in triplicate.

The quality of analytical data was evaluated on the basis of duplicate samples collected at selected times, followed by duplicate or triplicate analyses of each sample. The low-Fe and high-Fe oxidation experiments and jarosite aqueous alteration experiments were performed in duplicate. Dilute ICP/DCP standard solutions were used to monitor the accuracy of cation and anion analyses. Each standard was run as three replicates. For cation results, the standard error

ranges from ±0.06% to ±2.6% and averaged ±1.3%. For anion results, the standard error varied from ±3% to ±5%.


## 3.3 Results and Discussion

### 3.3.1 Fe(II) oxidation experiments

3.3.1.1 Fe(II) oxidation without phosphate

Without phosphate, the low-Fe oxidation experiment (low-Fe-Pht-free) precipitated poorly crystalline goethite (Figure 3.3). Its specific surface area was 71.6 m$^2$/g. The solution pH continuously decreased from 3.4 to 2.1. Throughout the experiment, the Cl$^-$ and Br$^-$ concentration in the solution remained almost constant. Cl$^-$ varied from 190 to 192 mM, and Br$^-$ concentration varied from 84.0 to 84.3 mM. Therefore, the Cl/Br molar ratio of the solution ranged from 2.21 to 2.28 (Figure 3.4 (A)), and its variation fell within the ±5% analytical uncertainties. Table 3.1 provides the composition of the solutions in each type of the experiment.

On the other hand, the high-Fe oxidation experiment (high-Fe-Pht-free) precipitated well crystalline jarosite (Figure 3.3). Its specific surface area was 2.9 m$^2$/g. The solution pH changed from 3.2 to 1.8. During the experiment, the Cl$^-$ concentration changed from 370 to 358 mM and Br$^-$ concentration changed from 186 to 177 mM. The Cl/Br molar ratio of the solution ranged from 1.87 to 2.02 (Figure 3.4 (A)), and its variation again fell within the ±5% analytical uncertainties. Given that the Cl$^-$/Br$^-$ molar ratio of the solution remained almost constant during the precipitation of goethite or jarosite, Cl$^-$ and Br$^-$ do not appear to fractionate from each other in the solution while these minerals form.

The result of the XRF analysis of precipitated goethite indicates that the solid phase did not contain detectable Cl$^-$ or Br$^-$. After being thoroughly washed by ultrapure water until the leachate

was halogen-free (determined using a 0.65 M AgNO₃ solution), the adsorbed part of halide anions on goethite was considered to be eliminated and then neither Cl nor Br were detectable in the sample (detection limits for Br = 0.219 wt% and Cl = 0.046 wt%). Therefore, even though we cannot rule out the incorporation of halogens by goethite (since our detection limits of Br and Cl were at the level of thousands to hundreds of parts per million), the amount of incorporated halide was negligible compared to its parent solution.

By contrast, jarosite formed in these experiments incorporated Cl⁻ and Br⁻ into its structure. Moreover, the jarosite was significantly enriched in Br⁻ with respect to Cl⁻. As shown in Table 3.3, the jarosite solid (Br,Cl-jarosite) incorporated 22.5 mmol/kg Cl⁻ and 493 mmol/kg Br⁻. Compared to its initial parent solution, the Cl⁻ concentration in the jarosite solid was only 0.061 times of that in the solution, but the Br⁻ concentration reached 2.65 times of that in the solution. Such partitioning behavior was also observed in the other two types of synthetic jarosite, which precipitated from similar but single-halogen bearing parent solutions. Also shown in Table 3.3, the Cl-jarosite formed from Cl-only parent solution contained only 0.105 times the concentration of Cl⁻ in the solid compared to the initial solution, and the Br-jarosite formed from Br-only parent solution was enriched in Br⁻ by a factor of 1.75 compared to its initial solution concentration. Such preferential incorporation of Br⁻ over Cl⁻ by the jarosite structure by at least an order of magnitude suggests a potential for fractionating Br⁻ from Cl⁻ in nature.

In the case of Br,Cl- jarosite, the Cl/Br ratio of the solid was only 0.046 compared to 2.02 for the solution on the same day. In addition, due to the high solution/solid ratio for the system (70 g/g in the case of Br,Cl-jarosite), different Cl/Br ratios in the solid may not be necessarily reflected in the solution chemistry. More implications of this observation for the Martian surface are discussed in Section 3.4.
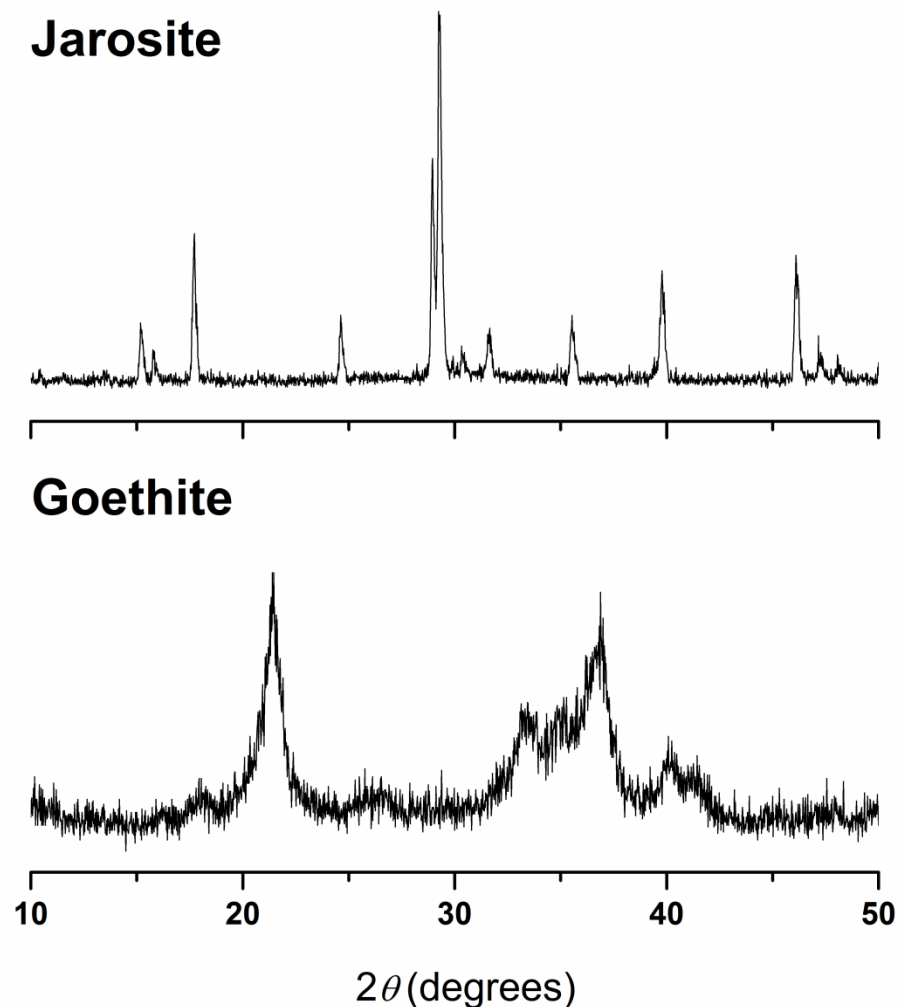
**Figure 3.3.** XRD patterns of jarosite and goethite obtained at the end of phosphate-free Fe(II) oxidation experiments. All peaks are attributed to jarosite or goethite, respectively, in each figure. Note that the goethite pattern has broader peaks and noticeably greater analytical noise, which is commonly caused by low degrees of crystallinity of the sample. Compared with commercially available pure jarosite and goethite powder standards, our jarosite was highly crystalline, and the goethite was poorly crystalline.
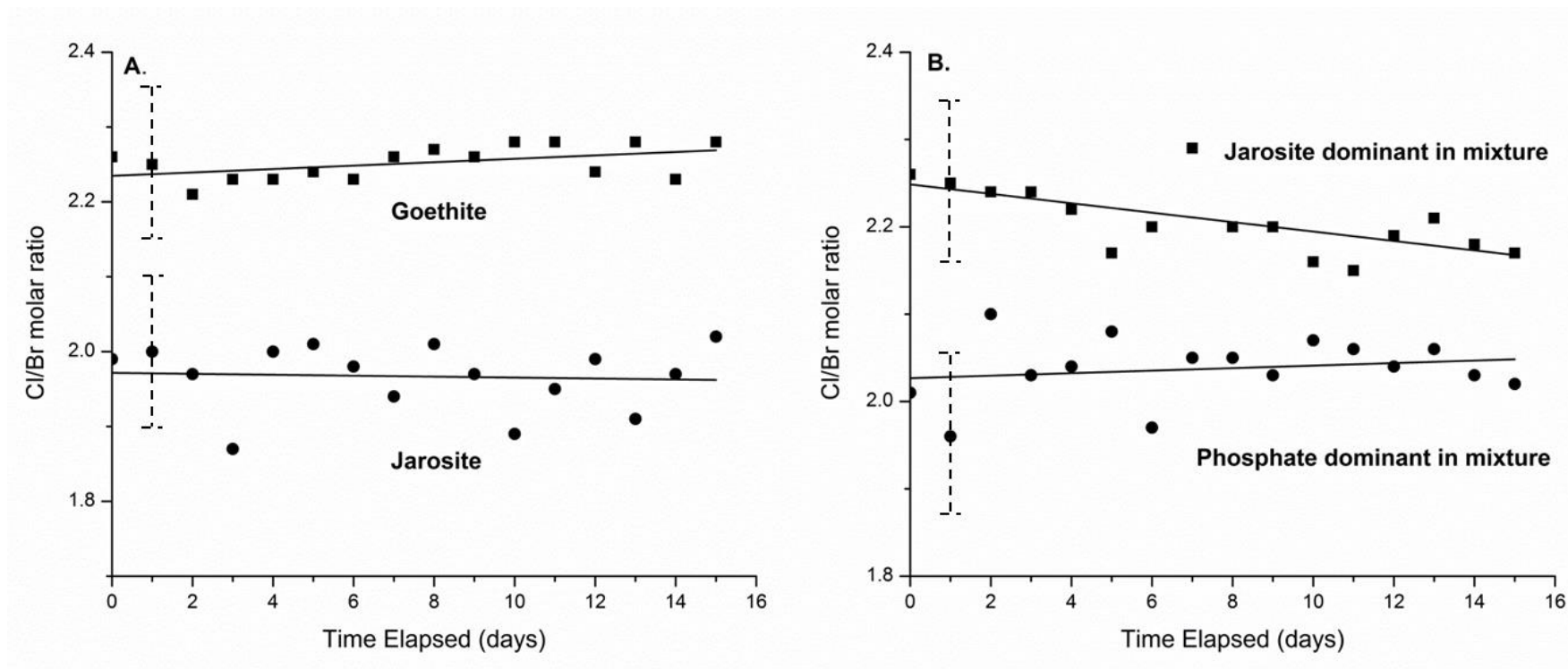
**Figure 3.4.** Cl/Br molar ratios in the solution throughout the Fe(II) oxidation experiment. The error bars (±5%) were shown on only one data point of each oxidation experiment plot, not on all data points, for clarity purpose. The trend lines in each plot were calculated by linear fitting of all data points. (A) Without phosphate, the Cl/Br ratios of the low-Fe oxidation experiment (precipitated goethite) and the high-Fe oxidation experiment (precipitated jarosite) remained almost constant at 2.21-2.28 and 1.87-2.02, respectively. (B) With phosphate, the low-Fe and high-Fe oxidation experiments both precipitated a mixture of jarosite and amorphous phosphates. The precipitates were dominated by phosphate under low-Fe condition and dominated by jarosite under high-Fe condition. The Cl/Br molar ratios remained almost constant at 2.15-2.29 and 1.96-2.08, respectively.

**Table 3.3.** Concentration of Cl⁻ and Br⁻ in precipitated jarosite solids and the molar ratios of Cl⁻ and Br⁻ concentrations between precipitates and initial solutions.

| Type of jarosite | $C_{aq}$ (mmol/L) | | $C_s$ (mmol/kg) | | $C_s/C_{aq}$ | |
|---|---|---|---|---|---|---|
| | Cl⁻ | Br⁻ | Cl⁻ | Br⁻ | Cl⁻ | Br⁻ |
| Cl-jarosite | 374 | - | 39.4 | - | 0.105 | - |
| Br-jarosite | - | 367 | - | 642 | - | 1.75 |
| Br,Cl-jarosite | 370 | 186 | 22.5 | 493 | 0.061 | 2.65 |

[a] $C_s$ denotes the concentration of final jarosite solid. $C_{aq}$ denotes the concentration of initial parent solution. The $C_s$ of Cl⁻ and Br⁻ in jarosite listed in this table are derived from the wt% concentrations listed in Table 3.2.

3.3.1.2 Fe(II) oxidation with phosphate

Addition of phosphate in the form of $KH_2PO_4$ introduced $K^+$ into the initial solutions thus facilitating the precipitation of jarosite in both low-Fe-Pht and high-Fe-Pht settings. Phosphate interacted with cations in the solution and precipitated unidentified amorphous phases, which were white in color. In the low-Fe-Pht experiment, amorphous phosphate precipitated on the first day without jarosite. On the 7th day (middle point of the experiment), a jarosite peak was distinguishable in the XRD pattern. On the 15th day (last day of the experiment), the jarosite signal was dominant in the XRD pattern. A similar sequence of mineralogical evolution was also observed in the high-Fe-Pht experiment, except that jarosite was dominant in the mixtures from the first day until the last.

The pH decreased from 3.6 to 2.5 in the low-Fe-Pht experiment and 2.9 to 1.8 in the high-Fe-Pht experiment. Due to the formation of amorphous phosphate phases, the phosphorus concentrations in the solution dropped below detection limit (i.e., 0.0001 mM) on the first day.

In the solution of the low-Fe-Pht experiment, the $Cl^-$ and $Br^-$ concentration varied slightly from 188 mM to 187 mM, and 83.4 mM to 86.4 mM respectively, and therefore the $Cl^-/Br^-$ molar ratio ranged from 2.15 to 2.29. In the solution of the high-Fe-Pht experiment, the $Cl^-$ and $Br^-$ concentration varied from 365 mM to 370 mM, and 182 mM to 184 mM respectively, and thus the $Cl^-/Br^-$ molar ratio ranged from 1.96 to 2.08 (Figure 3.4 (B)). The variation of $Cl^-/Br^-$ ratio was within the ±5% analytical uncertainties, and thus, we conclude that the $Cl^-$ and $Br^-$ did not fractionate from each other in the solution.

We were unable to separate jarosite from these mixtures for individual compositional analysis.

### 3.3.2 Stability of halogen-bearing jarosite

During the course of the 25 ℃ aqueous alteration experiments (methods described in Section 3.2.2), the amount of dissolved jarosite was very low and did not form any new phase. However, at 70 ℃, jarosite was dissolved and re-precipitated in the form of hematite (confirmed by XRD).

Regardless of temperature, the amount of dissolved jarosite within the same time intervals increased according to its type: Br,Cl-jarosite > Br-jarosite > HAL-free jarosite > Cl-jarosite (Figure 3.5). Thus, bromine-bearing jarosite (i.e., Br,Cl-jarosite containing 0.08 wt % Cl and 3.94 wt % Br and Br-jarosite containing 5.13 wt % Br) consistently dissolved more rapidly than either halogen-free jarosite (HAL-free jarosite) or jarosite containing only chlorine (Cl-jarosite containing 0.14 wt % Cl).

Based on the dissolution rates, we conclude that of the four types of jarosite, Cl-jarosite was the most stable phase and Br,Cl-jarosite was the least stable phase. Generally, major factors that affect the dissolution rate of a mineral particle include the grain size, crystallinity, structure stability, ionic strength of ambient solution, and temperature (e.g., Pritchett et al, 2012; Zahrai et al., 2012; Reyes et al., 2013). In our experiments, the four types of jarosite were dissolved in the same ambient solution, had similar specific surface area (Table 3.2, rows 1-4), and their dissolution sequence at both 25 ℃ and 70 ℃ were the same. Therefore, the main factors that influenced the dissolution rates are likely related to the crystallinity or structure stability of the particle itself. No structural information has yet been reported for halogen-bearing jarosite. Based on our compositional analyses (Table 3.2, Rows 1-4), deficiencies of $OH^-$ (<6.0), $SO_4^{2-}$ (<2.0) and $Fe^{3+}$ (<3.0) can be inferred in all the three types of halogen-bearing jarosite.
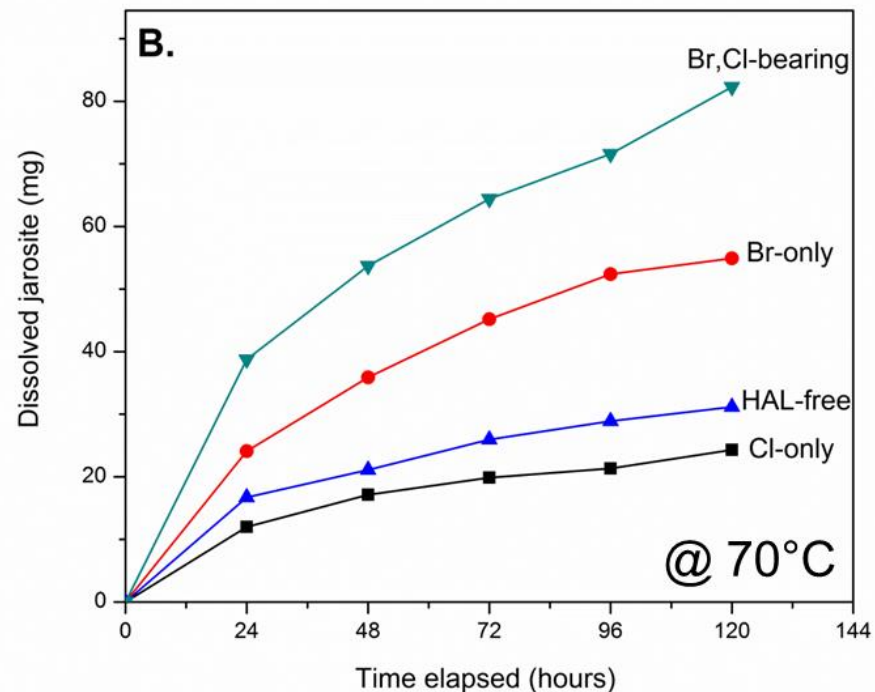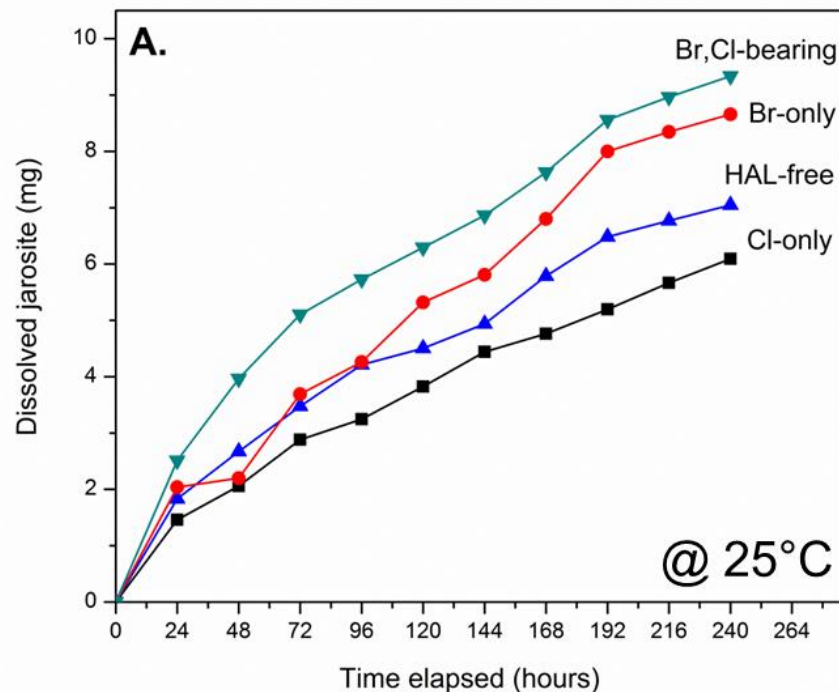
**Figure 3.5.** Aqueous alteration of halogen-bearing jarosite in ultrapure water at 25 °C and 70 °C. Regardless of temperature, the amount of jarosite dissolved increased according to the following sequence: Br,Cl-jarosite > Br-jarosite > HAL-free jarosite > Cl-jarosite. The difference was (A) at 25 °C, the amount of dissolved jarosite was low and no obvious phase change was observed; (B) at 70 °C, the amount of dissolved jarosite was much higher than at 25 °C, and significant amounts of hematite were detected in the final mixture.

The deficiencies of $OH^-$ in Br- and Cl-jarosite, which precipitated from single-halogen bearing parent solutions, were correlated to the amounts of incorporated $Br^-$ and $Cl^-$, whereas $SO_4^{2-}$ and $Fe^{3+}$ concentrations were generally low compared to HAL-free jarosite. On the other hand, Br,Cl-jarosite, which precipitated from a solution containing both $Br^-$ and $Cl^-$, had greater deficiencies of $OH^-$, $SO_4^{2-}$ and $Fe^{3+}$, but lower Br and Cl abundances compared to Br- and Cl-jarosite.

It has been shown that ionic substitutions could alter the unit cell parameters from ideal jarosite and consequently influence the dissolution rates and solubility of jarosite (e.g., *Elwood Madden et al,* 2012*; Kendall et al.,* 2013*; Savage et al.,* 2005). The incorporation of weight percent levels of $Br^-$ into our Br-jarosite and Br,Cl-jarosite samples may significantly distort the structure and make the bonds more susceptible to being attacked during aqueous alteration, and thus reduce the stability relative to halogen-free jarosite. The competition of $Br^-$ and $Cl^-$ for available substitution sites in Br,Cl-jarosite may further degrade the structure, and thus make Br,Cl-jarosite the least stable phase of all the four types of jarosite. On the other hand, the slight incorporation of $Cl^-$ in Cl-jarosite, even though it might also lead to structural distortion, somehow inhibited the dissolution, which in turn made the Cl-jarosite more stable compared to the halogen-free jarosite. To explain this observation, further investigation is indeed required.

Due to the lack of previous studies dealing with halogen-bearing jarosite for comparison, it is difficult to constrain the substitution sites for halide ions in jarosite. Two potential substitution sites are the $OH^-$ site and the $SO_4^{2-}$ site. The halide ions might substitute for $OH^-$ without causing charge imbalance. Alternatively, if the halide ions substitute for $SO_4^{2-}$, then other (-1) charged anions or coupled halide ions would be needed for charge balance. The $SO_4^{2-}$ site has been reported to be able to accommodate oxyanions such as chromate, arsenate and phosphate (e.g., *Baron and Palmer,* 1996*; Dutrizac and Chen,* 2010*; Savage et al.,* 2005), but whether it can

accommodate halides (especially $Br^-$) is unknown. From the perspective of ionic radii, the halide ions (crystal radii $Br^- = 1.82$ Å and $Cl^- = 1.67$ Å) are both larger than either $OH^-$ or $SO_4^{2-}$ (crystal radii $OH^- = 1.37$ Å and $SO_4^{2-} = 1.49$ Å) (*Shannon*, 1976). Therefore, with our current information, it remains unclear why $Br^-$ is favored over $Cl^-$ by the jarosite structure and which jarosite crystal site the $Br^-$ substitutes for. In addition, why slight incorporation of $Cl^-$ in Cl-jarosite could inhibit jarosite dissolution compared to HAL-free jarosite is also unclear. Further investigations on the crystallography of halogen-bearing jarosite and its effect on stability of jarosite are warranted for better understanding of these issues. Nevertheless, the incorporation of halogens indeed affected the stability of jarosite during aqueous alteration.

### 3.3.3 Adsorption selectivity on Fe minerals

To compare the adsorption selectivity of $Cl^-$, $Br^-$, $SO_4^{2-}$ and $H_2PO_4^-$ on HAL-free -hematite, -goethite and -jarosite, different combinations of anion and concentration conditions were tested using batch experiments. The settings of mixed anion solutions were (1) $Cl^-$ and $Br^-$, (2) $Cl^-$, $Br^-$, and $SO_4^{2-}$, and (3) $Cl^-$, $Br^-$, $SO_4^{2-}$, and $H_2PO_4^-$.

The distribution coefficients ($K_d$) of each anion on each adsorbent surface were calculated using equation (1) (*Chitrakar et al.,* 2006). The $K_d$ values are shown in Table 3.4. Propagated error by this calculation is estimated to be $\pm6\%$ to $\pm10\%$.

$K_d$ = anion adsorbed (mmol/g of solid)/ anion in solution (mmol/g of solution)     (1)

In the solutions containing only $Cl^-$ and $Br^-$, all the three HAL-free minerals demonstrated a similar selectivity sequence. When the $Cl^-/Br^-$ molar ratio was 1 ($Cl^- : Br^- = 10 : 10$ or $20 : 20$ mM), the selectivity sequence was $Br^- > Cl^-$ for all the three Fe-bearing phases. When the $Cl^-/Br^-$ molar ratio was 2 ($Cl^- : Br^- = 20 : 10$ mM), the selectivity sequence was $Cl^- > Br^-$. Therefore,

when the solution contained equal molar amounts of $Cl^-$ and $Br^-$, the HAL-free minerals, hematite, goethite, and jarosite, preferred adsorbing $Br^-$. However, the preference was modest such that once $Cl^-$ was dominant in the solution, all the HAL-free minerals selectively adsorbed $Cl^-$ over $Br^-$.

In the anion combinations of $Cl^-$ : $Br^-$ : $SO_4^{2-}$ at 10 : 10 : 10 (mM), all the three HAL-free minerals adsorbed $Br^-$ selectively over $SO_4^{2-}$. Changing the proportions of $Cl^-$ : $Br^-$ : $SO_4^{2-}$ to 20 : 10 : 40 (mM), where $SO_4^{2-}$ was the dominant species with almost equal amounts (by mass) of $Cl^-$ and $Br^-$, all the HAL-free minerals selectively adsorbed $SO_4^{2-}$.

To demonstrate how the adsorption behavior of $Cl^-$, $Br^-$, and $SO_4^{2-}$ changed in response to increasing $SO_4^{2-}$ concentrations, two sets of $Cl^-$-$Br^-$-$SO_4^{2-}$ adsorbent solutions were prepared by setting $Cl^-$ : $Br^-$ at 10 : 10 and 20 : 10 mM, and increasing $SO_4^{2-}$ from 10 to 40 mM with 10 mM interval. The results are shown in Figure 3.6. Note that the absorbent solutions and mineral slurry were both unbuffered so the equilibrium pH was different in each setting but generally acidic. In all the three HAL-free minerals, sorbed $SO_4^{2-}$ increased significantly while sorbed $Cl^-$ and $Br^-$ decreased accordingly. This suggests that in a halide-dominant solution system, $Br^-$ is able to compete with sulfate for adsorption on the Fe-mineral surface. However, in a solution system where $SO_4^{2-}$ dominates over $Br^-$ and $Cl^-$, halide anions are unable to compete with sulfate for adsorption.

**Table 3.4.** Distribution coefficient $K_d$ values of anions on halogen-free Fe minerals.

| Initial sorbate solution (mM) | HAL-free Hm (equilibrium pH 5) | | | | HAL-free Jt (equilibrium pH 4) | | | | HAL-free Gt (equilibrium pH 5) | | | | Adsorption selectivity |
|---|---|---|---|---|---|---|---|---|---|---|---|---|---|
| (1) $Cl^-$ : $Br^-$ | $K_d\_Cl^-$ | $K_d\_Br^-$ | | | $K_d\_Cl^-$ | $K_d\_Br^-$ | | | $K_d\_Cl^-$ | $K_d\_Br^-$ | $K_d\_SO_4^{2-}$ | | |
| 10 : 10 | $4.6\times10^4$ | $5.2\times10^4$ | | | $10^3$ | $2.7\times10^4$ | | | $5.0\times10^3$ | $2.6\times10^4$ | | | $Br^- > Cl^-$ |
| 20 : 20 | $8.0\times10^4$ | $2.0\times10^5$ | | | $3.2\times10^4$ | $6.6\times10^4$ | | | $3.6\times10^4$ | $7.2\times10^4$ | | | $Br^- > Cl^-$ |
| 20 : 10 | $3.5\times10^4$ | $3.0\times10^4$ | | | $3.8\times10^4$ | $3.2\times10^4$ | | | $3.9\times10^4$ | $3.0\times10^4$ | | | $Cl^- > Br^-$ |
| (2) $Cl^-$ : $Br^-$ : $SO_4^{2-}$ | $K_d\_Cl^-$ | $K_d\_Br^-$ | $K_d\_SO_4^{2-}$ | | $K_d\_Cl^-$ | $K_d\_Br^-$ | $K_d\_SO_4^{2-}$ | | $K_d\_Cl^-$ | $K_d\_Br^-$ | $K_d\_SO_4^{2-}$ | | |
| 10 : 10 : 10 | $3.0\times10^3$ | $3.6\times10^4$ | -- | | $3.0\times10^3$ | $3.9\times10^4$ | -- | | -- | $3.3\times10^4$ | -- | | $Br^->Cl^->SO_4^{2-}$ |
| 20 : 10 : 40 | -- | -- | $5.6\times10^4$ | | -- | -- | $4.1\times10^4$ | | -- | -- | $6.0\times10^4$ | | $SO_4^{2-} > (Cl^-$ and $Br^-$) |
| (3) $Cl^-$ : $Br^-$ : $SO_4^{2-}$ : $H_2PO_4^-$ | $K_d\_Cl^-$ | $K_d\_Br^-$ | $K_d\_SO_4^{2-}$ | $K_d\_H_2PO_4^-$ | $K_d\_Cl^-$ | $K_d\_Br^-$ | $K_d\_SO_4^{2-}$ | $K_d\_H_2PO_4^-$ | $K_d\_Cl^-$ | $K_d\_Br^-$ | $K_d\_SO_4^{2-}$ | $K_d\_H_2PO_4^-$ | |
| 20 : 10 : 40 : 10 | -- | -- | $4.8\times10^4$ | $5.0\times10^3$ | $6.0\times10^3$ | -- | $5.2\times10^4$ | -- | $1.3\times10^4$ | -- | $7.3\times10^4$ | -- | $SO_4^{2-}>(Cl^->)H_2PO_4^->Br^-$ |

[*]Jt = jarosite; Gt = goethite; Hm = hematite. HAL-free = halogen-free. Propagated error by this calculation is estimated to be ±6% to ±10%.

An interesting question is how phosphate would affect the adsorption behavior of $Cl^-$, $Br^-$ and $SO_4^{2-}$ in the solution where $SO_4^{2-}$ is dominant. To test this, the anion combination was set to be $Cl^-$ : $Br^-$ : $SO_4^{2-}$: $H_2PO_4^-$ at 20 : 10 : 40 : 10 (mM). In these proportions, HAL-free hematite adsorbed only $SO_4^{2-}$ and $H_2PO_4^-$, and $SO_4^{2-}$ was the dominant sorbed species. On the other hand, HAL-free jarosite and goethite adsorbed $SO_4^{2-}$ and $Cl^-$ without $H_2PO_4^-$, and $SO_4^{2-}$ was the preferentially adsorbed species.

Compared to extensively investigated terrestrial aqueous systems, such as seawater (e.g., Ruttenberg and Sulak, 2011), soil leachates (e.g., Arai and Livi, 2013), and acid mine drainage (e.g., Flores et al., 2012), our Martian simulation solution system was unique with much higher abundance of $Br^-$, lower amount of phosphate, and overwhelmingly dominant sulfate. Our preliminary adsorption experiments show that the adsorption behavior of $Cl^-$, $Br^-$, $SO_4^{2-}$ and $H_2PO_4^-$ on HAL-free -hematite, -goethite and -jarosite was controlled by the relative proportion of sulfate in the solution system. When sulfate concentration is lower than or equal to other anions, $Cl^-$ and $Br^-$ can compete with $SO_4^{2-}$ for available exchange sites by electrostatic interactions and phosphate can compete with $SO_4^{2-}$ by surface complexation (Gao and Mucci, 2001). However, when sulfate concentrations are increased to levels equal or double the combined molar concentrations of $Br^-$ and $Cl^-$, and with phosphate in the solution, adsorption of the low concentration anions are overwhelmed by $SO_4^{2-}$. A more comprehensive investigation is warranted for better understanding the adsorption behavior of halogens in these unique solutions that may be relevant for Mars but that differ from terrestrial aqueous systems.
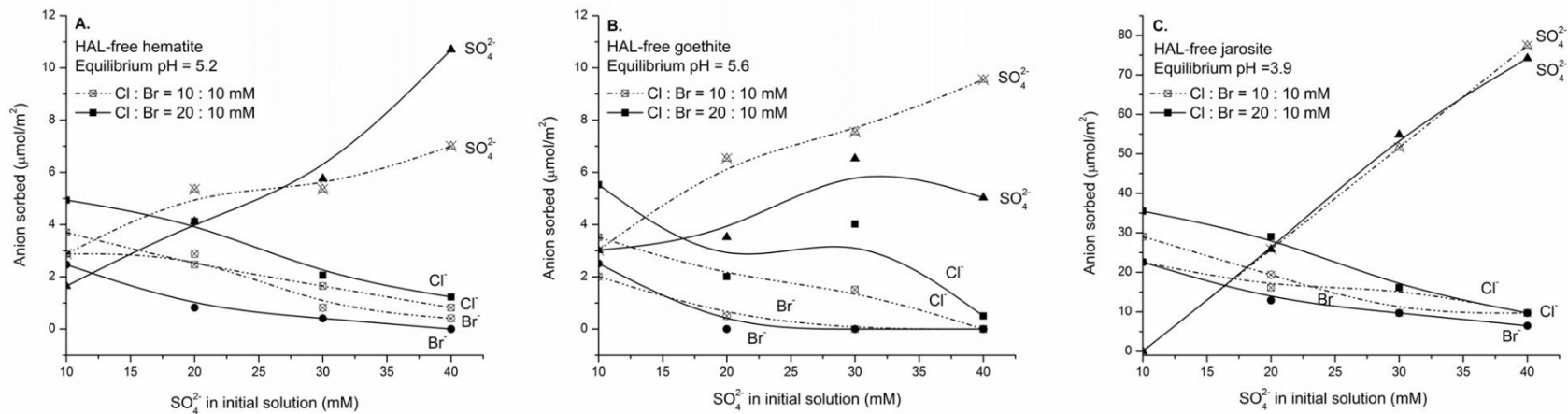
**Figure 3.6.** Adsorption sequence of Cl⁻-Br⁻-SO₄²⁻ with (A) HAL-free hematite, (B) HAL-free goethite, and (C) HAL-free jarosite. Empty symbols and dashed lines represent the conditions of Cl⁻ : Br⁻ = 10:10 mM. Solid symbols and solid lines represent Cl⁻ : Br⁻ = 20:10 mM. SO₄²⁻ increased from 10 to 40 mM with 10 mM intervals in both settings.

## 3.4 Implications and Conclusions

At Meridiani Planum, low pH and the basaltic provenance resulted in a Mg- and Fe-rich hydrological system that produced a highly distinctive evaporitic and diagenetic mineralogy that included jarosite and hematite, magnesium sulfates, and possibly other ferric and ferrous sulfates (Clark et al., 2005; McLennan et al., 2005; Tosca et al., 2005). Large molar S : Cl ratios of 20 : 1 in the strata of the Burns formation, and approximately 5 : 1 in associated soils, illustrate the dominance of sulfate over chloride salts in this geological setting (Clark et al., 2005). In one scenario of post-depositional diagenetic processes, hematite-rich concretions within the Burns formation sandstones grew within the phreatic zone during slow recharge of a high ionic strength groundwater system, which was likely dominated by the sulfate anion, but which also likely contained chloride and bromide. Phosphate anion could also have been present in such a fluid, but likely at limited concentrations due to the relatively low solubility of Ca-, Mg- and Fe-phosphates compared to sulfates and halides.

Our Fe oxidation experiments suggest that if jarosite precipitated from a $Br^-$ and $Cl^-$ containing solution, it may incorporate both $Br^-$ and $Cl^-$ into its structure. Importantly, such incorporation accumulated at least an order of magnitude more $Br^-$ than $Cl^-$ relative to the initial solution concentrations and thus significantly reduced the Cl/Br ratio of the solid compared to the solution. Due to high solution/solid ratio of the system (e.g., 70 g/g in our experiment), such changes in the Cl/Br ratio in the precipitate may not significantly affect the ratio of the solution. Therefore, since the "water : rock" ratio during the event from which jarosite was formed on Mars is largely unconstrained, it is in turn difficult to constrain whether such Br-Cl fractionation in jarosite might also be reflected in the residual solution. Nevertheless, such capability of incorporating large amounts of $Br^-$ compared to $Cl^-$ makes jarosite a plausible candidate for

holding elevated Br on the Martian surface if $Br^-$ was present in the fluid from which jarosite precipitated. The significant decrease of Cl/Br ratios in solids compared to the initial solution further suggests that the parent fluid could be depleted in $Br^-$ with respect to $Cl^-$, but still yield high Br precipitates. In the case of Meridiani Planum, it is thus possible that some high Br abundances detected by Opportunity rover are associated with jarosite, and such jarosite precipitates might originate from brines that were depleted in $Br^-$ concentration initially.

It is still debatable if goethite ever formed from Martian brines due to the lack of goethite in the Meridiani outcrop (Klingelhöfer et al., 2004; Clark et al., 2005). However, if it did, the precipitation of goethite is not expected to affect the Cl/Br ratios in either the solution or the solid.

The incorporation of $Br^-$ and $Cl^-$ in jarosite may affect the stability of jarosite. The general dissolution rate of the four types of synthetic jarosite was in the sequence: Br,Cl-jarosite > Br-jarosite > HAL-free jarosite > Cl-jarosite. We suggested above that weight percent levels of $Br^-$ incorporated into jarosite may distort its structure and make the bonds more susceptible to be attacked during aqueous alteration and thus reduce the stability relative to halogen-free jarosite. In contrast, the low levels of $Cl^-$ incorporated into jarosite somehow slows down the dissolution rate relative to halogen-free jarosite and thus increases the stability. Currently, the crystallographic information on halogen-bearing jarosite, why $Br^-$ is favored over $Cl^-$ by the jarosite structure, and for which site does the Br- substitute in jarosite, remain unclear. Also, how the incorporation of halogens affects jarosite stability is largely unknown. These issues require further systematic work. Nevertheless, our experiments do demonstrate that the initial $Cl^-/Br^-$ ratio from which the jarosite formed may be an important factor influencing jarosite stability.

Our preliminary competitive adsorption experiments for $Cl^-$, $Br^-$, $SO_4^{2-}$ and $H_2PO_4^-$ on halogen-free -hematite, -goethite and -jarosite show that, in a sulfate-dominant solution system where $SO_4^{2-}$ is much higher in abundance than any other anions, $Cl^-$, $Br^-$ and $H_2PO_4^-$ could not compete with $SO_4^{2-}$ on these Fe-mineral surfaces. Therefore, in the diagenetic fluid system where sulfate is most likely the highest abundance component, adsorption may not result in an enrichment of $Cl^-$, $Br^-$ or phosphate onto hematite, goethite, or jarosite. This observation is consistent with the findings from APXS soil data that there are no significant correlations between Cl or P and Np-Ox in soils at both MER landing sites (Greenwood and Blake, 2006).

Finally, a major concern about the partitioning behavior of these anions in terrestrial sedimentary systems is to distinguish between adsorption and incorporation onto/into the Fe-mineral precipitates, since adsorbed anions are potentially much more mobile and not likely to be retained during aqueous diagenesis. As discussed in a previous study of trace element behavior during these same diagenetic oxidation processes (Zhao and McLennan, 2013), this distinction may be of less concern on Mars, and especially for the Burns formation. At Meridiani Planum, mineralogical and geochemical evidence shows extremely limited liquid water interaction after the formation of the mineral assemblages currently present in the sedimentary rocks (Tosca and Knoll, 2009). Accordingly, these anions, regardless of whether initially held by diagenetic minerals through incorporation or adsorption, would be more likely to remain in place associated with the precipitates and thus contribute to the bulk elemental concentrations measured by the Opportunity rover – ultimately the data we are trying to understand.

# References

Arai, Y. and Livi, K. J. (2013) Underassessed phosphorus fixation mechanisms in soil sand fraction, *Geoderma,* **192**, 422-429, doi: 10.1016/j.geoderma.2012.06.021.

Baron, D. and Palmer, C. D. (1996) Solubility of jarosite at 4-35 ℃, *Geochim. Cosmochim. Acta,* **60**, 185-195.

Barrón, V., Torrent, J. and Greenwood, J. P. (2006) Transformation of jarosite to hematite in simulated Martian brines, *Earth Planet Sci. Lett.,* **251(3-4)**, 380-385, doi: 10.1016/j.epsl.2006.09.022.

Bibring, J. P., Arvidson, R. E., Gendrin, A., Gondet, B., Langevin, Y., Le Mouelic, S., Mangold, N., Morris, R. V., Mustard, J. F., Poulet, F., Quantin, C., Sotin, C. (2007) Coupled ferric oxides and sulfates on the Martian surface. *Science,* **317**, 1206-1210.

Brückner, J., Dreibus, G., Gellert, R., Squyres, S., Wänke, H., Yen, A., Zipfel, J. (2008) Mars Exploration Rovers: Chemical composition by the APXS. In *The Martian Surface: Composition, mineralogy, and physical properties* (ed. J. Bell). Cambridge Univ. Press, Cambridge, pp. 58-101.

Chitrakar, R., Tezuka, S., Sonoda, A., Sakane, K., Ooi, K., Hirotsu, T. (2006) Phosphate adsorption on synthetic goethite and akaganeite, *J. Colloid Interface Sci.,* **298**, 602-608.

Clark, B. C., Morris, R. V., McLennan, S. M., Gellert, R., Jolliff, B., Knoll, A. H., Squyres, S. W., Lowenstein, T. K., Ming, D. W., Tosca, N. J., Yen, A., Christensen, P. R., Gorevan, S., Brückner, J., Calvin, W., Dreibus, G., Farrand, W., Klingelhöefer, G., Waenke, H., Zipfel, J., Bell, J. F., Grotzinger, J., McSween, H. Y., Rieder, R. (2005) Chemistry and mineralogy of outcrops at Meridiani Planum. *Earth Planet. Sci. Lett.,* **240**, 73-94.

Cumplido, J., Barrón, V., Torrent, J. (2000) Effect of phosphate on the formation of nanophase lepidocrocite from Fe(II) sulfate, *Clays Clay Miner.,* **48(5)**, 503-510.

Dreibus, G. and Wänke, H. (1987) Volatiles on Earth and Mars: A comparison, *Icarus,* **71**, 225-240.

Dreibus, G. and Haubold, R. (2004) Phosphorus sorption by terrestrial basalt and granite and implications for the martian crust, *Icarus,* **167(1)**, 166-169, doi: 10.1016/j.icarus.2003.09.014.

Dutrizac, J. E. and Chen, T. T. (2010) The behaviour of phosphate during jarosite precipitation, *Hydrometallurgy,* **102(1-4)**, 55-65, doi: 10.1016/j.hydromet.2010.02.004.

Elwood Madden, M. E., Madden, A. S., Rimstidt, J. D., Zahrai, S., Kendall, M. R., Miller, M. A. (2012) Jarosite dissolution rates and nanoscale mineralogy, *Geochim. Cosmochim. Acta,* **91**, 306-321.

Eskandarpour, A., Sassa, K., Bando, Y., Okido, M., Asai, S. (2006) Magnetic removal of phosphate from wastewater using schwertmannite, *Mater. Trans.,* **47(7)**, 1832-1837, doi:10.2320/matertrans.47.1832.

Eskandarpour, A., Onyango, M. S., Ochieng, A., Asai, S. (2008) Removal of fluoride ions from aqueous solution at low pH using schwertmannite, *J. Hazard. Mater.,* **152(2)**, 571-579, doi: 10.1016/j.jhazmat.2007.07.020.

Flores, R. G., Andersen, S. L. F., Maia, L. K. K., Jose, H. J., Moreira, R. D. P. M. (2012) Recovery of iron oxides from acid mine drainage and their application as adsorbent or catalyst, *J. Environ. Manage*., **111**, 53-60, doi: 10.1016/j.jenvman.2012.06.017.

Galvez, N., Barrón, V. and Torrent, J. (1999) Effect of phosphate on the crystallization of hematite, goethite, and lepidocrocite from ferrihydrite, *Clays Clay Miner.,* **47(3)**, 304-311.

Gao, Y. (2001) Surface electrical properties of goethite and adsorption of phosphate and arsenate on iron oxyhydroxides in high ionic strength solutions, Ph.D thesis, Dept. of Earth and Planet. Sci., McGill University, Montreal, Canada.

Gao, Y. and Mucci, A. (2001) Acid base reactions, phosphate and arsenate complexation, and their competitive adsorption at the surface of goethite in 0.7 M NaCl solution, *Geochim. Cosmochim. Acta,* **65(14)**, 2361-2378.

Golden, D. C., Ming, D. W., Morris, R. V., Graff, T. G. (2008) Hydrothermal synthesis of hematite spherules and jarosite: Implications for diagenesis and hematite spherule formation in sulfate outcrops at Meridiani Planum, *Mars, Am. Mineral.,* **93(8-9)**, 1201-1214, doi: 10.2138/Am.2008.2737.

Greenwood, J. P. and Blake, R. E. (2006) Evidence for an acidic ocean on Mars from phosphorus geochemistry of Martian soils and rocks, *Geology,* **34(11)**, 953-956, doi: 10.1130/G22415a.1.

Grotzinger, J. P., Arvidson, R. E., Bell, J. F., Calvin, W., Clark, B. C., Fike, D. A., Golombek, M., Greeley, R., Haldemann, A., Herkenhoff, K. E., Jolliff, B. L., Knoll, A. H., Malin, M., McLennan, S. M., Parker, T., Soderblom, L., Sohl-Dickstein, J. N., Squyres, S. W., Tosca, N. J., Watters, W. A. (2005) Stratigraphy and sedimentology of a dry to wet eolian depositional system, Burns formation, Meridiani Planum, Mars. *Earth Planet. Sci. Lett.,* **240**, 11-72.

Karunatillake, S., Zhao, Y. -Y. S., McLennan, S. M., Skok, J. R., Button, N. E. (2013) Does Martian soil release reactive halogens to the atmosphere? *Icarus,* **226(2)**, 1438-1446, doi:10.1016/j.icarus.2013.07.018.

Kendall, M. R., Madden, A. S., Elwood Madden, M. E., Hu, Q. (2013) Effects of arsenic incorporation on jarosite dissolution rates and reaction products, *Geochim. Cosmochim. Acta,* **112**, 192-207.

Klingelhöfer, G., Morris, R. V., Bernhardt, B., Schroder, C., Rodionov, D. S., de Souza, P. A., Yen, A., Gellert, R., Evlanov, E. N., Zubkov, B., Foh, J., Bonnes, U., Kankeleit, E., Gutlich, P., Ming, D. W., Renz, F., Wdowiak, T., Squyres, S. W., Arvidson, R. E. (2004) Jarosite and hematite at Meridiani Planum from Opportunity's Mössbauer spectrometer. *Science,* **306**, 1740-1745.

Mautner, M. N. and Sinaj, S. (2002) Water-extractable and exchangeable phosphate in Martian and carbonaceous chondrite meteorites and in planetary soil analogs, *Geochim. Cosmochim. Acta,* **66(17)**, 3161-3174.

McLennan, S. M., Bell, J. F., Calvin, W. M., Christensen, P. R., Clark, B. C., de Souza, P. A., Farmer, J., Farrand, W. H., Fike, D. A., Gellert, R., Ghosh, A., Glotch, T. D., Grotzinger, J. P., Hahn, B., Herkenhoff, K. E., Hurowitz, J. A., Johnson, J. R., Johnson, S. S., Jolliff, B., Klingelhöfer, G., Knoll, A. H., Learner, Z., Malin, M. C., McSween, H. Y., Pocock, J., Ruff, S. W., Soderblom, L. A., Squyres, S. W., Tosca, N. J., Watters, W. A., Wyatt, M. B., Yen, A. (2005) Provenance and diagenesis of the evaporite-bearing Burns formation, Meridiani Planum, Mars. *Earth Planet. Sci. Lett.,* **240**, 95-121.

Morris, R. V., Klingelhöfer, G., Schröder, C., Rodionov, D. S., Yen, A., Ming, D. W., de Souza, P. A., Wdowiak, T., Fleischer, I., Gellert, R., Bernhardt, B., Bonnes, U., Cohen, B. A., Evlanov, E. N., Foh, J., Gütlich, P., Kankeleit, E., McCoy, T., Mittlefehldt, D. W., Renz, F., Schmidt, M. E., Zubkov, B., Squyres, S. W., Arvidson, R. E. (2006) Mössbauer mineralogy of rock, soil, and dust at Meridiani Planum, Mars: Opportunity's journey across sulfate-rich outcrop, basaltic sand and dust, and hematite lag deposits, *J. Geophys. Res.,* **111, E12S15**, doi: 10.1029/2006je002791.

Morris, R. V., Klingelhöfer, G., Bernhardt, B., Schröder, C., Rodionov, D. S., de Souza Jr., P. A., Yen, A., Gellert, R., Evlanov, E. N., Foh, J., Kankeleit, E., Gütlich, P., Ming, D. W., Renz, F., Wdowiak, T., Squyres, S. W., Arvidson, R. E. (2004) Mineralogy at Gusev Crater from the Mössbauer spectrometer on the Spirit Rover, *Science,* **305(5685)**, 833-836, doi:10.1126/science.1100020.

Munsell color (1994) Munsell soil color charts (revised edition), Macbeth division of kollmorgen instruments corporation, 405 little Britain road, New Windsor, NY 12553.

Murchie, S. L., Mustard, J. F., Ehlmann, B. L., Milliken, R. E., Bishop, J. L., McKeown, N. K., Noe Dobrea, E. Z., Seelos, F. P., Buczkowski, D. L., Wiseman, S. M., Arvidson, R. E., Wray, J. J., Swayze, G., Clark, R. N., Des Marais, D. J., McEwen, A. S., Bibring, J. –P. (2009) A synthesis of Martian aqueous mineralogy after 1 Mars year of observations from the Mars Reconnaissance Orbiter, *J. Geophys. Res.,* **114**, E00D06, doi: 10.1029/2009je003342.

Navrotsky, A., Forray, F. L., Drouet, C. (2005) Jarosite stability on Mars, *Icarus,* **176(1)**, 250-253, doi: 10.1016/j.icarus.2005.02.003.

Parfitt, R. L. (1982) Competitive adsorption of phosphate and sulfate on goethite (alpha-FeOOH) - a note, *New Zeal. J. Sci.,* **25(2)**, 147-148.

Palme, H. and Jones, A. (2003) Solar system abundances of the elements. In *Treatise on Geochemistry* (eds. H. D. Holland and K. K. Turekian), Elsevier, **vol. 1**, Section 1.03, Table 3, pp. 49.

Pritchett, B. N., Elwood Madden, M. E., Madden, A. S., Phillips, C. (2012) Salinity and temperature effects on the dissolution of natrojarosite and K-jarosite, paper presented at *43rd Lunar Planet Sci. Conf.,* **Abst. #2331**, Lunar Planetary Institute, Woodlands, TX.

Reyes, I. A., Patiño, F., Rivera, I., Flores, M. U., Reyes, M., Hernández, J. (2011) Alkaline reactivity of arsenical natrojarosite. *J. Braz. Chem. Soc.,* **22(12)**, 2260-2267, doi: 10.1590/S0103-50532011001200004.

Rieder, R., Gellert, R., Anderson, R. C., Brückner, J., Clark, B. C., Dreibus, G., Economou, T., Klingelhöffer, G., Lugmair, G. W., Ming, D. W., Squyres, S. W., d'Uston, C., Wänke, H., Yen, A., Zipfel, J. (2004) Chemistry of rocks and soils at Meridiani Planum from the alpha particle X-ray spectrometer. *Science,* **306**, 1746-1749.

Roach, L. H., Mustard, J. F., Lane, M. D., Bishop, J. L. Murchie, S. L. (2010) Diagenetic haematite and sulfate assemblages in Valles Marineris, *Icarus,* **207(2)**, 659-674, doi: 10.1016/j.icarus.2009.11.029.

Ruttenberg, K. C. and Sulak, D. J. (2011) Sorption and desorption of dissolved organic phosphorus onto iron (oxyhydr)oxides in seawater, *Geochim. Cosmochim. Acta,* **75(15)**, 4095-4112, doi: 10.1016/j.gca.2010.10.033.

Savage, K., Bird, D. K., O'Day, P. A. (2005) Arsenic speciation in synthetic jarosite, *Chem. Geol.,* **215**, 473-498.

Schilling, J. -G., Unni, C. K., Bender, M. L. (1978) Origin of chlorine and bromine in the oceans, *Nature,* **273**, 631-636, doi: 10.1038/273631a0.

Schwertmann, U. and Cornell, R. M. (2000) Iron oxides in the laboratory: preparation and characterization, second, completely revised and extended edition, Wiley-Vch, Weinheim.

Sefton-Nash, E. and Catling, D. C. (2008) Hematitic concretions at Meridiani Planum, Mars: their growth timescale and possible relationship with iron sulfates, *Earth Planet Sci. Lett.,* **269(3-4)**, 365-375, doi: 10.1016/j.epsl.2008.02.009.

Shannon, R. D. (1976) Revised effective ionic radii and systematic studies of interatomic distances in halides and chalcogenides, *Acta Cryst.,* **A32**, 751-767.

Torrent, J., Schwertmann, U., Barrón, V. (1992) Fast and slow phosphate sorption by goethite-rich Natural Materials, *Clays Clay Miner.,* **40(1)**, 14-21.

Torrent, J., Schwertmann, U., Barrón, V. (1994) Phosphate sorption by natural hematites, *Eur. J. Soil Sci.,* **45(1)**, 45-51.

Tosca, N. J., McLennan, S. M., Clark, B. C., Grotzinger, J. P., Hurowitz, J. A., Knoll, A. H., Schröder, C. and Squyres, S. W. (2005) Geochemical modeling of evaporation processes on Mars: Insight from the sedimentary record at Meridiani Planum. *Earth Planet. Sci. Lett.,* **240**, 122-148.

Tosca, N. J., McLennan, S. M., Dyar, M. D., Sklute, E. C., Michel, F. M. (2008) Fe oxidation processes at Meridiani Planum and implications for secondary Fe mineralogy on Mars. *J. Geophys. Res.,* **113**, E05005, doi:10.1029/2007JE003019.

Tosca N. J. and Knoll, A. H. (2009) Juvenile chemical sediments and the long term persistence of water at the surface of Mars, *Earth Planet. Sci. Lett*., **286**, 379-386.

Zahrai, S. K., Elwood Madden, M. E., Madden, A. S., Rimstidt, J. D. (2012) Comparing Na-jaroiste and K-jaroiste dissolution rates to determin the effects of crystal chemistry on jarosite lifetimes, paper presented at *43rd Lunar Planet Sci. Conf.*, **Abst. #1658**, Lunar Planetary Institute, Woodlands, TX.

Zhao, Y. -Y. S. and McLennan, S. M. (2013) Behavior of Ni, Zn and Cr during low temperature aqueous Fe oxidation processes on Mars, *Geochim. Cosmochim. Acta,* **109**, 365-383, doi: 10.1016/j.gca.2013.01.039.

# Chapter 4: Photochemical Controls on Oxy-chlorine Production and Br/Cl Fractionation at the Martian Surface

## Abstract

Experiments demonstrate that photo-oxidation of evaporative saline systems containing $Br^-$ and $Cl^-$ are able to produce substantial perchlorate and chlorate under conditions relevant to Mars, and result in Br/Cl fractionation due to preferential volatilization of Br over Cl into the atmosphere. Chlorate can co-occur with perchlorate, and even dominate over perchlorate, particularly in neutral to alkaline aqueous environments. Solid-gas heterogeneous reactions are the most effective pathway accounting for oxy-chlorine formation, and surfaces of sediment particles facilitate such heterogeneous reactions by providing effective interfaces, i.e., higher oxy-chlorine yields on finer-grain quartz particles. Bromine is strongly influenced by photochemical processes and at high abundance is capable of competing with Cl for available oxidants, reacting with Cl radicals, forming oxy-bromine species, and cycling at the Martian surface. The predicted variation of Br abundances in our model, due to photo-oxidation, is consistent with highly variable Br abundances detected on the Martian surface.

**4.1 Introduction**

Despite playing a key role in understanding Martian surficial processes, including both past and current habitability, the geochemistry of halogen elements chlorine (Cl) and bromine (Br) on Mars remains poorly understood. Recent measurements of Cl and Br abundances on the Martian surface reveal that:

(1) Cl is widely distributed (Boynton et al., 2007; Clark et al., 1982; Gellert et al., 2004; Keller et al., 2006; Rieder et al., 2004);

(2) Br is enriched and varies by three orders of magnitude in surface samples, which in turn primarily controls variations of Br/Cl ratios (Brückner et al., 2008; Gellert et al., 2004; Ming et al., 2008; Rieder et al., 2004). Although enrichment of Br has been related to aqueous processes, significant differences in Br concentrations for two Burns formation samples, spatially close to each other with similar S and Cl contents, is difficult to explain solely by $Cl^-$ and $Br^-$ aqueous chemistry in evaporative systems (Rieder et al., 2004);

(3) Perchlorate ($ClO_4^-$) exists at two widely separated locations (Phoenix and Curiosity landing sites) and in three different lithologies (surface soils, aeolian fines, ancient sedimentary rocks) (Hecht et al., 2009; Leshin et al., 2013; Ming et al., 2014), suggesting that oxy-chlorine species may be important components of total Cl abundances, ubiquitous on the Martian surface, and persistent through its history.

The hypothesis that oxy-chlorine species are widely distributed on the Martian surface has attracted considerable attention since it has broad implications for aqueous chemistry, brine stability, organics and habitability (Marion et al., 2010; Hanley et al., 2012; Kounaves et al., 2014). More importantly, it suggests that photochemical oxidation processes, which may have

been underappreciated, could play an important role influencing Cl behavior. Such processes could also affect Br (Sander et al., 2003), and may be one of the explanations for considerable Br variability observed on the Martian surface (Karunatillake et al., 2013).

The ultimate source of perchlorate on Mars is chloride (Cl$^-$), present in the form of solid, liquid, or gas at the Martian surface (e.g., Catling et al., 2010; Kang et al., 2008; Kounaves et al., 2010; Leshin et al., 2013; Rao et al., 2010; Schuttlefield et al., 2011). Due in part to limited understanding of how natural perchlorate forms on Earth, some key questions remain unclear including formation pathways, types of effective reactions (i.e., atmospheric gas-gas, or heterogeneous solid-gas or liquid-gas), roles of intermediate oxidation species between Cl$^-$ and ClO$_4^-$ (i.e., ClO$_3^-$, ClO$^-$, and ClO$_2^-$), type of oxidants, and other variables such as pH and temperature. Thus, for Mars, questions of great interest remain unanswered, such as (1) whether ClO$_3^-$, ClO$_2^-$ and ClO$^-$ are also present on the Martian surface; (2) what are the most likely efficient formation pathways; (3) which natural oxidants account for perchlorate formation, and so forth. In addition, due to the more attenuated atmosphere of Mars compared to Earth, relatively well-established atmospheric origins of perchlorate on Earth (Bao and Gu, 2004; Catling et al., 2010; Jackson et al., 2010) may not be quantitatively sufficient to explain the apparently abundant perchlorate detected on Mars, thus demanding alternative pathways, such as heterogeneous reactions (Smith et al., 2014).

Studies of terrestrial tropospheric Br suggest that Br preferentially volatilizes over Cl in brines having a Br/Cl ratio greater than seawater (e.g., Enami et al., 2007; Finlayson-Pitts, 2010; Lary, 2005) and such surface-atmosphere transfer is sufficient to influence Br mass balance and fractionate Br/Cl ratios in local regions (Risacher et al., 2006; Wood and Sanford, 2007). Some tropospheric Br sources identified on Earth may be relevant to Mars, including evaporative brine

and saltpan environments (Hönninger et al., 2004; Risacher et al., 2006; Wood and Sanford, 2007), brine films on suspended dust (Sander et al., 2003), and aerosol release from newly-formed ice on seawater (Kaleschke et al., 2004; Yang et al., 2008). At present, it is unknown if Br species other than $Br^-$ (e.g., Br, BrO, and $BrO_3$) are present on Mars, and how any Br would influence Cl during photochemical processes.

This work demonstrates that by evaporating brines containing $Br^-$ and $Cl^-$ (Appendix 2 Table S1) with ultraviolet (UV) radiation ($\lambda = 254$ nm; UVC range) and under current Earth or Mars atmosphere, substantial amounts of oxy-chlorine species ($ClO_4^-$ and $ClO_3^-$) and in some cases bromate ($BrO_3^-$) are produced, and that significant Br/Cl fractionation is present in the resulting evaporites. Variables we examined were brine compositions, pH, sediment grain size, atmospheric conditions, and length of UV irradiation. Our results indicate an efficient heterogeneous reaction pathway, alternative to the atmospheric gas-gas reaction, for perchlorate and chlorate to form. The experimental and analytical methods are described in detail in Appendix 2 of this thesis. Appendix 2 Table S2 summarizes all of the experiments conducted in this study as a "roadmap".

## 4.2 Results and Discussion

**Formation of perchlorate and chlorate**

$ClO_4^-$ and $ClO_3^-$ were detected in the final evaporites of most experiments undergoing UV radiation (detection limit 4 µg/kg). $ClO_2^-$ and $ClO^-$ were not detected but these species have order of magnitude higher detection limits ($ClO_2^-$ - 8 µg/g; $ClO^-$ - 64 µg/kg) and so it is not clear if the apparent absence of these species is due to being unstable under UV irradiation. $NO_3^-$ was not detected in any of the experimental products (detection limit 400 µg/g).

In the evacuated gas, $Cl^-$, $Br^-$, $ClO_4^-$ and $ClO_3^-$ were identified, but $ClO^-$ and $ClO_2^-$ were not detected. Bromate and sulfate also were not detected in the gas phase. Note that the gas-phase analyses were designed for species identification only and thus are not appropriate to use for quantifying the evaporating systems (see Appendix 2 for details of experimental design). See Appendix 2 Table S3 for the complete dataset.

Production of $ClO_4^-$ and $ClO_3^-$ increased with prolonged UV irradiation (Figure 4.1). The yields of $ClO_4^-$ and $ClO_3^-$ and the resultant $ClO_4^-/ClO_3^-$ ratios varied from brine to brine, likely controlled by brine chemistry, such as pH and cation abundances, and the nature of the final precipitates. $ClO_3^-$ dominated over $ClO_4^-$ in all of the experiments under neutral to alkaline conditions.

One extreme case of $ClO_4^-$ dominance occurred in an experiment with Brine #6, a pH 2 brine bearing $Fe^{3+}$ and evaporated under Earth atmosphere. In this experiment, orders of magnitude higher $ClO_4^-$ than $ClO_3^-$ were observed and the molar ratio $ClO_4^- / (ClO_4^- + ClO_3^-)$ ~1 throughout the experiment. This contrasts with the persistent high abundance of $ClO_3^-$ in the other brine experiments. Such extreme $ClO_4^-/ClO_3^-$ ratios are likely due to the highly acidic condition of this system. Excess protons could decompose $ClO_3^-$ with byproduct $ClO_2^-$, which led to additional $ClO_4^-$ formation (Rao et al., 2010). Accordingly, when this brine was evaporated under Martian atmosphere, in which the pH of the initial brine was greatly buffered by atmospheric $CO_2$, $ClO_3^-$ again dominated over $ClO_4^-$, as was observed in other neutral to alkaline brines (Brine #6 Ca-Mg-Fe-Cl-Br-$SO_4$; type 'B' experiments of Appendix 2 Table S2; results are shown in Table 4.1).
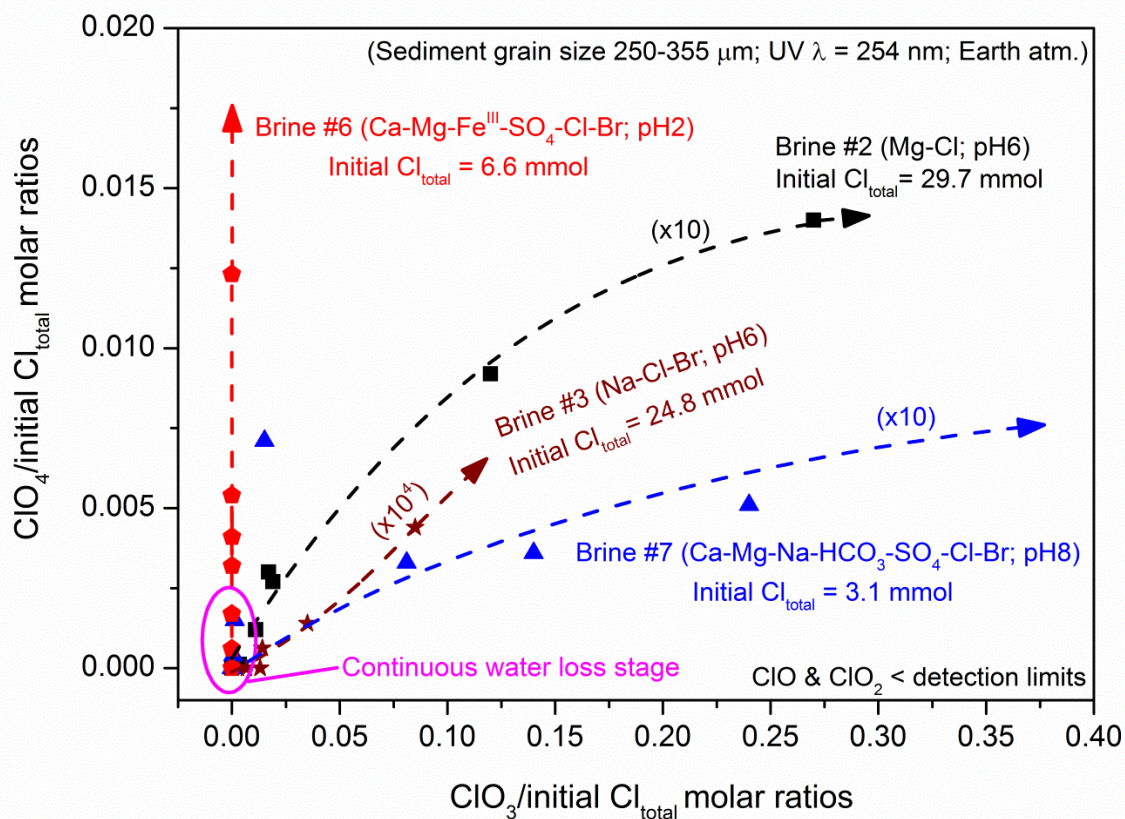
**Figure 4.1.** Molar ratios of $ClO_4^-/Cl_{total}$ versus $ClO_3^-/Cl_{total}$ in evaporating materials during extended time UV exposure experiments (UV time = 384 h) with Brines #2, #3, #6 and #7. Solid symbols represent samples collected every 48-72 h, and dash lines are the polynomial regression fit of the data points, and arrows show direction of increasing UV exposure time. In order to plot results on the same scale, perchlorate and chlorate concentrations were multiplied 10 times in Brines #2 (black) and #7 (blue), and $10^4$ times in Brine #3 (brown). Orders of magnitude lower yields of oxy-chlorine in Brine #3 was likely due to bromate production, which was $10^4$ times greater than levels of oxy-chlorine species. Samples within pink oval formed under "wet" conditions (i.e., excess water lost via evaporation > 0.2 g). Orders of magnitude differences in oxy-chlorine yields between "wet" and "dry" conditions indicate that heterogeneous solid-gas reactions better facilitate oxy-chlorine production.

**Table 4.1.** Comparison of $ClO_4^-$ and $ClO_3^-$ produced under Earth versus Mars atmosphere (quartz grain size = 250-355 μm; pressure 1 atm.)

| | $Cl^-$ | $Br^-$ | $SO_4^{2-}$ | $ClO_4^-$ | $ClO_3^-$ | $BrO_3^-$ | $Br^-/Cl^-$ | S loss | $ClO_4^-/Cl_{total}$ | $ClO_3^-/Cl_{total}$ | $ClO_4^-/Oxy\text{-}Cl_{total}$ |
|---|---|---|---|---|---|---|---|---|---|---|---|
| | mmol | mmol | mmol | μmol | μmol | μmol | molar | % | fraction | fraction | fraction |
| **Brine #4 Mg-$SO_4^{2-}$-$Cl^-$-$Br^-$ (pH 6)** | | | | | | | | | | | |
| Initial | 0.55 | 0.55 | 1.56 | < DL | < DL | < DL | 1.01 | | | | |
| Control | 0.57 | 0.56 | 1.51 | < DL | < DL | < DL | 0.99 | 3.2% | < DL | < DL | < DL |
| Final-Earth | 0.51 | 0.09 | 1.47 | 0.129 | 0.943 | < DL | 0.17 | 5.9% | 2.3E-04 | 1.7E-03 | 0.12 |
| Final-Mars | 0.43 | 0.28 | 1.47 | 0.061 | 1.525 | < DL | 0.65 | 5.8% | 1.1E-04 | 2.8E-03 | 0.04 |
| **Brine # 5 K-$SO_4^{2-}$-$Cl^-$-$Br^-$ (pH 6)** | | | | | | | | | | | |
| Initial | 0.20 | 0.23 | 0.83 | < DL | < DL | < DL | 1.15 | | | | |
| Control | 0.19 | 0.15 | 0.72 | < DL | < DL | < DL | 0.80 | 13.7% | < DL | < DL | < DL |
| Final-Earth | 0.20 | 0.12 | 0.80 | 0.016 | 0.146 | 9.7 | 0.59 | 3.7% | 8.0E-05 | 7.3E-04 | 0.10 |
| Final-Mars | 0.18 | 0.10 | 0.55 | 0.197 | 0.917 | < DL | 0.54 | 33.4% | 9.9E-04 | 4.6E-03 | 0.18 |
| **Brine #6 Ca-Mg-$Fe^{3+}$-$SO_4^{2-}$-$Cl^-$-$Br^-$ (pH 2)** | | | | | | | | | | | |
| Initial | 0.30 | 0.29 | 0.83 | < DL | < DL | < DL | 0.96 | | | | |
| Control | 0.05 | 0.17 | 0.81 | < DL | < DL | < DL | 3.72 | 3.0% | < DL | < DL | < DL |
| Final-Earth | 0.01 | 0.00 | 0.39 | 1.117 | 0.019 | < DL | 0.44 | 53.6% | 3.7E-03 | 6.4E-05 | 0.98 |
| Final-Mars | 0.10 | 0.11 | 0.87 | 0.202 | 0.823 | < DL | 1.08 | -4.7% | 6.7E-04 | 2.7E-03 | 0.20 |
| **Brine #7 Ca-Mg-Na-$HCO_3^-$-$SO_4^{2-}$-$Cl^-$-$Br^-$ (pH 8)** | | | | | | | | | | | |
| Initial | 2.02 | 2.87 | 11.15 | < DL | < DL | < DL | 1.42 | | | | |
| Control | 2.09 | 3.00 | 9.79 | < DL | < DL | < DL | 1.44 | 12.2% | < DL | < DL | < DL |
| Final-Earth | 1.06 | 0.95 | 4.45 | 1.447 | 4.552 | < DL | 0.90 | 60.1% | 7.2E-04 | 2.3E-03 | 0.24 |
| Final-Mars | 0.92 | 1.10 | 5.07 | 0.019 | 0.158 | < DL | 1.19 | 54.5% | 9.4E-06 | 7.8E-05 | 0.11 |

a.  Initial solutions and control samples (without UV irradiation) were all free of oxy-chlorine species and bromate.
b.  $ClO_2^-$ and $ClO^-$ were not detected in any sample. Detection limits in the final evaporative solid mixtures were 4 μg/kg ($ClO_3^-$ and $ClO_4^-$), 8 μg/g ($ClO_2^-$ and $BrO_3^-$), and 64 μg/kg ($ClO^-$).
c.  Direct comparison between different types of brines is not appropriate, since many variables need to be taken into account, such as brine composition and pH, initial amounts of $Cl^-$ and $Br^-$, final evaporites, evaporation rate, etc.

Another important feature revealed in Figure 4.1 is that $ClO_4^-$ and $ClO_3^-$ yields increased by one to two orders of magnitude after the systems became "dry" (i.e., weight loss from evaporating system < 0.2 g, although crystalline and adsorbed water may still have been present), suggesting that "dry" conditions better promoted oxy-chlorine species formation. In $Cl^-$ to $ClO_4^-$ oxidation experiments using ozone, Kang et al. (2008) also observed that the reaction was much more efficient for dry aerosol oxidation compared to solution phase oxidation. Accordingly, one of our UV experiments (Brine #1 Mg-Cl-Br; type 'D' experiments of Appendix 2 Table S2; results are shown in Appendix 2 Table S3) did not produce the same level of oxy-chlorine species as did other experiments, since excess water was persistent through to the end of the experiment. The excess water would be expected to dissolve intermediate species (e.g., $ClO^-$ and $ClO_2^-$), hinder interaction of halogens with gaseous oxidants, and slow down the rates of oxidation reactions.

Despite suggestions that surfaces of semiconducting minerals (e.g., anatase, rutile and ilmenite) best facilitate $ClO_4^-$ formation under UV (Schuttlefield et al., 2011), our experiments show that quartz ($SiO_2$) can also promote formation of oxy-chlorine species. As shown in Figure 4.2, production of $ClO_4^-$ and $ClO_3^-$ significantly correlated with sediment grain size. The highest abundances of $ClO_4^-$ and $ClO_3^-$ were produced on the finest grain size (size 90-125 μm), and as grain size coarsened, the yields decreased, to the point where $ClO_4^-$ was below detection limits when grain size reached >710 μm. Smaller grains have larger surface area, and may contribute to the efficiency of the reactions in two ways: (1) for gas-solid heterogeneous reactions, smaller grains of quartz provided a larger interface by adsorbing thin films of liquid or dry salt aerosols on their surface, so that the heterogeneous reactions could occur even before the whole brine system became entirely dry; (2) quartz grains were capable of generating oxidizing radicals on

133

the surface under UV irradiation (Xu et al., 2013), therefore, larger surface area of quartz may facilitate the formation of oxidants and thus promote the photo-oxidation processes. See section "Possbile oxidants".

Substantial $ClO_4^-$ and $ClO_3^-$ were produced under both Mars and Earth atmospheric conditions. Yields were much less for Mars conditions compared to the $O_2$-rich terrestrial atmosphere (Table 4.1). $ClO_4^-/ClO_3^-$ ratios produced by brines with pH 6-8 under Martian atmosphere followed similar trends as they did in the Earth atmosphere, except for the experiment with Brine #6 (pH 2), in which a reversed $ClO_4^-$ and $ClO_3^-$ pattern was present compared to that in the terrestrial atmosphere. The Martian atmosphere in our experimental setting was sufficient to buffer the initial system and thus shifted the pH from acidic to neutral, enabling preservation of the $ClO_3^-$ similar to that seen in other neutral to alkaline brines. This observation in turn confirms that pH is an important controlling factor of the $ClO_4^-/ClO_3^-$ ratios.

The influence of low pH ($\leq 2$) on Cl chemistry in our experiments is likely controlled by several factors. First, the zero point of charge (ZPC) of quartz is 2.0, therefore, at pH $\leq 2$, the quartz surface is positively charged and capable of absorbing greater amounts of negatively charged halogen anions (e.g., $Cl^-$, $ClO^-$, $ClO_2^-$) relative to higher pH conditions, which may increase the efficiency of heterogenous reactions on the quartz surface in producing $ClO_4^-$. Further, as discussed above, low pH may facilitate the $ClO_3^-$ decomposition and $ClO_2^-$ production, which may contribute to additional $ClO_4^-$ production and result in $ClO_4^-$ dominance over $ClO_3^-$. In addition, low pH (~ 2.5) could also increase the efficiency of transforming $Cl^-$ to other intermediate species, such as $Cl_2/OCl^-$, in an oxidizing aqueous system (Rao et al., 2010). Although producing these intermediate species may not necessarily increase the efficiency of
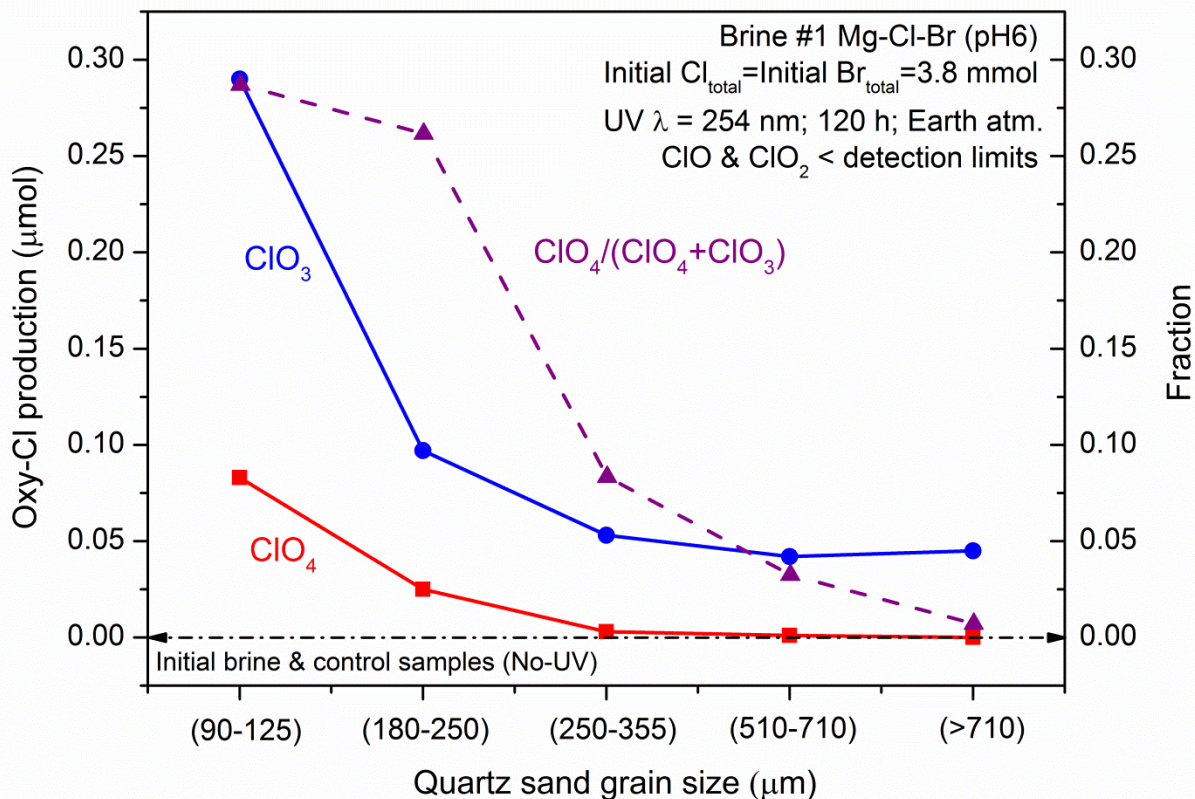
**Figure 4.2.** Significant correlation between yields of $ClO_4^-$ and $ClO_3^-$ and quartz grain size. Absolute $ClO_4^-$ and $ClO_3^-$ abundances are shown in solid symbols and lines, and $ClO_4^-$ fraction of total ($ClO_4^- + ClO_3^-$) is shown as solid symbols and a dash line. Dash arrow indicates initial brine and that control samples that were produced without UV were free of oxy-chlorine. $ClO_2^-$ and $ClO^-$ were not detected. As sediment grain size coarsened, concentrations of $ClO_4^-$ and $ClO_3^-$, and the $ClO_4^-$ / ($ClO_3^-$ + $ClO_4^-$) ratio all decreased. $ClO_4^-$ was absent from samples when sediment grain size > 710 μm.

producing $ClO_4^-$ (Rao et al., 2010), it could increase the volatility of Cl from a chloride aqueous system.

**$Br^-/Cl^-$ fractionation and S mobility**

Besides the production of oxy-chlorine species, substantial loss of bromide was also observed during photochemical oxidation. As shown in Figure 4.3, continuous loss of $Br^-$ occurred in all brines as a function of UV irradiation time (Figure 4.3 (A)). Loss of $Br^-$ was greater than $Cl^-$, suggesting that Br was preferentially volatilized over Cl, and thus controlled the $Br^-/Cl^-$ ratios in the final evaporites (Figure 4.3 (B)). These observations are consistent with Br/Cl fractionation observed at the Martian surface (e.g., Rieder et al., 2004; Gellert et al., 2006; Brückner et al., 2008; Karunatillake et al., 2013), and other studies of terrestrial troposphere and evaporation systems (e.g., Hönninger et al., 2004; Smoydzin and von Glasow, 2009; Wood and Sanford, 2007). On the other hand, there is no apparent correlation between the extent of Br/Cl fractionation and the production of oxy-chlorine species.

Bromate was detected in experiments involving two of the brines (Brine #3 $Na-Cl^--Br^-$ and Brine #7 $Ca-Mg-Na-HCO_3^--SO_4^{2-}-Cl^--Br^-$), but was not consistently present in all experiments. In samples with $BrO_3^-$ present, the oxy-chlorine abundance was low, suggesting competition between Br and Cl for available oxidants, although the conditions that encourage bromate formation are not known. In addition, results for experiments with Brines #1 and #2 show that when other variables are the same, yields of $ClO_4^-$ and $ClO_3^-$ are higher in bromide-free brine compared to bromide-bearing brine (Table 4.2).

The oxidation reaction of $Br^-$ by Cl radical is ~100 times faster than oxidation reactions involving the OH radical (Spicer et al., 1998). Hence, in the presence of $Br^-$, Cl may act as an

efficient oxidant rather than as a reducer, which in turn could influence the Cl cycle at the Martian surface.

In addition, sulfate behaved conservatively during photo-oxidation. Sulfate was not detected in evacuated gases from the reaction chamber as were halogen species, such as $Br^-$, $Cl^-$, $ClO_4^-$ and $ClO_3^-$. Given the oxidizing conditions, it also unlikely that sulfate was reduced to lower oxidation states and volatilized (e.g., $SO_2$ or $H_2S$). Therefore, sulfate variations in our experiments were primarily controlled by precipitation of sulfate-containing minerals, that is, removal from brines mainly due to formation of insoluble precipitates, such as Ca-sulfates and Fe-sulfates or Fe-oxides. Accordingly, the Br/S and Cl/S ratios of our evaporating systems were mainly controlled by the variation of Br and Cl. This is also consistent with the in-situ observations in Martian surface soil profiles (Karunatillake et al., 2013).
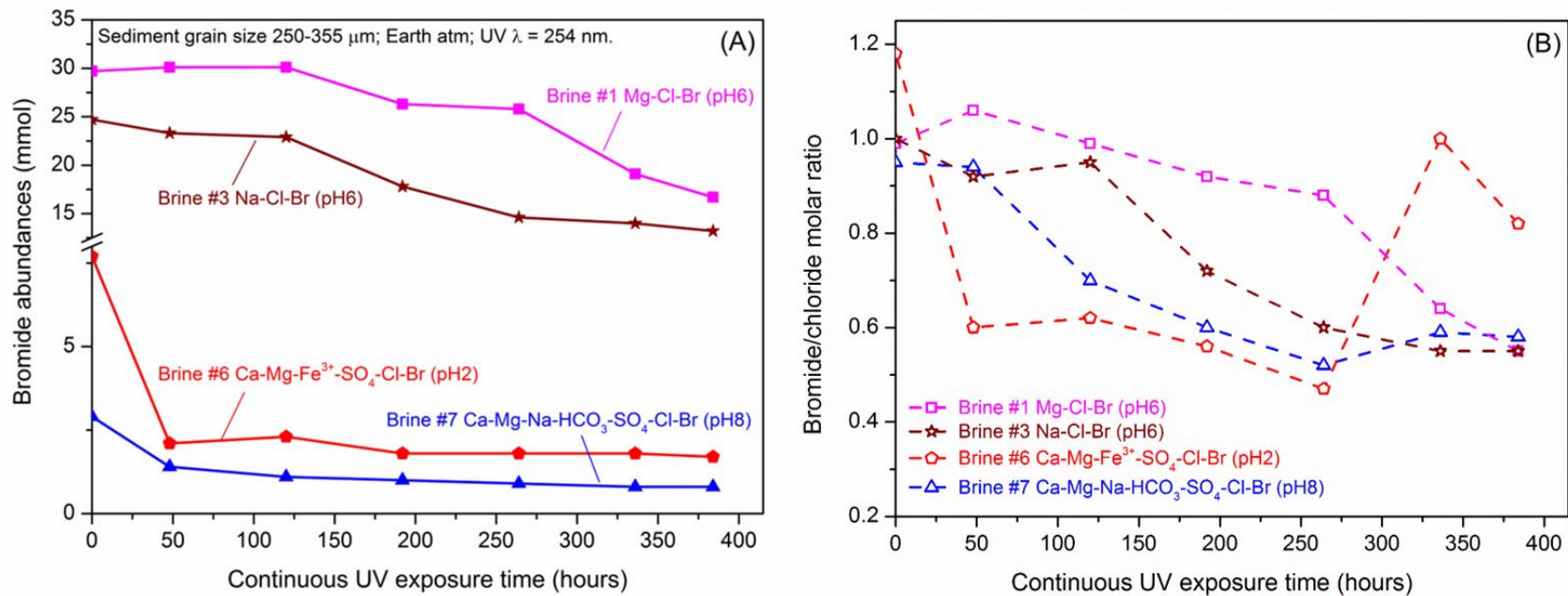
**Figure 4.3.** Br⁻/Cl⁻ fractionation in the evaporating materials during extended time UV exposure experiments (UV time = 384 h) with Brines #2, #3, #6 and #7. Loss of Br⁻ primarily controls the Br⁻/Cl⁻ variations in the evaporating materials. (A) Br⁻ abundances decreased (solid symbols and lines) with increasing UV irradiation time. (B) Br⁻/Cl⁻ molar ratios (open symbols and dash lines) also decrease as a function of increasing UV irradiation time. Note that there is a reversal of trend at the late stage of the Brine #6 experiment, caused by an increased loss of Cl⁻ relative to Br⁻, probably due to the greater acidity at this stage that also facilitated liberation of Cl⁻.

**Possible oxidants**

The primary oxidants in our evaporation experiments are largely unknown, since the experiments were not designed to distinguish specific oxidants. However, because the wavelength of our UV lamp (90% $\lambda = 254$ nm and 10% $\lambda > 254$ nm) is sufficient only to break O-H in the water molecule (bond energy 459 kJ/mol; required $\lambda < 260$ nm) but not the O-O bond in the oxygen molecule (bond energy 498 kJ/mol; required $\lambda < 240$ nm), we conclude the initial oxidants produced by the UV source, even in the presence of $O_2$ molecules, were likely OH· and H· radicals rather than ozone or the O· radical. Subsequent photochemical reactions could further involve $O_2$ or other halogen radicals, however, ozone should not be the primary oxidant accounting for the oxyanion formation in our experiments, as suggested in many terrestrial perchlorate studies (e.g., Bao and Gu, 2004; Catling et al., 2010; Jackson et al., 2010)

Another possible source of oxidant radicals may be generated directly on the quartz surface via photocatalysis. Xu et al. (2013) demonstrated that besides intensively studied anatase, rutile and hematite, quartz is capable of generating $H_2O_2$ on its surface under UV irradiation ($\lambda = 254$ nm) at pH 6. Given the strong correlation between oxychlorine production and quartz grain size, it is possible that smaller grain size of quartz facilitated to produce higher amount of oxidants on its surface, by providing larger surface area. The mineral surface-associated radical formation processes may be particularly important in our experiments to explain the high yields of oxy-chlorine and bromate under conditions in which ozone was likely absent. Further investigations are necessary to constrain the efficiency of oxidant production via quartz under conditions relevant to our experiments.

We conducted supplementary experiments to examine whether interaction of hydrogen peroxide ($H_2O_2$) with $Br^-$ and $Cl^-$ containing brines could produce oxy-chlorine species or

fractionate Br$^-$/Cl$^-$ in the solution without UV radiation (see Appendix 2 Table S5) and results were negative. Reactions of H$_2$O$_2$ with Br$^-$ or Cl$^-$ catalytically decomposed H$_2$O$_2$ and released O$_2$, and such reaction rates showed no difference between Br$^-$ or Cl$^-$, and thus should not cause Br$^-$/Cl$^-$ fractionation in solution (e.g., Bray and Livingston, 1923; Livingston and Bray, 1926; Livington and Bray, 1925). Conditions involving UV radiation were not examined because with UV, photolysis of H$_2$O$_2$ could occur and form OH· radicals (H$_2$O$_2$ $_{(aq)}$ + hυ (λ = 254 nm) → 2 OH $_{(aq)}$), which would then be similar to the conditions in our evaporation experiments.

## 4.3 Implications for Mars

Our experiments demonstrate that with UV radiation, substantial perchlorate and chlorate can be produced by photo-oxidation of chloride in both liquid and solid saline systems, even under the current Martian atmosphere. As a model study, the UV flux (λ = 254 nm) adapted in our experiments (8.5 mW/cm$^2$) was much higher than the estimated flux that can reach the current Martian surface (5 µW/cm$^2$; Cockell et al., 2005). However, even with less UV$_{254}$ flux on Mars, substantial amounts of oxychlorine species are still likely to be produced with the aid of other shorter wavelength fluxes and on the order of up to a billion years of near-continuous irradiation. Subsequent aqueous related activies could further enrich the oxychlorine species at local areas, particularly in environments that lack consumption mechanisms for oxychlorine after its formation (e.g., low pH aqueous activities, organics, meteorite bombardments, etc).

Solid-gas and liquid-gas heterogeneous reactions to produce oxy-chlorine species appear more efficient than simple atmospheric origins. Such reactions can occur directly in saline systems or on the surface of sediment particles as coatings of brine or dry salt. Inert sediment

particles (e.g., quartz) can facilitate the reactions by providing effective interfaces, i.e., higher oxy-chlorine yields on finer grain sediment particles.

Consistent with our findings, chlorate has been reported, along with natural perchlorate, on Earth, including in the Atacama Desert, in Death Valley and in Antarctica (Rao et al., 2010a). Recently, chlorate was also reported in a sawdust fraction of SNC meteorite EETA79001 (Kounaves et al., 2014). Since direct transformation from chlorate to perchlorate is not efficient (Rao et al., 2010), once formed, $ClO_4^-/ClO_3^-$ ratios can remain constant at neutral to alkaline pHs, where decomposition of perchlorate or chlorate would not likely occur. At low pH, chlorate is less stable than perchlorate, and decomposition of chlorate could lead to additional perchlorate formation. Therefore, the pH of the environment where oxy-chlorine species form or are preserved is critical in controlling the $ClO_4^-/ClO_3^-$ ratios. Acidic conditions favor perchlorate dominance over chlorate, and even extreme molar ratios of $ClO_4^- / (ClO_4^- + ClO_3^-) = 1$ could be present under conditions similar to our Brine #6 experiment.

Due to the lack of complete perchlorate, chlorate and pH datasets for most natural perchlorate samples, it is difficult to evaluate the original relationships between perchlorate and chlorate, including possible influences of pH on $ClO_4^-/ClO_3^-$ ratios in natural systems. As shown in Table S6, with the very limited data reported so far, chlorate is present with perchlorate in available terrestrial natural samples, consistent with our experiments. Molar $ClO_4^-/ClO_3^-$ ratios of samples from Atacama Desert and Death Valley (both containing caliche, suggesting pH > 7-8) were typically less than one, and in many cases, chlorate is much higher than perchlorate. Although the perchlorate and chlorate present in these terrestrial samples are likely formed in the atmosphere involving ozone (Jackson et al., 2010), and thus different from our proposed

heterogeneous reaction formation, it does support that high pH could facilitate preservation of chlorate.

Our experiments predict that chlorate is likely present in the total oxy-chlorine component, at equal or higher levels than perchlorate, at both the Phoenix and Curiosity rover landing sites where the aqueous environment was neutral to slightly alklaine (Grotzinger et al., 2014; Hecht et al., 2009). At other locations where acidic condition prevailed, such as Meridiani Planum (McLennan et al., 2005), oxy-chlorine species could form, but likely would be dominated by perchlorate, due to the predicted decomposition of chlorate.

The Wet Chemistry Lab (WCL) onboard the Phoenix lander carried out the first direct measurents of soluble salts in surface soil on Mars (Hecht et al., 2009; Kounaves et al., 2010). At the landing site, three dry surface soil samples (named Rosy Red, Sorceress 1 and Sorceress 2) were scooped and added to liquid water heated to a temperature between $5 - 10$ ºC, and then the dissolved ions of the soil leachate solutions were analyzed by an array of Ion Selective Electrodes (ISEs) The sensitivity of the ISEs used for measurement was in the relative order $SO_4^{2-} \leq F^- \leq Cl^- \leq Br^- \leq NO_3^- \leq ClO_3^- \leq I^- \leq ClO_4^- \leq SCN^-$, so it is possible the high intensity of $ClO_4^-$ overwhelmed the $ClO_3^-$ or $NO_3^-$ signal (Hanley et al., 2012). The initial report of WCL solution results suggested there were unmeasured anions present in the leachate solution samples (6.49 mM monovalent or 3.25 mM divalent equivalent; Hecht et al., 2009), however, with subsequent work to constrain soluble sulfate concentrations, charge balances of two out of three samples is now thought to be negative (Kounaves et al., 2010a). Such negative charge balances are not likely caused by unidentified cations, but more likely by an overestimation of anion concentrations, particularly for $Cl^-$, $ClO_4^-$ or $SO_4^{2-}$ (Toner et al., 2014). In addition, other unidentified anions such as $ClO_3^-$ and $NO_3^-$ may also be present (Toner et al., 2014). Because the

original Phoenix WCL analysis is characterized by relative errors in concentration between about 20–50% due to high levels of noise and anomalous signal fluctuations (Hecht et al., 2009; Kounaves et al., 2010), Toner et al. (2014) reanalyzed the WCL data using improvements of original analysis and a series of geochemical modeling methods, to better characterize ion concentrations. This study concluded that of the Rosy Red result is more robust than the other two analyses (Sorceress 1 and Sorceress 2), and geochemical modeling using Rosy Red data suggested lower $Cl^-$ and $Ca^{2+}$ concentrations than the original report by Hecht et al. (2009) and Kounaves et al. (2010).

Based on the WCL data discussion and our experimental results, if any additional $ClO_3^-$ is also present, at comparable levels as perchlorate, the estimated proportion of oxy-chlorine species to total chlorine would be >90% as reported by Hecht et al. (2009) (see Appendix 2 Table S6), and even greater using the data analysis approach suggested by Toner et al. (2014). Therefore, the Phoenix soil appears unique compared to other Martian or terrestrial samples due to its very high proportion of oxy-chlorine which dominates over chloride. Such high abundances and high proportions of oxy-chlorine species, does not likely result directly from any known photochemical processes. However, whether the high abundances are caused by accumulation of oxy-chlorine species over extensive geological time, or particular conditions of arctic environment may efficiently promote the heterogeneous reactions, or aqueous activities such as evaporation or freeze-thaw processes might facilitate concentrating of these species, are currently unknown.

At Gale Crater, the Sample Analysis at Mars (SAM) instruments onboard the Curiosity rover was able to identify oxy-chlorine species in the evolved gases during pyrolysis of the Rocknest aeolian fines (RN) and the John_Klein (JK) and Cumberland (CB) drill materials

(Leshin et al., 2013; Ming et al., 2014). However, SAM is unable to uniquely distinguish specific oxy-chlorine species. Simulation experiments were conducted in laboratories on Earth, however, pure common perchlorate salts were unable to reproduce the exact pattern matching the $O_2$- and HCl-release profiles and decomposition temperatures obtained in the RN, JK, and CB samples (Leshin, et al., 2013; Ming et al., 2014). The search for plausible candidates or mineral combinations is ongoing (Ming et al., 2014; Sutter et al., 2014). For example, it has been suggested that mixing perchlorate with Fe-oxides/oxyhydroxides or mixing chlorate with hematite could lower $O_2$-release temperatures as found in the RN, JK and CB samples (Rudloff et al., 1970). In any case, further experimental evaluation is required to resolve these questions. Our results indicate that because of the near neutral aqueous waters from which the sedimentary rocks at Yellowknife Bay were deposited (Grotzinger et al., 2013), perchlorate and chlorate are both likely preserved, and thus might co-exist in these samples. Although it is difficult to estimate the likely $ClO_4/ClO_3$ ratios in these Martian samples due to the lack of understanding of possible geochemical cycles of perchlorate and chlorate at Gale Crater, it might be helpful to consider combined perchlorate and chlorate as a component in further simulation experiments, with starting molar $ClO_4/ClO_3$ ratios 1 to 0.1, to evaluate if there is any influence on evolved $O_2$- and HCl-release profiles compared to Gale Crater materials.

As shown in Appendix 2 Table S6, the oxy-chlorine proportion of total chlorine in Martian samples is at least one order of magnitude higher than any terrestrial samples. The significant difference might be in part due to the formation pathways, in that terrestrial samples are thought to mostly form in the atmosphere involving ozone (Jackson et al., 2010), whereas the Martian samples may have formed by the heterogeneous reactions proposed in this study. In addition, with higher solar fluxes and much longer prevailing dry conditions on the Martian surface, the

144

efficiency of producing oxy-chlorine species could be accordingly higher than that on Earth. Finally, perchlorate and chlorate deliquescence under Martian surface conditions, and subsequent evaporation or freeze-thaw processes might further concentrate these species on a local scale.

Bromine may be more reactive on the Martian surface than previously thought due to photo-oxidation processes (Karunatillake et al., 2013). Although the initial settings of molar $Br^-$/$Cl^- = 1$ for our experiments is unrealistic for either Mars or Earth natural systems, it provides a clear view of how $Br^-$ would behave once in high abundances. At high Br abundances and Br/Cl molar ratios much greater than terrestrial seawater (molar Br/Cl = 0.0015), Br is capable of competing with Cl for available oxidants, reacting with Cl radicals, forming oxy-bromine species, and preferentially volatilizing over Cl into the atmosphere, potentially leading to highly variable Br/Cl ratios on a local scale.

We propose a model to explain the photochemical influences on Br and Cl at the Martian surface (Figure 4.4). Two main sources of halogens are: (1) volcanic degassing and (2) $Br^-$ and $Cl^-$ containing brine-salt systems. With UV radiation, $Br^-$ and $Cl^-$ can be photo-oxidized and mobilized, and form three major transfer pathways:

(1) Mobilization and volatilization directly into the atmosphere. By direct volcanic degassing or photo-oxidation processes on saline salts or liquid, Br and Cl can be volatilized into the atmosphere, in the form of Br·, BrCl or BrO (Sanders, 2003) and Cl·, ClO, $ClO_2$ (Rao et al., 2010). In addition, blowing sand and dust devils/storms could also temporally raise salt solids or aerosols into the atmosphere (Renno and Kok, 2008). Br is preferentially volatilized over Cl during photo-oxidation processes, and may result in Br/Cl fractionation of the initial saline systems. The volatilized species could be transported over long distance if there are no effective removal agents present such as dust particles or clouds.

145

(2) Direct removal from atmosphere. Direct deposition or adsorption onto dust particles could lead to halogens being removed from the atmosphere. Dust particles provide important interfaces, and enable Br and Cl to be photo-oxidized into higher oxidation states. On the ground, oxyanion species could also form in brines or on saltpans.

(3) Migration and relocation via aqueous activities. Once formed, perchlorate, chlorate and bromate mobility are mainly controlled by aqueous processes, given that they are hygroscopic and highly soluble (Catling et al., 2010; Hanley et al., 2012). Therefore, with surface or subsurface aqueous activity, these halogen species could be re-dissolved, mobilized and concentrated via evaporation. Even on the current arid and cold Martian surface, the very low eutectic point and highly hygroscopic properties of oxy-chlorine species enable them to be present as liquid for a few hours of the day so that re-distribution and concentration could occur (e.g., Chevrier et al., 2009; Hanley et al., 2012; Kounaves et al., 2014). With much less water, thin liquid films that form on the surface of the regolith could act as a temporary trap, facilitating migration and enrichment of halogen species (Boxe et al., 2012; Cull et al., 2010).

It has been suggested that the presence of oxy-chlorine species might be able to support some form of habitability on Mars (Hecht et al., 2009; Kounaves et al., 2014), and certain rare microorganisms can utilize perchlorate reduction for metabolism (Coates and Achenbach, 2004). However, this type of metabolism likely develops via extreme biological adaption and evolution. For instance, nitrate-reducing bacteria on Earth could not tolerate the toxic end product $ClO_2^-$ produced by reducing (per)chlorate (Coates and Achenbach, 2004). Therefore, even though widely distributed (per)chlorate may be theoretically habitable, as demonstrated in this study, it would provide no advantages for the origin of life on Mars.
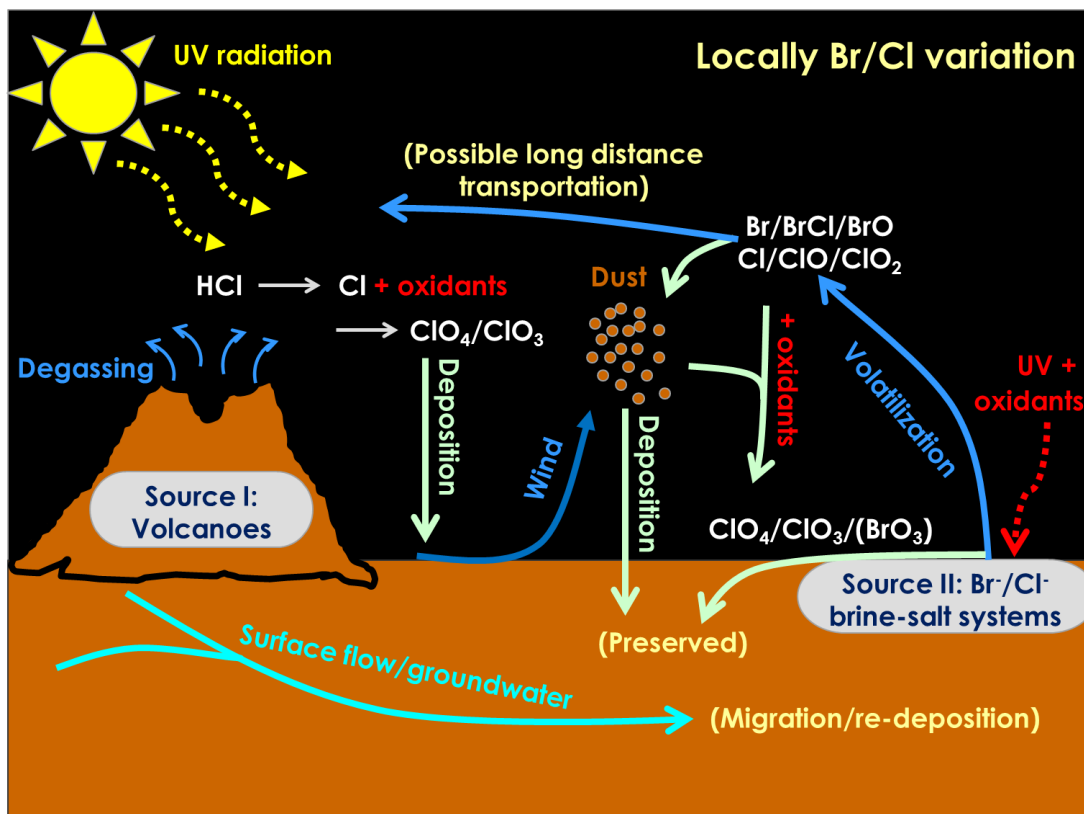
**Figure 4.4.** Model of photochemical controls on Br and Cl at the Martian surface. The two main sources of halogens on the Martian surface are: (1) volcanic degassing and (2) Br$^-$- and Cl$^-$-containing brine-salt systems. With UV radiation, Br$^-$ and Cl$^-$ can be photo-oxidized and mobilized, and follow three major transfer pathways: (1) direct transfer into the atmosphere (blue); (2) direct deposition from the atmosphere (light yellow), and (3) migration via aqueous activity (light green). Mobility of Br compared to Cl is greater than previously thought due to preferential volatilization into the atmosphere, and may result in local variations of Br/Cl ratios. Br variation and Br/Cl fractionation observed in this model are consistent with Br and Cl measurements in in-situ samples on the Martian surface.

**Acknowledgements**

# References

Bao, H. M. and Gu, B. H. (2004) Natural perchlorate has a unique oxygen isotope signature. *Environ. Sci. Technol.,* **38**, 5073-5077.

Boxe, C. S., Hand, K. P., Nealson, K. H., Yung, Y. L., Yen, A. S. and Saiz-Lopez, A. (2012) Adsorbed water and thin liquid films on Mars. *International Journal of Astrobiology*, **11**, 169-175, doi: 10.1017/S1473550412000080.

Boynton, W. V., Taylor, G. J., Evans, L. G., Reedy, R. C., Starr, R., Janes, D. M., Kerry, K. E., Drake, D. M., Kim, K. J., Williams, R. M. S., Crombie, M. K., Dohm, J. M., Baker, V., Metzger, A. E., Karunatillake, S., Keller, J. M., Newsom, H. E., Arnold, J. R., Brückner, J., Englert, P. A. J., Gasnault, O., Sprague, A. L., Mitrofanov, I., Squyres, S. W., Trombka, J. I., d'Uston, L., Wanke, H. and Hamara, D. K. (2007) Concentration of H, Si, Cl, K, Fe, and Th in the low- and mid-latitude regions of Mars. *J. Geophys. Res.,* **112**, E12S99, doi: 10.1029/2007JE002887.

Bray, W. C. and Livingston, R. S. (1923) The catalytic decomposition of hydrogen peroxide in a bromine-bromide solution, and a study of the steady state. *J. Am. Chem. Soc.* **45**, 1251-1271.

Brückner, J., Dreibus, G., Gellert, R., Squyres, S., Wänke, H., Yen, A., Zipfel, J. (2008) Mars Exploration Rovers: Chemical composition by the APXS. In *The Martian Surface: Composition, mineralogy, and physical properties* (ed. J. Bell). Cambridge Univ. Press, Cambridge, pp. 58-101.

Catling, D. C., Claire, M. W., Zahnle, K. J., Quinn, R. C., Clark, B. C., Hecht, M. H. and Kounaves, S. (2010) Atmospheric origins of perchlorate on Mars and in the Atacama. *J. Geophys. Res.,* **115**, E00E11, doi: 10.1029/2009JE003425.

Chevrier, V. F., Hanley, J. and Altheide, T. S. (2009) Stability of perchlorate hydrates and their liquid solutions at the Phoenix landing site, Mars. *Geophys. Res. Lett.,* **36**, L10202, doi: 10.1029/2009GL037497.

Clark, B. C., Baird, A. K., Weldon, R. J., Tsusaki, D. M., Schnabel, L. and Candelaria, M. P. (1982) Chemical composition of Martian fines. *J. Geophys. Res.* **87**, 59-67.

Coates, J. D. and Achenbach, L. A. (2004) Microbial perchlorate reduction: rocket-fuelled metabolism. *Nat. Rev. Microbiol.* **2**, 569-580.

Cockell, C. S., Schuerger, A. C., Billi, D., Friedmann, E. I., and Panitz, C. (2005) Effects of a simulated martian UV flux on the cyanobacterium, Chroococcidiopsis sp. 029. *Astrobiology*, **5(2)**, 127-140.

Cull, S. C., Arvidson, R. E., Catalano, J. G., Ming, D. W., Morris, R. V., Mellon, M. T. and Lemmon, M. (2010) Concentrated perchlorate at the Mars Phoenix landing site: Evidence for thin film liquid water on Mars. *Geophys. Res. Lett.,* **37**, L22203, doi:10.1029/2010GL045269.

Enami, S., Vecitis, C. D., Cheng, J., Hoffmann, M. R. and Colussi, A. J. (2007) Global inorganic source of atmospheric bromine. *J. Phys. Chem. (A)*, **111**, 8749-8752.

Finlayson-Pitts, B. J. (2010) Halogens in the Troposphere. *Anal. Chem.,* **82 (3)**, 770-776, doi: 10.1021/ac901478p.

Gellert, R., Rieder, R., Anderson, R.C., Bruckner, J., Clark, B.C., Dreibus, G., Economou, T., Klingelhofer, G., Lugmair, G.W., Ming, D.W., Squyres, S.W., d'Uston, C., Wanke, H., Yen, A. and Zipfel, J. (2004) Chemistry of rocks and soils in Gusev crater from the alpha particle x-ray spectrometer. *Science*, **305**, 829-832.

Grotzinger, J. P., Sumner, D. Y., Kah, L. C., Stack, K., Gupta, S., Edgar, L., Rubin, D., Lewis, K., Schieber, J., Mangold, N., Milliken, R., Conrad, P. G., DesMarais, D., Farmer, J., Siebach, K., Calef, F., Hurowitz, J., McLennan, S. M., Ming, D., Vaniman, D., Crisp, J., Vasavada, A., Edgett, K. S., Malin, M., Blake, D., Gellert, R., Mahaffy, P., Wiens, R. C., Maurice, S., Grant, J. A., Wilson, S., Anderson, R. C., Beegle, L., Arvidson, R., Hallet, B., Sletten, R.S., Rice, M., Bell, J., Griffes, J., Ehlmann, B., Anderson, R. B., Bristow, T. F., Dietrich, W. E., Dromart, G., Eigenbrode, J., Fraeman, A., Hardgrove, C., Herkenhoff, K., Jandura, L., Kocurek, G., Lee, S., Leshin, L. A., Leveille, R., Limonadi, D., Maki, J., McCloskey, S., Meyer, M., Minitti, M., Newsom, H., Oehler, D., Okon, A., Palucis, M., Parker, T., Rowland, S., Schmidt, M., Squyres, S., Steele, A., Stolper, E., Summons, R., Treiman, A., Williams, R., Yingst, A. and Team, M.S. (2014) A Habitable Fluvio-Lacustrine Environment at Yellowknife Bay, Gale Crater, Mars. *Science*, **343 (6169)**, doi: 10.1126/science.1242777.

Hanley, J., Chevrier, V. F., Berget, D. J. and Adams, R. D. (2012) Chlorate salts and solutions on Mars. *Geophys. Res. Lett.,* **39**, L08201, doi: 10.1029/2012GL051239.

Hecht, M. H., Kounaves, S. P., Quinn, R. C., West, S. J., Young, S. M. M., Ming, D. W., Catling, D. C., Clark, B. C., Boynton, W. V., Hoffman, J., DeFlores, L. P., Gospodinova, K., Kapit, J. and Smith, P. H. (2009) Detection of Perchlorate and the Soluble Chemistry of Martian Soil at the Phoenix Lander Site. *Science*, **325**, 64-67.

Hönninger, G., Bobrowski, N., Palenque, E. R., Torrez, R. and Platt, U. (2004) Reactive bromine and sulfur emissions at Salar de Uyuni, Bolivia. *Geophys. Res. Lett.,* **31**, L04101, doi: 10.1029/2003GL018818.

Jackson, W. A., Böhlke, J. K., Gu, B. H., Hatzinger, P. B. and Sturchio, N. C. (2010) Isotopic composition and origin of indigenous natural perchlorate and co-occurring nitrate in the southwestern United States. *Environ. Sci. Technol.,* **44**, 4869-4876.

Kaleschke, L., Richter, A., Burrows, J., Afe, O., Heygster, G., Notholt, J., Rankin, A. M., Roscoe, H. K., Hollwedel, J., Wagner, T. and Jacobi, H. W. (2004) Frost flowers on sea ice as a source of sea salt and their influence on tropospheric halogen chemistry. *Geophys. Res. Lett.,* **31**, L16114, doi: 10.1029/2004GL020655.

Kang, N., Jackson, W. A., Dasgupta, P. K. and Anderson, T. A. (2008) Perchlorate production by ozone oxidation of chloride in aqueous and dry systems. *Sci. Total Environ.,* **405**, 301-309.

Karunatillake, S., Zhao, Y. Y. S., McLennan, S. M., Skok, J. R. and Button, N. E. (2013) Does Martian soil release reactive halogens to the atmosphere? *Icarus,* **226 (2)**, 1438-1446, http://dx.doi.org/10.1016/j.icarus.2013.07.018.

Keller, J. M., Boynton, W. V., Karunatillake, S., Baker, V. R., Dohm, J. M., Evans, L. G., Finch, M. J., Hahn, B. C., Hamara, D. K., Janes, D. M., Kerry, K. E., Newsom, H. E., Reedy, R. C., Sprague, A. L., Squyres, S. W., Starr, R. D., Taylor, G. J. and Williams, R. M. S. (2006) Equatorial and midlatitude distribution of chlorine measured by Mars Odyssey GRS. *J. Geophys. Res.,* **111**, E03S08, doi: 10.1029/2006JE002679, 112, E3.

Kounaves, S. P., Carrier, B. L., O'Neil, G. D., Stroble, S. T. and Claire, M. W. (2014) Evidence of martian perchlorate, chlorate, and nitrate in Mars meteorite EETA79001: Implications for oxidants and organics. *Icarus*, **229**, 206-213.

Kounaves, S. P., Hecht, M. H., Kapit, J., Gospodinova, K., DeFlores, L., Quinn, R. C., Boynton, W. V., Clark, B. C., Catling, D. C., Hredzak, P., Ming, D. W., Moore, Q., Shusterman, J., Stroble, S., West, S.J. and Young, S. M. M. (2010a) Wet Chemistry experiments on the 2007 Phoenix Mars Scout Lander mission: Data analysis and results. *J. Geophys. Res.,* **115**, E00E10, doi: 10.1029/2009JE003424.

Kounaves, S. P., Hecht, M. H., Kapit, J., Quinn, R. C., Catling, D. C., Clark, B. C., Ming, D. W., Gospodinova, K., Hredzak, P., McElhoney, K. and Shusterman, J. (2010b) Soluble sulfate in the martian soil at the Phoenix landing site. *Geophys. Res. Lett.,* **37**, L09201, doi: 10.1029/2010GL042613.

Kounaves, S. P., Stroble, S. T., Anderson, R. M., Moore, Q., Catling, D. C., Douglas, S., McKay, C. P., Ming, D. W., Smith, P. H., Tamppari, L. K. and Zent, A. P. (2010c) Discovery of Natural Perchlorate in the Antarctic Dry Valleys and Its Global Implications. *Environ. Sci. Technol.,* **44**, 2360-2364.

Lary, D. J. (2005) Halogens and the chemistry of the free troposphere. *Atmos. Chem. Phys.*, **5**, 227-237.

Leshin, L. A., Mahaffy, P. R., Webster, C. R., Cabane, M., Coll, P., Conrad, P. G., Archer, P. D., Atreya, S. K., Brunner, A. E., Buch, A., Eigenbrode, J. L., Flesch, G. J., Franz, H. B., Freissinet, C., Glavin, D. P., McAdam, A. C., Miller, K. E., Ming, D. W., Morris, R. V., Navarro-Gonzalez, R., Niles, P. B., Owen, T., Pepin, R. O., Squyres, S., Steele, A., Stern, J. C., Summons, R. E., Sumner, D. Y., Sutter, B., Szopa, C., Teinturier, S., Trainer, M. G., Wray, J. J., Grotzinger, J. P. and Team, M. S. (2013) Volatile, isotope, and organic analysis of Martian fines with the Mars Curiosity rover. *Science*, **341 (6153)**, doi: 10.1126/science.1238937.

Livingston, R. S. and Bray, W. C. (1926) The catalytic decomposition of hydrogen peroxide in an acid chlorine-chloride solution. *J. Am. Chem. Soc.,* **48**, 405-406.

Livington, R. S. and Bray, W. C. (1925) The catalytic decomposition of hydrogen peroxide in an acid chlorine-chloride solution. *J. Am. Chem. Soc.,* **47**, 2069-2082.

Marion, G. M., Catling, D. C., Zahnle, K. J. and Claire, M. W. (2010) Modeling aqueous perchlorate chemistries with applications to Mars. *Icarus,* **207**, 675-685.

McLennan, S. M., Bell, J. F., Calvin, W. M., Christensen, P. R., Clark, B. C., de Souza, P. A., Farmer, J., Farrand, W. H., Fike, D. A., Gellert, R., Ghosh, A., Glotch, T. D., Grotzinger, J. P., Hahn, B., Herkenhoff, K. E., Hurowitz, J. A., Johnson, J. R., Johnson, S. S., Jolliff, B., Klingelhöfer, G., Knoll, A. H., Learner, Z., Malin, M. C., McSween, H. Y., Pocock, J., Ruff, S. W., Soderblom, L. A., Squyres, S. W., Tosca, N. J., Watters, W. A., Wyatt, M. B., Yen, A. (2005) Provenance and diagenesis of the evaporite-bearing Burns formation, Meridiani Planum, Mars. *Earth Planet. Sci. Lett.,* **240**, 95-121.

Ming, D. W., Archer, P. D., Glavin, D. P., Eigenbrode, J. L., Franz, H. B., Sutter, B., Brunner, A. E., Stern, J. C., Freissinet, C., McAdam, A. C., Mahaffy, P. R., Cabane, M., Coll, P., Campbell, J. L., Atreya, S. K., Niles, P. B., Bell, J. F., Bish, D. L., Brinckerhoff, W. B., Buch, A., Conrad, P. G., Des Marais, D. J., Ehlmann, B. L., Fairen, A. G., Farley, K., Flesch, G. J., Francois, P., Gellert, R., Grant, J. A., Grotzinger, J. P., Gupta, S., Herkenhoff, K. E., Hurowitz, J. A., Leshin, L. A., Lewis, K. W., McLennan, S. M., Miller, K. E., Moersch, J., Morris, R. V., Navarro-Gonzalez, R., Pavlov, A. A., Perrett, G. M., Pradler, I., Squyres, S. W., Summons, R. E., Steele, A., Stolper, E. M., Sumner, D. Y., Szopa, C., Teinturier, S., Trainer, M. G., Treiman, A. H., Vaniman, D. T., Vasavada, A. R., Webster, C. R., Wray, J. J., Yingst, R. A. and Team, M. S. (2014) Volatile and Organic Compositions of Sedimentary Rocks in Yellowknife Bay, Gale Crater, Mars. *Science*, **343 (6169)**, doi: 10.1126/science.1245267.

Ming, D. W., Gellert, R., Morris, R. V., Arvidson, R. E., Brukner, J., Clark, B. C., Cohen, B. A., d'Uston, C., Economou, T., Fleischer, I., Klingelhofer, G., McCoy, T. J., Mittlefehldt, D. W., Schmidt, M. E., Schroder, C., Squyres, S. W., Treguier, E., Yen, A. S. and Zipfel, J. (2008) Geochemical properties of rocks and soils in Gusev Crater, Mars: Results of the Alpha Particle X-Ray Spectrometer from Cumberland Ridge to Home Plate. *J. Geophys. Res.,* **113**, E12S39, doi: 10.1029/2008JE003195.

Rao, B., Anderson, T. A., Redder, A. and Jackson, W. A. (2010) Perchlorate formation by ozone oxidation of aqueous chlorine/oxy-chlorine species: role of ClxOy radicals. *Environ. Sci. Technol.*, **44**, 2961-2967.

Rao, B., Hatzinger, P. B., Bohlke, J. K., Sturchio, N. C., Andraski, B. J., Eckardt, F. D. and Jackson, W. A. (2010b) Natural chlorate in the environment: Application of a new IC-ESI/MS/MS method with a ($ClO_3^-$)-O-18 internal standard. *Environ. Sci. Technol.*, **44**, 8429-8434.

Reno N. and Kok J. (2008) electrical activity and dust lifting on earth mars and beyond, *Space Sci. Rev.*, **137**, 419-434, doi: 10.1007/s11214-008-9377-5.

Rieder, R., Gellert, R., Anderson, R. C., Bruckner, J., Clark, B. C., Dreibus, G., Economou, T., Klingelhoffer, G., Lugmair, G. W., Ming, D. W., Squyres, S. W., d'Uston, C., Wanke, H., Yen, A. and Zipfel, J. (2004) Chemistry of rocks and soils at Meridiani Planum from the alpha particle X-ray spectrometer. *Science*, **306**, 1746-1749.

Risacher, F., Fritz, B. and Alonso, H. (2006) Non-conservative behavior of bromide in surface waters and brines of Central Andes: A release into the atmosphere? *Geochim. Cosmochim. Acta,* **70**, 2143-2152.

Rudloff, W. K. and Freeman, E. S. (1970) Catalytic effect of metal oxides on thermal decomposition reactions. II. Catalytic effect of metal oxides on the thermal decomposition of potassium chlorate and potassium perchlorate as detected by thermal analysis methods. *J. Phys. Chem.,* **74**, 3317-3324, doi: 10.1021/j100712a002.

Sander, R., Keene, W. C., Pszenny, A. A. P., Arimoto, R., Ayers, G. P., Baboukas, E., Cainey, J. M., Crutzen, P. J., Duce, R. A., Hönninger, G., Huebert, B. J., Maenhaut, W., Mihalopoulos, N., Turekian, V. C. and Van Dingenen, R. (2003) Inorganic bromine in the marine boundary layer: a critical review. *Atmos. Chem. Phys.,* **3**, 1301-1336.

Schuttlefield, J. D., Sambur, J. B., Gelwicks, M., Eggleston, C. M. and Parkinson, B. A. (2011) Photooxidation of chloride by oxide minerals: Implications for perchlorate on Mars. *J. Am. Chem. Soc.,* **133**, 17521-17523.

Smith, M. L., Claire, M. W., Catling, D. C. and Zahnle, K. J. (2014) The formation of sulfate, nitrate and perchlorate salts in the martian atmosphere. *Icarus*, **231**, 51-64.

Spicer, C. W., Chapman, E. G., Finlayson-Pitts, B. J., Plastridge, R. A., Hubbe, J. M., Fast, J. D. and Berkowitz, C. M. (1998) Unexpectedly high concentrations of molecular chlorine in coastal air. *Nature*, **394**, 353-356.

Sutter, B., Archer, P. D., Ming, D. W., Niles, P. B., Eigenbrode, J. L., Franz, H., Glavin, D. P., McAdam, A. C., Mahaffy, P., Stern, J. C., Navarro-Gonzalez, R., McKay, C. P. (2014) The investigation of chlorates as a possible source of oxygen and chlorine detected by the sample analysis at Mars (SAM) instrument in Gale Crater, Mars. 45th Lunar and Planetary Science Conference, **Abst #2136**, Lunar Planetary Institute, Woodlands, TX.

Toner, J. D., Catling, D. C. and Light, B. (2014) The formation of supercooled brines, viscous liquids, and low-temperature perchlorate glasses in aqueous solutions relevant to Mars. *Icarus,* **233**, 36-47.

Wood, W. W. and Sanford, W. E. (2007) Atmospheric bromine flux from the coastal Abu Dhabi sabkhat: A ground-water mass-balance investigation. *Geophys. Res. Lett.,* **34**, L14405, doi: 10.1029/2007GL029922.

Xu, J., Sahai, N., Eggleston, C. M., Schoonen, M. A. A. (2013) Reactive oxygen species at the oxide/water interface: Formation mechanisms and implications for prebiotic chemistry and the origin of life. *Earth Planet. Sci. Lett.,* **363**, 156-167, doi: 10.1016/j.epsl.2012.12.008.

Yang, X., Pyle, J. A. and Cox, R. A. (2008) Sea salt aerosol production and bromine release: Role of snow on sea ice. *Geophys. Res. Lett.,* **35**, L16815, doi: 10.1029/2008GL034536.

## Chapter 5: Conclusions and Future Work

In this work, I experimentally evaluated the geochemistry of trace element cations ($Ni^{2+}$, $Zn^{2+}$ and $Cr^{3+}$) and the halide anions ($Br^-$ and $Cl^-$) during diagenetic oxidation processes of ferrous sulfates to ferric oxides. In addition, the geochemistry of Br and Cl during photochemical-related evaporation processes was explored experimentally. The purpose of this research was to better understand some of the possible controls on the distributions and speciation of these elements on the Martian surface, as observed by the 1975 Viking 1 and 2 landers (Cl abundances), 1996 Pathfinder rover *Sojourner* (Cl abundances), 2001 Mars Odyssey orbital gamma-ray spectrometer (global Cl near-surface distribution), 2003 Mars Exploration rovers (MER), *Spirit* and *Opportunity* (Cl, Br, Cr, Ni, Zn abundances), 2007 *Phoenix* Mars Lander (soluble Cl abundances and speciation) and the 2011 Mars Science Laboratory (MSL) rover *Curiosity* (Cl, Br, Cr, Ni, Zn abundances and Cl speciation).

During the diagenetic mineralogical evolution defined as Pathway 1 (melanterite → jarosite → hematite) and Pathway 2 (melanterite → schwertmannite → goethite → hematite), the preferred uptake of initially equal concentrations of $Cr^{3+}$, $Ni^{2+}$ and $Zn^{2+}$ via these different pathways are in different orders. Uptake of $Cr^{3+}$ by the precipitates was orders of magnitude greater than was uptake of $Ni^{2+}$ and $Zn^{2+}$ for both pathways, due to probable substitution of $Cr^{3+}$ for $Fe^{3+}$ in mineral structures. In contrast $Ni^{2+}$ and $Zn^{2+}$ likely were mainly adsorbed onto mineral surfaces. Uptake of $Ni^{2+}$ and $Zn^{2+}$ by schwertmannite and goethite was in the order $Ni^{2+} > Zn^{2+}$, but this pattern was reversed in the case of jarosite (i.e., $Zn^{2+} > Ni^{2+}$). Therefore, the high Ni content and high Ni/Zn ratios observed in the hematitic spherule-bearing targets (and

interpreted as sedimentary concretions) detected at Meridiani Planum by the Mars rover *Opportunity*, can be readily explained by the evolution pathway described above, involving goethite (i.e., Pathway 2). Other diagenetic pathways, such as via jarosite, could only be valid if there was an additional source of Ni to the system (e.g., meteoritic components or an especially high-Ni basalt provenance).

The anions $Br^-$ and $Cl^-$, which the data from Mars indicate should also to be present in such diagenetic solutions, also demonstrate different partitioning behavior via the different mineralogical evolution pathways. For aqueous solutions with initial molar $Cl^-/Br^- > 1$, jarosite incorporated at least an order of magnitude more Br than Cl and, consequently, was greatly enriched in Br over Cl in its mineral structure. Such preferential Br-enrichment was not found in goethite (i.e., Pathway 2). Incorporation of large amounts of $Br^-$ would greatly decrease jarosite stability during aqueous alteration. Accordingly, these experiments suggest that jarosite could be a plausible candidate for holding elevated Br and thus causing at least some of the fractionated Br/Cl ratios observed at the Martian surface. The changes in decomposition rates of jarosite, observed when incorporating halide anions, also should be considered when attempting to interpret the aqueous history of Meridiani Planum by using jarosite as a "stopwatch".

Photo-oxidation (ultraviolet $\lambda = 254$ nm) experiments of evaporative saline systems containing $Br^-$ and $Cl^-$ produced perchlorate and chlorate at up to ~2% levels of total chlorine abundances under conditions relevant to the current, and possibly ancient, surface of Mars. In addition, significant Br/Cl fractionation was present in the resulting evaporites, due to preferential volatilization of Br over Cl into the atmosphere. Formation of perchlorate and chlorate by solid-gas heterogeneous reactions were observed to be considerably more efficient compared to liquid-gas reactions or to the commonly proposed atmospheric gas-gas reactions.

Accordingly, I propose a model for halogen cycling on Mars (see Figure 1.6) to describe the photochemical influences on Br and Cl geochemistry, which in part explains the variation of Br abundances that have been detected on the Martian surface, and also suggests that chlorate is likely present along with perchlorate at Martian surface, particularly at neutral to alkaline aqueous environments.

The characteristics of the diagenetic solutions from which the hematitic concretions originated are largely unconstrained. Accordingly, in design of the trace element (Ni, Zn and Cr) experiments, one shortcoming was that each element was evaluated individually, to avoid various complications, such as needing to evaluate the effects of mixing ratios of trace elements or the possibility of competing trace elements influencing precipitated mineral morphologies. Based on the results of this study, a logical next step would be to evaluate more complex systems, which, of course, would also be more representative of natural conditions on Mars.

Halogen-bearing jarosite, particularly Br-bearing jarosite, are of great interest because of the potential for fractionating Cl/Br ratios, yet the experimental approach used in this study was inadequate to evaluate detailed crystallographic controls. Thus, questions remained about why $Br^-$ is favored over $Cl^-$ by the jarosite structure, and for which site $Br^-$ does substitute in jarosite. These aspects will require further work. Such work should involve synthesis of a series of halogen-bearing jarosite samples with increasing amounts of incorporated halogens (e.g., Br-, Cl- and Br, Cl-bearing) and systematically collecting crystallographic information for each type of sample for comparison.

Finally, several aspects of the photochemical work, that require additional clarification, could be further evaluated by extending the experimental conditions or by adjusting the experimental designs. Issues that remained included: the effects of other wavelengths of UV

radiation (both shorter or longer than 254 nm); distinguishing possible oxidants and their efficiency within the system; systematically evaluating the influence of pH on the formation and preservation of chlorate (e.g., by using one brine composition with different initial pHs); determining what conditions promote the formation of bromate rather than perchlorate and chlorate; determining the isotopic signatures of $^{36}Cl$, $^{37}Cl$, $^{18}O$, $^{17}O$ and $^{16}O$ in the produced perchlorate and other species and comparing these to natural terrestrial samples and other synthetic laboratory samples, in order to obtain additional insight into the origin and formation pathway of the oxy-chlorine species.

**Appendix 1: Supplemental Materials for Chapter 3**

This appendix contains two parts of supplemental information.

Part A is the Scanning Electron Microscopy (SEM) images of six synthetic Fe-bearing minerals described in Section 3.2.4 and Table 2.

Part B is a supplemental material to Section 3.3.3 and provides the details of determining adsorption isotherms of single adsorbate $Cl^-$ and $Br^-$ for the three HAL-free Fe-minerals. The experimental methods and results are summarized.

**Part A. Scanning Electron Microscopy (SEM) images of synthetic Fe-bearing minerals.**
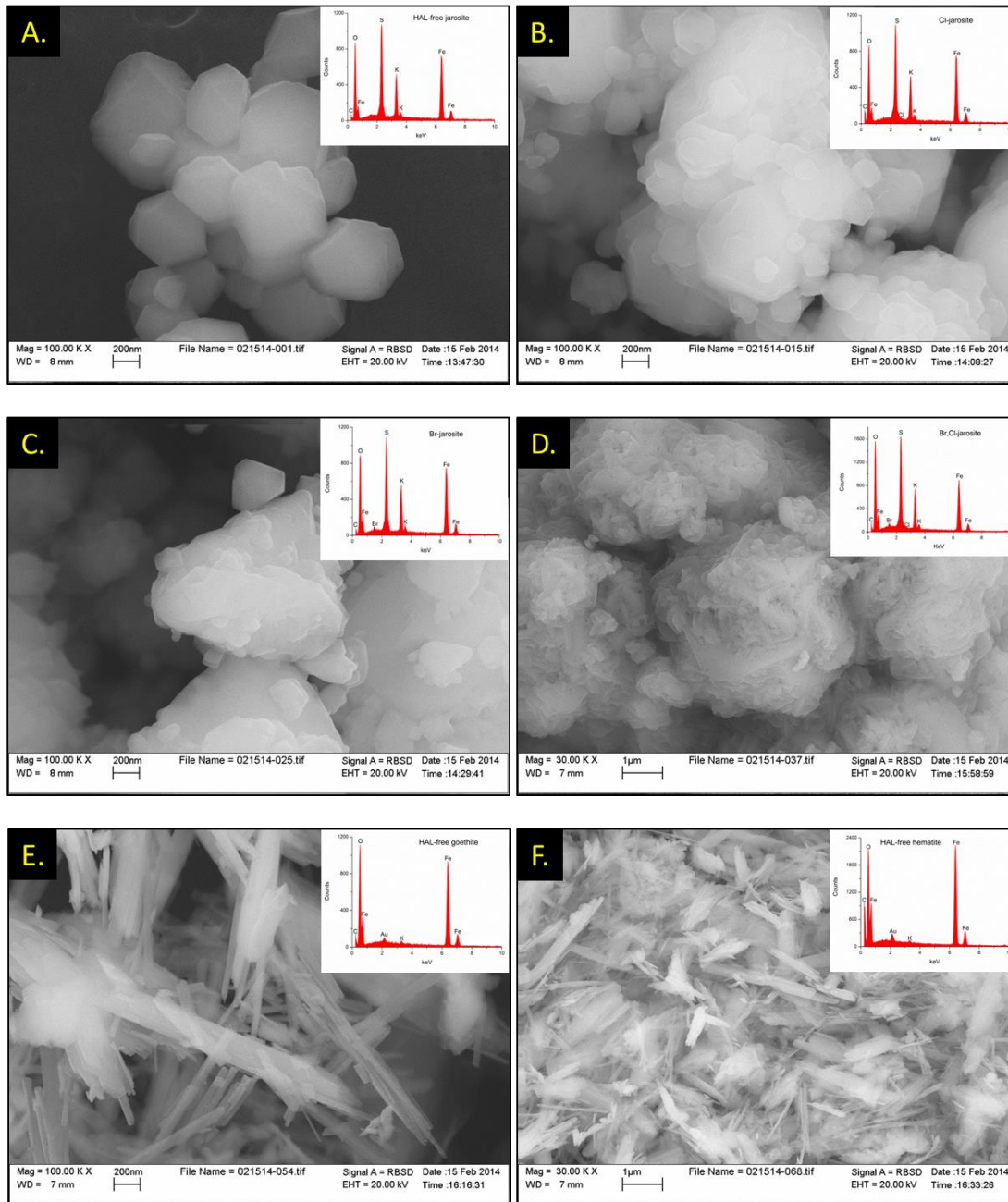


**Figure S1**. SEM images of synthetic Fe-bearing minerals described in Section 3.2.4 and Table 2. Elements detected by Energy-Dispersive X-ray Spectrometer (EDS; insets in SEM images) were consistent with the X-ray fluorescence spectrometry (XRF) analyses. The Au detected in goethite and hematite samples was introduced by the gold-coating pretreatment prior to the SEM analysis. In jarosite samples, the Au peak overlaps a S peak. (A) HAL-free jarosite. (B) Cl-jarosite. (C) Br-jarosite. (D) Br,Cl-jarosite. (E) HAL-free goethite. (F) HAL-free hematite.

**Part B. Adsorption isotherms of Cl⁻ and Br⁻ for HAL-free -hematite, -goethite, and -jarosite**

In the preliminary adsorption experiments, adsorption isotherms of single adsorbate Cl⁻ and Br⁻ of the three Fe-minerals were determined before making multi-adsorbate solutions of Cl⁻, Br⁻, $SO_4^{2-}$ and $H_2PO_4^-$ (results that are discussed in Section 3.3). Here, the experimental methods and results of determining adsorption isotherms are summarized.

**Experimental methods:**

NaCl and NaBr adsorbate solutions (unbuffered) were prepared at concentrations of 0.5, 1, 1.5, 2, 3, 5, 7 and 10 mM. In each experiment, 25 mL of adsorbate solution were transferred to a 50 mL centrifuge tube and then 1 mL of mineral slurry (0.1 g/mL; unbuffered) was added to the tube. These tubes were then capped and put in a water bath maintained at 25 ℃ for 3 days for the reactions to reach equilibrium (based on previous kinetic studies dealing with similar systems (e.g., Gao, 2001; Chitrakar et al., 2006). During the reaction period, the tubes were agitated by hand every 24 h. At the end of each experiment, all the tubes were centrifuged and the supernatant solutions were collected and passed through 0.2 µm filters. The pH of each solution was measured immediately after sampling.

**Results:**

The adsorption isotherms of Cl⁻ and Br⁻ (from NaCl or NaBr solution) on HAL-free -hematite, -goethite, and -jarosite are shown in Figure S2. Similar trends of uptake of Cl⁻ or Br⁻ (in the range of 0~10 mM) were observed on all three HAL-free minerals. Uptake of Br⁻ on the mineral surface increased with increasing equilibrium concentrations of Br⁻. On the other hand, sorbed Cl⁻ scattered in a narrow range with increasing equilibrium concentrations, and was much lower than sorbed Br⁻.

The isotherm data were modeled using Freundlich and Langmuir equations. $Cl^-$ data were poorly fit by either Freundlich or Langmuir models ($R^2$ ranged from 0.55 to 0.83). On the other hand, adsorption isotherms of $Br^-$ were better fitted with the Freundlich equation $x/m = KC^n$, where $(x/m)$ is the amount of bromide adsorbed on the solid phase (mg Br/g), C is the equilibrium bromide concentration in the solution phase (mg Br/kg), and K (mg/g) and n (dimensionless) are Freundlich constants. The constant n refers to the interaction between exchange sites in the adsorbent and $Br^-$ ions. A high value for n (>1) indicates favorable adsorption (e.g., Chitrakar et al., 2006). Uptake of $Br^-$ on goethite is considerably higher than that on hematite or jarosite. Freundlich isotherm constants and $R^2$ values of isotherms of bromide on all three HAL-free minerals are given in Table S1.

**Table S1.** Freundlich isotherm constants of Br- calculated for HAL-free -hematite, -goethite and -jarosite

| HAL-free minerals | Solution | Freundlich constants | | | |
|---|---|---|---|---|---|
| | | logK | K | n | $R^2$ |
| Hematite | NaBr | 1.14 | 13.7 | 1.3 | 0.989 |
| Goethite | NaBr | 2.99 | 985 | 2.2 | 0.984 |
| Jarosite | NaBr | 0.595 | 3.94 | 1.0 | 0.984 |

* HAL-free = halogen-free.

**References:**

Chitrakar, R., S. Tezuka, A. Sonoda, K. Sakane, K. Ooi, and T. Hirotsu (2006) Phosphate adsorption on synthetic goethite and akaganeite, *J. Colloid Interface Sci.*, **298**, 602-608.

Gao, Y. (2001) Surface electrical properties of goethite and adsorption of phosphate and arsenate on iron oxyhydroxides in high ionic strength solutions, Ph.D thesis, Dept. of Earth and Planet. Sci., McGill University, Montreal, Canada.
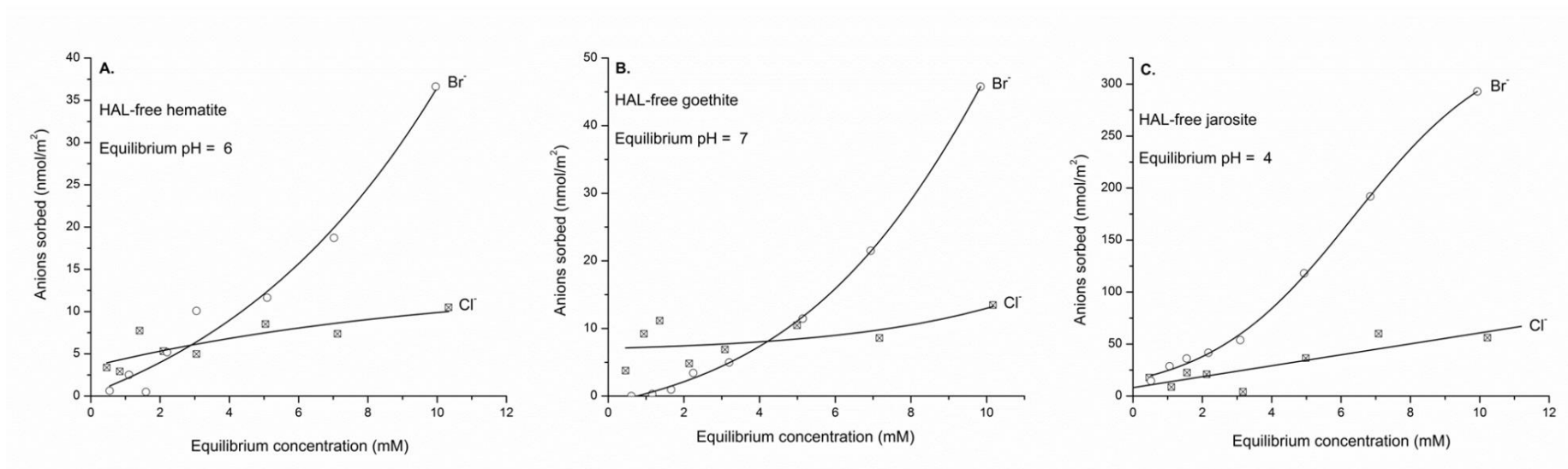
**Figure S2.** Adsorption isotherms of Cl⁻ and Br⁻ with (A) HAL-free hematite, (B) HAL-free goethite, and (C) HAL-free jarosite. The initial absorbate solutions were unbuffered. Sorbed Cl⁻ scattered over a narrow range whereas sorbed Br⁻ increased with increasing equilibrium concentrations.

164

**Appendix 2: Supplemental Materials for Chapter 4**

This appendix contains following supplemental information:

1. Experimental and analytical methods of UV experiments
2. Experiment of $H_2O_2$ solution interaction with $Br^-$ and $Cl^-$ containing brines

Figure S1

Table S1 to S6

References

## 1.  Experimental and analytical methods of UV experiments

The experimental apparatus used for the UV experiments is illustrated in Figure S1. The 1-liter borosilicate reaction chamber was built to withstand high-vacuum conditions ($10^{-6}$ mbar), with a 254-nm ultraviolet (UV) light source inserted directly into the chamber (UVP Pen-ray PCQ Lamp. Part number 90-0049-06. The lamp emits 8.5 mW/cm$^2$ at 2 cm distance from the light source; 90% $\lambda = 254$ nm and 10% $\lambda > 254$ nm). Circulating water in the outer jacket of the chamber was maintained at 25 °C for all of the experiments. The starting materials were placed in a quartz dish at the bottom of the chamber. The brines of interest were slurried with pure quartz grains (sea sand (washed), 100% quartz, ACROS Organics$^{TM}$; chosen to simulate inert sediments). During the experiments, the chamber was fully covered with heavy duty foil to avoid interference from other light sources as well as to eliminate UV leaks.

Seven types of brines were examined in this study. An initial molar ratio of Br$^-$/Cl$^-$ of ~1 was used for all brines. Brine #1 was Mg-Cl$^-$-Br$^-$ (initial pH 6). Brine #2 was a variant of Brine #1 but without Br$^-$ (Mg-Cl$^-$; pH 6). Brine #3 was Na-Cl$^-$-Br$^-$ (pH 6). Brines #4 and #5 were sulfate dominant brines, Mg-SO$_4^{2-}$-Cl$^-$-Br$^-$ (pH 6) and K-SO$_4^{2-}$-Cl$^-$-Br$^-$ (pH 6). Brine #6 was designed to simulate Meridiani Planum aqueous conditions, an acidic sulfate dominant brine bearing Fe (Ca-Mg-Fe$^{3+}$-SO$_4^{2-}$-Cl$^-$-Br$^-$; pH 2). Brine #7 was designed to simulate the Phoenix landing site conditions, a slightly alkaline, bicarbonate dominant brine (Ca-Mg-Na-HCO$_3^-$-SO$_4^{2-}$-Cl$^-$-Br$^-$; pH 8). See Table S1 for further details. Table S2 serves as a "roadmap" listing the details of all types of experiments (A - F) conducted in this study.

In a typical experiment (UV continuously on for 120 h; experiment types A-C and control experiments type E in Table S2), the initial brine and quartz grain mixture (quartz/brine mass ratio ~ 4) was placed in the chamber and evaporated to dryness by intermittently pumping. After

24 h of pumping (vacuum at 40 mbar), the pump was stopped and the chamber was re-filled with simulated atmospheric gas (loaded at 1 bar) and then sealed for 24 h for the reaction to occur ("reaction period"). After two such pump-reaction cycles, the pump was operated for an additional 24 h marking the end of the experiment. The evaporating mixtures typically became dry after the first 24 h of pumping. Final solid mixtures were then collected, re-dissolved in ultrapure water (EasyPure; 18.2 m$\Omega$) and supernatants were filtered with a 0.2 $\mu$m membrane and analyzed for anion concentrations. This type of experiment was used to investigate the effects of sediment grain size and atmospheric composition (Mars simulate atmosphere had a composition of 95.35% $CO_2$, 1.62% Ar, 2.83% $N_2$, and 0.2% $O_2$).

To demonstrate how halogen species change as a function of increasing UV exposure time, an extended duration UV exposure experiment (UV continuously on 384 h) was carried out using larger initial samples to facilitate additional analyses (experiment types D in Table S2). Quartz grain size was kept constant at 250-355 $\mu$m and only Earth atmosphere was used. The initial quartz/brine mass ratio = 1. During this type of experiment, an aliquot of the brine-quartz mixture was sampled after each pump-reaction cycle (24 h pumping and 24-48 h for reaction). The first 20 minutes of evacuated gases from the chamber, immediately after the "reaction period", were bubbled through 50 g of ultrapure water and the solution samples with the dissolved gas species were also collected and analyzed.

Major anions $Cl^-$, $Br^-$, $NO_3^-$, $SO_4^{2-}$ and oxyanions including $ClO^-$, $ClO_2^-$, $ClO_3^-$, $ClO_4^-$ and $BrO_3^-$ were analyzed at Texas Tech University. In contrast to the order of stability of Cl compounds ($ClO_3^- < ClO_4^-$), the Br compounds are in the order $BrO_3^- > BrO_4^-$ (Keith and Solomon, 1970). Therefore, although bromate is the only oxy-bromine species we attempted to identify, if present, bromate is likely the most stable oxy-bromine species.

Major anions ($Cl^-$, $Br^-$, $NO_3^-$, and $SO_4^{2-}$) were determined by ion chromatography using EPA Method 300.0.

Anions perchlorate ($ClO_4^-$) and chlorate ($ClO_3^-$) were separately measured by sequential ion chromatography-mass spectroscopy-mass spectroscopy (IC-MS/MS) following the method of Rao et al. (2007, 2010). $ClO_4^-$ and $ClO_3^-$ were quantified using a Dionex LC 20 ion chromatography system consisting of GP50 pump, CD25 conductivity detector, AS40 automated sampler and Dionex IonPac AS16 (250 X 2 mm) analytical column. The IC system was coupled with an Applied Biosystems-MDS SCIEX API $2000^{TM}$ triple quadrupole mass spectrometer equipped with a Turbo-IonSpray$^{TM}$ source. A hydroxide (NaOH) eluent at 0.3 mL min$^{-1}$ was followed by 90% acetonitrile (0.3 mL min$^{-1}$) as a post-column solvent. To overcome matrix effects, all samples were spiked with $Cl^{18}O_3$ (produced in house) or $Cl^{18}O_4$ (Dionex) internal standards.

The anions chlorite ($ClO_2^-$) and bromate ($BrO_3^-$) were quantified using an ion chromatograph (IC) consisting of a Dionex LC20 conductivity detector, an AS40 automated sampler, an IonPac AG9-HC (4 x 50 mm) guard column followed by an IonPac AS9-HC (4 x 250 mm) analytical column, and a Thermo Scientific Dionex AMMS 300, 4 mm suppressor. A 9 mM sodium carbonate ($Na_2CO_3$) eluent at 1.0 mL/min was followed by a 0.04 sulfuric acid ($H_2SO_4$) reagent solution at 3.0 mL/min as a post-column solvent. A 25 µl loop was used for sample loading.

Hypochlorite ($ClO^-$) was analyzed by buffering the samples at a pH ≈ 8.5 in 3 ml of 50% 100 mM potassium phosphate ($K_2HPO_4$) and 50% 100 mM potassium iodide (KI). At a pH of approximately 8.5, interferences from $ClO_2^-$, $ClO_3^-$, and $ClO_4^-$ are negligible. The resulting tri-iodide species ($I_3^-$) brought about from the excess iodide ($I^-$) from the KI in the buffering solution,

was measured using a DU$^®$ 730 Series Life Science UV/Vis Beckman Coulter$^®$ Spectrophotometer at 351 nm ($\varepsilon = (2.54 \pm 0.02)$ x 104 M$^{-1}$ cm$^{-1}$). The spectrophotometer cell had a 10 mm light path. ClO$^-$ was calculated based on the reaction stoichiometry of the species with iodide (1 mole I$_3^-$/mole of ClO$^-$ species).

In the solution samples, the detection limit of Cl$^-$, Br$^-$, and SO$_4^{2-}$ is 500 µg/L, of NO$_3^-$ is 5000 µg/L, of ClO$_3^-$ and ClO$_4^-$ is 0.05 µg/L, of ClO$_2^-$ and BrO$_3^-$ is 100 µg/L, and of ClO$^-$ is 8 µg/L. Calculated back to the solids, based on dilution factors, the detection limits in the evaporative solids were: Cl$^-$, Br$^-$, and SO$_4^{2-}$ - 40 µg/g, NO$_3^-$ - 400 µg/g, ClO$_2^-$ and BrO$_3^-$ - 8 µg/g, ClO$_3^-$ and ClO$_4^-$ - 4 µg/kg, and ClO$^-$ - 64 µg/kg.

Major cations (Mg$^{2+}$, K$^+$, Na$^+$, Ca$^{2+}$, Fe$^{3+}$) of the initial solution samples were analyzed at Stony Brook by Direct Current Argon Plasma Atomic Emission Spectrophotometry (DCP-AES).

Final concentrations are reported relative to the total solid mixtures after evaporation but corrected for any sample removal (particularly important for the extended time UV exposure experiments) to provide a basis for comparison from sample to sample. In addition, control experiments were conducted with same procedure but without UV irradiation. All of the initial brines and control samples were free of oxyanion species. Control experiments of Brine #7 (pH 8) showed that under alkaline condition, precipitation of insoluble minerals such as Ca-sulfates did not cause Br/Cl fractionation. In contrast, in the control experiment using Brine #6 (pH 2), there was significant loss of Cl$^-$ and Br$^-$ while the sulfate concentration remained almost constant. Therefore, any loss of Cl$^-$ and Br$^-$ is likely due to volatilization of HCl and HBr under acidic condition, and not by co-precipitation of insoluble minerals such as gypsum. Complete datasets are presented in Tables 4.1, S3 and S4.
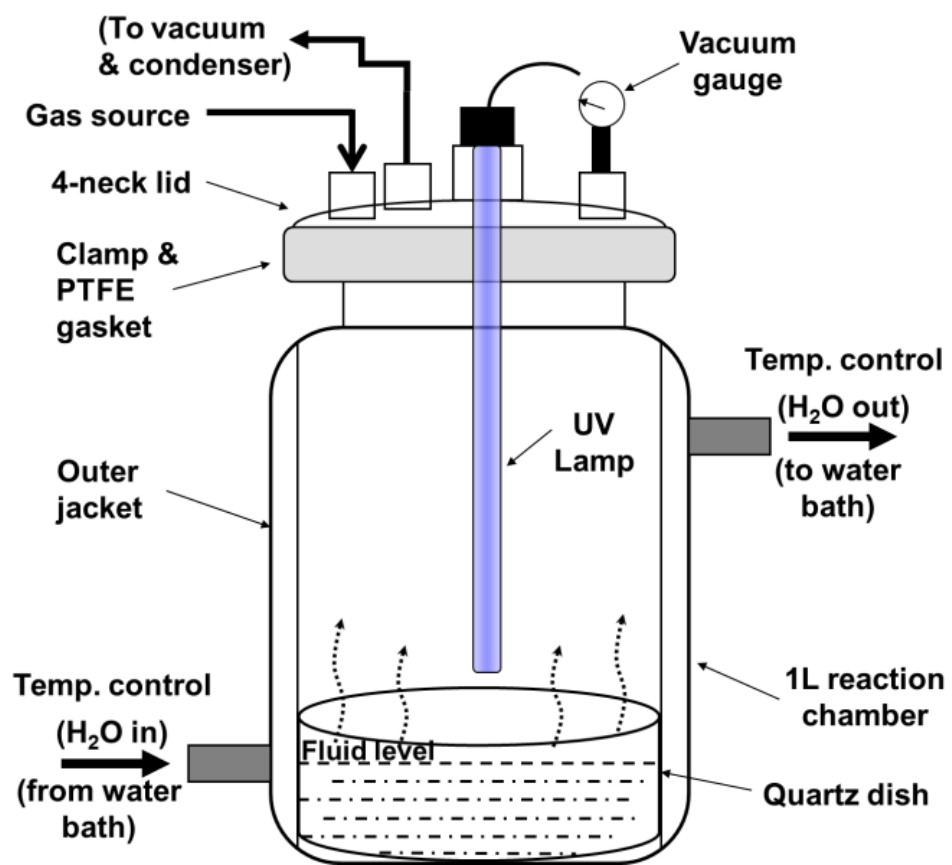
**Figure S1.** Experimental apparatus used in this study.

**Table S1.** Initial compositions of the seven brines used in this study (unit of concentration: mM)[a].

| Index | Types of brine | pH | Cations (mM) | | | | | Anions (mM) | | | | Notes |
|---|---|---|---|---|---|---|---|---|---|---|---|---|
| | | | $Mg^{2+}$ meas. | $Ca^{2+}$ meas. | $Na^+$ meas. | $Fe^{3+}$ meas. | $K^+$ | $Cl^-$ meas. | $Br^-$ meas. | $SO_4^{2-}$ meas. | $HCO_3^{-}$ [b] cal. | |
| Brine #1 | Mg-Cl-Br | 6 | 2799.1 | - | - | - | - | 2798.5 | 2778.6 | - | - | |
| Brine #2 | Mg-Cl | 6 | 2643.2 | - | - | - | - | 2695.8 | | - | - | Bromide free |
| Brine #3 | Na-Cl-Br | 6 | - | - | 1897.3 | - | - | 1777.0 | 1928.3 | - | - | |
| Brine #4 | Mg-SO$_4$-Cl-Br | 6 | 1256.3 | - | - | - | - | 321.5 | 325.1 | 920.4 | - | |
| Brine #5 | K-SO$_4$-Cl-Br | 6 | - | - | - | - | 379.0 | 89.9 | 103.3 | 377.5 | - | |
| Brine #6 | Ca-Mg-Fe-Cl-Br-SO$_4$ | 2 | 42.4 | 9.3 | - | 33.9 | - | 20.5 | 19.1 | 72.2 | - | Simulate Meridiani Planum landing site |
| Brine #7 | Mg-Ca-Na-HCO$_3$-SO$_4$-Cl-Br | 8 | 42.7 | 10.0 | 62.7 | - | - | 11.3 | 10.6 | 42.1 | 62.7 | Simulate Phoenix landing site |

a. Meas. = measured. Cal. = calculated. The A.C.S reagents and 18.2 mΩ EasyPure ultrapure water were used in making all the brines.
b. The $HCO_3^-$ was added as $NaHCO_3$. Its concentration was calculated based on measured $Na^+$ concentration.

**Table S2.** Experiments carried out in this study.

| | Variables evaluated | UV time and sampling strategy | Brine types used (initial pH) | Atmospheric condition | Quartz grain size | Results displayed |
|---|---|---|---|---|---|---|
| (A) | Sediment grain size | UV continuous on for 120 h; sampled once at the end of experiment | Brine #1 Mg-Cl-Br (pH 6) | Earth | 90-125 µm<br><br>180-250 µm<br><br>250-355 µm<br><br>510-710 µm<br><br>>710 µm | Figure 4.2; Table S4 |
| (B) | Atmospheric composition | UV continuous on for 120 h; sampled once at the end of experiment | Brine #4 Mg-$SO_4$-Cl-Br (pH 6)<br><br>Brine #5 K- $SO_4$-Cl-Br (pH 6)<br><br>Brine #6 Ca-Mg-Fe(III)-$SO_4$-Cl-Br (pH 2)<br><br>Brine #7 Ca-Mg-Na-$HCO_3$-$SO_4$-Cl-Br (pH 8) | Earth and Mars for each brine; 1 atm. pressure for both gases | 250-355 µm | Table 4.1 |
| (C) | Effect of Br to Cl chemistry | UV continuous on for 120 h; sampled once at the end of experiment | Brine #1 Mg-Cl-Br (pH 6)<br><br>Brine #2 Mg-Cl  (pH 6) | Earth | 90-125 µm | Table 4.2 |
| (D) | Brine chemistry and length of UV | UV continuous on for 384 h; sampled every 48-72 h during the | Brine #1 Mg-Cl-Br (pH 6)<br><br>Brine #2 Mg-Cl (pH 6) | Earth | 250-355 µm | Figure 4.1; Figure 4.3; Table S3 |

| | | | | | | |
|---|---|---|---|---|---|---|
| | irradiation | experiment. Evacuated gases were bubbled into DI water and resulting solutions collected for phase identification | Brine #3 Na-Cl-Br (pH 6)<br><br>Brine #6 Ca-Mg-Fe(III)-$SO_4$-Cl-Br (pH 2)<br><br>Brine #7 Ca-Mg-Na-$HCO_3$-$SO_4$-Cl-Br (pH 8) | | | |
| (E) | Controls: evaporation without UV radiation | No UV; 120 h; sampled once at the end of experiment | Brine #1 Mg-Cl-Br (pH 6)<br><br>Brine #2 Mg-Cl (pH 6)<br><br>Brine #3 Na-Cl-Br (pH 6)<br><br>Brine #4 Mg-$SO_4$-Cl-Br (pH 6)<br><br>Brine #5 K-$SO_4$-Cl-Br (pH 6)<br><br>Brine #6 Ca-Mg-Fe(III)-$SO_4$-Cl-Br (pH 2)<br><br>Brine #7 Ca-Mg-Na-$HCO_3$-$SO_4$-Cl-Br (pH 8) | Earth | 250-355 μm | Data listed with appropriate experiments |
| (F) | $H_2O_2$ solution interaction with brines without UV | No UV or ambient light; sampled the final solution at the end of experiment | Brine #1 Mg-Cl-Br (pH 6)<br><br>Brine #2 Mg-Cl (pH 6)<br><br>Brine #3 Na-Cl-Br (pH 6) | Earth | No sediments | Table S5 |

**Table S3.** Anion compositions of extended time UV exposure experiments ('D' experiments in Table S2; Earth atmosphere; sediment quartz grain size = 250-355 μm; UV λ = 254 nm) [a].

| Brine #1 Mg-Cl$^-$-Br$^-$ (pH 6) (No dry point) | | | | | | | | | | | |
|---|---|---|---|---|---|---|---|---|---|---|---|
| | Cl$^-$ | Br$^-$ | ClO$_4^-$ | ClO$_3^-$ | BrO$_3^-$ | Br$^-$/Cl$^-$ | Cl$^-$ loss[b] | Br$^-$ loss[b] | ClO$_4^-$/Cl$_{total}$ | ClO$_3^-$/Cl$_{total}$ | ClO$_4^-$/Oxy-Cl$_{total}$ |
| Time Elapsed | mmol | mmol | μmol | μmol | μmol | molar | % | % | fraction | fraction | fraction |
| Evacuated gas[c] | 8.5E-04 | 6.3E-04 | < DL | < DL | < DL | 0.74 | | | | | |
| Initial | 29.9 | 29.7 | < DL | < DL | < DL | 0.99 | | | | | |
| 48 h | 28.6 | 30.1 | < DL | 5.1E-03 | < DL | 1.06 | 4.5% | -1.5% | 0 | 1.7E-07 | 0 |
| 120 h | 30.3 | 30.1 | < DL | 9.3E-02 | < DL | 0.99 | -1.3% | -1.2% | 0 | 3.1E-06 | 0 |
| 192 h | 28.6 | 26.3 | < DL | 6.0E-02 | < DL | 0.92 | 4.4% | 11.5% | 0 | 2.0E-06 | 0 |
| 264 h | 29.5 | 25.8 | 0.002 | 3.6E-02 | < DL | 0.88 | 1.3% | 13.0% | 7.0E-08 | 1.2E-06 | 0.06 |
| 336 h | 29.8 | 19.1 | 0.002 | 8.4E-02 | < DL | 0.64 | 0.2% | 35.8% | 8.0E-08 | 2.8E-06 | 0.03 |
| 384 h | 30.2 | 16.7 | 0.005 | 1.8E-01 | < DL | 0.55 | -1.1% | 43.8% | 1.7E-07 | 5.9E-06 | 0.03 |
| Brine #2 Mg-Cl$^-$ (pH 6) | | | | | | | | | | | |
| | Cl$^-$ | Br$^-$ | ClO$_4^-$ | ClO$_3^-$ | BrO$_3^-$ | Br$^-$/Cl$^-$ | Cl$^-$ loss | Br$^-$ loss | ClO$_4^-$/Cl$_{total}$ | ClO$_3^-$/Cl$_{total}$ | ClO$_4^-$/Oxy-Cl$_{total}$ |
| Time Elapsed | mmol | mmol | μmol | μmol | μmol | molar | % | % | fraction | fraction | fraction |
| Evacuated gas | 1.6E-02 | - | 3.5E-04 | 3.3E-03 | < DL | - | | - | | | 0.10 |
| Initial | 29.7 | - | < DL | < DL | < DL | - | | - | | | |
| 48 h | 29.2 | - | 0.35 | 10.51 | < DL | - | 1.6% | - | 1.2E-05 | 3.5E-04 | 0.03 |
| 120 h (dry point) | 29.5 | - | 3.57 | 31.72 | < DL | - | 0.8% | - | 1.2E-04 | 1.1E-03 | 0.10 |
| 192 h | 29.5 | - | 7.92 | 55.51 | < DL | - | 0.6% | - | 2.7E-04 | 1.9E-03 | 0.12 |
| 264 h | 31.1 | - | 8.90 | 51.12 | < DL | - | -4.6% | - | 3.0E-04 | 1.7E-03 | 0.15 |

| Time Elapsed | Cl⁻ | Br⁻ | ClO₄⁻ | ClO₃⁻ | BrO₃⁻ | Br⁻/Cl⁻ | Cl⁻ loss | Br⁻ loss | ClO₄⁻/Cl$_{total}$ | ClO₃⁻/Cl$_{total}$ | ClO₄⁻/Oxy-Cl$_{total}$ |
|---|---|---|---|---|---|---|---|---|---|---|---|
| 336 h | 29.1 | - | 27.44 | 355.70 | < DL | - | 2.0% | - | 9.2E-04 | 1.2E-02 | 0.07 |
| 384 h | 30.2 | - | 42.11 | 803.66 | < DL | - | -1.6% | - | 1.4E-03 | 2.7E-02 | 0.05 |
| **Brine #3 Na-Cl⁻-Br⁻ (pH 6)** | | | | | | | | | | | |
| | Cl⁻ | Br⁻ | ClO₄⁻ | ClO₃⁻ | BrO₃⁻ | Br⁻/Cl⁻ | Cl⁻ loss | Br⁻ loss | ClO₄⁻/Cl$_{total}$ | ClO₃⁻/Cl$_{total}$ | ClO₄⁻/Oxy-Cl$_{total}$ |
| Time Elapsed | mmol | mmol | μmol | μmol | μmol | molar | % | % | fraction | fraction | fraction |
| Evacuated gas | 1.7E-04 | 6.3E-04 | 3.0E-05 | 3.6E-05 | < DL | 3.70 | | | | | 0.46 |
| Initial | 24.8 | 24.7 | < DL | < DL | < DL | 1.00 | | | | | |
| 48 h | 25.3 | 23.3 | < DL | 0.007 | < DL | 0.92 | -1.9% | 5.5% | 0 | 3.0E-07 | 0 |
| 120 h (dry point) | 24.0 | 22.9 | < DL | 0.017 | 38.1 | 0.95 | 3.2% | 7.3% | 0 | 6.7E-07 | 0 |
| 192 h | 24.7 | 17.8 | < DL | 0.033 | 35.3 | 0.72 | 0.5% | 28.0% | 0 | 1.3E-06 | 0 |
| 264 h | 24.3 | 14.6 | 0.002 | 0.034 | 125.7 | 0.60 | 2.1% | 40.8% | 6.2E-08 | 1.4E-06 | 0.04 |
| 336 h | 25.5 | 14.0 | 0.004 | 0.088 | 303.1 | 0.55 | -2.8% | 43.2% | 1.4E-07 | 3.5E-06 | 0.04 |
| 384 h | 24.1 | 13.2 | 0.011 | 0.212 | 570.1 | 0.55 | 2.8% | 46.4% | 4.4E-07 | 8.5E-06 | 0.05 |

(Continued)

| Brine #6 Ca-Mg-Fe$^{3+}$-SO$_4^{2-}$-Cl$^-$-Br$^-$ (pH 2) | | | | | | | | | | | | |
|---|---|---|---|---|---|---|---|---|---|---|---|---|
| | Cl$^-$ | Br$^-$ | SO$_4^{2-}$ | ClO$_4^-$ | ClO$_3^-$ | BrO$_3^-$ | Br$^-$/Cl$^-$ | Cl$^-$ loss | Br$^-$ loss | SO$_4^{2-}$ loss | ClO$_4^-$/Cl$_{total}$ | ClO$_3^-$/Cl$_{total}$ | ClO$_4^-$/Oxy-Cl$_{total}$ |
| Time Elapsed | mmol | mmol | mmol | µmol | µmol | µmol | molar | % | % | % | fraction | fraction | fraction |
| Evacuated gas | 4.5E-03 | 6.3E-04 | < DL | 2.5E-03 | 1.0E-02 | < DL | 0.14 | | | | | | 0.20 |
| Initial | 6.6 | 7.7 | 18.6 | < DL | < DL | < DL | 1.18 | | | | | | |
| 48 h | 3.5 | 2.1 | 12.8 | 6.5E-02 | < DL | < DL | 0.60 | 47.2% | 73.0% | 31.1% | 9.9E-06 | 0 | 1.00 |
| 120 h (dry point) | 3.7 | 2.3 | 12.8 | 4.0E+00 | 1.2E-03 | < DL | 0.62 | 44.6% | 70.5% | 31.4% | 6.1E-04 | 1.8E-07 | 1.00 |
| 192 h | 3.3 | 1.8 | 10.7 | 1.1E+01 | 2.4E-03 | < DL | 0.56 | 49.9% | 76.1% | 42.5% | 1.7E-03 | 3.6E-07 | 1.00 |
| 264 h | 3.8 | 1.8 | 10.2 | 3.5E+01 | 8.9E-02 | < DL | 0.47 | 41.9% | 76.6% | 45.2% | 5.4E-03 | 1.3E-05 | 1.00 |
| 336 h | 1.8 | 1.8 | 8.2 | 2.7E+01 | 2.5E-02 | < DL | 1.00 | 72.5% | 76.4% | 56.0% | 4.1E-03 | 3.8E-06 | 1.00 |
| 384 h | 2.0 | 1.7 | 8.8 | 2.1E+01 | 9.6E-03 | < DL | 0.82 | 69.3% | 78.4% | 52.7% | 3.2E-03 | 1.5E-06 | 1.00 |

| Brine #7 Ca-Mg-Na-HCO$_3^-$-SO$_4^{2-}$-Cl$^-$-Br$^-$ (pH 8) | | | | | | | | | | | | |
|---|---|---|---|---|---|---|---|---|---|---|---|---|
| | Cl$^-$ | Br$^-$ | SO$_4^{2-}$ | ClO$_4^-$ | ClO$_3^-$ | BrO$_3^-$ | Br$^-$/Cl$^-$ | Cl$^-$ loss | Br$^-$ loss | SO$_4^{2-}$ loss | ClO$_4^-$/Cl$_{total}$ | ClO$_3^-$/Cl$_{total}$ | ClO$_4^-$/Oxy-Cl$_{total}$ |
| Time Elapsed | mmol | mmol | mmol | µmol | µmol | µmol | molar | % | % | % | fraction | fraction | fraction |
| Evacuated gas | 2.5E-03 | 5.0E-04 | < DL | 2.4E-04 | 1.4E-03 | < DL | 0.20 | | | | - | | 0.15 |
| Initial | 3.1 | 2.9 | 9.7 | < DL | < DL | < DL | 0.95 | | | | | | |
| 48 h | 1.5 | 1.4 | 5.1 | 0.12 | 0.21 | < DL | 0.94 | 51.8% | 51.3% | 47.4% | 4.0E-05 | 6.9E-05 | 0.36 |
| 120 h (dry point) | 1.6 | 1.1 | 4.4 | 0.47 | 0.40 | < DL | 0.70 | 49.2% | 61.8% | 54.2% | 1.5E-04 | 1.3E-04 | 0.54 |
| 192 h | 1.6 | 1.0 | 3.9 | 2.19 | 4.59 | < DL | 0.60 | 48.3% | 67.0% | 60.2% | 7.1E-04 | 1.5E-03 | 0.32 |
| 264 h | 1.7 | 0.9 | 4.9 | 1.02 | 25.26 | 56.3 | 0.52 | 46.3% | 70.0% | 49.9% | 3.3E-04 | 8.1E-03 | 0.04 |

| 336 h | 1.3 | 0.8 | 4.0 | 1.13 | 44.11 | 40.7 | 0.59 | 56.9% | 73.0% | 58.4% | 3.6E-04 | 1.4E-02 | 0.02 |
|---|---|---|---|---|---|---|---|---|---|---|---|---|---|
| 384 h | 1.4 | 0.8 | 3.9 | 1.57 | 73.65 | 46.1 | 0.58 | 55.8% | 72.4% | 59.7% | 5.1E-04 | 2.4E-02 | 0.02 |

a. Final results were reported as the abundances in the total final evaporating mixtures prior to sampling, which equates to initial brine plus quartz grain minus weight loss due to the evaporation. The Cl and Br species detected in the evacuated gases and as produced oxy-Cl and oxy-Br speices did not necessarily accounted for all the loss of chloride and bromide from the evaporating system. Not all evacuated gases were collected in our experiments. Some species which were undetected may be also present.

b. The standard error for $Cl^-$ and $Br^-$ was ±5%, and for $SO_4^{2-}$ was ±1%. Therefore, the propagated error for columns 'Cl$^-$ loss' and 'Br$^-$ loss' was estimated to be ±10%. The negative values in these two columns were mainly due to analytical errors, which were concluded as no apparent changes.

c. Evacuated gas was collected in ultrapure water and the solutions were analyzed for species identification and semi-quantification.

d. $ClO_2^-$ and $ClO^-$ were not detected in any of the samples. The $BrO_3^-$ was undetected in most of the samples. Detection limits in the final evaporating mixtures: 4 µg/kg ($ClO_3^-$ and $ClO_4^-$), 8 µg/g ($ClO_2^-$ and $BrO_3^-$), and 0.64 µg/g ($ClO^-$).
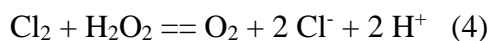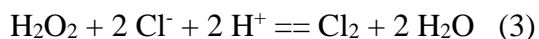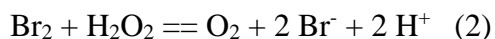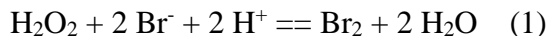
**Table S4.** Anion compositions for experiments examining quartz grain size effects ('A' experiments in Table S2; Earth atmosphere; UV continuously on 120 h).

| | $Cl^-$ | $Br^-$ | $ClO_4^-$ | $ClO_3^-$ | $ClO_2^-$ | $ClO^-$ | $BrO_3^-$ | $Br^-/Cl^-$ | $Cl^-$ loss | $Br^-$ loss | $ClO_4^-/Cl_{total}$ | $ClO_4^-/Oxy\text{-}Cl_{total}$ |
|---|---|---|---|---|---|---|---|---|---|---|---|---|
| | mmol | mmol | µmol | µmol | µmol | µmol | µmol | molar | % | % | fraction | fraction |
| Initial brine only | 3.85 | 3.82 | < DL | < DL | < DL | < DL | < DL | 0.99 | | | | |
| quartz grain size 90-125 µm | 2.86 | 1.46 | 0.083 | 0.290 | < DL | < DL | < DL | 0.51 | 25.7% | 61.7% | 2.2E-05 | 0.22 |
| quartz grain size 180-250 µm | 3.48 | 1.69 | 0.025 | 0.097 | < DL | < DL | < DL | 0.49 | 9.6% | 55.7% | 6.4E-06 | 0.20 |
| quartz grain size 250-355 µm | 2.55 | 1.49 | 0.003 | 0.053 | < DL | < DL | < DL | 0.58 | 33.7% | 61.0% | 8.9E-07 | 0.06 |
| quartz grain size 510-710 µm | 3.16 | 1.46 | 0.001 | 0.042 | < DL | < DL | < DL | 0.46 | 18.0% | 61.9% | 2.6E-07 | 0.02 |
| quartz grain size >710 µm | 3.15 | 1.22 | < DL | 0.045 | < DL | < DL | < DL | 0.39 | 18.2% | 68.0% | 0.00 | 0.00 |

## 2. $H_2O_2$ solution interaction with $Br^-$ and $Cl^-$ containing brines.

Since the Viking Landers first observed that Martian surface soils are chemically reactive and capable of decomposing organic molecules (Klein, 1978; Levin and Straat, 1976; Oyama et al., 1977), a number of oxidant candidates have been proposed to explain soil reactivity, but no consensus has been reached regarding the nature of the oxidants (Zent and Mckay, 1994). Of the proposed oxidizing compounds, hydrogen peroxide ($H_2O_2$) has received most attention because of its potentially ubiquitous distribution both in the Martian atmosphere (Bullock et al., 1994; Encrenaz et al., 2004) and on surface soil particles (Hurowitz et al., 2007; Pradhan et al., 2010; Quinn and Zent, 1999), and the relatively well established pathways to photochemically produce other oxidants, such as hydroxyl radical ($OH\cdot$) and hydroperoxyl radical ($HO_2\cdot$) (Chu and Anastasio, 2005; France et al., 2007). In this scenario, $H_2O_2$ either formed initially in the Martian atmosphere and then diffused into surface soils, or was present directly on the surface of soil particles. One question relevant to our studies is that once any $H_2O_2$ comes into contact with $Br^-$ and $Cl^-$ bearing brines, would it oxidize halide anions to higher oxidation states or might it liberate $Br^-$ or $Cl^-$ from the solution and thus cause Br/Cl fractionation?

Previous studies demonstrated that a core reaction of $H_2O_2$ with $Cl^-$ or $Br^-$ solutions at room temperature is catalytic decomposition of $H_2O_2$, because $H_2O_2$ could not only oxidize $Br^-$ to Br and $Cl^-$ to Cl, but also reduce Br to $Br^-$ and Cl to $Cl^-$, by the following reactions (Bray and Livingston, 1923; Livington and Bray, 1925).

$H_2O_2 + 2\ Br^- + 2\ H^+ == Br_2 + 2\ H_2O$    (1)

$Br_2 + H_2O_2 == O_2 + 2\ Br^- + 2\ H^+$   (2)

$H_2O_2 + 2\ Cl^- + 2\ H^+ == Cl_2 + 2\ H_2O$   (3)

$Cl_2 + H_2O_2 == O_2 + 2\ Cl^- + 2\ H^+$   (4)

These reactions occur simultaneously, thus the sum of these reactions is the decomposition of $H_2O_2$ and release of oxygen molecule.

$2 H_2O_2 == 2 H_2O + O_2$ (5)

It is still uncertain whether chlorine and bromine could be liberated from these reactions (Footnote 1 in Bray and Livingston, 1923). The chlorine and bromine are not likely formed in a neutral halide brine, but might be liberated in the reaction with HBr or HCl under acidic condition (Maass and Hatcher, 1922). In this work, we used three near-neutral brines (pH 6) containing both $Br^-$ and $Cl^-$ (molar $Br^-/Cl^-$ ratio = 1), to examine if the interaction with concentrated $H_2O_2$ solutions (30 wt% $H_2O_2$; 8.8 mM) enables oxidation of $Br^-$ and $Cl^-$ to higher oxidation states, and if the Br and Cl could be liberated even at low levels.

Experimental method:

Brines #1, #2, #3 were used in contact with 8.8 mM $H_2O_2$ solutions (experiment type F in Table S2). About 3.3 g of the brine and 5.4 g of 8.8 mM $H_2O_2$ solution were added to a 50 mL polypropylene tube (covered with heavy duty foil and placed in a dark box without a cap). Each type of brine experiment had three replicates. Periodically the tube was swirled by hand to release the formed bubbles from the solution until all bubbles had disappeared. The solution was then collected and diluted for analyses.

Results and discussion:

Besides the release of generated bubbles, no other changes were observed in the solutions. In the final solutions there was no significant $Br^-$ and $Cl^-$ loss, and no oxy-chlorine species or bromate was detected (Table S5). Weight loss from the solution was consistent with the $O_2$ gas release, which has been reported in previous studies (e.g., Bray and Livingston, 1923; Livington

180

and Bray, 1925). Therefore, our results agree well with previous studies (Bray and Livingston, 1923). Without UV irradiation, the interaction of $H_2O_2$ with halide bearing solutions (at close to neutral conditions) is a series of catalytic reactions to release oxygen molecules, without forming higher oxidation states of halogens or liberating halogens from solution. No significant change to halogens in the brine is thus expected.

We did not examine the same processes in the presence of UV radiation, since the effective oxidant under those conditions is likely OH· instead of $H_2O_2$ ($H_2O_{2\ (aq)} + h\upsilon$ ($\lambda = 254$ nm) $\rightarrow$ 2 OH $_{(aq)}$), and the influence of OH radical on halogens has been described extensively (e.g., Finlayson-Pitts, 2010; Frinak and Abbatt, 2006; Jung et al., 2010; Mozurkewich, 1995; von Glasow and Crutzen, 2007).

**Table S5.** Results of experiments examining halide bearing brines interacting with $H_2O_2$ solutions[a] ('F' experiments in Table S2).

| | Brine types | Initial brine g | Initial $H_2O_2$ solution g | Loss of gas phases g | Avg. Cl⁻ mmol | Avg. Br⁻ mmol | Oxy-chlorine species [b] mmol | $BrO_3^-$ [b] mmol |
|---|---|---|---|---|---|---|---|---|
| Initial | Na-Cl-Br | 3.32 ± 0.004 | 5.38 ± 0.004 | 0.97 ± 0.01 | 6.79 ± 0.002 | 6.61 ± 0.002 | < DL | < DL |
| Final | | | | | 6.87 ± 0.41 | 6.57 ± 0.27 | < DL | < DL |
| Initial | Mg-Cl-Br | 3.30 ± 0.004 | 5.36 ± 0.032 | 1.43 ± 0.005 | 7.62 ± 0.005 | 6.90 ± 0.004 | < DL | < DL |
| Final | | | | | 7.55 ± 0.17 | 6.70 ± 0.04 | < DL | < DL |
| Initial | Mg-Cl | 3.31 ± 0.003 | 5.36 ± 0.016 | 0.92 ± 0.026 | 6.63 ± 0.006 | | < DL | < DL |
| Final | | | | | 6.59 ± 0.05 | | < DL | < DL |

a. Each type of brine had three replicates, and the average and standard deviation are reported.
b. Oxy-chlorine species represented by $ClO_4^-$, $ClO_3^-$, $ClO_2^-$, and $ClO^-$. Detection limits of oxy-species in the solution were: 0.05 µg/L ($ClO_3^-$ and $ClO_4^-$), 100 µg/L ($ClO_2^-$ and $BrO_3^-$), and 8 µg/L ($ClO^-$).

**Table S6.** Perchlorate, chlorate and chloride data for Mars and selected terrestrial natural samples.

| Samples | Location | Description | $ClO_4^-$ | $ClO_3^-$ | $Cl^-$ | $Cl_{total}$[a] | $(ClO_4+ClO_3)/$ $Cl_{total}$ molar ratio | $ClO_4/$ $ClO_3$ molar ratio | pH | Data sources[b] |
|---|---|---|---|---|---|---|---|---|---|---|
| Phoenix landing site surface soils | Mars, north pole | Average of Rosy Red, Sorceress 1 and Sorceress 2 | 2.4 mM | ≤2.4 mM[c] | 0.47 mM | NA | ≤0.91[c] | NA | 7.7 | [1] |
| Phoenix landing site surface soils | Mars, north pole | Rosy Red (initial data reported by [1]) | 2.7 mM | ≤2.7 mM[c] | 0.6 mM | NA | ≤0.90[c] | NA | 7.74 | [1] |
| Phoenix landing site surface soils | Mars, north pole | Rosy Red (re-analysis data reported by [2]) | 2.89 mM | ≤2.89 mM[c] | 0.39 mM | NA | ≤0.94[c] | NA | 7.67 | [2] |
| Rocknest aeolian fines | Mars, Gale Crater | Average of four separate portions of the fifth scooped sample; calculated based on evolved gas abundances during SAM pyrolysis experiments. | (equiv. $Cl_2O_7$) 0.4 wt% | | NA | 0.69 wt% | 0.225[d] | NA | neutral | [3], [4] |
| Cumberland drill fines | Mars, Gale Crater, Yellowknife Bay, Sheepbed formation | Mudstone drill material; ~ 6 cm deep; average of four runs; calculated based on evolved gas abundances during SAM pyrolysis experiments equivalent to oxychlorine $Cl_2O_7$ | (equiv. $Cl_2O_7$) 0.95 wt% | | NA | 1.41 wt% | 0.261[d] | NA | neutral | [3] |
| John_Klein drill fines | Mars, Gale Crater, Yellowknife Bay, Sheepbed formation | Mudstone drill material; ~ 6 cm deep; average of four runs; calculated based on evolved gas abundances during SAM pyrolysis experiments equivalent to oxychlorine $Cl_2O_7$ | (equiv. $Cl_2O_7$) 0.125 wt% | | NA | 0.4 wt% | 0.121[d] | NA | neutral | [3] |
| Martian meteorite EETA79001 | Mars, proposed launch from a segment of Olympus Mons aureole | A sawdust portion of the meteorite | 0.6 ppm | 1.4 ppm | 3.2 ppm | NA | 0.202 | 0.36 | 8.4 | [5] |

| | | | | | | | | | | |
|---|---|---|---|---|---|---|---|---|---|---|
| Soil P1 | Atacama, Chile | 6 m depth, caliche | 240 ppm | 340 ppm | 8 wt% | NA | 2.9E-03 | 0.63 | NA | [6] |
| Soil P2 | Atacama, Chile | 6 m depth, halite caliche | 330 ppm | 330 ppm | 46 wt% | NA | 5.6E-04 | 0.89 | NA | [6] |
| Soil P4 | Atacama, Chile | 50 cm depth, chunk of $NaNO_3$ | 130 ppm | 530 ppm | 6.1 wt% | NA | 4.4E-03 | 0.22 | NA | [6] |
| DV3 | Death Valley, California | Confidence Hills-1 caliche | 0.25 ppm | 41 ppm | 32 wt% | NA | 5.5E-05 | 0.01 | NA | [6] |
| DV4 | Death Valley, California | Bully Hill caliche | 0.8 ppm | 0.6 ppm | 8 wt% | NA | 6.8E-06 | 1.19 | NA | [6] |
| DV5 | Death Valley, California | Saratoga Hills-1 caliche | 0.95 ppm | 32 ppm | 6.3 wt% | NA | 2.2E-04 | 0.03 | NA | [6] |
| DV6 | Death Valley, California | Zabriskie caliche | 1.7 ppm | 57 ppm | 14 wt% | NA | 1.8E-04 | 0.03 | NA | [6] |
| AN1 | University Valley, Antarctica | Surface sample | 0.202 ppm | 0.037 ppm | 540 ppm | NA | 1.6E-04 | NA | NA | [6] |

a. NA = data not available. The column of $Cl_{total}$ reports data obtained by direct measurement only. In the case the $Cl_{total}$ data is not available, sum of ($ClO_4 + ClO_3 + Cl^-$) is used as the total Cl in order to calculate molar ratios of ($ClO_4 + ClO_3$)/ $Cl_{total}$.

b. Data sources: [1] Hecht et al., 2009; [2] Toner et al., 2014; [3] Ming et al., 2014; [4] Blake et al., 2013; [5] Kounaves et al., 2014; [6] Rao et al., 2010.

c. Chlorate is not detected in the Phoenix sample, however, this might be due to the signal being overwhelmed by perchlorate. We assume an upper limit on molar $ClO_4/ClO_3 = 1$ to calculate an upper limit on the ($ClO_4+ClO_3$)/ $Cl_{total}$ molar ratio.

d. Oxy-chlorine species are assumed in the form of $Cl_2O_7$ based on SAM pyrolysis experiments. We use it as total perchlorate and chlorate in the calculation of ($ClO_4+ClO_3$)/ $Cl_{total}$ molar ratios of Gale Crater samples.

# References

Blake, D. F., Morris, R. V., Kocurek, G., Morrison, S. M., Downs, R. T., Bish, D., Ming, D. W., Edgett, K. S., Rubin, D., Goetz, W., Madsen, M. B., Sullivan, R., Gellert, R., Campbell, I., Treiman, A. H., McLennan, S. M., Yen, A. S., Grotzinger, J., Vaniman, D. T., Chipera, S. J., Achilles, C. N., Rampe, E. B., Sumner, D., Meslin, P. Y., Maurice, S., Forni, O., Gasnault, O., Fisk, M., Schmidt, M., Mahaffy, P., Leshin, L. A., Glavin, D., Steele, A., Freissinet, C., Navarro-Gonzalez, R., Yingst, R. A., Kah, L. C., Bridges, N., Lewis, K. W., Bristow, T. F., Farmer, J. D., Crisp, J. A., Stolper, E. M., Marais, D. J. D., Sarrazin, P. and Team, M. S. (2013) Curiosity at Gale Crater, Mars: Characterization and analysis of the Rocknest sand shadow. *Science*, **341 (6153)**, doi: 10.1126/science.1239505.

Bray, W. C. and Livingston, R. S. (1923) The catalytic decomposition of hydrogen peroxide in a bromine-bromide solution, and a study of the steady state. *J. Am. Chem. Soc.* **45**, 1251-1271.

Bullock, M. A., Stoker, C. R., Mckay, C. P. and Zent, A. P. (1994) A coupled soil atmosphere model of $H_2O_2$ on Mars. *Icarus*, **107**, 142-154.

Chu, L. and Anastasio, C. (2005) Formation of hydroxyl radical from the photolysis of frozen hydrogen peroxide. *J. Phys. Chem. (A),* **109**, 6264-6271.

Encrenaz, T., Bezard, B., Greathouse, T. K., Richter, M. J., Lacy, J. H., Atreya, S. K., Wong, A. S., Lebonnois, S., Lefevre, F. and Forget, F. (2004) Hydrogen peroxide on Mars: Evidence for spatial and seasonal variations. *Icarus,* **170**, 424-429.

Finlayson-Pitts, B. J. (2010) Halogens in the Troposphere. *Anal. Chem.,* **82 (3)**, 770-776, doi: 10.1021/ac901478p.

France, J. L., King, M. D. and Lee-Taylor, J. (2007) Hydroxyl (OH) radical production rates in snowpacks from photolysis of hydrogen peroxide ($H_2O_2$) and nitrate ($NO_3^-$). *Atmos. Environ.,* **41**, 5502-5509.

Frinak, E. K. and Abbatt, J. P. D. (2006) $Br_2$ production from the heterogeneous reaction of gas-phase OH with aqueous salt solutions: Impacts of acidity, halide concentration, and organic surfactants. *J. Phys. Chem. (A),* **110**, 10456-10464.

Hecht, M. H., Kounaves, S. P., Quinn, R. C., West, S. J., Young, S. M. M., Ming, D. W., Catling, D. C., Clark, B. C., Boynton, W. V., Hoffman, J., DeFlores, L. P., Gospodinova, K., Kapit, J. and Smith, P. H. (2009) Detection of perchlorate and the soluble chemistry of Martian soil at the Phoenix Lander site. *Science,* **325**, 64-67.

Hurowitz, J. A., Tosca, N. J., McLennan, S. M. and Schoonen, M. A. A. (2007) Production of hydrogen peroxide in Martian and lunar soils. *Earth Planet. Sci. Lett.,* **255**, 41-52.

Jung, Y. J., Baek, K. W., Oh, B. S. and Kang, J. W. (2010) An investigation of the formation of chlorate and perchlorate during electrolysis using Pt/Ti electrodes: The effects of pH and reactive oxygen species and the results of kinetic studies. *Water Res.,* **44**, 5345-5355.

Keith, J. N. and Solomon, I. J. (1970) Ammonium perbromate, *Inorganic Chemistry*, **9(6)**, 1560-1561.

Klein, H. P. (1978) Viking biological experiments on Mars. *Icarus,* **34**, 666-674.

Kounaves, S. P., Carrier, B. L., O'Neil, G. D., Stroble, S. T. and Claire, M. W. (2014) Evidence of martian perchlorate, chlorate, and nitrate in Mars meteorite EETA79001: Implications for oxidants and organics. *Icarus,* **229**, 206-213.

Levin, G. V. and Straat, P. A. (1976) Viking labeled release biology experiment - interim results. *Science*, **194**, 1322-1329.

Livington, R. S. and Bray, W. C. (1925) The catalytic decomposition of hydrogen peroxide in an acid chlorine-chloride solution. *J. Am. Chem. Soc.,* **47**, 2069-2082.

Maass, O. and Hatcher, W. H. (1922) The properties of pure hydrogen peroxide (III), *J. Am. Chem. Soc.,* **44(11)**, 2472-2480, doi: 10.1021/ja01432a015.

Ming, D. W., Archer, P. D., Glavin, D. P., Eigenbrode, J. L., Franz, H. B., Sutter, B., Brunner, A. E., Stern, J. C., Freissinet, C., McAdam, A. C., Mahaffy, P. R., Cabane, M., Coll, P., Campbell, J. L., Atreya, S. K., Niles, P. B., Bell, J. F., Bish, D. L., Brinckerhoff, W. B., Buch, A., Conrad, P. G., Des Marais, D. J., Ehlmann, B. L., Fairen, A. G., Farley, K., Flesch, G. J., Francois, P., Gellert, R., Grant, J. A., Grotzinger, J. P., Gupta, S., Herkenhoff, K. E., Hurowitz, J. A., Leshin, L. A., Lewis, K. W., McLennan, S. M., Miller, K. E., Moersch, J., Morris, R. V., Navarro-Gonzalez, R., Pavlov, A. A., Perrett, G. M., Pradler, I., Squyres, S. W., Summons, R. E., Steele, A., Stolper, E. M., Sumner, D. Y., Szopa, C., Teinturier, S., Trainer, M. G., Treiman, A. H., Vaniman, D. T., Vasavada, A. R., Webster, C. R., Wray, J. J., Yingst, R. A. and Team, M. S. (2014) Volatile and Organic Compositions of Sedimentary Rocks in Yellowknife Bay, Gale Crater, Mars. *Science*, **343 (6169)**, doi: 10.1126/science.1245267.

Mozurkewich, M. (1995) Mechanisms for the release of halogens from sea-salt particles by free-radical reactions. *J. Geophys. Res.,* **100**, 14199-14207.

Oyama, V. I., Berdahl, B. J. and Carle, G. C. (1977) Preliminary findings of viking gas-exchange experiment and a model for Martian surface chemistry. *Nature*, **265**, 110-114.

Pradhan, M., Kalberer, M., Griffiths, P. T., Braban, C. F., Pope, F. D., Cox, R. A. and Lambert, R. M. (2010) Uptake of gaseous hydrogen peroxide by submicrometer titanium dioxide aerosol as a function of relative humidity. *Environ. Sci. Technol.,* **44**, 1360-1365.

Quinn, R. C. and Zent, A. P. (1999) Peroxide-modified titanium dioxide: A chemical analog of putative Martian soil oxidants. *Origins of Life and Evolution of Biospheres*, **29**, 59-72.

Rao, B., Anderson, T. A., Orris, G. J., Rainwater, K. A., Rajagopalan, S., Sandvig, R. M., Scanlon, B. R., Stonestrom, D. A., Walvoord, M. A. and Jackson, W. A. (2007) Widespread natural perchlorate in unsaturated zones of the southwest United States. *Environ. Sci. Technol.,* **41**, 4522-4528.

Rao, B., Hatzinger, P. B., Bohlke, J. K., Sturchio, N. C., Andraski, B. J., Eckardt, F. D. and Jackson, W. A. (2010b) Natural chlorate in the environment: Application of a new IC-ESI/MS/MS method with a $(ClO_3^-)$-O-18 internal standard. *Environ. Sci. Technol.*, **44**, 8429-8434.

von Glasow, R. and Crutzen, P. J. (2007) Tropospheric halogen chemistry, in: Heinrich, D.H., Karl, K.T. (Eds.), Treatise on Geochemistry. Pergamon, Oxford, pp. 1-67.

Zent, A.P. and Mckay, C.P. (1994) The chemical-reactivity of the Martian soil and implications for future missions. *Icarus,* **108 (1)**, 146-157, http://dx.doi.org/10.1006/icar.1994.1047.

**Appendix 3: Paper Reprint**

**Does Martian Soil Release Reactive Halogens to the Atmosphere?**

# Does martian soil release reactive halogens to the atmosphere?

CrossMark

Suniti Karunatillake [a,b,*], Yu-Yan Sara Zhao [a], Scott M. McLennan [a], J.R. Skok [b], Nicole E. Button [b]

[a] Stony Brook University, Department of Geosciences, Earth and Space Sciences Building, Stony Brook, NY 11794-2100, United States
[b] Department of Geology and Geophysics, Lousiana State University, Baton-Rouge, LA 70803, United States

A R T I C L E   I N F O

A B S T R A C T

Detailed statistical examination of Cl, Br, and S distributions, in martian soil profiles at Gusev Crater and Meridiani Planum, indicates decreasing Br abundance and weakening Br–S association towards the surface. All three elements decrease towards the surface in the order Cl < S < Br. Furthermore, Br variability decouples from potential cations such as Mg at the surface relative to the subsurface. These observations support a relative loss of surficial Br compared to S and Cl, all highly mobile elements in aqueous environments. We propose that Br may have converted preferentially to gas phases (e.g., BrO), driven either by UV photolysis or by chemical oxidants. Such volatilization pathways may in turn impart a global signature on Mars by acting as controls on oxidants such as ozone and perchlorates. S/Cl mass ratios vary with depth ($\sim$4–5 in the subsurface; 1.8–3.6 on the surface) as well, with a strong correlation of S and Cl near the surface but more variable at depth, consistent with differential vertical mobility, but not volatilization of Cl. Elevated S/Cl in subsurface soil also suggests that the ratio may be higher in bulk soil – a key repository of martian geologic and climatic records – than previously thought.

## 1. Introduction

The halogens chlorine and bromine are probably the most mobile elements known on Mars. Halogen distributions reveal constraints on surficial processes; indeed Br is perhaps the most important trace element used to evaluate evaporative processes on Earth (Warren, 2006). To date, Cl and Br variations in martian soils and rocks have been interpreted almost exclusively with their behavior in aqueous fluid–mineral systems, including aqueous alteration, evaporative processes, and post-depositional fluid migration (Clark et al., 2005; Knoll et al., 2008; Marion et al., 2009; Rao et al., 2009; Yen et al., 2005).

On Earth, halogens remobilize by both aqueous and atmospheric processes. Recent work (Hönninger et al., 2004; Risacher et al., 2006) further suggests that atmospheric processes can also affect rock/sediment geochemistry in highly arid evaporative settings. Accordingly, even though aqueous processes may explain variations in the Mars soil data, these recent studies in terrestrial settings question the exclusion of atmospheric effects in the martian context (Zhao et al., 2013).

To evaluate the potential for volatility effects, we examine the geochemical relationships among Br, Cl, and other mobile elements in martian soils to evaluate whether atmospheric processes could

have affected their distribution. Such pathways typically yield reactive halogen species known to destroy ozone (Finlayson-Pitts, 2010), though not yet incorporated into models of oxidant distribution on Mars, such as for perchlorates (Marion et al., 2010), $H_2O_2$ (Hurowitz et al., 2007), and atmospheric ozone (Lefèvre et al., 2008). For our analysis, we use geochemical data obtained by the Mars Exploration Rovers Spirit and Opportunity at Gusev Crater and Meridiani Planum, respectively.

In assessing halogen volatility, we also examine whether the S/Cl ratio may vary substantially more in the martian soil profile than suggested previously (Gellert et al., 2006). This analysis helps to assess the volatility of Cl, as well as to constrain the extent to which the proposed compositional uniformity of martian soil (e.g., Yen et al., 2005) holds true both at depth and across the surface. Soil excavations by the rovers enabled us to generate continuous profiles of compositional variation with depth at specific locations (e.g., Squyres et al., 2006).

Both aspects of our investigation relate to soil as a key repository of many complex processes operating at the surface of Mars over geological time. Its varying composition reflects complex interactions among impact, volcanic, eolian, glacial, aqueous, and atmospheric influences. While a daunting task, unraveling the relative importance of such processes can shed considerable insight into the geologic and climatic evolution of the planet.

### 1.1. Halogen atmospheric chemistry: Implications for Mars

In terrestrial settings, Br may convert from soluble bromide ($Br^-$) to a variety of gas phase bromine species (e.g., Br, $Br_2$, BrO,

* Corresponding author. Address: Geology & Geophysics, Louisiana University, E300 Howe-Russell BLDG (Postal: E235), Baton Rouge, LA 70803, United States.
E-mail address: wk43@cornell.edu (S. Karunatillake).
URLs: http://www.linkedin.com/pub/suniti-karunatillake/7/56b/8b6, http://www.researcherid.com/rid/A-5934-2009 (S. Karunatillake).

HBr, HOBr) and enter the atmosphere via numerous chemical pathways, many of which include photochemical reactions (Simpson et al., 2007). Salt aerosols, released from frost flowers on newly formed sea ice or lake ice and blowing snow especially in polar regions (Buys et al., 2012; Kaleschke, 2004; Yang et al., 2008), offer a primary natural mechanism for such transport. Modified analogs of this may occur on Mars, from atmospheric moisture as hoarfrost or from phase changes in brine films associated with soil. As another mechanism with obvious potential relevance for Mars (e.g., Smith, 2008) halogens may transfer from thin water films on eolian dust (Sander et al., 2003). Similar processes also mobilize chlorine into the atmosphere, but terrestrial marine brines that remain after ice formation and form the aerosols are relatively enriched in Br compared to Cl (Vogt et al., 1996; Yang et al., 2008). As a consequence, Br converts preferentially into the gas phase compared to Cl, which in turn fractionates Br/Cl ratios significantly.

Despite evidence for a limited role for aqueous activity on Mars through much of its geological history (Hurowitz and McLennan, 2007), Br/Cl fractionation may remain in effect for brine films on eolian dust. Beyond the known volatilization of Br from aerosols at the marine boundary layer, recent studies also indicate preferential Br transfer into the atmosphere during simple evaporation of brines (Smoydzin and Von Glasow, 2009; Wood and Sanford, 2007) and possibly directly from salt pans in arid environments (Hönninger et al., 2004). In one experiment, Wood and Sanford (2007) evaporated Br-spiked Abu Dhabi sabkha brines mixed with sand under vacuum and UV light at 80 °C. While Cl concentrations remained constant, they found that a remarkable 83% of the Br migrated to the atmosphere and that the Cl/Br ratio in the re-dissolved salts increased by nearly a factor of 6 over the original brine. These observations indicate that surface–atmosphere transfer of Br in hyper-arid regions such as Andean salt pans, analogous in terms of aqueous activity to the typical surface conditions on Mars, may influence the Br mass balance and fractionate Cl/Br ratios (Risacher et al., 2006).

On Earth, the mobility of Br via the atmosphere is of limited relevance to the overall global aqueous balance of the element. Br resides in the atmosphere only briefly (several minutes to several days) and at low concentrations (10's of ng/g) (Simpson et al., 2007; von Glasow and Crutzen, 2007). In contrast, Br resides in the oceans about $10^8$ times longer at concentrations about $10^6$ times greater (Broecker et al., 1982). The immense size of oceans diminishes the importance of saline lakes to global mass balance.

Compared to Earth, several factors make halogen atmospheric mobility on Mars possible. Mars presents compelling evidence for evaporite minerals at the surface despite insufficient evidence for ancient marine environments. Its surface experiences high solar UV-C (200–280 nm), UV-B (280–315 nm), and to a lesser degree UV-A (315–400 nm) fluxes (Cockell et al., 2000; Rontó et al., 2003). The martian surface has also been exposed to the atmosphere and to dust storms over long timescales, perhaps exceeding $10^9$ years (Carr, 2008). Accordingly, the atmosphere may affect the near surface environment significantly. The amount and composition of the martian atmosphere certainly differs fundamentally from Earth's, with outstanding questions on sedimentary processes (e.g., Grotzinger et al., 2013) and unknown implications to the halogen atmospheric chemistry. Nevertheless, volatilization may only require thin films of brine forming from the deliquescence of salts at low temperatures (Fairén et al., 2009; Zorzano et al., 2009) in salt pan analogs or on dust grains as discussed above. Subsurface $H_2O$ ice, as recently shown in situ at the Phoenix site (Smith et al., 2009) and locally within craters (Byrne et al., 2009), may further facilitate such processes.

The fate of any volatilized halogens remains an additional unknown on Mars. However, volatile halogens on Earth exchange easily between solid, aqueous, and gaseous phases (Simpson et al., 2007), likely enabling a steady state to be reached over the ~2.5–3.5 Ga geologic ages of Meridiani (Andrews-Hanna et al., 2007) and Gusev (Parker et al., 2010). Even though modern Mars seems to lack sabkhas and playas, their analogs could have existed cyclically in places like Meridiani (e.g., Hayes et al., 2011) and Gusev (Wang et al., 2008) enabling a steady state. Factors such as wind patterns, atmospheric temperature profiles, and atmospheric dust load may also offer varying environments for volatile phases to condense and redistribute.

Terrestrial $BrO_x$ species exist only for several hours during daytime (Simpson et al., 2007). The reactive species BrO in the terrestrial troposphere would eventually convert to BrCl or $BrONO_2$ within a few hours after sunset (Wayne et al., 1995). Clouds and aerosols enable subsequent surface deposition. Despite the unknown significance of such pathways on Mars, the dearth of removal agents such as clouds might extend the atmospheric lifetime of volatilized halogens, facilitating long-distance transportation. Fine particles suspended by dust storms or dust devils may offer adsorption surfaces with which to convert from gas to solid phases, depositing subsequently on the martian surface under dry conditions.

What evidence supports an atmospheric effect on halogen chemistry in surface materials of Mars? The 2007 Phoenix lander discovered significant quantities of perchlorate ($ClO_4^-$) in the water-soluble fraction of soils at the Phoenix polar landing site. The mineralogy hosting the perchlorates is uncertain, but data are consistent with $Mg(ClO_4)_2 \cdot nH_2O$. Measurements indicate that perchlorates may contain most of the chlorine in polar soil (Hecht et al., 2009). Analysis of Rocknest soil at Gale Crater also supports perchlorate presence (Archer et al., 2013; Sutter et al., 2013). Although aqueous processes may influence perchlorate geochemistry on Mars (Marion et al., 2010), the perchlorate ions on Mars may ultimately originate atmospherically (Catling et al., 2010). Terrestrial perchlorates, found in the stratosphere and as mineralization in hyperarid environments, result from photochemical oxidative processes involving volatile chlorine species (Catling et al., 2010) as discussed by Bao and Gu (2004).

## 2. Data and methods

For this analysis, we examined Alpha Particle X-ray Spectrometer (APXS)-derived geochemical relationships among Br, Cl, Mg, Na, and S in soils from Gusev Crater (sols 14-1368) and Meridiani Planum (sols 11-1368). MERAnalyst makes both data sets available to the public (http://an.rsl.wustl.edu/mer/MERB/merb_apxsoxide.htm), including introduction, key work (e.g., Gellert et al., 2006; Ming et al., 2008), notes on data evolution, and oxide data as *.csv files. The *.csv file header row includes sol identifier (spectrum), team consensus on target type (type), stoichiometric oxide mass fraction, and corresponding uncertainty at two standard errors. Target type contributed to our own classification by distinguishing soil targets from rocks and by identifying different soil preparation methods. Several different sampling methods of soil at the two sites show varying effects of local mineralogy. For example, local alkaline volcanics make some soils in Gusev Crater P-rich, and bedrock-derived hematitic spherules make some Meridiani Planum soils Fe-rich.

Soil excavations constitute a critical component of the data at both Gusev and Meridiani. In the Columbia Hills of Gusev Crater, some surface soils and associated subsurface soils exposed by a failed rover wheel differ dramatically (Yen et al., 2008). For this study, we term such excavations "involuntary." The mission also sampled soil intentionally as "trenches" by rotating a single rover
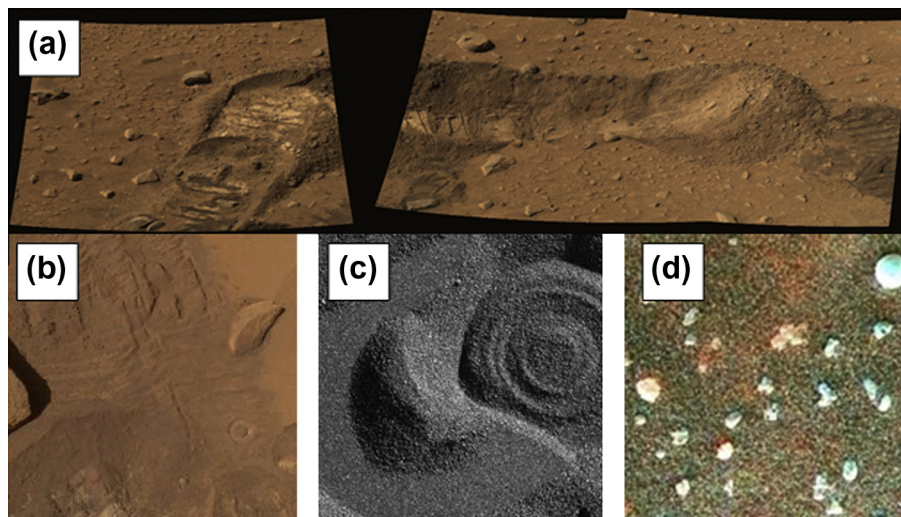
**Fig. 1.** Examples of different soil sampling methods we used to distinguish soil types: (a) trench activity at Gusev shown by a Pancam mosaic generated of Boroughs on Sol 142 (available online1). Boroughs is approximately 20 cm wide and 11 cm deep. (b) Disturbed soil sample at Gusev imaged by the Pancam on Sol 343 (online 2) bearing the Mossbauer contact plate imprint roughly 5 cm across. (c) MI $\sim 3 \times 3$ cm on Sol 236 of Meridiani soil sample brushed with the RAT (online 3). (d) MI on Sol 10 of undisturbed soil at Meridiani colorized with Pancam data (online 4). Photo credits: JPL/NASA/Cornell/USGS, MER-Analyst (online 5), and Pancam Images (online 6). Online 1: http://pancam.astro.cornell.edu/pancam_instrument/142A_new.html. Online 2: http://pancam.astro.cornell.edu/pancam_instrument/images/True/Sol343A_P2573_1_True_R-AD_thumb.jpg. Online 3: http://pds-geosciences.wustl.edu/mer/mer1-m-mi-3-rdr-sci-v1/mer1mi_1xxx/extras/sol0236/B0236auk_rawenh.tif. Online 4: http://pancam.astro.cornell.edu/pancam_instrument/images/merges/images/1MP010IOF02ORT24P2933L256F1_ec-th.jpg. Online 5: http://an.rsl.wustl.edu/mer/. Online 6: http://pancam.astro.cornell.edu/pancam_instrument/images.html.

wheel in place (Fig. 1a), as "disturbances" by brief wheel rotation scuffs (Fig. 1b) or wheel motion over soil, as "brushed" by spinning the Rock Abrasion Tool's brush mechanism against the soil (Fig. 1c), or as pristine surface samples undisturbed by the rover (Fig. 1d). Microscopic Images (MI) taken before and after subsurface soil exposure generally accompanied subsurface sampling. For sufficiently deep trenches, APXS observations of the adjacent surface, interior wall, and floor (Wang et al., 2006) offered the best chemical insight to date of the martian soil profile. Trenches in particular were expected to characterize the bulk soil for comparisons with depth-sensitive chemical remote sensing by the Mars Odyssey Gamma Ray Spectrometer (GRS) at regional scales (Karunatillake et al., 2007).

With the goal of identifying relationships among the elements of interest in the context of atmosphere–surface interactions, we subdivided the Gusev soils ($n = 60$) into six categories, with some overlap allowing samples to appear in more than one category: moderate S content soils ($n = 53$), basaltic soils (45), trench soils (6), disturbed soils (29), disturbed normal soils (15), and surficial soils (25). The details of these categories follow:

1. The moderate S category consisted of all soil with elemental S mass fractions less than 4%.
2. In addition to the S threshold, basaltic soil excluded potential sinter/bleached soil and hydrothermally altered samples such as those discussed by Ruff et al. (2011) and Yen et al. (2008), respectively.
3. Trench soil excluded involuntary excavations, such as Paso Robles soil, made by the Spirit Rover's immobile wheel. For additional insight into the soil profiles we compared surface, wall, and floor samples at each of the three Gusev trench sites.
4. Disturbed soil included all shallow subsurface samples, such as wheel scuffs and involuntary excavations, but excluded trench soil.
5. On the other hand, disturbed normal soil also excluded Paso Robles (hydrothermal origin) and Kenosha Comets (sinter/bleached) samples.
6. Surficial soil consisted of normal soil from undisturbed surfaces.

We list the sol, feature name, and APXS-derived composition for samples of each soil category in the worksheet "Gusev" of the Supplementary Excel file "S1SoilCategories." The first two worksheets of this file contain the first 1368 sols of data for each landing site extracted from the MERAnalyst *.csv files. Remaining worksheets enumerate sol and target names for each soil category at the two landing sites. Columns in the first two worksheets include the classification as soil (header: "soil?"). For samples identified as soil, several additional columns of moderate S, basaltic, trench, disturbed, disturbed normal, and undisturbed surficial soil identify classification into each of the six overlapping categories. Remaining columns present oxide – elemental, in the case of Br and Cl – percentage mass fractions. µg/g mass fractions describe the abundances of minor elements Br, Ni, and Zn. We assessed available images (MIs, panoramic camera, navigation camera, hazard camera) and mission reports to assign a given sample to each category. This also enabled us to identify samples uniquely even in cases of ambiguous or conflicting target names.

Compositional complexities from the presence of hematitic spherules (aka "blueberries") – considered sedimentary in origin – prompted us to divide Meridiani soil ($n = 38$) into seven overlapping categories. As with Gusev data, we identify samples of each category in the worksheet "Meridiani" of the Supplementary Excel file "S1SoilCategories." Most categories remain similar to those used at Gusev, as evident below:

1. Moderate S content soil ($n = 37$).
2. Basaltic soil (23) which, in addition to moderate S content, excluded soil enriched in hematitic spherules.
3. Trench soil (4).
4. Disturbed soil (8).
5. Disturbed soil with moderate S content and low hematite content (5). Such soil contained less than 20% $FeO_T$ with negligible hematitic spherule visibility in available MI and Pancam images.
6. Surficial soil (26). All contained moderate sulfur mass fractions, at less than 4%.
7. Surficial soil without excessive hematite (15).

As key statistical parameters, we used linear correlation coeffi-
cients, slopes, and intercepts, along with their error bounds for
Br–S, Br–Cl, Br–Mg, Br–Na, Cl–S, Cl–Mg, and Cl–Na pairs. Standard
errors of the correlation coefficients ($r$) decreased primarily with
the number of data and increased with relative scatter of data from
a least squares line fit (Karunatillake et al., 2012). Adjusted coeffi-
cient of determination ($R^2$) as well as standard errors of regression
slopes and intercepts varied accordingly (Karunatillake et al.,
2012). We computed these detailed statistical parameters not only
for each elemental pair, but also for each of the 13 soil categories at
Gusev and Meridiani. As with Br–S in Section 3, we communicate
the results summarily with scatter plots of mutually dependent
regression parameters of correlation and slope. To provide context,
we describe the underlying data with scatter plots of Br–S and
Br–Mg for strong and weak correlation extremes. In addition to
highlighting key observations, our methodology prevents a bewil-
dering array of 97 scatter plots and corresponding regression
results.

Given our primary interest in elemental trends rather than spe-
cific values, and evidence for high instrumental precision (Rieder
et al., 2004), we included data with lower Br concentrations, where
specifically reported, in our statistical analysis. Nevertheless, even
in the context of elemental trends, our results may be sensitive to
the greater uncertainties associated with Br. The trace element Br
is a special case usually assigned a detection limit of about
30 μg/g despite lower reported values in the literature (Rieder
et al., 2004).

## 3. Results and discussion

Our observations of Gusev trench soil indicate broad consis-
tency with the loss of surficial Br to the atmosphere, driven by
UV photolysis (Wood and Sanford, 2007), by chemical oxidants
perhaps including –OH radicals (Urbansky, 1998), or by the auto-
catalytic pathway involving HOBr (Simpson et al., 2007). First,
the Br concentration is consistently higher in the subsurface rela-
tive to the surface at Gusev. Second, while Br, S, and Cl increase
in the subsurface, the proportional increase relative to the surface,
roughly in the order Br > S > Cl, yield higher Br/Cl, lower S/Br, and
higher S/Cl ratios in the subsurface. Table 1 illustrates this trend
by comparing averages of surface ratios (undisturbed) with sub-
surface (trench) ratios.

Trends across soil categories confirm the vertical variations in
Br observed at the trenches. That Br correlates strongly with S in
the subsurface is evident in Fig. 2 summary plot showing the twin
regression parameters of correlation and slope. Fig. 3 provides
bivariate scatter plot context for the strongest elemental associa-
tion in summary plots of correlation and slope (e.g., Fig. 2). For
example, the Br–S scatter plot for the trench category at Gusev
(Fig. 3a) generates the trench datum in Fig. 2. Despite few data,
the correlation coefficient of 0.9 (±0.2 at 1 standard error) corre-
sponds to 73% of the Br variability modeled by S alone, as indicated
by the adjusted coefficient of determination ($R^2$) (Karunatillake
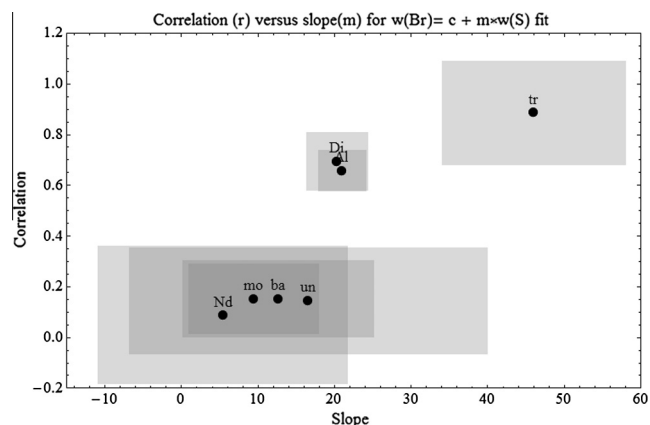et al., 2012).



**Fig. 2.** Plot of correlation coefficient versus slope of linear regressions for Br–S in
different soil classes at Gusev. These mutually dependent regression parameters
summarily illustrate Br–S mass fraction trends. Labels indicate soil type as
described in detail in Section 2: trench (tr), disturbed (Di), all data (Al), moderate
S (mo), undisturbed surface soil (un), basaltic soil (ba), normal disturbed soil (Nd).
The Supplementary Excel file "S1SoilCategories" identifies samples of each type.
Shaded rectangles correspond to 1 standard error in each parameter.

Fig. 3b shows the scatter of Br with Mg in Gusev's Trench
soil category, where 90% of Br variability can be modeled with
Mg alone. Fig. 3c shows MIs of corresponding samples. Our
one standard error bars (using gray shading to avoid visual clut-
ter) for slope and correlation in Fig. 2 account both for data
scatter and the number of data, where fewer data cause higher
uncertainty than evident visually in scatter plots (e.g., Fig. 3a
and b).

In summary, the Br/Cl ratio is lower at the surface (Table 1), Br
correlates strongly with S at depth yielding a higher Br/S ratio, and
nearly all of the variability in Br can be modeled by S and Mg vari-
ations alone (Figs. 2 and 3a and b) in subsurface (trench) soil. The
substantially stronger correlation of Br with Mg (Fig. 3b) compared
to that with S (Figs. 2 and 3a) suggests coupling between Br and Mg
beyond indirect association from subsurface Mg and S correlation.
Such indirect variation arise, for example, from the presence of Mg-
sulfates in soil along with co-migration of halides and sulfates dur-
ing aqueous processes.

Fig. 4 shows an example of a bivariate scatter plot to provide
context for the weakest association between Br and S, found in
the Meridiani surficial soil category. Beyond the visual contrast
with the scatter plot from the Gusev trench (Fig. 3a), a factor of 4
higher uncertainty in slope (translating to a factor of 23 higher rel-
ative uncertainty), despite more data, reflects our analytical ap-
proach that integrates both scatter and the number of data in
uncertainty estimates (Karunatillake et al., 2012). Fig. 5, a plot of
correlation coefficients versus regression slopes, summarizes the
data in Fig. 4 as the surficial soil type at Meridiani.

Br regresses with S at distinctly higher correlation and slope in
trench soil than in most other soil categories (Fig. 2) at Gusev. A
similar trend at Meridiani (Fig. 5) remains discernable despite
insufficient data for trench soil ($n = 4$) inducing substantial uncer-
tainty. Also consistent with stronger coupling of Br and S at depth,
only the correlation within disturbed soil exceeds the ~0.5 value of
trench soil.

Several factors contribute to subsurface trends. Some subsur-
face soil may reflect a history of alteration and consolidation over
longer periods than eolian infill of secondary crater depressions,
termed hollows by the MER team (e.g., Squyres, 2004). Further-
more, compositional trends with depth vary from one trench to an-
other. Such variability makes the depth gradient difficult to
quantify across the three trenches (Boroughs, Big Hole, Road Cut)
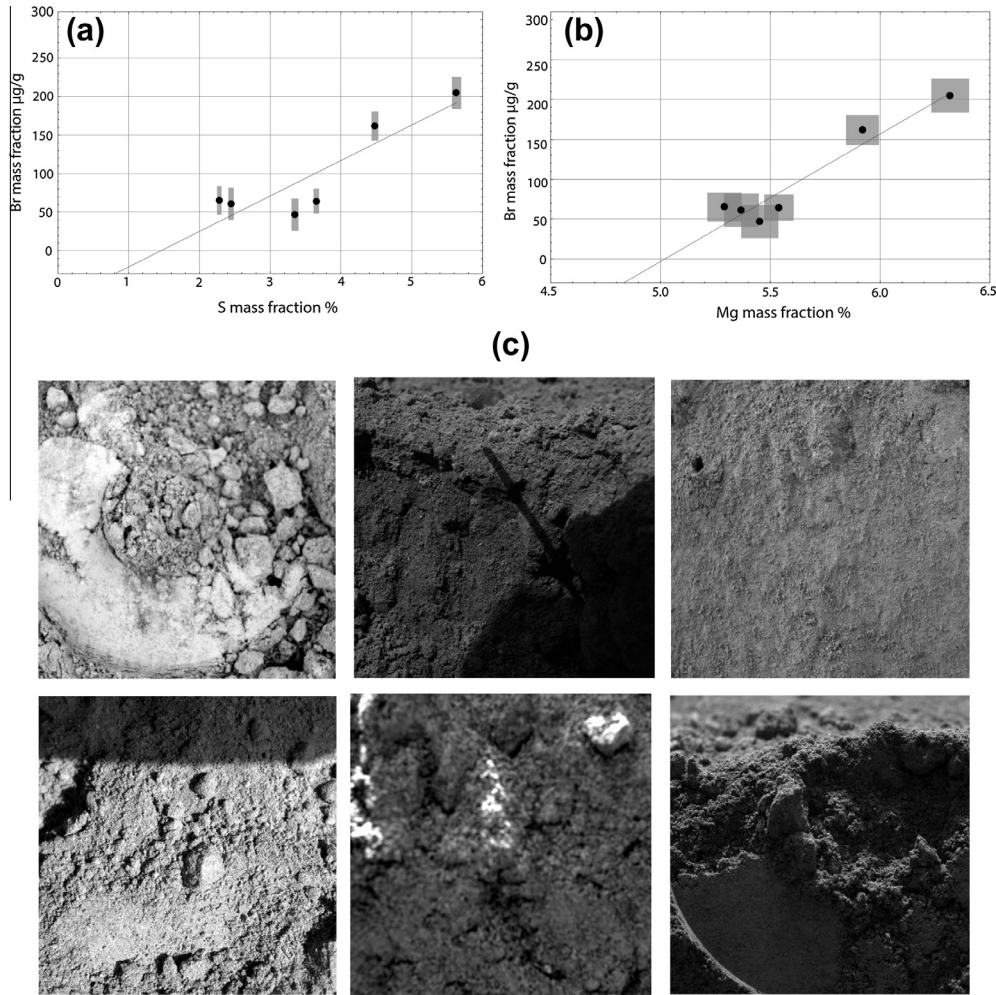at Gusev. Among these, Boroughs type soil seems areally abundant,

**Table 1**
Average mass fraction ratios of Br to Cl and S to Cl compared between undisturbed
surface and trench soil samples at Gusev Crater. Differences between surface and
depth (trench) indicate variability of Br and S relative to Cl. The values indicate that
Br, but not S, increases approximately 2× more than Cl at depth.

| Mass ratio type | Soil category | Mean ratio | Standard error |
|---|---|---|---|
| Br/Cl | Undisturbed | $0.3 \times 10^{-2}$ | $0.1 \times 10^{-2}$ |
| | Trench | $0.6 \times 10^{-2}$ | $0.1 \times 10^{-2}$ |
| S/Cl | Undisturbed | 3.6 | 0.1 |
| | Trench | 5.1 | 0.9 |

**Fig. 3.** Correlation of Br (µg/g) with S and Mg in Gusev trench soil samples. Bivariate regression of Br with S (a) yields a slope, $m = 46 \pm 12$; and intercept, $C = -67 \pm 46$, at one standard error including a strong correlation coefficient of ∼0.9. Similarly, with a slope, $m = 160 \pm 23$, and intercept, $C = -800 \pm 100$, Br yields an ∼1.0 correlation with Mg (b). Consequently, S and Mg alone model more than 90% of the variability in Br within trench soil, despite the statistical constraint of only six samples. Gray shading about each datum indicates 1 standard error uncertainty. Sample images by the MI shown in left–right top–bottom order (c): Bighole_RS2 (sol 114); Bighole_Trico (sol 115); Boroughs_Hellskitchen_side (141); Boroughs_Mills_bottom (140); Road cut_Floor3 (49); and Road Cut_WallMI (50). Each image has dimensions of ∼3 × 3 cm.
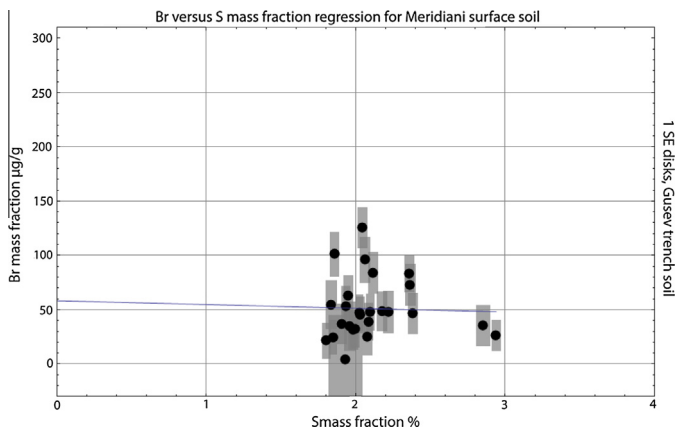


**Fig. 4.** Scatter plot of Br versus S revealing that Br (as µg/g) does not correlate with S within undisturbed surface soil at Meridiani. Provides contextual detail for the surficial soil type in the Br–S correlation and slope summary plot (Fig. 5). Regression results model $w$(Br) with slope, $m = -3 \pm 20$, and intercept, $C = 58 \pm 43$, at 1 standard error. The roughly factor of four higher uncertainty of the slope (corresponding to 23× higher relative uncertainty) when compared with Gusev trench data (Figs. 2 and 3) reflects scatter overwhelming any correlation.

perhaps geologically old, and most representative of chemical processes over geologic time scales (Karunatillake et al., 2007). Furthermore, the Boroughs trench shows evidence for increasing Br depletion towards shallower 4–5 cm depths from 7 to 10 cm depths. Despite ambiguities, all three trenches show consistently lower Br mass fractions and correspondingly lower Br/Cl ratios at the surface (Fig. 6, surface samples highlighted as circles) relative to deeper wall and floor samples (Fig. 6, solid squares and disks, respectively).

Meridiani soil analyses suggest that Br varies at depth in a manner roughly similar to that at Gusev. For example, Br decreases towards the surface, thus acting as the primary control on elemental ratios (compare Fig. 6 with Fig. 7) as evident in consistently lower Br/Cl ratios and Br mass fractions at the surface (Fig. 7 open circles) relative to depth (Fig. 7 solid squares and circles) in trenches. Meridiani samples differ in some ways, including less clear variation in the correlation of Cl (Fig. 8) and Br (Fig. 5) with S across different soil types. Furthermore, Cl and Br correlate strongly at Meridiani in trench soil but not at Gusev (Fig. 9).

Do volatilized halogens – Br in particular – transported throughout the martian surface remain a viable model despite differences in the detailed trends of Br, Cl, and S at Gusev relative to those at Meridiani? Established differences in petrogenetic
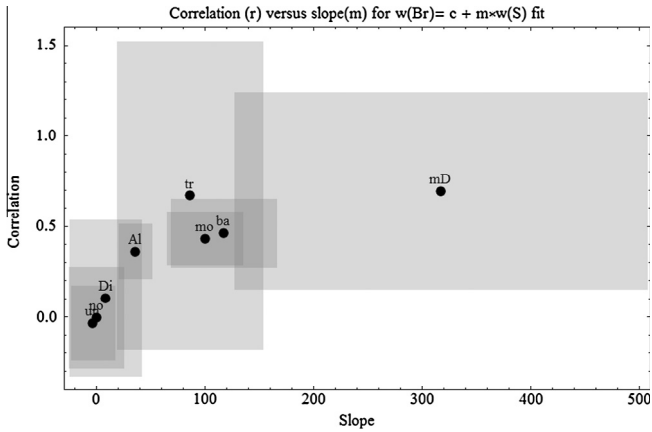
Fig. 5. Plot of correlation coefficient versus slope of linear regressions for Br–S in different soils classes. These mutually dependent regression parameters summarily illustrate Br–S association trends at Meridiani. Labels identify the seven soil types as described in detail in Section 2: moderate S content soils (mo), basaltic soils (ba), trench soils (tr), disturbed soils (Di), disturbed soils with moderate S content and low hematite content (mD), surficial soils (un), surficial soils without excessive hematite (no). The Supplementary Excel file "S1SoilCategories" identifies samples of each type. Shaded rectangles correspond to 1 standard error in each parameter.
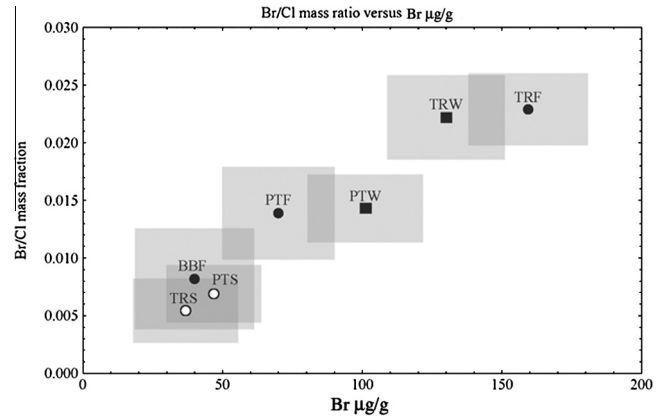


Fig. 7. Trench profile at Meridiani. Labels identify specific trenches, BB: Beagle Burrow; PT: Peanut Trench; TR: Trench. Suffixes identify location at trench site, S: Surface, W: Wall, and F: Floor. We propagated highly conservative numerical uncertainties from reported values for Br and Cl at 2 standard errors, shown as shaded rectangles. Consequently, the values may be more precise than they appear. Note the difference across floor, wall, and surface with highest ratios at the floor sampling the deepest. The ratio also varies roughly linearly with Br, indicating a relatively uniform Cl content.
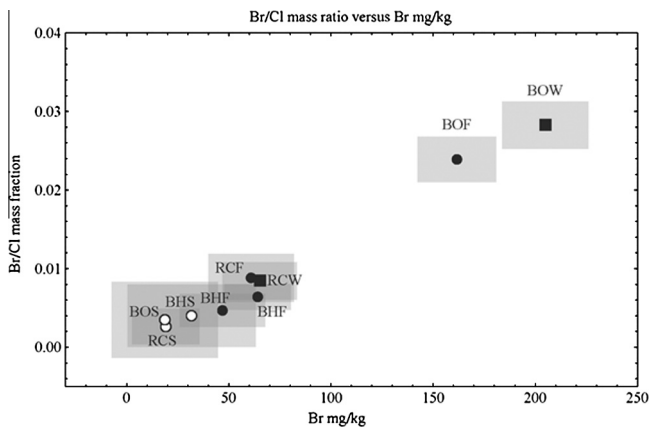


Fig. 6. Trench profile at Gusev for the mass fraction ratio Br/Cl. Labels identify specific trenches, BO: Boroughs; RC: Road Cut; BH: Big Hole. Suffixes and shapes identify location at trench site, S: surface as circle, W: wall as solid square, and F: floor as disk. We propagated highly conservative numerical uncertainties from reported values for Br and Cl at 2 standard errors, shown as shaded rectangles. Consequently, the values are more precise than they appear. Note the difference across floor, wall, and surface with highest ratios at the floor sampling the deepest. The ratio also varies roughly linearly with Br, indicating a relatively uniform Cl content.
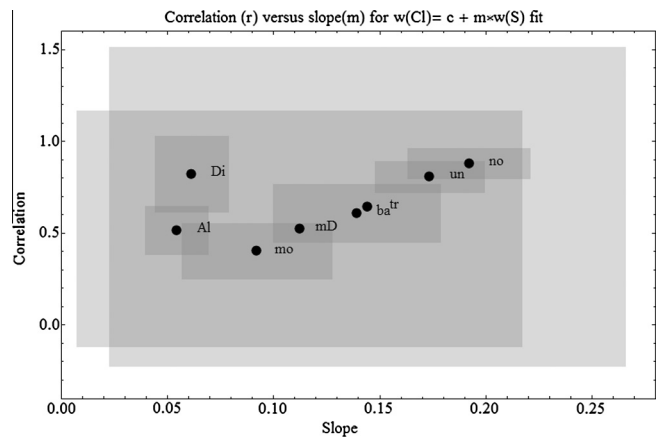


Fig. 8. Plot of correlation coefficient versus slope of linear regressions for Cl versus S mass fraction in different soils classes at Meridiani. These mutually dependent regression parameters summarily illustrate Cl–S association. Labels identify the seven soil types as described in detail in Section 2: moderate S content soils (mo), basaltic soils (ba), trench soils (tr), disturbed soils (Di), disturbed soils with moderate S content and low hematite content (mD), surficial soils (un), and surficial soils without excessive hematite (no). The Supplementary Excel file "S1SoilCategories" identifies samples of each type. Shaded rectangles correspond to 1 standard error in each parameter.

processes at the two sites (McLennan et al., 2005; McSween et al., 2010, 2008) may drive some of the differences. For example, Meridiani outcrops likely originate from sedimentary processes sustained by temporally and spatially varying ground water tables analogous to terrestrial playas (McLennan et al., 2005). In contrast, most float rocks and outcrop at Gusev appear igneous, with those in the Columbia Hills suggesting limited aqueous alteration (McSween et al., 2010, 2008). Gusev sedimentary rocks seem coupled to volcanism – and in places impact related processes – such as Home Plate deposited in a pyroclastic surge (Lewis et al., 2008) and carbonate-bearing Comanche precipitating in hydrothermal environments (Morris et al., 2010). Local rocks at each site may contribute to soil via comminution and chemical weathering (Yen et al., 2005). For example, hematite lag deposits at Meridiani not only constitute a local component of soil (Fleischer et al., 2010)

but also suggest mechanical weathering (Squyres et al., 2009) and sediment contribution from sedimentary S-rich host rock. If so, the high variability of Br in Meridiani rocks relative to other elements (Clark et al., 2005, p. 83) may obscure similarities with the halogen distributions in Gusev soil.

### 3.1. The variability of S/Cl across landing sites

Differences in labile element trends between Meridiani and Gusev motivated us to evaluate the common conclusion that martian soil remains quite uniform in elemental composition across the vast distances that separate different landing sites (Gellert et al., 2006; Yen et al., 2005). The ratio of S and Cl mass fractions in particular has been considered to be nearly constant at ∼3.6 (Gellert et al., 2006, p. 73). Key models of Cl and S evolution on Mars also suggest a similarity of sources such as volcanic exhalations or
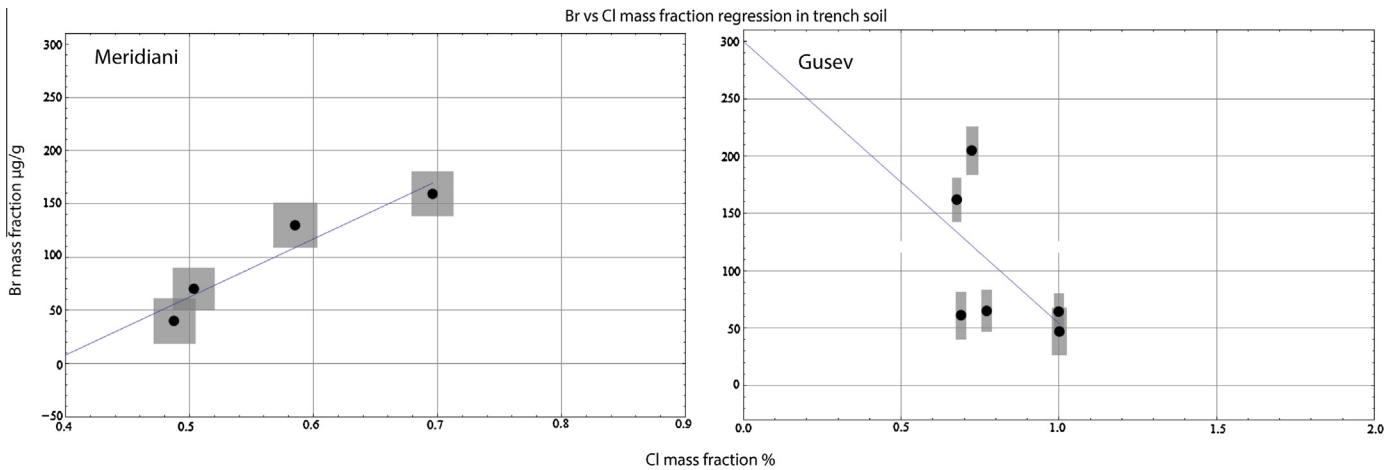
**Fig. 9.** Correlation of Br (mass fraction as μg/g) with Cl within trench soil compared between Meridiani (left) and Gusev (right). Despite the few samples, Br regression shows less uncertainty in slope (550 ± 120) at Meridiani, versus −250 ± 180 at Gusev, indicating less scatter. Accordingly, Cl models nearly ∼90% of Br variability at Meridiani compared to only ∼15% at Gusev. Unlike at Meridiani, Br also appears to anticorrelate with Cl at Gusev. Shaded rectangles signify one standard error uncertainty of each datum.
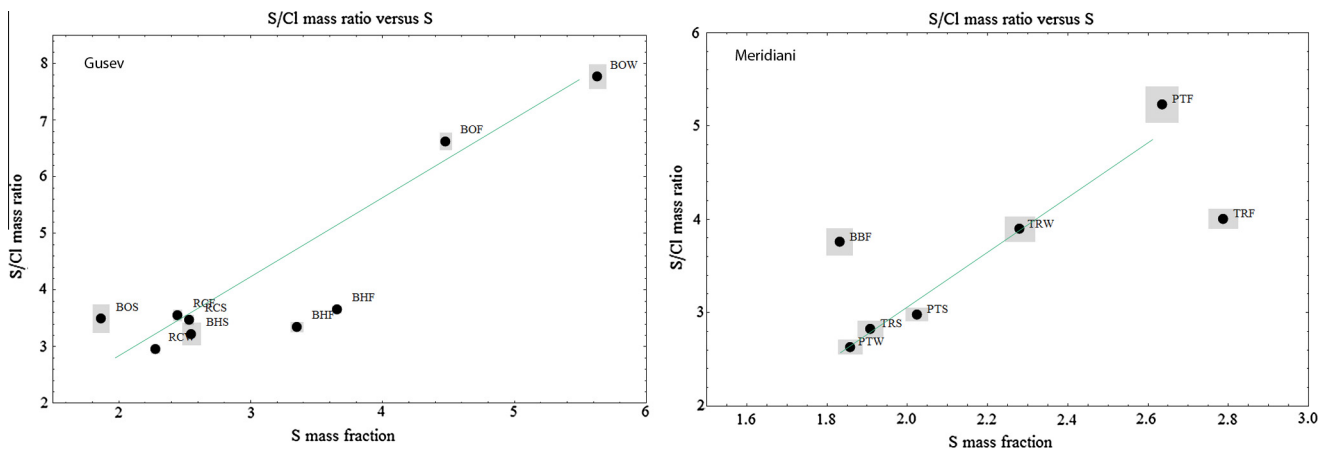


**Fig. 10.** Trench profile of S/Cl mass ratios versus S at Gusev (left) and Meridiani (right). Labels identify specific trenches at Gusev, BO: Boroughs; RC: Road Cut; and BH: Big Hole. Suffixes identify position within each trench, S: Surface, W: Wall, and F: Floor. Corresponding labeling at Meridiani indicate Beagle Burrow (BB), Peanut Trench (PT), and Trench (TR). We propagated highly conservative numerical uncertainties from reported values for Br and Cl at 2 standard errors, shown as shaded rectangles. Consequently, the values may be more precise than they appear. Note the difference across floor, wall, and surface with lowest ratios occurring at the surface. While less pronounced than with the Br/Cl ratio, linearity in trends (accentuated with the green lines) suggest S/Cl variations driven more by S than Cl.

secondary minerals from fluids (McSween et al., 2008, para. 19). Nevertheless, soils from different landing sites, despite broadly similar chemical composition, when examined in detail exhibit variations among landing sites, explained largely by differences in local geology; across each landing site, explained largely by variable geology and aqueous processes; and within vertical profiles. A variety of aqueous processes may explain the latter, perhaps extending to atmospheric processes for Br variability.

Some data across different landing sites suggest a variable S/Cl ratio. Analyses of trench soil samples at Gusev and Meridiani suggest a S/Cl ratio substantially higher than 3.6 at decimeter-scale depths of GRS sensitivity (Karunatillake et al., 2007). In contrast, Phoenix data indicate much lower S/Cl ratios approximating 1.8 (Kounaves et al., 2010), although this value only represents water-soluble salts in the soil. Collectively, such observations further suggest that the variability of the S/Cl ratio on Mars may have been underestimated. Our work also indicates a higher S/Cl ratio with depth at both Gusev (summarized in Table 1) and Meridiani, from ∼3.6 at the surface to values of 4–5 in the subsurface (Fig. 10 shows trench profiles at both sites). While the S–Cl correlation weakens only at depth, positive Cl intercepts (Fig. 11), amounting

to ∼15% of the typical 0.6–0.7% Cl mass fraction in basaltic soil, occur even in soil categories where S and Cl correlate strongly. Consequently, the two elements may fractionate significantly in bulk martian soil at depth scales on the order of decimeters or more.

Aqueous and photochemical processes on Earth and recent experiments suggest that Br may volatilize preferentially, imparting a stronger volatility signature relative to Cl (Vogt et al., 1996; Yang et al., 2008; Zhao et al., 2013). Once volatilized, gaseous inorganic Br may reside in the atmosphere almost three times longer than gaseous inorganic Cl, reflecting more efficient cycling of Br than Cl in the terrestrial atmosphere (Rancher and Kritz, 1980). However, perchlorates in the martian arctic zone, as observed by Phoenix (Hecht et al., 2009), support Cl volatility with soil acting as a sink over geologic time scales (Catling et al., 2010). S may also volatilize (Halevy and Schrag, 2009; Halevy et al., 2007) on Mars.

Cl may volatilize, but the preferential decrease of Br towards the surface (Figs. 6 and 7 and Table 1) supports a more pronounced loss of Br to the atmosphere relative to Cl and S, at least at the Gusev landing site. Two pathways may contribute to this at unconstrained relative significance: (1) the soil surface may incorporate atmospherically sourced perchlorate preferentially, altering the S/
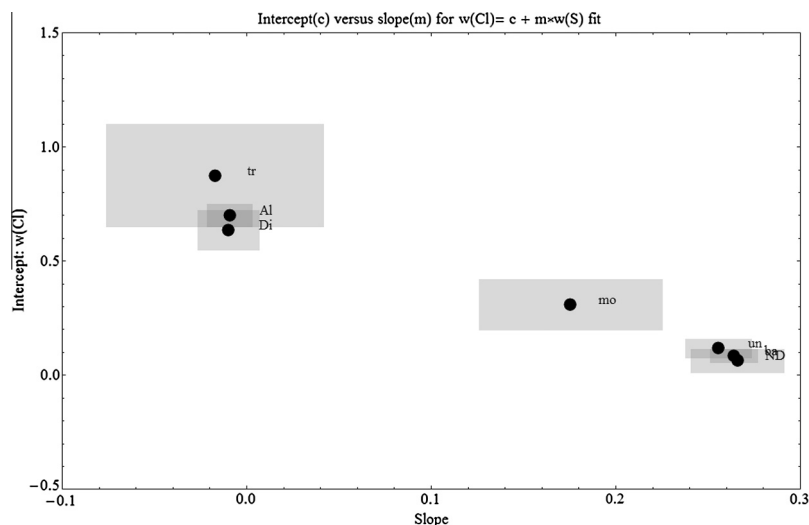
**Fig. 11.** Scatter plot showing the mutually dependent parameters of intercept versus slope in the regression of Cl with S at Gusev. Labels indicate soil type as described in detail in Section 2: trench (tr), disturbed (Di), all data (Al), moderate S (mo), undisturbed surface soil (un), basaltic soil (ba), normal disturbed soil (ND). The Supplementary Excel file "S1SoilCategories" identifies samples of each type. Shaded rectangles correspond to 1 standard error in each parameter. Cl and S dissociate in deeper soil, in turn disrupting the correlation within the set of all samples. Positive intercepts, even in surficial soil where Cl and S associate strongly, reveal the fractionation of Cl and S.

Cl ratio at the surface relative to the subsurface; (2) with halide phases less volatile and less soluble than bromide phases (Yang et al., 2008) as discussed in Section 1.1, Cl may redistribute in less concentrated brines while Br volatilizes from concentrated brine. This may impart a stronger aqueous signature to the Cl distribution than to that of Br.

Pathways to form perchlorate naturally remain unclear (e.g., Bao and Gu, 2004) both on Earth and Mars. Gaseous Cl species can oxidize to perchlorate in the atmosphere by photochemical processes (Catling et al., 2010). However, perchlorate can also form by aqueous $Cl^-$ interacting with oxidants, such as ozone (Rao et al., 2010). In the latter case, photochemical processes may contribute indirectly as a provider of oxidants, while perchlorate forms via liquid–gas reactions in situ during evaporation. In such processes, dissolution of Cl species may dominate over the volatilization. More laboratory work remains essential to constrain the relative significance of aqueous mobility relative to volatility of halogens on Mars.

## 4. Conclusions and future work

Our soil analyses yield two key results. First, halogen variability in the soil profile is consistent with loss to the atmosphere. Accordingly, the more readily volatilized Br shows strong evidence of decreasing concentration and weakening correlation with S toward the surface. Consequently, analogs of some terrestrial processes that volatilize Br, such as frost flower facilitation (Zhao et al., 2008), low-temperature UV-photolysis oxidation (Saiz-Lopez et al., 2008), and salt pan UV-photolysis (Wood and Sanford, 2007), could be significant on Mars. Brine films on dust grains may also accelerate halogen volatilization (Sander et al., 2003).

We find our observations sufficiently compelling, necessitating additional work to distinguish volatility pathways from the alternative of evaporative processes and post-depositional fluid migration (e.g., Amundson et al., 2008; Clark et al., 2005; Yen et al., 2005). To this end, we have begun a laboratory program experimentally evaporating UV-exposed bromide–chloride and bromide–chloride–sulfate brines under conditions more representative of Mars (Zhao et al., 2013) than the single experiment reported by Wood and Sanford (2007). Preliminary laboratory observations appear to strengthen the potential for halogen volatility to impart a discernable chemical signature (Zhao et al., 2013).

Second, the soil profile shows more variable S/Cl mass ratios than previously thought. The soil profile samples Mars at greater depth than the hundreds of microns by most remote sensing missions, in richer detail than at multi-meter resolution of compositional effects on dielectric properties by radar methods (Carter et al., 2009; Watters et al., 2007), and with greater fidelity of bulk soil than surface measurements. As a mix of surface material exposed to recent eolian processes with subsurface soil that may record varying climatic and aqueous conditions over geologic time scales, bulk soil presents the key to understanding martian surface evolution (McSween et al., 2010). Based on our observations, such soil – likely sampled globally by the GRS – bears a bi-modal S/Cl distribution with low values at the surface approximating 3.6, and higher subsurface values in the 4–5 range. Due to reasons discussed in Section 3.1, we posit further that aqueous processes may overprint S/Cl variability, unlike that of Br driven more by atmospheric release.

## Appendix A. Supplementary material

Supplementary data associated with this article can be found, in the online version, at http://dx.doi.org/10.1016/j.icarus.2013.07.018.

# References

Amundson, R. et al., 2008. On the in situ aqueous alteration of soils on Mars. Geochim. Cosmochim. Acta 72, 3845–3864.

Andrews-Hanna, J.C., Phillips, R.J., Zuber, M.T., 2007. Meridiani Planum and the global hydrology of Mars. Nature 446, 163–166.

Archer Jr., P.D. et al., 2013. Possible detection of perchlorates by evolved gas analysis of Rocknest soils: Global implications. Lunar Planet Sci. 44. Abstract 2168.

Bao, H., Gu, B., 2004. Natural perchlorate has a unique oxygen isotope signature. Environ. Sci. Technol. 38, 5073–5077.

Broecker, W.S., Peng, T., Beng, Z., 1982. Tracers in the Sea. Columbia University.

Buys, Z., Brough, N., Huey, G., Tanner, D., Von Glasow, R., Jones, A.E., 2012. $Br_2$, BrCl, BrO and surface ozone in coastal Antarctica: A meteorological and chemical analysis. Atmos. Chem. Phys. Discuss. 12, 11035–11077.

Byrne, S. et al., 2009. Distribution of mid-latitude ground ice on Mars from new impact craters. Science 325, 1674–1676.

Carr, M.H., 2008. The Surface of Mars. Cambridge University Press, New York.

Carter, L.M., Campbell, B.A., Watters, T.R., Phillips, R.J., Putzig, N.E., Safaeinili, A., Plaut, J.J., Okubo, C.H., Egan, A.F., Seu, R., Biccari, D., Orosei, R., 2009. Shallow radar (SHARAD) sounding observations of the Medusae Fossae Formation, Mars. Icarus 199, 295–302.

Catling, D.C. et al., 2010. Atmospheric origins of perchlorate on Mars and in the Atacama. J. Geophys. Res. 115, E00E11.

Clark, B.C. et al., 2005. Chemistry and mineralogy of outcrops at Meridiani Planum. Earth Planet. Sci. Lett. 240, 73–94.

Cockell, C.S., Catling, D.C., Davis, W.L., Snook, K., Kepner, R.L., Lee, P., McKay, Christopher P., 2000. The ultraviolet environment of Mars: Biological implications past, present, and future. Icarus 146, 343–359.

Fairén, A.G., Davila, A.F., Gago-Duport, L., Amils, R., McKay, Christopher P., 2009. Stability against freezing of aqueous solutions on early Mars. Nature 459, 401–404.

Finlayson-Pitts, B.J., 2010. Atmospheric chemistry. Proc. Natl. Acad. Sci. USA 107, 6566–6567.

Fleischer, I., Agresti, D.G., Klingelhöfer, G., Morris, R.V., 2010. Distinct hematite populations from simultaneous fitting of Mössbauer spectra from Meridiani Planum, Mars. J. Geophys. Res. 115, E00F06.

Gellert, R. et al., 2006. Alpha Particle X-ray Spectrometer (APXS): Results from Gusev Crater and calibration report. J. Geophys. Res. 111, E02S05.

Grotzinger, J.P., Hayes, A.G., Lamb, M.P., McLennan, S.M., 2013. Sedimentary processes on Earth, Mars, Titan, and Venus. In: Mackwell, S.J. (Ed.), Comparative Climatology of Terrestrial Planets. University of Arizona.

Halevy, I., Schrag, D.P., 2009. Sulfur dioxide inhibits calcium carbonate precipitation: Implications for early Mars and Earth. Geophys. Res. Lett. 36, L23201.

Halevy, I., Zuber, M.T., Schrag, D.P., 2007. A sulfur dioxide climate feedback on early Mars. Science 318, 1903–1907.

Hayes, A.G., Grotzinger, J.P., Edgar, L.A., Squyres, S.W., Watters, W.A., Sohl-Dickstein, J., 2011. Reconstruction of eolian bed forms and paleocurrents from cross-bedded strata at Victoria Crater, Meridiani Planum, Mars. J. Geophys. Res. 116, E00F21.

Hecht, M.H. et al., 2009. Detection of perchlorate and the soluble chemistry of martian soil at the Phoenix lander site. Science 325, 64–67.

Hönninger, G., Bobrowski, N., Palenque, E.R., Torrez, R., Platt, U., 2004. Reactive bromine and sulfur emissions at Salar de Uyuni, Bolivia. Geophys. Res. Lett. 31, L04101.

Hurowitz, J.A., McLennan, S.M., 2007. A ∼3.5 Ga record of water-limited, acidic weathering conditions on Mars. Earth Planet. Sci. Lett. 260, 432–443.

Hurowitz, J.A., Tosca, Nicholas J., McLennan, S.M., Schoonen, M.A.A., 2007. Production of hydrogen peroxide in martian and lunar soils. Earth Planet. Sci. Lett. 255, 41–52.

Kaleschke, L., 2004. Frost flowers on sea ice as a source of sea salt and their influence on tropospheric halogen chemistry. Geophys. Res. Lett. 31, L16114.

Karunatillake, S. et al., 2007. Chemical compositions at Mars landing sites subject to Mars Odyssey Gamma Ray Spectrometer constraints. J. Geophys. Res. 112, E08S90.

Karunatillake, S. et al., 2012. Martian case study of multivariate correlation and regression with planetary datasets. Earth, Moon, Planets 108, 253–273.

Knoll, A.H. et al., 2008. Veneers, rinds, and fracture fills: Relatively late alteration of sedimentary rocks at Meridiani Planum, Mars. J. Geophys. Res. 113, 1–27.

Kounaves, S.P. et al., 2010. Soluble sulfate in the martian soil at the Phoenix landing site. Geophys. Res. Lett. 37, L09201.

Lefèvre, F. et al., 2008. Heterogeneous chemistry in the atmosphere of Mars. Nature 454, 971–975.

Lewis, K.W. et al., 2008. Structure and stratigraphy of Home Plate from the Spirit Mars Exploration Rover. J. Geophys. Res. 113, E12S36.

Marion, G.M., Catling, D.C., Kargel, J.S., 2009. Br/Cl partitioning in chloride minerals in the Burns formation on Mars. Icarus 200, 436–445.

Marion, G.M., Catling, D.C., Zahnle, K.J., Claire, M.W., 2010. Modeling aqueous perchlorate chemistries with applications to Mars. Icarus 207, 675–685.

McLennan, S.M. et al., 2005. Provenance and diagenesis of the evaporite-bearing Burns formation, Meridiani Planum, Mars. Earth Planet. Sci. Lett. 240, 95–121.

McSween, H.Y. et al., 2008. Mineralogy of volcanic rocks in Gusev Crater, Mars: Reconciling Mössbauer, Alpha Particle X-ray Spectrometer, and miniature thermal emission spectrometer spectra. J. Geophys. Res. 113, E06S04.

McSween, H.Y., McGlynn, I.O., Rogers, A.D., 2010. Determining the modal mineralogy of martian soils. J. Geophys. Res. 115, E00F12.

Ming, D.W. et al., 2008. Geochemical properties of rocks and soils in Gusev Crater, Mars: Results of the Alpha Particle X-ray Spectrometer from Cumberland ridge to home plate. J. Geophys. Res. 113, E12S39.

Morris, R.V. et al., 2010. Identification of carbonate-rich outcrops on Mars by the Spirit Rover. Science 329, 421–424.

Parker, M.V.K., Zegers, T., Kneissl, T., Ivanov, B., Foing, B., Neukum, G., 2010. 3D structure of the Gusev Crater region. Earth Planet. Sci. Lett. 294, 411–423.

Rancher, J., Kritz, M.A., 1980. Diurnal fluctuations of Br and I in the tropical marine atmosphere. J. Geophys. Res. 85, 5581–5587.

Rao, M.N., Nyquist, L.E., Sutton, S.R., Dreibus, G., Garrison, D.H., Herrin, J., 2009. Fluid-evaporation records preserved in salt assemblages in Meridiani rocks. Earth Planet. Sci. Lett. 286, 396–403.

Rao, B., Anderson, T.A., Redder, A., Jackson, W.A., 2010. Perchlorate formation by ozone oxidation of aqueous chlorine/oxy-chlorine species: Role of $Cl_xO_y$ radicals. Environ. Sci. Technol. 44, 2961–2967.

Rieder, R. et al., 2004. Chemistry of rocks and soils at Meridiani Planum from the Alpha Particle X-ray Spectrometer. Science 306, 1746–1749.

Risacher, F., Fritz, B., Alonso, H., 2006. Non-conservative behavior of bromide in surface waters and brines of Central Andes: A release into the atmosphere? Geochim. Cosmochim. Acta 70, 2143–2152.

Rontó, G. et al., 2003. Solar UV irradiation conditions on the surface of Mars. Photochem. Photobiol. 77, 34–40.

Ruff, Steven W. et al., 2011. Characteristics, distribution, origin, and significance of opaline silica observed by the Spirit Rover in Gusev Crater, Mars. J. Geophys. Res. 116, E00F23.

Saiz-Lopez, A. et al., 2008. On the vertical distribution of boundary layer halogens over coastal Antarctia: Implications for $O_3$, $HO_x$, $NO_x$ and the Hg lifetime. Atmos. Chem. Phys. Discuss. 8, 887–900.

Sander, R. et al., 2003. Inorganic bromine in the marine boundary layer: A critical review. Atmos. Chem. Phys. 3, 1301–1336.

Simpson, W.R. et al., 2007. Halogens and their role in polar boundary-layer ozone depletion. Atmos. Chem. Phys. Discuss. 7, 4285–4403.

Smith, M.D., 2008. Spacecraft observations of the martian atmosphere. Annu. Rev. Earth Planet. Sci. 36, 191–219.

Smith, P.H. et al., 2009. $H_2O$ at the Phoenix landing site. Science 325, 58–61.

Smoydzin, L., Von Glasow, R., 2009. Modelling chemistry over the Dead Sea: Bromine and ozone chemistry. Atmos. Chem. Phys. Discuss. 9, 4525–4565.

Squyres, S.W., 2004. The Spirit Rover's Athena science investigation at Gusev Crater, Mars. Science 305, 794–799.

Squyres, S.W. et al., 2006. Two years at Meridiani Planum: Results from the Opportunity Rover. Science 313, 1403–1407.

Squyres, S.W. et al., 2009. Exploration of Victoria crater by the Mars rover opportunity. Science 324, 1058–1061.

Sutter, B. et al., 2013. The detection of evolved oxygen from the Rocknest eolian bedform material by the Sample Analysis at Mars (SAM) instrument at the Mars Curiosity landing site. Lunar Planet. Sci. 44, 2046.

Urbansky, E.T., 1998. Perchlorate chemistry: Implications for analysis and remediation. Bioremed. J. 2, 81–95.

Vogt, R., Crutzen, P.J., Sander, R., 1996. A mechanism for halogen release from sea-salt aerosol in the remote marine boundary layer. Nature 383, 327–329.

Von Glasow, R., Crutzen, P.J., 2007. Tropospheric halogen chemistry. In: Heinrich, D.H., Turekian, K.K. (Eds.), Treatise on Geochemistry. Pergamon, Oxford, pp. 1–67.

Wang, A. et al., 2006. Sulfate deposition in subsurface regolith in Gusev Crater, Mars. J. Geophys. Res. 111, E02S17.

Wang, A. et al., 2008. Light-toned salty soils and coexisting Si-rich species discovered by the Mars Exploration Rover Spirit in Columbia Hills. J. Geophys. Res. 113, E12S40.

Warren, J.K., 2006. Evaporites: Sediments, Resources, and Hydrocarbons. Springer, Berlin, New York.

Watters, T.R. et al., 2007. Radar sounding of the Medusae Fossae Formation Mars: Equatorial ice or dry, low-density deposits? Science 318, 1125–1128.

Wayne, R.P. et al., 1995. Halogen oxides: Radicals, sources and reservoirs in the laboratory and in the atmosphere. Atmos. Environ. 29, 2677–2881.

Wood, W.W., Sanford, W.E., 2007. Atmospheric bromine flux from the coastal Abu Dhabi sabkhat: A ground-water mass-balance investigation. Geophys. Res. Lett. 34, L14405.

Yang, X., Pyle, J.a., Cox, R.a., 2008. Sea salt aerosol production and bromine release: Role of snow on sea ice. Geophys. Res. Lett. 35, L16815.

Yen, A.S. et al., 2005. An integrated view of the chemistry and mineralogy of martian soils. Nature 436, 49–54.

Yen, A.S. et al., 2008. Hydrothermal processes at Gusev Crater: An evaluation of Paso Robles class soils. J. Geophys. Res. 113, E06S10.

Zhao, T.L. et al., 2008. A three-dimensional model study on the production of BrO and Arctic boundary layer ozone depletion. J. Geophys. Res. 113, D24304.

Zhao, Y.-Y.S., McLennan, S.M., Jackson, A.W., Karunatillake, S., 2013. Photochemical effects on bromine and chlorine distributions during brine evaporation on the martian surface. Lunar Planet. Sci. 44, 3002.

Zorzano, M.-P., Mateo-Martí, E., Prieto-Ballesteros, O., Osuna, S., Renno, N., 2009. Stability of liquid saline water on present day Mars. Geophys. Res. Lett. 36, L20201.